Metal oxo clusters, from theory to innovation; Synthesis, mechanism & novel application in recyclable polymers

Inauguraldissertation

Zur

Erlangung der Würde eines Doktors der Philosophie

vorgelegt der

Philosophisch-Naturwissenschaftlichen Fakultät

der Universität Basel

und

der Ghent University

Von

Dietger Van den Eynden

von Belgien

2023

Genehmigt von der Philosophisch-Naturwissenschaftlichen Fakultät

Auf Antrag von

Prof. Dr. Jonathan De Roo & Prof. Dr. Klaartje De Buysser

Prof. Dr. Edwin Constable

Prof. Dr. Thomas Bürgi

Basel, den 19.09.2023   Prof. Dr. Marcel Mayor (Dekan)

Acknowledgements

One of the most important parts of this thesis is to thank all the people who have contributed to it. For this reason, I have put off writing this part for far too long, not because I think it is difficult, but because there is this little voice in my head: "I'm afraid I'll forget someone, or that my thanks won't be enough to express how grateful I am for everyone's support". This thesis is the result of a huge amount of work done by many people, and I will try to thank them in the rest of my acknowledgements. In my original timeline, this part should have been written around June, and as you can see at the end of my acknowledgements, this did not quite work out. At the moment my dissertation is mostly written, all that's left is to add a few references here and there and to filter out spelling mistakes (which I'm sure there will be). It feels satisfying to finish 4 years of PhD, in which I have always given 120%. Finalising my acknowledgements is the cherry on top. At the same time, it is strange to think that it will soon be over (if all goes well), it feels bittersweet. In the unlikely event that I've forgotten you, come and find me and we'll have a beer for old times' sake.

First of all, I would like to thank Prof. Dr. Jonathan De Roo and Prof. Dr. Klaartje De Buysser for being my main supervisors.
To Jonathan, I would first like to thank you for giving me the opportunity to come to Switzerland as your PhD student. This step has allowed me to grow both personally and scientifically. Thank you for all the knowledge you have imparted to me over the years. From making figures and slides to learning how to properly present scientific research. You have indoctrinated me to such an extent that I find myself internally correcting slides when watching other people's presentations. Thank you for giving me the freedom (within certain limits) to direct my research towards topics that fascinate

me and for believing in me. I have always found our scientific discussions very stimulating and constructive. If I compare the scientist I was before I started my PhD with the one I am now, I will be forever grateful to you because you have had a great influence on making me the scientist I am today. I wish you all the best in your future research.

To Klaartje, I would also like to thank you for the scientific discussions we had and for the opportunity to pursue my PhD in a collaborative spirit. Most of all, however, I would like to thank you for showing me that there is a great personal aspect to science. In our field it is easy to get lost in the data/results and forget the people behind it. Being part of your group taught me that it is good to reflect and that sometimes science is just science and not the most important part of life. I'll never forget the congratulations you wrote in your email to me telling me I passed my bachelor's after I thought I didn't because of crystallography, I was super happy! (Especially as I really didn't like crystallography and didn't want to do it again).

To Prof. Dr. Edwin Constable, thank you for being my second supervisor throughout my PhD. Your immense experience in chemistry always provided new insights to advance my research during our annual meetings. Finally, I would like to thank Prof. Dr. Thomas Bürgi for agreeing to be my external supervisor and Prof. Dr. Malte Oppermann for chairing my defense.

A big thank you, from the bottom of my heart, to the members of the De Roo group for making these 4 years a pleasant journey. Through numerous paper parties, group trips and cakes. I especially enjoyed the team building this year, it was the first time I've seen someone walk through a high quality French window. Special thanks to Rohan for his help in the start of my PhD and fitting the PDF for my clusters, to Jikson for the cluster catalysis and mechanism fittings and to Carlotta for still trying to find the PDF for the *in situ* measurements. I would also like to thank 2 of our master students. First of all, Ale, you're just amaaaaazing, nothing more, nothing less. Second, Antonia, you've shown great determination in a (not so) easy project. Special thanks to Ajmal for catching spelling mistakes. Thanks to the other members, Chris, Evelina, Evert, Jibin, Liza, Mahsa and Nico. I am also grateful to Isa and Claudia for keeping the administration ship at bay, and to Philipp and Grischa for building our special equipment for our *in situ* synchrotron measurements.

I would also like to thank the members of the SCRIPTS group in Ghent,

namely Ewout, Hannes, Isabel, John, Klaartje and Laura, together with the staff of S3, for the good times I had whenever I was in Belgium. To Loren and Eline, you both spent a year in Basel doing research on the not always pretty HfO_2 nanoparticles. Loren, I am grateful for the drinks we had together and for the pictures I took after your paper celebration, which still make me smile every time I see them. I don't think Mira has forgiven you for throwing up in the bath, though. Eline, I am grateful for all the help I have received from you, whatever the task, you are always there to help someone else. I completely understand that you never get any work done yourself. I am especially grateful that my efforts to create the Wheel of Fortune were not in vain because of you.

Next, I would like to express my gratitude to many scientific collaborators who have been part of my PhD. First of all, I would like to thank Prof. Dr. Ivan Infante, Roberta Pascazio and Dr. Juliette Zito for hosting me for 2 weeks at IIT Genova and teaching me the ins and outs of molecular dynamics. Staying in the computational field, I would like to thank Dr. Mike Devereux and Prof. Dr. Markus Meuwly for teaching me Density Functional Theory (DFT). Also special thanks to Dr. Tapas Debsharma and Prof. Dr. Filip Du Prez for collaborating with me on chapter 5 and teaching me rheology. Thanks to Dr. Angelo Muliali and Prof. Dr. Tatjana Parac-Vogt for their contributions to chapter 3 of this thesis. Thanks to Ona Segura Lecina (Buonsanti group) for showing me how colloidal atomic layer deposition works, to Prof. Dr. Stefan Hengsberger for showing me the nanoindentation technique and and to Ilaria Onori (Weder group) for showing me dynamic mechanical analysis and performing some measurements for me. Thanks to Dr. Suren Nehmat (Tiefenbacher group) for the 'easy' nanoparticle titration. Thanks to Dr. Mariano Calcabrini (Ibáñez group), I hope I could teach you at least some NMR. I am grateful to Dr. Olga Safonova, Dr. Adam Hugh Clark, Dr. Sanjit Ghose and Dr. Cheng Hung Lin for their excellent support of our *in situ* synchrotron measurements. I would also like to thank the NCCR Molecular System Engineering for the financial support during my PhD.

While the scientific collaborators were essential to this thesis, I would never have got here without the help of many non-scientific people. First of all, my family, Mom, Dad and kleine. Thank you Mom and Dad for raising me the way you did and supporting me all this time, I think you did a great

job! It feels good to know that you are there for me in every situation and that I can always count on you. It took me 28 years to learn that it is wise to listen to you because you are right 99% of the time, something I did not believe as a child... Without you I would not be the person I am today and I would not be finishing my PhD. I will be forever grateful for the opportunities you gave me, for this is a debt I will never be able to repay. Kleine, although we didn't always see eye to eye when we were little, I'm glad we grew up together. Being 6 years younger, you always kept my inner child alive. I hope we can still enjoy our inflatable unicorn and beer cooler (we still have to convince mom and dad of the latter).

To Grandma and Grandpa Cow (for those who are not familiar with this concept, this is not an insult. My grandparents had cows and it was an easy word to remember as a child, I wasn't always smart, you know) I would like to thank them for all the good times I spent on the farm. I still remember driving a tractor a couple times my size when the grass had to be dried and Grandpa was shouting instructions that I could hardly hear because of the noise. Or enjoying an ice-cold Coke on a hot July evening after all the hay bales had been put into the barn. To Grandma and Grandpa Fish (same reasoning as above, they live in the same street so using the name of the village to make the distinction was not an option) thank you for the wonderful times we spent together on holiday and for teaching me how to ride a bike. You taught it that well to me that I am still able to do it! Finally, I would also like to thank my aunts, uncles and other relatives for the wonderful family celebrations we have had together.

To my best friend Domien, I'm very grateful for everything you've taught me. Whenever I was upset about something trivial, you were always the first to put the situation I got myself into perspective. Usually by laughing in my face first and only then thinking of solutions. I will never forget hiding our game boys under the pillow when Mom and Dad went to sleep during a sleepover, or getting up every 30 minutes to see if it was already snowing outside. You taught me to look on the bright side, even when things seem hard, because it could always be worse. I miss you...

To Geert, Ine, Willem, Sander and Simon, you brightened my time as a student at Ghent University. Geert, by deriving every possible equation in our quantum chemistry course, which made the course text 5 times bigger and not easier unfortunately. Or when you woke up in the lift at the pharmacy

campus after a night out, if only you were wearing a GoPro that night. Ine, the girl from Antwerp, studying in Ghent and proud of it, always ready for a beer or fries (or both). You made some questionable decisions, like joining the 'AB', but we still had a lot of fun and I think I'm ready to forgive your mistakes! Willem, by flooding our fume hood during organic chemistry practicals when I turned my back for 2 seconds to weigh something. Maybe it's for the best that you became a civil engineer, your practical chemistry skills left something to be desired. Sander, the way we met may have been unconventional, and maybe it was just as good the second time around. They say that first impressions are crucial. I don't think mine was very good, but I think that says more about you than me. Finally, Simon, I cherish our time at 'de Wase', ordering a few 'meters' and waking up refreshed the next day to play some Call of Duty. Maybe not the healthiest, but some of the best nights I have had in Ghent.

Foemp and Kiri, two of my oldest and dearest friends. I have known you since I was 3 years old and somehow we have managed to stay friends for a quarter of a century. We've had some crazy times together in the 'Chiro' that I wouldn't change for the world. I still remember 'leefweek' when I could barely keep my eyes open in class and it was only Wednesday. And then instead of taking it a bit slower we typically accelerated because the weekend was coming up. We don't see each other as much as we used to, but whenever I have something, I know you'll be there. I would like to thank you both for your continued support over the years and I hope there are many more to come!

To my new 'Swiss' friends Moritz, Stefano, Mareike, Raffaele, Marco, Susanne and Ricco. Thanks for the nice evenings we spent together, whether it was playing board games or making panzarotti, it was always very enjoyable. I would especially like to thank Camille for all her help during the first year of my PhD.

Last but not least, to my girlfriend Miranda, I cannot express my gratitude enough for everything you have done for me over the last years. You have made my transition to Switzerland so much easier and more enjoyable. Without you this thesis would be nowhere close the document it is today. So with this I grant you an honorary doctor title for tolerating me for the last few years, I know it hasn't always been easy, but I know we will ace everything together no matter what comes up.

With this my acknowledgements come to an end. Again thanks to everyone who has been a part of my PhD, without you it would not have been the same. Now nothing remains but saying goodbye to my PhD and welcoming the new challenge life throws at me.

Bazel, 3rd of August 2023
Dietger Van den Eynden

Contents

List of Acronyms

A

ACN	Acetonitrile
AIBN	Azobisisobutyronitrile
ATR	Attenuated Total Reflection

B

BADGE	Bisphenol A Diglycidyl Ether
BPO	Benzoyl Peroxide

C

CAN	Covalent Adaptable Network
CDCl$_3$	Deuteriated Chloroform
CD$_3$OD	Deuteriated Methanol
CN	Coordination Number
COPASI	Complex Pathway Simulator
CT	Computed Tomography

D

DBU	1,8-Diazabicyclo[5.4.0]undec-7-ene
DCM	Dichloromethane
DLS	Dynamic Light Scattering
DMA	Dynamic Mechanical Analysis
DMF	Dimethylformamide
DOSY	Diffusion Ordered Spectroscopy
DSC	Differential Scanning Calorimetry
DW	Debye-Waller

E

ESI	Electron Spray Ionisation
EtOAc	Ethyl Acetate
EXAFS	Extended X-ray Absorption Fine Structure

F

FT–IR	Fourier Transform – Infrared
FWHM	Full Width at Half Maximum

G

GPC	Gel Permeation Chromatography

H

HR	High Resolution

I

IR	Infrared

M

MMA	Methyl Methacrylate
mCPBA	meta-Chloroperoxybenzoic Acid
MeOH	Methanol
MOF	Metal Organic Framework
MS	Mass Spectroscopy

N

nm	Nanometer
NMR	Nuclear Magnetic Resonance
NP	Nanoparticle

P

PD	Polydispersity
PDF	Pair Distibution Function

R

ROP	Ring-Opening Polymerization
r_w	Goodness of Fit

S

SEC   Size Exclusion Chromotography

T

TAD   Triazolinediones
TEM   Transmission Electron Microscopy
TFA   Trifluoroacetic acid
TGA   Thermogravimetric Analysis
T_g Glass Transition Temperature
THF   Tetrahydrofuran
T_m Melting Temperature
TOPO   Trioctylphosphine Oxide
$t_{1/2}$ Half Life Time

X

XRD   X-Ray Diffraction

Z

Zr_{12} Dimeric $[Zr_6O_4(OH)_4(OOCR)_{12}]_2$ Cluster
Zr_6 Monomeric $Zr_6O_4(OH)_4(OOCR)_{12}$ Cluster

1

Introduction

1.1 It's a fascinating universe

The Oxford dictionary defines the word curious as 'having a strong desire to know about something' or 'strange and unusual'.[a] This curiosity has motivated scientist throughout history to investigate phenomena observed around us. One fascinating example, albeit not well-known, is the size distribution of stellar objects. Plotting the frequency of objects with a certain mass against their actual mass gives a mass function. Although these objects exhibit a vast range of masses, low mass objects are substantially more prevalent. This observation is nothing spectacular on its own, the real fascinating aspect is when this mass function is fitted with a power law (See Equation 1.1). It was found that the exponent of this is fit is consistently approximately equal to -2, regardless of whether the mass distribution ranks only the masses of stars or a combination of different objects (such as galaxies, planets, and stars). This observation was first documented by Salpeter E. in 1955, for his fit he obtained -2.35 as value for a.[1]

---

[a] Oxford University Press, 2022, Curious (adj.), Oxford English Dictionary, viewed 10 June 2023, https://www.oxfordlearnersdictionaries.com/definition/english/curious

$$\phi(m) = K.m^a \qquad (1.1)$$

Inspired by this work, Kautsh *et al.* studied whether this phenomenon was also applicable on more common objects.[2] As an example they chose to plot and fit the size distribution of a Lego™ set and found that also here the exponent was approximately -2 (-2.13). The Youtube channel 'Physics for the birds' pointed out that while this study appeared to confirm the universal law, their study only entails 1 Lego set which is not statistically relevant. To increase the study population, the author wrote a Python script to allow for automatic scanning and analysis of different Lego sets. His findings further supported the theory, all of his exponentials are approximately -2.

I believe that both definitions of the word curious are interconnected. This thesis is no different, it is a result of my curious nature. Despite our well-defined goals and calculated hypothesis, the chemistry behind our system consistently produced unusual and unexpected results. These outcomes, however, stimulated my curiosity and encouraged me to comprehend our research more deeply. Because of this, I like to believe that this thesis is a product of my curious nature, trying to understand and control metal oxo clusters while overcoming the challenges I encountered.

1.2   The world through a magnifying glass

Studying natural phenomena has lead scientist to document their findings. This is reflected in Naturalis Historia, a collection of books written by Pliny the elder back in AD 77.[3] Besides being the largest scientific work to have survived from the Roman Empire, it covers a wide range of topics, including science, medicine and fine arts. Although not always understood, phenomena such as magnetism are already described in these books. Over the following centuries, science has continuously acquired knowledge in both fundamental understanding and control of synthesising innovating materials. While bulk materials were being developed, nanomaterials remained unnoticed until this point.
We jump now to the year 1959, where Richard Feynman gave a lecture at CallTech titled: There's plenty of room at the bottom.[4] Here, he encouraged scientists to push the limits of material science to create increasingly smaller materials, ultimately aiming to achieve atomic-level control. This would enable synthesis of innovative materials with unrivalled control and quality. He recognised that as technology advances, so should our understanding and control of material synthesis. The time leap from this point onwards is considerably shorter, taking only 25 years for the nanoparticle

field to gain significant momentum. Since then numerous nanoparticles have been reported in literature, with moderate control over size, shape and composition.[5] Although there are many nanoparticles available, those outside the scientific community often poorly understand the prefix 'nano'. From this one could ask 2 questions. First of all, 'What exactly is a nanoparticle/nanocrystal?' and secondly, 'Why would anyone want to use them?
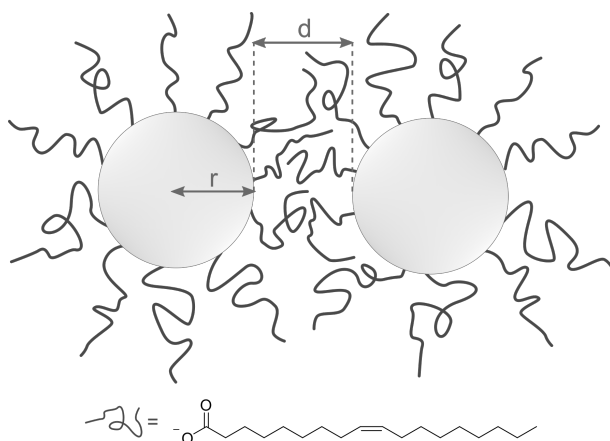
Figure 1.1: Concept of sterical stabilization in nanoparticles. With r being the radius of the nanoparticles and d the distance between both. The sterical repulsion will avoid agglomeration between both particles. Oleic acid (chemical structure) is shown as a prototypical ligand in nanoparticle chemistry.

Let us tackle the first question. Generally, when people talk about nanoparticles or nanocrystals they indicate objects that are smaller than 100 nm (10^{-7} m). The distinction between a nanoparticle and a nanocrystal is merely whether the core is amorphous or crystalline respectively. From here on, I will only refer to them as nanoparticle for simplicity. In order to avoid agglomeration of these nano-sized objects people have stabilized them in 2 ways. They can either be electrostatically stabilized, where agglomeration is avoided based on the electrostatic repulsion between charged (positive or negative) particles. This type of stabilization will not be further discussed in this thesis. A more common way to stabilize nanoparticles is steric stabilization. Here, the surface of the particles is decorated with a ligand shell typically consisting of long and flexible organic molecules, creating a hybrid object. The inorganic, solid core of the particle defines the physical properties of these materials such as e.g. luminescence. The organic ligand shell on the other hand, dictates the chemical properties of the system

(e.g. solubility) and additionally avoids agglomeration. Upon collision of 2 nanoparticles the ligand shell will deform. When two nanoparticles collide, their ligand shells deform. If the nanoparticles continue to approach each other, the steric repulsion between their ligand shells increases. Eventually, this steric repulsing will cause the particles to separate, without agglomeration, and thus retaining their size in the nanometer range. (See Figure 1.1)

As 1 nm equals 10^{-9} m these materials are miniature versions of their bulk counterpart and require advanced techniques to be studied. Which is most likely the reason why they only gained momentum in the 1990s. It is not always easy to imagine just how small these materials actually are. A rule of thumb that may be helpful is that the size ratio between a nanoparticle and a football is the same as the ratio between a football and the earth. Figure 1.2 illustrates the size comparison between nanomaterials and common everyday objects.
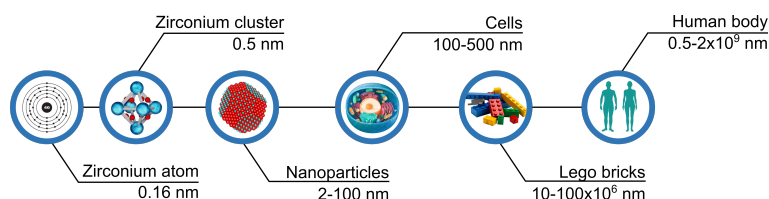
Figure 1.2: Comparison of nanometer sized object versus common objects with macroscopic dimensions. Ranging from a single atoms, to a collection of a finite amount of atoms (clusters and nanoparticles) to bulk materials/objects.

The second question can be answered by looking at some of their applications. Quantum dots, for example, have a tunable band gap based on their size, typically 2-10 nm, and have been successfully applied in Samsung's™ Q-LED televisions.[6] Nanoparticles display a very high surface to volume ratio due to their small size, making them a very attractive candidate for more sustainable and improved catalysts. Depending on the material used, they can also be used as CT contrast agents in medical and engineering applications.[7] Finally, due to their finite size, they can easily be incorporated in polymer resins, combining the versatility of polymers with the high-end properties of nanoparticles. For the above mentioned reasons, people worldwide have taken interest in these fascinating materials. A great deal of research has been carried out into the formation mechanism of these materials. More recently, the field has realised that the surface chemistry is

of paramount importance for most applications and has therefore received more attention.

However, nanoparticle synthesis still poses significant challenges in terms of size control and doping. Because of this these topics are heavily studied by many scientists. Nanoparticles exhibit a size distribution, the most narrow size distribution is approximately 5%, indicating that a particle synthesised with an average size of 5 nm will range in size from 4.75 nm to 5.25 nm. The process of doping nanoparticles is yet to be fully understood, and the amount of dopant is often determined post-synthesis, as it is not always correlated with the initial amount of dopant used before synthesis. Further development in this field could lead to the discovery of new materials that enhance existing processes, which could address some of the major global challenges such as climate change and overpopulation.
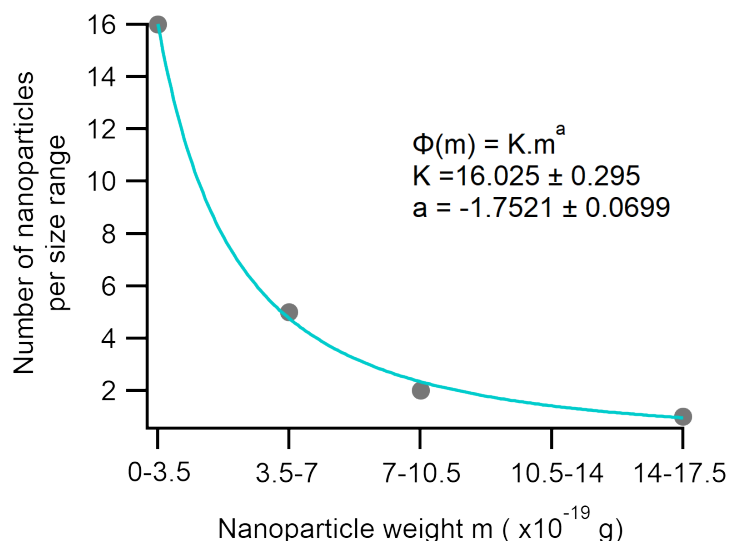
Figure 1.3: Weight distribution curve of group 4 metal oxo nanoparticles synthesised via both the Trioctyl phosphine oxide (TOPO) synthesis and benzyl alcohol (BnOH) synthesis. The fit shows an exponent of -1.75 which is reasonably close to the -2 found for stellar objects.

Out of curiosity, I tested how the weight distribution (see section 1.1) of nanoparticles looks like and see if also here an exponent of -2 is observed. For this purpose, I computed the weight of group 4 metal (Ti, Zr and Hf) oxo nanoparticles synthesised via both benzylalcohol (BnOH) and tri-octylphosphine oxide (TOPO) synthesis, of various sizes, see equation A.1-

A.4.[8] These masses are binned according to their mass and the amount of particles found in each bin is plotted as a function of this bin size. (See Figure 1.3) Surprisingly, even though the sampling population is very small, the same trend is observed. The exponent is -1.75, which is reasonably close given the assumptions made to determine the particle weight. (Homogeneous size and perfect spheres) This law seems to apply to other systems outside stellar objects and Lego, how curiously fascinating!

Understanding now the concept of nanoparticles, we are equipped to read the remainder of this thesis. The aim of this work is to understand and control a dormant type of nanomaterial, specifically metal oxo clusters. Despite being reported in various compositions in the nineties, they received little attention thereafter. This is likely because the most common characterization technique used was single crystal XRD, which requires the scientist to go through the tedious and time-consuming process of growing high-quality crystals. In addition, the formation mechanism of these materials was studied as it was mainly speculation up until now. Finally, after optimizing the synthetic route and elucidating the formation mechanism, this knowledge was used to create versatile and tunable building blocks from the metal oxo clusters. Throughout this dissertation we will follow the story of an underdeveloped yet promising material into a well-understood and controlled building block for material science.

1.3   State of the art

Clusters exist in a various sizes and compositions. Cluster have been reported for a significant portion of the periodic table of elements.[8–10] They can be divided into different types, such as metal clusters, lanthanide clusters, semiconductor clusters and metal oxo clusters. Generally, they consist of an inorganic core (< 100 atoms) capped with an organic ligand layer similar to their bigger counterparts nanoparticles (> 1000 atoms) mentioned earlier. Unlike nanoparticles, the clusters are atomically precise. Meaning that the exact number of atoms in the core is known, which reduces the polydispersity to zero. The latter makes them ideal building blocks for high-end applications, as each building blocks is identical. To make an analogy with the real world, nanoparticles can be compared with Duplo™ as small and valuable building blocks however, they are rather robust. In contrast, the atomically precise cluster can be compared to Lego. As they have a precise composition and are even smaller, allowing for more detailed constructs.

Here we will focus on group 4 metal oxo clusters. While properties such as surface chemistry, ligand exchanges, binding affinities, nucleation mechanisms and synthetic pathways have been extensively studied for group 4 metal oxo nanoparticles, they are often lacking or incomplete for clusters. Therefore, clusters are a vast area that can and should be further explored. Despite this knowledge gap clusters are found in a multitude of applications. (*vide infra*)

1.3.1   Group 4 metal oxo clusters

In group 4, titanium, zirconium and hafnium oxo clusters have been reported. Here, we define oxo clusters as an arrangement of a finite number of metal atoms connected by oxo bridges. A prototypical example for both zirconium and hafnium is the octahedron with the chemical composition: $M_6O_4(OH)_4(OOCR)_{12}$. Titanium on the other hand, forms ring-shaped structures with 8 metal atoms, $Ti_8O_8(OOCR)_{16}$. As their surface is covered by ligands, such clusters can be considered as the smallest possible nanoparticle, with the added advantage that they are atomically precise (polydispersity = 0 %). They can be crystallized and their structure determined via single crystal XRD. Although many mixed oxoalkoxy clusters exist, such (carboxylate-capped) clusters have already been extensively reviewed.[11–14] In addition, there are oxoalkoxy cluster with phosphonate and phosphinate ligands.[13;15] However, oxoalkoxy compounds are not stable to atmospheric water. Clusters with different nuclearities have been reported for all 3 elements, **Ti**$_{2-44}$, **Zr**$_{3-26}$ & **Hf**$_{4-17}$. A limited amount of group 4 mixed metal clusters e.g. TiZr, TiHf & TiZrHf clusters have also been reported in literature however, their structural configuration differs from the previously mentioned octahedron and these structures are generally not fully condensed. In this work we focus on fully condensed (= no alkoxy ligands) oxo clusters with carboxylate ligands synthesised by non-aqueous methods, as these are the most representative models for oxide nanoparticles. A comprehensive overview of clusters synthesised from water (e.g., capped with sulfate ligands) can be found elsewhere.[14]

These clusters are readily obtained by reaction between a metal alkoxide and excess carboxylic acid. For titanium, elevated temperatures are typically used, whereas zirconium and hafnium clusters can be synthesised at room temperature.[16;19] How they are formed is still largely unknown. One generally accepted observation is that the oxo bridges on the cluster core are formed by an *in situ* esterification reaction between alkoxides and carboxylic acids. This reaction forms M-OH functionalities which can further condense to form M-O-M bridges. Alternatively, esterification between free
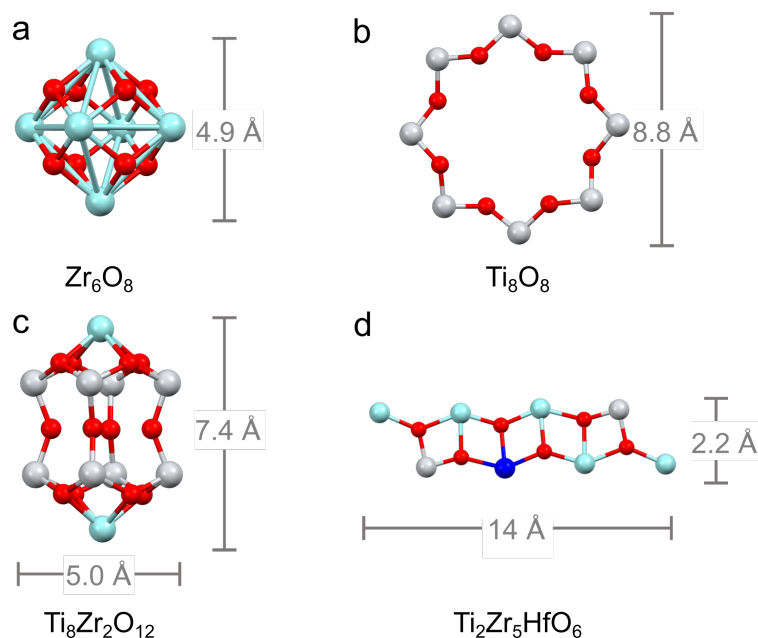
Figure 1.4: Overview of reported group 4 metal oxo clusters. For simplicity only their cores (without H) are displayed with their respective size in Å. The atoms are colored based on atom type, O in red, Ti in grey, Zr in blue and Hf in dark blue. (a) The mono-metallic octahedron shaped Zr (and Hf) metal oxo clusters, (b) shows the mono-metallic Ti oxo clusters. [16] (c) and (d) show 2 examples of crystallized mixed metal clusters. [17;18]

alcohol and carboxylic acid produces water which in turn can hydrolyse the metal centers. For zirconium clusters, there is one study that postulates a **Zr$_3$**-species as a reaction intermediate. [20] Attempts to add small amounts of water to control cluster formation have tended to be less reproducible. [21] It should not come as a surprise that titanium forms clusters with a different shape compared to zirconium and hafnium. Zirconium and hafnium are referred to as twin metals due to the lanthanide contraction. As a result, many properties are almost identical, including ionic radii (Zr^{4+} = 84 pm, Hf^{4+} = 83 pm) [22] and Pauling electronegativity (Zr = 1.33, Hf = 1.3). [23] This ultimately results in the formation of isostructural clusters of zirconium and hafnium. On the other hand, Ti^{4+} has a smaller ionic radius of 74 pm and has a higher Pauling electronegativity (= 1.54). [22;23] Titanium is smaller in size, has a maximum coordination number of 6, whereas zirconium and hafnium have a maximum coordination number of 8. [8] Due to its different reactivity and shape, titanium clusters will be omitted and only zirconium

and hafnium clusters will be studied.

1.3.2   Zirconium and hafnium clusters
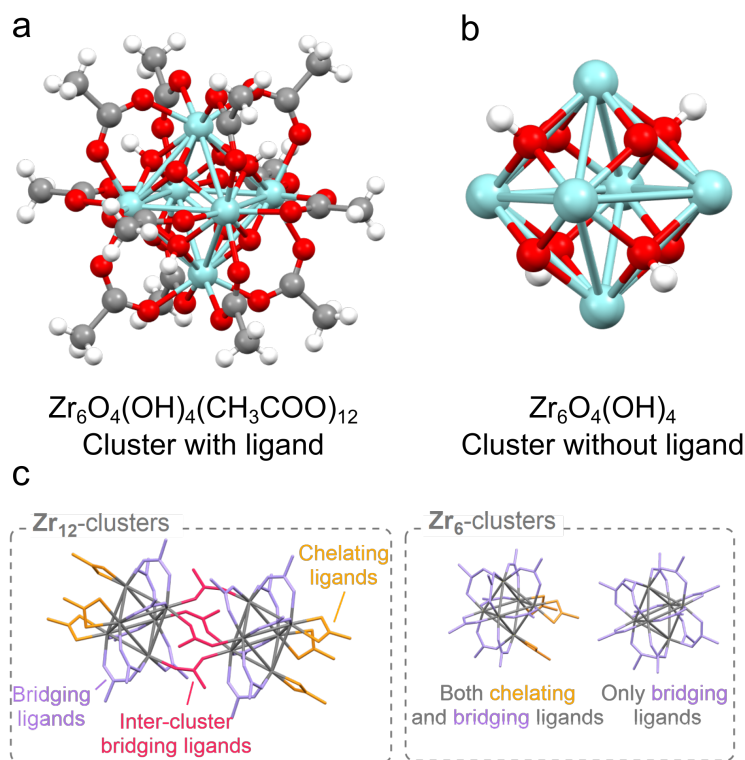
Figure 1.5: (a) The prototypical structure of an octahedron shaped Zr oxo cluster with ligands and (b) the core alone. Hafnium clusters display the same octahedron structure. (c) The different binding modes of the ligands for the dimeric **Zr$_{12}$** clusters (left) and the for the monomeric **Zr$_6$** clusters. (right)

As previously stated, the reaction between $Zr(OPr)_4$ or $Hf(OBu)_4$ with excess carboxylic acid, results in the formation of octahedron shaped clusters at room temperature in quantitative yields. Metal atoms are localized at each corner of the octahedron cluster, and are connected by μ_3-oxygen bridges across all 8 triangular planes. Of the 8 oxygen atoms present in the cluster core, 4 have an additional proton to achieve charge neutrality. (See Figure 1.5a-b) The core of the clusters carries a total charge of 12^+, which is balanced by 12 negatively charged carboxylates. The longest Zr−Zr dis-

tance in the octahedral cluster is 0.5 nm. All metal atoms exhibit an 8-fold coordination, and the metal-oxygen arrangement closely resembles that of bulk, cubic zirconia/hafnia.

The general chemical formula for one octahedron is $M_6O_4(OH)_4(RCOO)_{12}$ or $\mathbf{M_6}$ for short, and these structures are referred to as monomeric clusters. These monomers have either both chelating ligands (ligands attached to 1 metal atom) and bridging ligands (ligands attached to 2 metal atoms) or only bridging ligands. (See Figure 1.5c) For some ligands the clusters dimerise, henceforth referred to as dimers. Here, 4 ligands exhibit a bridging confirmation between 2 octahedrons. The remaining ligands adopt either bridging or chelating binding modes. The overall chemical formula is simply the double of the monomeric structure and is written as $[M_6O_4(OH)_4(OOCR)_{12}]_2$, hereafter noted as $\mathbf{M_{12}}$.

Although it has never been explicitly stated by others, it appears that the monomer forms when the ligand is sterically imposed on the α-position of the carboxylic acid. In cases where there is no sterical hindrance, the dimer is always obtained. These carboxylate ligands are flexible and can be exchanged for other carboxylic acid via exchange reactions similar to nanoparticle ligand exchange. The dimer does not convert into the monomer after ligand exchange at room temperature.[24] Ligand exchanges where the binding group of the ligand is varied has not yet been investigated. In addition to the 12 carboxylate ligands, other hydrogen-bonded carboxylic acids can be found in the crystal structure database.

1.3.3   Polymeric nanocomposites

Nanocomposites are hybrid materials consisting of a polymer resin in which objects are embedded that are, at least in 1 dimension, smaller than 100 nm.[25] The design of synthetic nanocomposites draws inspiration from natural composites, such as nacre, which exhibit outstanding mechanical properties.[26;27] In addition to nanosheets and tubes, inorganic nanoparticles have gained popularity due to their high surface to volume ratio.[28–31] Three main approaches for synthesising nanocomposites.

1. Mixing as-synthesised nanoparticles and polymers

2. *In situ* nanoparticles synthesis inside a polymer matrix

3. Mixing nanoparticles with monomers and subsequent polymerisation

The first approach, which involves mechanical force to ensure proper mixing, is popular due to its simplicity and has been proven successful for

Al_2O_3 nanoparticles.[32] The second method has been employed for Au & Pd,[33] SiO_2[34] and TiO_2[35] nanoparticles. In this approach, the precursors are mixed with the polymer and the resulting nanoparticles are instantly surface functionalised by the polymer. Neither of these approaches are easily applicable to other types of nanoparticles, because specific conditions are needed in order to achieve homogeneous nanocomposites.[36] The third approach is the most flexible one in terms of tunability. The colloidal stability of nanoparticles relies greatly on the ligand shell, as previously elaborated. Adjusting the ligand shell allows for maximizing the enthalpic compatibility between the nanoparticles and the monomers.[31;37] By doing so, the probability of agglomeration, a common issue in nanocomposite synthesis, can be minimized.[38] Moreover, this allows for surface functionalisation with reactive ligands such as epoxides[39], methacrylates[40] or click chemistry groups[41] allowing the nanoparticles to react with the polymer resin. Incorporation of these inorganic nanoparticles generally enhances material properties, such as mechanical or electrical characteristics.

Polymers are typically divided in two classes.[42] On one hand, there are thermoplastics, which are non cross-linked materials which allow for reprocessing but usually display poor mechanical strength. Plexiglass is an example of a thermoplastic material.[43] Thermosets on the other hand, are fully crosslinked polymer networks. They display excellent mechanical properties but cannot be reprocessed, one of the first ever thermosets was bakelite.[44] Recently, a new and exciting type of polymers emerged, bridging the gap between thermoplastics and thermosets, which are called covalent adaptable networks (CANs).[45] The cross-links in these materials can be activated to become reversible. Thus, in the absence of activation (heat or UV) these materials behave as fully cross-linked thermosets. However, upon activation the cross-links become reversible and the material acts as a thermoplastic allowing the material to be recycled.

Since their discovery, a vast amount of chemistry's has been explored and 2 distinctive cases of CANs were assigned.[46] The reversible cross-links can react through either a dissociative or an associative mechanism. The latter is a special case and are known as vitrimers, in these materials the amount of cross-links is constant at any time. (See Figure 1.6) Some examples of reversible chemistry's include transesterification, transamination and transalkylation.[46–50]

One of the most interesting properties of covalent adaptable networks is their ability to relax stress by rearranging their internal structure, through the reversible cross-links. This stress relaxation behaviour is studied using rheology.[51] During such an experiment, the sample is heated to a certain temperature after which a constant deformation is applied, causing stress on

the sample. Then the relaxation modulus (G), which is defined as the stress normalised to the deformation, is studied over time. The stress relaxation is often described using the Maxwell model. (See Equation 1.2) In this equation τ indicates the relaxation time and can be defined as the time the sample needs in order to reach 37% (1/e) of it's original relaxation modulus.

$$\frac{G}{G_0} = e^{\left(\frac{-t}{\tau}\right)} \tag{1.2}$$

In order to increase the mechanical properties several nanocomposites were synthesised using a covalent adaptable network as polymer resin. The addition koalin clay or Al_2O_3 to a PDMS (polydimethylsiloxane) based vitrimer increased the mechanical properties of these materials.[52] Similar results were found for SiO_2 particles functionalised with either epoxide[53] or amidoxime[54] functionalities. Finally, amine functionalised carbon dots were applied to form cross-linked materials through the imine formation with polydextran aldehyde (PDA).[55] The latter, more mechanically robust materials, could be 3D-printed demonstrating their applicability.
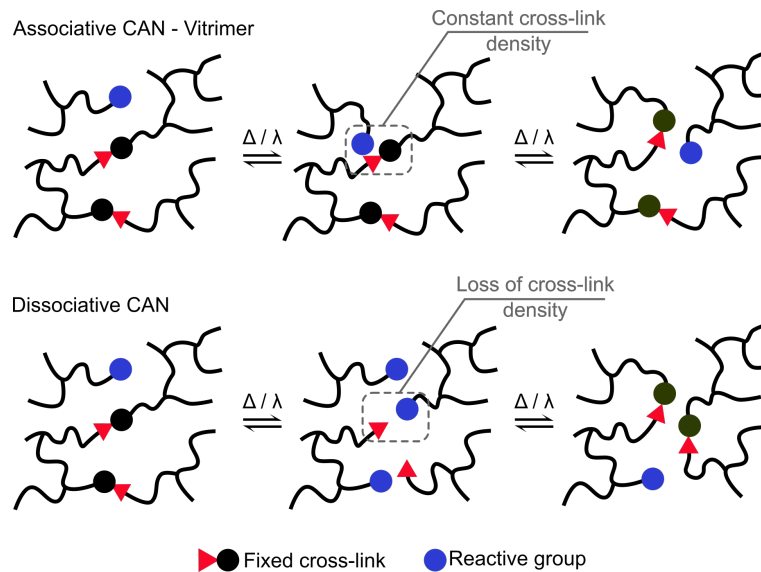

Figure 1.6: Overview of both associative (top) and dissociative (bottom) covalent adaptable networks. An associative covalent adaptable network is also called a vitrimer and maintain its network integrity upon activation contrary to a dissociative CAN.

1.3.4 Group 4 clusters as inorganic monomers

Similar to the nanocomposites above, group 4 metal oxo clusters have been embedded in polymer resins. $\mathbf{Zr_6}$-methacrylate clusters have 12 methacrylate ligands, each with a polymerisable double bond. Schubert *et al.* used these clusters as cross-linkers during the radical polymerisation of methylmethacrylate or styrene.[56–58] While cluster fractions of 0.5-1 mol% (equivalent to 3.2-6.3 w%) yield glassy, transparent polymers, 2 mol% or 100 mol% (no monomer added) yield a white solid. In contrast to undoped polymer, the cluster-polymer composites were insoluble. They only swell in solvent, the extent of which decreases with increasing cluster concentration (= increasing cross-linking density). The composites also have a higher thermal stability because thermal depolymerisation is inhibited. Improved performance was achieved by using $\mathbf{Zr_4}$-methacrylate clusters and incorporation in polymer composites.[59–61] These cluster reacts similarly and can achieve an even higher cross-linking density, possibly due to its more open structure.[57;62;63] polymerisation with 10 w% of $\mathbf{Zr_4}$-methacrylate, results in a improved bend strength (47 MPa) and improved bend modulus (1900 MPa). The composite retains its strength even after 7 days storage in water. In general, there are two effects in such composites: cross-linking and inert filler effect.[64] The higher cross-linking ability causes the decrease in the swellability and the increase in glass transition temperature. The filler effect delays the thermal degradation. Oxo clusters also improved the mechanical properties of shape memory materials without compromising the shape memory effect itself.[65] Next to the mechanical properties, also the (di)electrical properties (conductivity, dielectric constant, etc) are influenced by the inclusion of oxo clusters.[66]

The $\mathbf{Zr_4}$-methacrylate cluster has also been used in a photopolymerisation process with methylmethacrylate monomer to produce hard and transparent coatings.[67] Depending on the type of carboxylic acid, the clusters can also be used in other types of polymerisation reactions. $\mathbf{Zr_6}$ clusters capped with 5-norbornene-2-carboxylic acid were used as cross-linkers in ring opening metathesis polymerisations.[68] $\mathbf{Zr_{12}}$ clusters capped with 3-mercaptopropionic acid were embedded in polymethylmethacrylate using a photothiol-ene polymerisation.[69;70] The cluster-reinforced polymer featured improved hardness. The above composite materials fit in a wider class of cluster-reinforced polymers featuring also titanium, tin, silicon, and tungsten oxo clusters.[21;71;72] The effect of oxo clusters on the structural and functional properties of these organic-inorganic composites has been reviewed in detail elsewhere.[73]
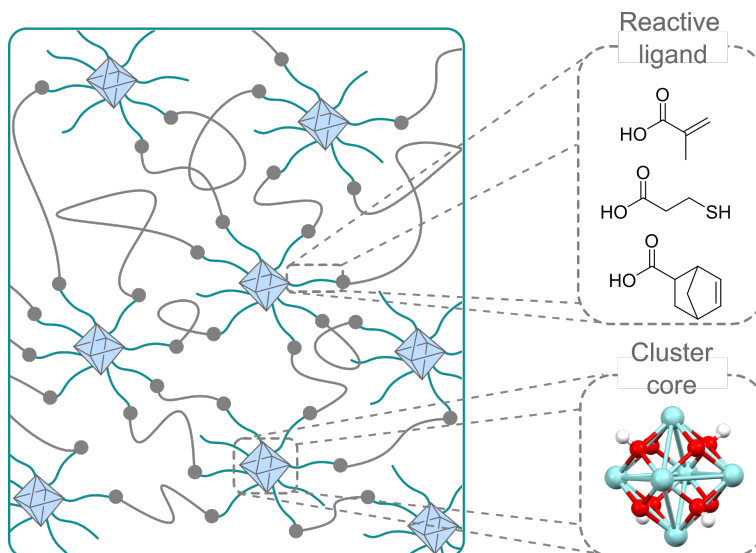
Figure 1.7: Schematic overview of the polymerisation using clusters as cross-linkers. On the right, the reported ligands from literature are depicted. For simplicity not all ligands are represented on the cluster core.

Going one step further, $\mathbf{Zr}_4$ or $\mathbf{Hf}_4$-methacrylate clusters were co-polymerised with (hydrolyzed) methacryloxymethyl-triethoxysilane and subsequently calcined at 800 - 1000 °C.[74;75] The resulting all-inorganic composites consisted of silica and ZrO_2 or HfO_2 nanoparticles. A fraction of the nanoparticles was crystalline but the majority was amorphous. By combining both $\mathbf{Zr}_4$ and $\mathbf{Hf}_4$-methacrylate clusters, the ternary system ZrO_2-HfO_2-SiO_2 was achieved.[76] This strategy of using composite precursors has been thoroughly reviewed elsewhere.[77]

Different polymerisation reactions have been studied as well. By synthesising mercaptopropionate-capped clusters, they could be reacted with trifunctional alkene and thiol monomers to obtain polymers. Recently, it has been shown that this click chemistry can be exploited in lithographic applications. They show that polymerizing the clusters can be achieved in both ways by surface functionalisation with either thiols or alkene and reacting with the respective monomer.[69] Ring opening polymerisations (ROP) of $\mathbf{Zr}_6$ clusters has been studied as well. The clusters were synthesised using 5-norbornene-2-carboxylate followed by subsequent polymerisation via reaction with Grubs catalyst in dichloromethane (DCM), with or without additional norbornene monomer. The reaction was rapidly completed within 1 h and was confirmed via Gel Permeation Chromatography (GPC).[68]

1.3.5 Further applications

Zirconium and hafnium oxo clusters have received increasing attention as building block for extreme UV patterning, and 3D printing.[78;79] The principle is similar to that of the composites, but here the photo-sensitivity of the methacrylate ligands is used to cross-link the cluster and thus change their solubility. The resolution of the laser determines the resolution of the final pattern or even 3D structure.

Zr$_6$-methacrylate and **Zr**$_{12}$-vinylacetate clusters have been used to activate hydrogen peroxide.[80] Under these oxidative conditions, Zr-peroxo complexes are formed, which act as catalysts for the oxidation of methyl p-tolyl sulfide to its corresponding sulfoxide and sulfone. This is a model reaction for the oxidative desulfurization of fuels. On the other hand, $Hf_{18}O_{10}(OH)_{26}(SO_4)_{13} \cdot (H_2O)_{33}$ clusters have been used as heterogeneous catalyst for the selective hydrolysis of proteins.[81]

Finally, group 4 metal oxo clusters have been extensively studied for their use as the inorganic nodes in Metal Organic Frameworks (MOFs). In 2008, the **Zr**$_6$ cluster was first used as building block to create MOFs (UiO-66 and UiO-67) by direct reaction between an aromatic dicarboxylic acid and $ZrCl_4$ in DMF (120 °C, 24 hours).[82] Such MOFs had an exceptionally high thermal stability (540 °C) and are stable in water, DMF, benzene and acetone. Dehydroxylation of the cluster core starts at 250 °C and is completed at 300 °C.[82] Two of the four -OH bridges leave the structure with an additional proton, yielding a Zr_6O_6 cluster core with a Lewis acidic seven-coordinated zirconium. Although the cluster structure is changed considerably, this process maintains the overall integrity of the MOF and is reversible.[82] The incorporation of trifluoroacetate during the synthesis and its subsequent thermal removal further increases the Lewis acidity of UiO-66, as evidenced by the enhanced cyclization rate of citronellal to isopulegol.[83] Zr-MOFs are also catalytically active towards peptide bond hydrolysis, thus acting as artificial proteases.[84;85] Many other zirconium MOFs have been developed in the last two decades and are reviewed elsewhere.[86;87] Also hafnium based MOFs are known, which are often isoreticular with the zirconium MOFs.[88–91]

In 2010, the **Zr**$_6$-methacrylic cluster was used as a well-defined precursor for UiO-66.[92] The reaction conditions were mild (120 °C, 24 hours), but the MOF crystal size was smaller compared to the direct synthesis method from $ZrCl_4$. More interestingly, the direct synthesis of a MOF from $ZrCl_4$ and trans,trans muconic acid failed, while a nanocrystalline MOF (isostructural to UiO-66) was obtained with the **Zr**$_6$-methacrylic cluster, even at room temperature. In another example, the **Zr**$_{12}$-acetate cluster was used as precursor and, depending on the linker, the dimeric nature of

the cluster was retained in the final MOF.[93] Mixed metal clusters have also been used as precursors for MOFs.[18;87] Recently, several MOFs have been synthesised at room temperature by mechanochemical synthesis from the $\mathbf{Zr}_6$-methacrylate cluster or the $\mathbf{Zr}_{12}$-acetate cluster.[94;95] In this way, the highest quality UiO-97 was obtained, with a surface area of 2250 m^2/g, and excellent catalytic activity in the hydrolysis of dimethyl 4-nitrophenyl phosphate (a nerve agent).[94] Multimetallic MOFs have recently been produced via mechanochemical synthesis by combining $\mathbf{Zr}_{12}$-acetate and $\mathbf{Hf}_{12}$-acetate clusters with bridging ligands.[91] The above results suggest that the zirconium and hafnium oxo clusters remain intact during MOF synthesis.

1.4 Outline

Based on the possible applications, these clusters are definitely worth studying. This thesis follows the story of how an underdeveloped field was further unraveled, by carefully studying the synthesis and formation mechanism before moving towards application. In order to avoid questioning the reliability of the synthetic methods, paving the way for future research on these fascinating materials. Allowing for further developing these clusters in applications such as catalysis and aerogels. Furthermore, it is hoped that the mechanistic insights can aid the search for novel clusters with different metals.

Chapter two generalises the synthesis and extends the ligand library to longer carboxylates. The newly developed toolbox allows for structure determination without the need for crystallization, which was not possible until now. The inorganic core was studied with Pair Distribution Function (PDF) and High Resolution Mass Spectroscopy (HRMS). The organic ligand shell was studied using Fourier Transform InfraRed (FTIR), Nuclear Magnetic Resonance (NMR) and Thermogravimetric Analyis (TGA). It was also shown that the dimer and monomer can be converted into each other under the right conditions. Furthermore, the findings for zirconium could be generalized to hafnium. Finally, it was shown that the clusters outperform nanoparticles as catalysts in esterification reactions due to their maximized surface to volume ratio.

In the third chapter the reaction mechanism is elucidated. Here the cluster formation is studied via *in situ* synchrotron EXAFS measurements. Initially, the interaction between the metal alkoxide and carboxylic acid were studied to identify the real precursor. A $\mathbf{Zr}_3$ species was identified as an intermediate towards the octahedron formation. In addition, the effect of different reaction conditions on the ester formation reaction is investigated

by NMR. Combining our data allowed us to propose a more detailed reaction mechanism, from precursor to octahedron. Finally, we showed that the cluster synthesis can also be performed in EtOAc excluding the toxic DCM as reaction solvent.

In chapter four the clusters are investigated as inorganic monomers. Here we study the effect of different parameters on the polymerisation of (meth-)acrylate capped clusters using methyl methacrylate as co-monomer. The knowledge gained in chapter 2 allows us to prepare clusters with mixed ligand shells. We found that clusters capped with either oleic or linoleic acid could not be polymerised under our current conditions, in contrast to clusters functionalised with 10-undecenoic acid. Mixed acrylate capped clusters on the other hand, were readily polymerised. We found that the T_g does not change considerably despite a large variety in sample composition.

As a final part of this thesis the clusters are studied as inorganic monomers in covalent adaptable networks. 10-undecenoic acid and oleic acid were epoxidized using mCPBA. Afterwards, the clusters are functionalised with this custom-made ligand in different ratios. In order to synthesise a polymer network, these different clusters are reacted with multi-functional carboxylic acid species (Pripol 1040) and a difunctional epoxy molecule (BADGE), inspired by the first vitrimer reported by Leibler *et al.* back in 2011.[96] We found that these materials are able to effectively relax stress applied to the system. However the exchange mechanism appears to dissociative in nature, which we assigned to a ligand exchange on the cluster core. Finally, it was shown that these clusters improve the mechanical properties of these materials.

References

[1] Salpeter, E. E. The Luminosity Function and Stellar Evolution. *Astrophysical journal* **1955**, *121*, 161.

[2] Kautsch, S. J.; Veras, D.; Hansotia, K. K. The pedagogical representation of mass functions with LEGO and their origin. *European Journal of Physics* **2021**, *42*, 035605.

[3] Whalley, J. I.; Pliny,; Victoria,; Albert, M. *Pliny the Elder, Historia naturalis*; Victoria and Albert Museum London: London, 1982.

[4] Feynman, R. P. There's plenty of room at the bottom. *Resonance* **2011**, *16*, 890–905.

[5] Hens, Z.; De Roo, J. Atomically Precise Nanocrystals. *J. Am. Chem. Soc.* **2020**, *142*, 15627–15637.

[6] Hens, Z.; Moreels, I. Light absorption by colloidal semiconductor quantum dots. *Journal of Materials Chemistry* **2012**, *22*, 10406–10415.

[7] Shilo, M.; Reuveni, T.; Motiei, M.; Popovtzer, R. Nanoparticles as computed tomography contrast agents: current status and future perspectives. *Nanomedicine* **2012**, *7*, 257–269.

[8] Van den Eynden, D.; Pokratath, R.; De Roo, J. Nonaqueous Chemistry of Group 4 Oxo Clusters and Colloidal Metal Oxide Nanocrystals. *Chem Rev* **2022**, *122*, 10538–10572.

[9] Chakraborty, I.; Pradeep, T. Atomically Precise Clusters of Noble Metals: Emerging Link between Atoms and Nanoparticles. *Chemical Reviews* **2017**, *117*, 8208–8271.

[10] Schnepf, A. In *Metalloid Clusters*; Dehnen, S., Ed.; Springer International Publishing: Cham, 2017; pp 135–200.

[11] Rozes, L.; Sanchez, C. Titanium Oxo-Clusters: Precursors for a Lego-Like Construction of Nanostructured Hybrid Mater. *Chem. Soc. Rev.* **2011**, *40*, 1006–1030.

[12] Rozes, L.; Steunou, N.; Fornasieri, G.; Sanchez, C. Titanium-Oxo Clusters, Versatile Nanobuilding Blocks for the Design of Advanced Hybrid Mater. *Monatsh. Chem.* **2006**, *137*, 501–528.

[13] Coppens, P.; Chen, Y.; Trzop, E. Crystallography and Properties of Polyoxotitanate Nanoclusters. *Chem. Rev.* **2014**, *114*, 9645–9661.

[14] Zhang, Y.; de Azambuja, F.; Parac-Vogt, T. N. The Forgotten Chemistry of Group(IV) Metals: A Survey on the Synthesis, Structure, and Properties of Discrete Zr(IV), Hf(IV), and Ti(IV) Oxo Clusters. *Coord. Chem. Rev.* **2021**, *438*, 213886.

[15] Guerrero, G.; Mehring, M.; Hubert Mutin, P.; Dahan, F.; Vioux, A. Syntheses and Single-Crystal Structures of Novel Soluble Phosphonato- and Phosphinato-Bridged Titanium Oxo Alkoxides. *J. Chem. Soc., Dalton Trans.* **1999**, *10*, 1537–1538.

[16] Frot, T.; Cochet, S.; Laurent, G.; Sassoye, C.; Popall, M.; Sanchez, C.; Rozes, L. $Ti_8O_8(OOCR)_{16}$, a New Family of Titanium-Oxo Clusters: Potential NBUs for Reticular Chemistry. *Eur. J. Inorg. Chem.* **2010**, *2010*, 5650–5659.

[17] Gross, S.; Kickelbick, G.; Puchberger, M.; Schubert, U. Mono-, Di-, and Trimetallic Methacrylate-Substituted Metal Oxide Clusters Derived from Hafnium Butoxide. *Monatsh. Chem.* **2003**, *134*, 1053–1063.

[18] Yuan, S.; Qin, J.-S.; Xu, H.-Q.; Su, J.; Rossi, D.; Chen, Y.; Zhang, L.; Lollar, C.; Wang, Q.; Jiang, H.-L.; et al., $[Ti_8Zr_2O_{12}(COO)_{16}]$ Cluster: An Ideal Inorganic Building Unit for Photoactive Metal-Organic Frameworks. *ACS Cent. Sci.* **2018**, *4*, 105–111.

[19] Kickelbick, G.; Schubert, U. Oxozirconium Methacrylate Clusters: $Zr_6(OH)_4O_4(OMc)_{12}$ and $Zr_4O_2(OMc)_{12}$ (OMc = Methacrylate). *Ber. Dtsch. Chem. Ges.* **1997**, *130*, 473–478.

[20] Kickelbick, G.; Feth, M. P.; Bertagnolli, H.; Puchberger, M.; Holzinger, D.; Gross, S. Formation of Organically Surface-Modified Metal Oxo Clusters from Carboxylic Acids and Metal Alkoxides: a Mechanistic Study. *J. Chem. Soc., Dalton Trans.* **2002**, *20*, 3892–3898.

[21] Schubert, U. Cluster-Based Inorganic-Organic Hybrid Mater. *Chem. Soc. Rev.* **2011**, *40*, 575–582.

[22] Shannon, R. D. Revised Effective Ionic Radii and Systematic Studies of Interatomic Distances in Halides and Chalcogenides. *Acta Crystallogr.* **1976**, *32*, 751–767.

[23] *Inorganic Chemistry : Principles of Structure and Reactivity*, 4th ed.; Huheey, J., Keiter, E., Keiter, R., Eds.; HarperCollins: New York, 1993; pp 188–189.

[24] Puchberger, M.; Kogler, F. R.; Jupa, M.; Gross, S.; Fric, H.; Kickelbick, G.; Schubert, U. Can the Clusters $Zr_6O_4(OH)_4(OOCR)_{12}$ and $[Zr_6O_4(OH)_4(OOCR)_{12}]_2$ Be Converted into Each Other? *Eur. J. Inorg. Chem.* **2006**, *2006*, 3283–3293.

[25] Fu, S.; Sun, Z.; Huang, P.; Li, Y.; Hu, N. Some basic aspects of polymer nanocomposites: A critical review. *Nano Materials Science* **2019**, *1*, 2–30.

[26] Sun, J.; Bhushan, B. Hierarchical structure and mechanical properties of nacre: a review. *RSC Advances* **2012**, *2*, 7617–7632.

[27] Bechtle, S.; özcoban, H.; Lilleodden, E. T.; Huber, N.; Schreyer, A.; Swain, M. V.; Schneider, G. A. Hierarchical flexural strength of enamel: transition from brittle to damage-tolerant behaviour. *Journal of The Royal Society Interface* **2011**, *9*, 1265–1274.

[28] Albdiry, M. T.; Yousif, B. F.; Ku, H.; Lau, K. T. A critical review on the manufacturing processes in relation to the properties of nanoclay/polymer composites. *Journal of Composite Materials* **2012**, *47*, 1093–1115.

[29] Du, J.; Cheng, H.-M. The Fabrication, Properties, and Uses of Graphene/Polymer Composites. *Macromolecular Chemistry and Physics* **2012**, *213*, 1060–1077.

[30] Rahmat, M.; Hubert, P. Carbon nanotube-polymer interactions in nanocomposites: A review. *Composites Science and Technology* **2011**, *72*, 72–84.

[31] Amanda Dantas de, O.; Cesar Augusto Gonçalves, B. In *Polymer Nanocomposites with Different Types of Nanofiller*; Subbarayan, S., Ed.; IntechOpen: Rijeka, 2018; p Ch. 6.

[32] Ash, B.; Schadler, L.; Siegel, R. Glass transition behavior of alumina/polymethylmethacrylate nanocomposites. *Materials Letters* **2002**, *55*, 83–87.

[33] Mayer, A. B. R. Formation of noble metal nanoparticles within a polymeric matrix: nanoparticle features and overall morphologies. *Materials Science and Engineering: C* **1998**, *6*, 155–166.

[34] Musto, P.; Ragosta, G.; Scarinzi, G.; Mascia, L. Toughness enhancement of polyimides by in situ generation of silica particles. *Polymer* **2004**, *45*, 4265–4274.

[35] Wang, S.; Wang, M.; Lei, Y.; Zhang, L. Anchor effect in poly(styrene maleic anhydride)/TiO_2 nanocomposites. *Journal of Materials Science Letters* **1999**, *18*, 2009–2012.

[36] Chiara, I.; AnnaMaria, P.; Roberto, C.; Maria Lucia, C.; Marinella, S. Colloidal Inorganic Nanocrystal Based Nanocomposites: Functional Materials for Micro and Nanofabrication. *Materials* **2010**, *3*, 1316–1352.

[37] Li, Y.; Krentz, T. M.; Wang, L.; Benicewicz, B. C.; Schadler, L. S. Ligand Engineering of Polymer Nanocomposites: From the Simple to the Complex. *ACS Applied Materials & Interfaces* **2014**, *6*, 6005–6021.

[38] Reynaud, E.; Jouen, T.; Gauthier, C.; Vigier, G.; Varlet, J. Nanofillers in polymeric matrix: a study on silica reinforced PA6. *Polymer* **2001**, *42*, 8759–8768.

[39] Tao, P.; Li, Y.; Siegel, R. W.; Schadler, L. S. Transparent dispensible high-refractive index ZrO_2/epoxy nanocomposites for LED encapsulation. *Journal of Applied Polymer Science* **2013**, *130*, 3785–3793.

[40] Lü, C.; Gao, J.; Fu, Y.; Du, Y.; Shi, Y.; Su, Z. A Ligand Exchange Route to Highly Luminescent Surface-Functionalized ZnS Nanoparticles and Their Transparent Polymer Nanocomposites. *Advanced Functional Materials* **2008**, *18*, 3070–3079.

[41] Ranjan, R.; Brittain, W. J. Synthesis of high density polymer brushes on nanoparticles by combined RAFT polymerization and click chemistry. *Macromolecular Rapid Communications* **2008**, *29*, 1104–1110.

[42] Scheutz, G. M.; Lessard, J. J.; Sims, M. B.; Sumerlin, B. S. Adaptable Crosslinks in Polymeric Materials: Resolving the Intersection of Thermoplastics and Thermosets. *Journal of the American Chemical Society* **2019**, *141*, 16181–16196.

[43] Ebnesajjad, S. In *7 - Surface Preparation of Thermoplastics, Thermosets, and Elastomers*; Ebnesajjad, S., Ed.; William Andrew Publishing: Oxford, 2011; pp 107–134.

[44] Baekeland, L. H. The Synthesis, Constitution, and Uses of Bakelite. *Journal of Industrial & Engineering Chemistry* **1909**, *1*, 149–161.

[45] Kloxin, C. J.; Scott, T. F.; Adzima, B. J.; Bowman, C. N. Covalent Adaptable Networks (CANs): A Unique Paradigm in Cross-Linked Polymers. *Macromolecules* **2010**, *43*, 2643–2653.

[46] Denissen, W.; Winne, J. M.; Du Prez, F. E. Vitrimers: permanent organic networks with glass-like fluidity. *Chemical Science* **2016**, *7*, 30–38.

[47] Yu, K.; Taynton, P.; Zhang, W.; Dunn, M. L.; Qi, H. J. Reprocessing and recycling of thermosetting polymers based on bond exchange reactions. *RSC Advances* **2014**, *4*, 10108–10117.

[48] Yang, Y.; Pei, Z.; Zhang, X.; Tao, L.; Wei, Y.; Ji, Y. Carbon nanotube-vitrimer composite for facile and efficient photo-welding of epoxy. *Chemical Science* **2014**, *5*, 3486–3492.

[49] Denissen, W.; Rivero, G.; Nicolaÿ, R.; Leibler, L.; Winne, J. M.; Du Prez, F. E. Vinylogous Urethane Vitrimers. *Advanced Functional Materials* **2015**, *25*, 2451–2457.

[50] Obadia, M. M.; Mudraboyina, B. P.; Serghei, A.; Montarnal, D.; Drockenmuller, E. Reprocessing and Recycling of Highly Cross-Linked Ion-Conducting Networks through Transalkylation Exchanges of C-N Bonds. *Journal of the American Chemical Society* **2015**, *137*, 6078–6083.

[51] Zhang, V.; Kang, B.; Accardo, J. V.; Kalow, J. A. Structure-Reactivity-Property Relationships in Covalent Adaptable Networks. *Journal of the American Chemical Society* **2022**, *144*, 22358–22377.

[52] Spiesschaert, Y.; Guerre, M.; Imbernon, L.; Winne, J. M.; Du Prez, F. Filler reinforced polydimethylsiloxane-based vitrimers. *Polymer* **2019**, *172*, 239–246.

[53] Legrand, A.; Soulié-Ziakovic, C. Silica-Epoxy Vitrimer Nanocomposites. *Macromolecules* **2016**, *49*, 5893–5902.

[54] Wang, H.; Xu, J.; Wang, H.; Cheng, X.; Wang, S.; Du, Z. Mechanically robust inorganic/organic hybrid polyurethane films with excellent self-healing and anti-corrosion ability. *Progress in Organic Coatings* **2022**, *167*, 106837.

[55] Lu, C.-H.; Yeh, Y.-C. Synthesis and Processing of Dynamic Covalently Crosslinked Polydextran/Carbon Dot Nanocomposite Hydrogels with Tailorable Microstructures and Properties. *ACS Biomaterials Science & Engineering* **2022**, *8*, 4289–4300.

[56] Trimmel, G.; Fratzl, P.; Schubert, U. Cross-Linking of Poly(methyl methacrylate) by the Methacrylate-Substituted Oxozirconium Cluster $Zr_6(OH)_4O_4(Methacrylate)_{12}$. *Chem. Mater.* **2000**, *12*, 602–604.

[57] Schubert, U.; Trimmel, G.; Moraru, B.; Tesch, W.; Fratzl, P.; Gross, S.; Kickelbick, G.; Hüsing, N. Inorganic-Organic Hybrid Polymers from Surface-Modified Oxometallate Clusters. *Mater. Res. Soc. Symp. Proc.* **2000**, *628*, CC2.3.

[58] Kogler, F. R.; Schubert, U. Crosslinking Vs. Filler Effect of Carboxylate-Substituted Zirconium Oxo Clusters on the Thermal Stability of Polystyrene. *Polymer* **2007**, *48*, 4990–4995.

[59] Vigolo, M.; Borsacchi, S.; Soraru, A.; Geppi, M.; Smarsly, B. M.; Dolcet, P.; Rizzato, S.; Carraro, M.; Gross, S. Engineering of Oxoclusters-Reinforced Polymeric Mater. with Application as Heterogeneous Oxydesulfurization Catalysts. *Appl. Catal.* **2016**, *182*, 636–644.

[60] Benedetti, C.; Cazzolaro, A.; Carraro, M.; Graf, R.; Landfester, K.; Gross, S.; Munoz-Espi, R. Dual Role of Zirconium Oxoclusters in Hybrid Nanoparticles: Cross-Linkers and Catalytic Sites. *ACS Appl. Mater. Interfaces* **2016**, *8*, 26275–26284.

[61] Bragaggia, G.; Beghetto, A.; Bassato, F.; Reichenbächer, R.; Dolcet, P.; Carraro, M.; Gross, S. Tuning the Activity of a Hybrid Polymer-Oxocluster Catalyst: A Composition-Selectivity Correlation. *Polymers* **2021**, *13*, 3268.

[62] Schubert, U.; Völkel, T.; Moszner, N. Mechanical Properties of an Inorganic-Organic Hybrid Polymer Cross-linked by the Cluster $Zr_4O_2(\text{methacrylate})_{12}$. *Chem. Mater.* **2001**, *13*, 3811–3812.

[63] Trimmel, G.; Gross, S.; Kickelbick, G.; Schubert, U. Swelling Behavior and Thermal Stability of Poly(methylmethacrylate) Crosslinked by the Oxozirconium Cluster $Zr_4O_2(\text{methacrylate})_{12}$. *Appl. Organomet. Chem.* **2001**, *15*, 401–406.

[64] Kreutzer, J.; Qin, X.-H.; Gorsche, C.; Peterlik, H.; Liska, R.; Schubert, U. Variation of the Crosslinking Density in Cluster-Reinforced Polymers. *Mater. Today Commun.* **2015**, *5*, 10 – 17.

[65] Gibin, G.; Lorenzetti, A.; Callone, E.; Dirè, S.; Dolcet, P.; Venzo, A.; Causin, V.; Marigo, A.; Modesti, M.; Gross, S. Smart and Covalently Cross-Linked: Hybrid Shape Memory Mater. Reinforced through Covalent Bonds by Zirconium Oxoclusters. *ChemPlusChem.* **2016**, *81*, 338–350.

[66] Gross, S.; Di Noto, V.; Schubert, U. Dielectric Investigation of Inorganic-Organic Hybrid Film Based on Zirconium Oxocluster-Crosslinked PMMA. *J. Non. Cryst. Solids* **2003**, *322*, 154–159.

[67] Graziola, F.; Girardi, F.; Bauer, M.; Di Maggio, R.; Rovezzi, M.; Bertagnolli, H.; Sada, C.; Rossetto, G.; Gross, S. UV-Photopolymerisation of Poly(methyl methacrylate)-Based Inorganic-Organic Hybrid Coatings and Bulk Samples Reinforced with Methacrylate-Modified Zirconium Oxocluster. *Polymer* **2008**, *49*, 4332–4343.

[68] Gao, Y.; Kogler, F. R.; Peterlik, H.; Schubert, U. Ring-opening metathesis polymerizations with norbornene carboxylate-substituted metal oxo clusters. *Journal of Materials Chemistry* **2006**, *16*, 3268–3276.

[69] Faccini, F.; Fric, H.; Schubert, U.; Wendel, E.; Tsetsgee, O.; Muller, K.; Bertagnolli, H.; Venzo, A.; Gross, S. [Small Omega]-Mercapto-Functionalized Hafnium- and Zirconium-Oxoclusters as Nanosized Building Blocks for Inorganic-Organic Hybrid Mater.: Synthesis, Characterization and Photothiol-ene Polymerization. *J. Mater. Chem.* **2007**, *17*, 3297–3307.

[70] Sangermano, M.; Gross, S.; Priola, A.; Rizza, G.; Sada, C. Thiol-ene Hybrid Organic/Inorganic Nanostructured Coatings Based on Thiol-Functionalized Zirconium Oxoclusters. *Macromol. Chem. Phys.* **2007**, *208*, 2560–2568.

[71] Schubert, U. Polymers Reinforced by Covalently Bonded Inorganic Clusters. *Chem. Mater.* **2001**, *13*, 3487–3494.

[72] Faustini, M.; Nicole, L.; Ruiz-Hitzky, E.; Sanchez, C. History of Organic-Inorganic Hybrid Mater.: Prehistory, Art, Science, and Advanced Applications. *Adv. Funct. Mater.* **2018**, *28*, 1704158.

[73] Gross, S. Oxocluster-Reinforced Organic-Inorganic Hybrid Mater.: Effect of Transition Metal Oxoclusters on Structural and Functional Properties. *J. Mater. Chem.* **2011**, *21*, 15853–15861.

[74] Armelao, L.; Eisenmenger-Sittner, C.; Groenewolt, M.; Gross, S.; Sada, C.; Schubert, U.; Tondello, E.; Zattin, A. Zirconium and Hafnium Oxoclusters as Molecular Building Blocks for Highly Dispersed ZrO_2 or HfO_2 Nanoparticles in Silica Thin Films. *J. Mater. Chem.* **2005**, *15*, 1838–1848.

[75] Armelao, L.; Gross, S.; Müller, K.; Pace, G.; Tondello, E.; Tsetsgee, O.; Zattin, A. Structural Evolution upon Thermal Heating of Nanostructured Inorganic-Organic Hybrid Mater. to Binary Oxides MO_2-SiO_2

(M = Hf, Zr) as Evaluated by Solid-State NMR and FTIR Spectroscopy. *Chem. Mater.* **2006**, *18*, 6019–6030.

[76] Armelao, L.; Bertagnolli, H.; Bleiner, D.; Groenewolt, M.; Gross, S.; Krishnan, V.; Sada, C.; Schubert, U.; Tondello, E.; Zattin, A. Highly Dispersed Mixed Zirconia and Hafnia Nanoparticles in a Silica Matrix: First Example of a $ZrO_2-HfO_2-SiO_2$ Ternary Oxide System. *Adv. Funct. Mater.* **2007**, *17*, 1671–1681.

[77] Gross, S.; Müller, K. Sol-Gel Derived Silica-Based Organic-Inorganic Hybrid Mater. as Composite Precursors for the Synthesis of Highly Homogeneous Nanostructured Mixed Oxides: an Overview. *J. Sol-Gel Sci. Technol.* **2011**, *60*, 283–298.

[78] Wu, L.; Liu, J.; Vockenhuber, M.; Ekinci, Y.; Castellanos, S. Hybrid EUV Resists with Mixed Organic Shells: A Simple Preparation Method. *Eur. J. Inorg. Chem.* **2019**, *2019*, 4136–4141.

[79] Huang, J.-Y.; Xu, H.; Peretz, E.; Wu, D.-Y.; Ober, C. K.; Hanrath, T. Three-Dimensional Printing of Hierarchical Porous Architectures. *Chem. Mater.* **2019**, *31*, 10017–10022.

[80] Faccioli, F.; Bauer, M.; Pedron, D.; Soraru, A.; Carraro, M.; Gross, S. Hydrolytic Stability and Hydrogen Peroxide Activation of Zirconium-Based Oxoclusters. *Eur. J. Inorg. Chem.* **2015**, *2015*, 210–225.

[81] Moons, J.; de Azambuja, F.; Mihailovic, J.; Kozma, K.; Smiljanic, K.; Amiri, M.; Cirkovic Velickovic, T.; Nyman, M.; Parac-Vogt, T. N. Discrete Hf_{18} Metal-oxo Cluster as a Heterogeneous Nanozyme for Site-Specific Proteolysis. *Angew. Chem. Int. Ed.* **2020**, *59*, 9094–9101.

[82] Cavka, J. H.; Jakobsen, S.; Olsbye, U.; Guillou, N.; Lamberti, C.; Bordiga, S.; Lillerud, K. P. A New Zirconium Inorganic Building Brick Forming Metal Organic Frameworks with Exceptional Stability. *J. Am. Chem. Soc.* **2008**, *130*, 13850–13851.

[83] Vermoortele, F.; Bueken, B.; Le Bars, G.; Van de Voorde, B.; Vandichel, M.; Houthoofd, K.; Vimont, A.; Daturi, M.; Waroquier, M.; Van Speybroeck, V.; et al., Synthesis Modulation as a Tool To Increase the Catalytic Activity of Metal-Organic Frameworks: The Unique Case of UiO-66(Zr). *J. Am. Chem. Soc.* **2013**, *135*, 11465–11468.

[84] Ly, H. G. T.; Fu, G.; Kondinski, A.; Bueken, B.; De Vos, D.; Parac-Vogt, T. N. Superactivity of MOF-808 toward Peptide Bond Hydrolysis. *J. Am. Chem. Soc.* **2018**, *140*, 6325–6335.

[85] Loosen, A.; de Azambuja, F.; Smolders, S.; Moons, J.; Simms, C.; De Vos, D.; Parac-Vogt, T. N. Interplay between Structural Parameters and Reactivity of Zr_6-Based MOFs as Artificial Proteases. *Chem. Sci.* **2020**, *11*, 6662–6669.

[86] Chen, Z.; Hanna, S. L.; Redfern, L. R.; Alezi, D.; Islamoglu, T.; Farha, O. K. Reticular Chemistry in the Rational Synthesis of Functional Zirconium Cluster-Based MOFs. *Coord. Chem. Rev.* **2019**, *386*, 32 – 49.

[87] Yuan, S.; Qin, J.-S.; Lollar, C. T.; Zhou, H.-C. Stable Metal-Organic Frameworks with Group 4 Metals: Current Status and Trends. *ACS Cent. Sci.* **2018**, *4*, 440–450.

[88] Jakobsen, S.; Gianolio, D.; Wragg, D. S.; Nilsen, M. H.; Emerich, H.; Bordiga, S.; Lamberti, C.; Olsbye, U.; Tilset, M.; Lillerud, K. P. Structural Determination of a Highly Stable Metal-Organic Framework with Possible Application to Interim Radioactive Waste Scavenging: Hf-UiO-66. *Phys. Rev. B* **2012-09**, *86*, 125429.

[89] Beyzavi, M. H.; Klet, R. C.; Tussupbayev, S.; Borycz, J.; Vermeulen, N. A.; Cramer, C. J.; Stoddart, J. F.; Hupp, J. T.; Farha, O. K. A Hafnium-Based Metal-Organic Framework as an Efficient and Multifunctional Catalyst for Facile CO_2 Fixation and Regioselective and Enantioretentive Epoxide Activation. *J. Am. Chem. Soc.* **2014**, *136*, 15861–15864.

[90] Beyzavi, M. H.; Vermeulen, N. A.; Howarth, A. J.; Tussupbayev, S.; League, A. B.; Schweitzer, N. M.; Gallagher, J. R.; Platero-Prats, A. E.; Hafezi, N.; Sarjeant, A. A.; et al., A Hafnium-Based Metal-Organic Framework as a Nature-Inspired Tandem Reaction Catalyst. *J. Am. Chem. Soc.* **2015**, *137*, 13624–13631.

[91] Salvador, F. E.; Miller, V.; Shimada, K.; Wang, C.-H.; Wright, J.; Das, M.; Chen, Y.-P.; Chen, Y.-S.; Sheehan, C.; Xu, W.; et al., Mechanochemistry of Group 4 Element-Based Metal-Organic Frameworks. *Inorg. Chem.* **2021**, *21*, 16079–16084.

[92] Guillerm, V.; Gross, S.; Serre, C.; Devic, T.; Bauer, M.; Férey, G. A Zirconium Methacrylate Oxocluster as Precursor for the Low-Temperature Synthesis of Porous Zirconium(iv) Dicarboxylates. *Chem. Comm.* **2010**, *46*, 767–769.

[93] Bezrukov, A. A.; Törnroos, K. W.; Le Roux, E.; Dietzel, P. D. C. Incorporation of an Intact Dimeric Zr_{12} Oxo Cluster from a Molecular Precursor in a New Zirconium Metal-Organic Framework. *Chem. Comm.* **2018**, *54*, 2735–2738.

[94] Fidelli, A. M.; Karadeniz, B.; Howarth, A. J.; Huskic, I.; Germann, L. S.; Halasz, I.; Etter, M.; Moon, S.-Y.; Dinnebier, R. E.; Stilinovic, V.; et al., Green and Rapid Mechanosynthesis of High-Porosity NU- and UiO-type Metal-Organic Frameworks. *Chem. Comm.* **2018**, *54*, 6999–7002.

[95] Huang, Y.-H.; Lo, W.-S.; Kuo, Y.-W.; Chen, W.-J.; Lin, C.-H.; Shieh, F.-K. Green and Rapid Synthesis of Zirconium Metal-Organic Frameworks via Mechanochemistry: UiO-66 Analog Nanocrystals Obtained in One Hundred Seconds. *Chem. Comm.* **2017**, *53*, 5818–5821.

[96] Montarnal, D.; Capelot, M.; Tournilhac, F.; Leibler, L. Silica-Like Malleable Materials from Permanent Organic Networks. *Science* **2011**, *334*, 965–968.

2

Metal oxo clusters as smallest conceivable nanoparticle[a]

> *Research is to see what everybody else has seen, and to think what nobody else has thought.*
> – Albert Szent-Györgyi

2.1   Introduction

As mentioned above, clusters can be regarded as the smallest conceivable nanoparticles. This is because the inorganic core consists of the smallest amount of atoms organized as a crystallographic unit cell which is capped by organic ligands, creating hybrid objects. Although there are similarities, there are also important differences. First of all, the clusters are atomically precise, meaning that the number of metal atoms and ligands is exactly defined. As a result, their polydispersity (PD) is zero whereas for nanoparticles the PD is 5% in the best case scenario. Secondly, their ligand density,

---

expressed as the number of ligands per squared nanometer, of the clusters is lower. 0.5 nm clusters have a ligand density of 2.4 ligands per nm^2 compared to 3-4 for nanoparticles. Finally, they have a maximized surface to volume ratio. All the metal atoms are located on the surface making them interesting candidates for catalysis. By comparison, a 5 nm nanoparticle has approximately 20 % of the metal atoms on the surface, while the other 80 % is buried in the bulk of the nanoparticle.

Although the aforementioned properties sound amazing it is not all sunshine and rainbows. Historically, clusters have been characterized by single crystal XRD. This required them to be synthesised using short and rigid carboxylic acids, which limited their solubility and, inevitably, their application. Since we approach these clusters as nanoparticles rather than inorganic complexes, we intend to use longer and more bulky carboxylic acids, thus eliminating single crystal as a characterization technique. Unfortunately, commonly used nanoparticles techniques such as transmission electron microscopy (TEM) and dynamic light scattering (DLS) cannot be used since the cluster size reaches the lower detection limit of these techniques. Hence a new toolbox was necessary to fully characterize these cluster. In the remainder of this chapter it is shown how these challenges were overcome, developing novel fatty acid capped clusters.

2.1.1 Synthesis of Zr and Hf oxo clusters

Zirconium propoxide (70 w% in propanol) or zirconium butoxide (80 w% in butanol) reacts with an excess of acetic acid (8 equivalents) to form the **Zr_{12}**-acetate cluster, which is a dimer of **Zr_6**. The reaction is performed in dichloromethane (DCM) solvent to obtain higher quality crystals and both acetic acid and DCM are co-crystallized with the cluster.[1] The balanced chemical equation is shown in Figure 2.1a. After reacting overnight, we further washed the crystalline powder with a solution of acetic acid in DCM to remove reaction by-products and other zirconium species. Although the powder can be handled in air, it is recommended for long term storage to keep the clusters in a glovebox or desiccator, since they react slowly with atmospheric water and become partially insoluble.
Zr_{12}-propionate is similarly synthesised and purified as **Zr_{12}**-acetate. We extended the synthetic strategy to longer carboxylic acid ligands (see Figure 2.1b), but the resulting clusters cannot be crystallized anymore and therefore other purification techniques are required. The **Zr_{12}**-butanoate is washed overnight in acetonitrile (ACN), while **Zr_{12}**-hexanoate, **Zr_6**-methylbutanoate and **Zr_6**-methylheptanoate clusters can be precipitated with ACN and isolated by centrifugation. Dissolution in DCM and repeating the pre-
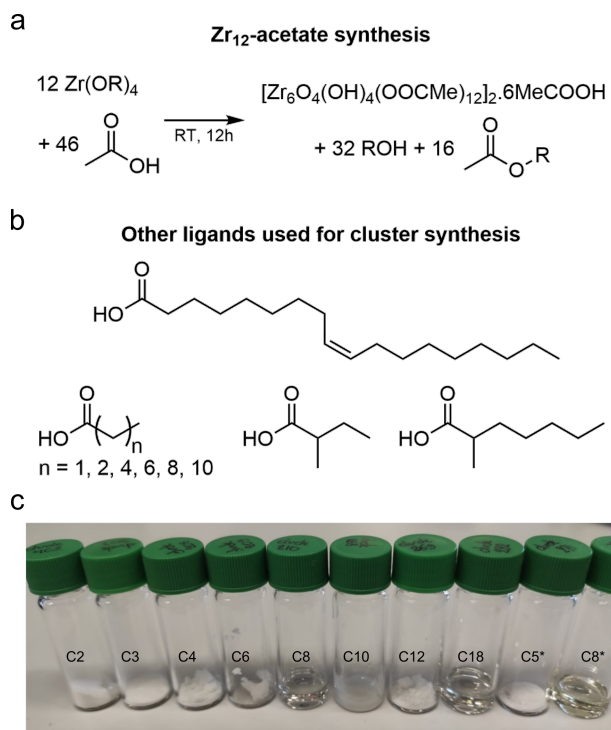
Figure 2.1: (a) Balanced chemical equation for the synthesis of **Zr$_{12}$**-acetate clusters from zirconium propoxide (or butoxide) and acetic acid. The final product has co-crystallized acetic acid and dichloromethane (the latter is not shown). (b) Chemical structures of the other carboxylic acids used here for cluster synthesis. (c) Finally, the aggregation of the as synthesised cluster with corresponding carboxylic acids. C2-C18 = **Zr$_{12}$**-acetate to **Zr$_{12}$**-oleate, C5* = **Zr$_6$**-methylbutanoate and C8* = **Zr$_6$**-methylheptanoate.

cipitation cycle twice, delivers the purified clusters. This type of purification is typical for colloidal nanoparticles,[2] and thus reinforces the idea of fatty acid capped clusters as atomically precise models for nanoparticles. For the clusters with even longer ligands (octyl, decyl, dodecyl and oleyl chains), the first precipitation is performed with acetonitrile, while acetone is the preferred anti-solvent for the two consecutive steps to precipitate the clusters, and separate it from, e.g. the ester co-product. The physical appearance of the clusters ranges from semi-crystalline solids (acetate, propionate, methylbutanoate) to waxy solids (butanoate, hexanoate, decanoate, dodecanoate) or viscous oils (octanoate, oleate, methylheptanoate). (See Figure

2.1c) The same synthetic procedure can be repeated, replacing $Zr(OPr)_4$ for $Hf(OBu)_4$, in order to obtain $\mathbf{Hf}_{12}$ or $\mathbf{Hf}_6$ clusters.

2.2   Developing a new toolbox

These new acids would greatly improve the solubility since they consist of longer aliphatic chains compared to the existing ligands. However, these acids imply that the clusters can no longer be crystallized. This means that a new toolbox is necessary. Further in this chapter, the toolbox will be developed for zirconium clusters and afterwards the toolbox will be applied on hafnium clusters.

PDF was used to study the cluster core. This technique has already established itself as a useful technique for studying nanoparticles but has rarely been used to study clusters. Since the inorganic/organic ratio is much smaller for clusters compared to nanoparticles we had to adapt the nanoparticle PDF methodology to meet our needs. The organic ligand shell was studied using FTIR, NMR and TGA which was challenging due to the carboxylates having multiple binding modes. Finally, the core with ligand shell was visualized using HRMS.

2.2.1   Structural analysis by X-ray PDF

While the $\mathbf{Zr}_{12}$-acetate and $\mathbf{Zr}_{12}$-propionate clusters are known in literature, the others are not. To prove their structure, we analyzed the clusters with X-ray total scattering and Pair Distribution Function (PDF) analysis. Total scattering takes into account both Bragg and diffuse scattering. The real space PDF is ideal to study nanomaterials, local effects and amorphous materials.[3–5] We measured the experimental PDF of all the above clusters and ordered them according to increasing carbon content, see Figure 2.2. Focusing first on the PDF of acetate capped clusters and comparing with the structure from single crystal XRD,[1] we easily recognize the Zr-O distance at 2.2 Å and the Zr-Zr distances within one $\mathbf{Zr}_6$ cluster at 3.5 Å and 5 Å. We label them as intra-$\mathbf{Zr}_6$ distances. The longer range Zr-Zr distances are specific to the $\mathbf{Zr}_{12}$ dimer and are present at 5.7 Å, 8.4 Å, and 11.5 Å. They are labeled as inter-$\mathbf{Zr}_6$ distances. When the chain length increases, the same features remain present in the PDF, except for the case of methylbutanoate and methylheptanoate where the inter-$\mathbf{Zr}_6$ distances are missing. The peak at 5.7 Å does not completely disappear but changes shape and has a lower intensity. The residual intensity stems from intra-$\mathbf{Zr}_6$ Zr-O distances (not the first coordination sphere but longer range correlations).

The above observations suggest that both the Zr_6-methylbutanoate and Zr_6-methylheptanoate clusters are monomers while the others are dimers. This is in agreement with our earlier hypothesis that branching of the carboxylic acid at the alpha position is the deciding factor between monomer and dimer.[6] A higher degree of oligomerization on the other hand, was excluded based on the absence of features beyond 11.5 Å, and on the crystal structure of Zr_{12}-acetate which exclusively consist of Zr_{12} clusters. With increasing chain length, we also observe the growth of a peak at 1.5 Å, which we assign to C-C distances in the ligand chain.
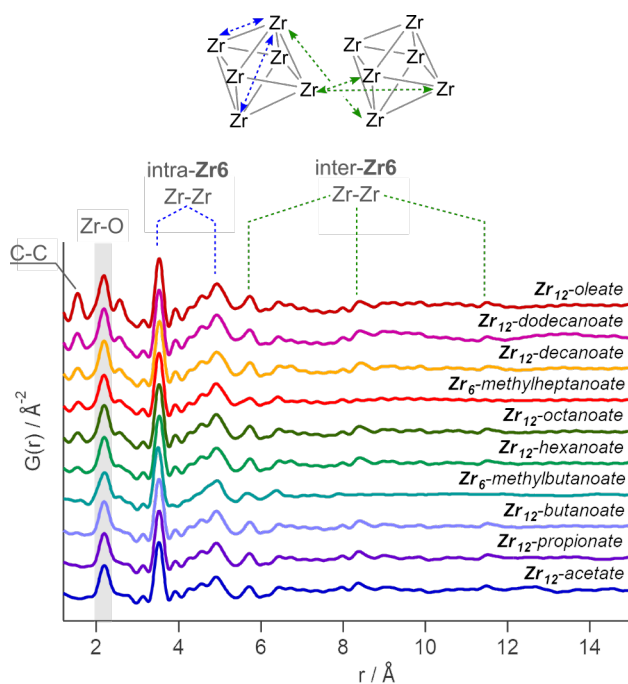
Figure 2.2: Experimental PDF of zirconium oxo clusters with different capping ligands. The C-C, Zr-O, and Zr-Zr distances are assigned. We make a distinction between the Zr-Zr distances within one Zr_6 cluster and the Zr-Zr distances that are characteristic for the dimer.

Apart from this model-free analysis, we sought to quantitatively fit the PDFs. We focus again first on Zr_{12}-acetate to refine our approach since a single crystal XRD structure is available for this cluster (CCDC-604528).[1] To demonstrate the importance of the organic ligands to the PDF, we theoretically calculated the PDF of Zr_{12}-acetate, including either (i) no carbon atoms, (ii) only the carbonyl carbon atoms, or (iii) all carbon atoms, see

Figure A.1. The carbon atoms contribute significantly to the PDF, especially between 4 Å and 8 Å. This result stands in stark contrast to the regular practice of ignoring the ligands in the PDF refinement of nanoparticles and larger clusters.[7–16] The ligand effect is further demonstrated by fitting the Zr_{12}-acetate PDF with various models, see Figure 2.3. For each structure model, we refined thermal motion parameters while keeping the structure (i.e. the atomic positions) unchanged. In a first attempt, similar to traditional approaches, we only used the Zr_6 cluster core as a model. The model could capture the basic Zr-O and intra-Zr_6 Zr-Zr distances but gave overall a poor agreement and a significant misfit in the Zr-O distance. Using the dimer structure, the inter-Zr_6 Zr-Zr distances are well described. By including the oxygen atoms from the coordinated acetates, a significant reduction in R_w is achieved and the Zr-O peak is now accurately fitted. By including the carbon atoms from the coordinated acetate, we obtain a decent fit, with an $R_w = 0.14$.

The crystal structure of Zr_{12}-acetate contains also hydrogen bonded ligands and co-crystallized DCM molecules. When the hydrogen bonded ligands are explicitly included, only a marginally better fit is obtained, see Figure A.2. Alternatively, we added an exponentially decaying sinusoidal function as a second phase, resulting in a slightly (but significantly) better fit with R_w value 0.11, see Figure A.3. This second phase describes disordered but still structured intensity and has previously been used to model solvent restructuring, or a regular array of high/low density regions.[17;18]. While it is gratifying to obtain an excellent fit for the data, we sought to determine whether we could distinguish the Zr_{12}-acetate structure from other reported clusters structures that were previously determined by single crystal XRD. We thus attempted to fit the experimental PDF of Zr_{12}-acetate clusters with the reported structures of Zr_{12}-propionate, Zr_6-trimethylacetate, Zr_6-methacrylate, Zr_6-isobutyrate, Zr_6-acetate, Zr_4 -methacrylate, Zr_4-formate isopropoxide, Zr_3-acetate isopropoxide, Zr_3-acetate tert-butoxide, Zr_{10}-salicylate, and Zr_{26}-formate, see Figure A.4.[1;19–25] For these refinements, we removed the excess carbons in the structures to arrive at models with acetate ligands. The models based on Zr_3, Zr_4, Zr_{10} and $Zr26$ had all a very poor agreement with the data. The Zr_6 structure models also delivered poor fits ($R_w = 0.24$ - 0.31). The second best agreement was obtained for the Zr_{12}-propionate model ($R_w = 0.18$). While this model is structurally very similar to the Zr_{12}-acetate model, the Zr-Zr distances are slightly larger in the propionate model (Table A.7). We conclude that PDF is able to pick up the correct structure from a series of possible clusters structures, based on the goodness of fit.

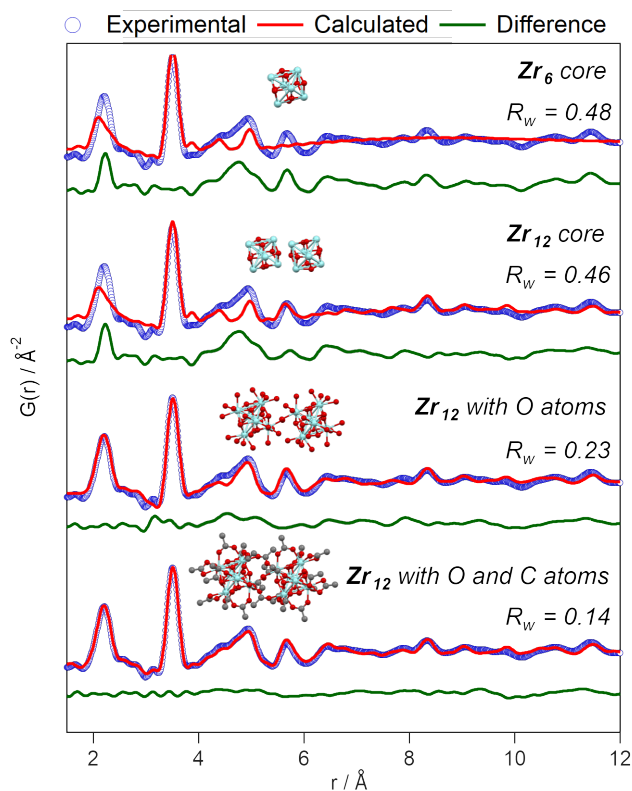The developed strategy is now applied to the other oxo clusters. Figure

Figure 2.3: PDF refinement of the **Zr**$_{12}$-acetate cluster with various models, derived from the reported crystal structure.[1] The best fit is obtained when including the oxygen and carbon atoms from the acetate ligands. The refined parameters are given in Table A.2.

2.4 shows the PDF refinement for four selected oxo clusters, capped with either butanoate, methylbutanoate, octanoate or oleate. In each case, we use a cluster model along with a decaying sine wave. For **Zr**$_{12}$-butanoate and **Zr**$_{12}$-octanoate, we find that the **Zr**$_{12}$-acetate structure model gives a satisfactory fit (Figure 2.4), which is clearly better than the refinement with a **Zr**$_6$-acetate structural model (Figure A.5). The latter structure has all bridging ligands and was reported after crystallization from aqueous solution.[19] In contrast, the **Zr**$_6$-methylbutanoate cluster, is best described by the **Zr**$_6$ model and gives a worse fit for the **Zr**$_{12}$ model. The **Zr**$_{12}$-oleate cluster was best described by the **Zr**$_{12}$-propionate structure model with the slightly larger Zr-Zr distances. Again, the **Zr**$_6$ model delivered a

worse fit (Figure A.5). We can thus distinguish the $\mathbf{Zr_6}$ structures from the $\mathbf{Zr_{12}}$ structures, based on the refinement. However, we notice that the R_w increases with increasing chain length (indicating a worse fit). The origin lies in the fact that we did not explicitly include all the carbons of the long ligands in the models. The short-range C-C distances (at 1.5 and 2.6 Å) are not fitted in the refinement. However, the sinusoidal function seems to describe the long-range C-C distances quite well, presumably because the ligand chain is disordered. This hypothesis is confirmed by the increase in the relative amplitude of the sine wave from $\mathbf{Zr_{12}}$-acetate to $\mathbf{Zr_{12}}$-oleate (Table A.2, A.4). The improvement in R_w upon including the sinusoid is small for acetate (0.03) while large for oleate (0.09) (see Figure A.6).
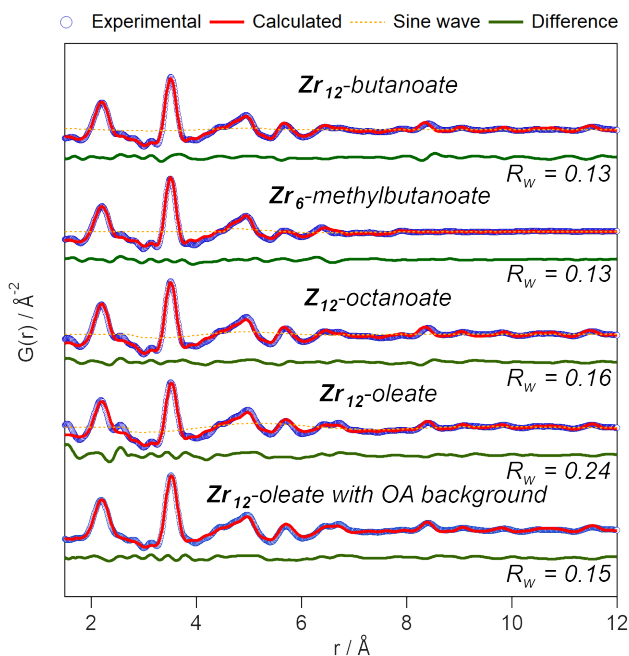
Figure 2.4: PDF refinement for $\mathbf{Zr_{12}}$-butanoate and $\mathbf{Zr_{12}}$-octanoate using the $\mathbf{Zr_{12}}$-acetate structure model. PDF refinement of $\mathbf{Zr_6}$-methylbutanoate using the $\mathbf{Zr_6}$-acetate structure model. Finally, the PDF refinement of $\mathbf{Zr_{12}}$-oleate using the $\mathbf{Zr_{12}}$-propionate structure model, with or without background correction in reciprocal space. If applied in the refinement, the exponentially dampening sine wave is shown (orange dotted lines). The refined parameters are given in Table A.5.

A more effective way of dealing with the long ligands is measuring the free ligand explicitly as a background and subtracting its scattering from

the data in reciprocal space. For Zr_{12}-oleate, this leads to a significant improvement of the fit. The short-range C-C distances disappeared from the PDF (Figure 2.4) and the sine wave is completely obsolete (Table A.4). The goodness of fit is now comparable to the case of the clusters with shorter chains. Note that the presence of longs ligands reduces the signal-to-noise ratio during the data collection (due to a lower fraction of oxo clusters in the X-ray beam). We conclude that, after initial training on the acetate clusters, our PDF analysis is able to confirm the structure of these previously unreported clusters. Our synthetic procedures indeed lead to the formation of soluble Zr_6 oxo clusters, forming monomers or dimers depending on the sterical hindrance of the ligand. We further emphasize that good refinements can only be achieved by including the binding group of the ligand explicitly in the model (even after background subtraction). This is much more important for the small clusters discussed here, than for larger clusters or nanoparticles. For the latter two, there is a larger core of strongly scattering atoms, and relatively fewer, weakly scattering ligands. However, small nanoparticles have typically worse goodness of fits compared to larger ones and it might be worth to consider including ligands explicitly to obtain better refinements.[7]

2.2.2   The organic ligand shell

For PDF modelling we need to include the carboxylate head group, but PDF is in general not very sensitive to the organic fraction. Detailed information on the presence of uncoordinated ligands or coordination modes is hard to obtain from PDF. We turn now to FTIR, TGA and NMR. In Figure 2.5, we show the FTIR spectra of selected oxo clusters (the complete FTIR spectra of all clusters are presented in Figure A.7). The C$-$H stretches (2800-3000 cm^{-1}) gain intensity with increasing chain length. The small, sharp peak around 3450 cm^{-1} and the broad peak between 3500 and 3000 cm^{-1} were assigned to the OH moieties onto the cluster, which are involved in hydrogen bonding. While all these samples were extensively purified by multiple precipitation/re-dissolution cycles, it is clear that there is still protonated carboxylic acid in the sample (observed at 1710 cm^{-1}), presumably hydrogen bonded to the cluster. Such hydrogen bonding is also observed for the co-crystallized acetic acid in the single-crystal structure of Zr_{12}-acetate, see Figure 2.6b. Our efforts to purify the clusters further and remove the hydrogen bonded acid were not successful or even compromised the integrity of the cluster core, see appendix A (Figures A.9 and A.14-A.15). Since Attenuated Total Reflection (ATR) FTIR is not quantitative, we used TGA to quantify the amount of excess carboxylic acid. We find about 1.1 - 3.7

excess ligand molecules per $\mathbf{Zr}_6$ monomer, see Table 2.1. (Mathematical equations are found in appendix A, Equation A.5-11) There is no clear trend among the different clusters. Only the $\mathbf{Zr}_{12}$-acetate stands out with 5.5 excess ligands per monomer.
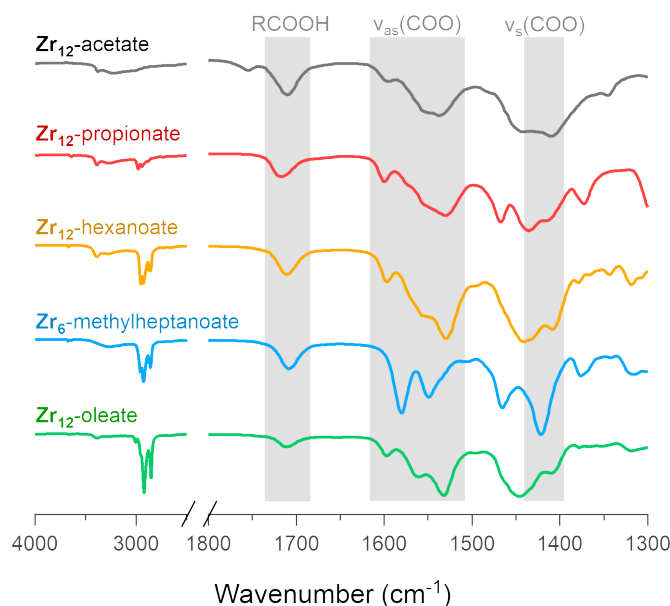

Figure 2.5: FTIR spectra of $\mathbf{Zr}_{12}$-acetate, -propionate, -hexanoate, -oleate and $\mathbf{Zr}_6$-methylheptanoate. The weak band at 1750 cm^{-1} in the spectrum of $\mathbf{Zr}_{12}$-acetate is assigned to a small amount of acetic acid that is not involved in hydrogen bonding of any kind.[26] An ester impurity is ruled out because of the absence of any signal around 4 ppm in ^{1}H NMR, (See Figure A.8).

Returning to the FTIR spectrum, the bands in the region 1500-1600 cm^{-1} are assigned to the asymmetric stretch of the carboxylate, $\nu_{as}(COO)$. While the symmetric stretch, $\nu_s(COO)$, is expected around 1400-1450 cm^{-1}, there is significant overlap with CH_2 and CH_3 deformation bands which are expected around 1440-1460 cm^{-1}. Focusing here on the qualitative differences, we first draw the attention to the spectrum of $\mathbf{Zr}_6$-methylheptanoate. In contrast to the IR spectrum of $\mathbf{Zr}_6$-pivalate,[27] $\nu_{as}(COO)$ is split in two bands (1580 and 1550 cm^{-1}).While the $\mathbf{Zr}_6$-pivalate has all bridging carboxylates, the band splitting for $\mathbf{Zr}_6$-methylheptanoate indicates that the part of the methylheptanoate ligands are in the chelating mode. When comparing the pattern of the $\nu_{as}(COO)$ bands in $\mathbf{Zr}_6$-methylheptanoate with those

Table 2.1: TGA data on bottom up synthesised clusters. The values in the table is the remaining mass of ZrO_2 in %. Note that for the acetate cluster the value in the table is on top of the extra acid from the crystal structure $Zr_{12}O_8(OH)_8(CH_3COO)_{24}.6\,CH_3COOH.3.5\,DCM$.

Ligand	Theoretical value (%)	experimental value (%)	Extra acid/monomer
Acetic acid	53.3	48	2.5
Propionic acid	47.5	42.8	2.3
Butanoic acid	42.9	39	1.9
Methylbutanoic acid	39	34	2.8
Hexanoic acid	35.9	31.9	2.2
Octanoic acid	30.8	25.2	3.7
Methyl heptanoic acid	30.8	29.1	1.1
Decanoic acid	27	23.2	2.6
Dodecanoic acid	24.1	19.4	3.7
Oleic acid	18.2	14.8	3.4

of $\mathbf{Zr}_{12}$-oleate, we find striking differences. For $\mathbf{Zr}_6$-methylheptanoate, the most intense band is at 1580 cm^{-1} while for $\mathbf{Zr}_{12}$-oleate, the most intense band is at 1532 cm^{-1}. In addition, $\mathbf{Zr}_{12}$-oleate has a band with the highest wavenumber; 1597 cm^{-1}. Typically the wavelength difference between $\nu_{as}(COO)$ and $\nu_s(COO)$ is used as a diagnostic tool to distinguish between chelating ($\Delta\nu < 110\ cm^{-1}$), bridging ($\Delta\nu = 140 - 190\ cm^{-1}$) or monodentate ($\Delta\nu = 200 - 320\ cm^{-1}$) binding modes.[28;29] This is an empirical rule-of-thumb and in case of multiple bands it is difficult to assign the paired $\nu_s(COO)$. With these limitations in mind, we tentatively calculate $\Delta\nu = 190\ cm^{-1}$ for the band at 1597 cm^{-1}, and assign it to the ligands that bridge the two clusters. More importantly, the same $\nu_{as}(COO)$ pattern of $\mathbf{Zr}_{12}$-oleate is retrieved for all the $\mathbf{Zr}_{12}$ clusters (see also Figure A.7). Furthermore, the $\nu_{as}(COO)$ pattern of $\mathbf{Zr}_6$-methylheptanoate is quasi identical to that of $\mathbf{Zr}_6$-methylbutanoate. This is an exciting observation since it provides a very fast method to distinguish between the $\mathbf{Zr}_6$ and $\mathbf{Zr}_{12}$ clusters.

The ^{1}H NMR spectra of selected oxo clusters are shown in Figure 2.6 a. For $\mathbf{Zr}_{12}$-propionate, hexanoate and oleate, we recognize three different resonances for the alpha CH$_2$ moiety, indicating three different distinguishable carboxylate environments (see also Figure A.11 for the other $\mathbf{Zr}_{12}$ clusters). On the other hand, Zr$_6$-methylheptanoate has only two alpha CH resonances (see Figure A.11 for $\mathbf{Zr}_6$-methylbutanoate). It is striking that the NMR pattern seems to roughly agree with the $\nu_{as}(COO)$ pattern in FTIR. For $\mathbf{Zr}_{12}$-acetate, we find four methyl resonances. Diffusion ordered spectroscopy (DOSY), shows that three resonances (1.7-2 ppm) have the same diffusion coefficient, while the fourth (2.1 ppm) diffuses more quickly,

see Figure 2.6 b. The resonance at 2.1 ppm thus corresponds to the excess acetic acid, as also determined by FTIR and TGA. The measured diffusion coefficient ($D = 1106 \mu m/s$) is lower than the reference of free acetic acid ($D = 1851 \mu m/s$), and we conclude that the excess acetic acid is in fast exchange between two states: (i) free and (ii) hydrogen bonded to the cluster.[30]
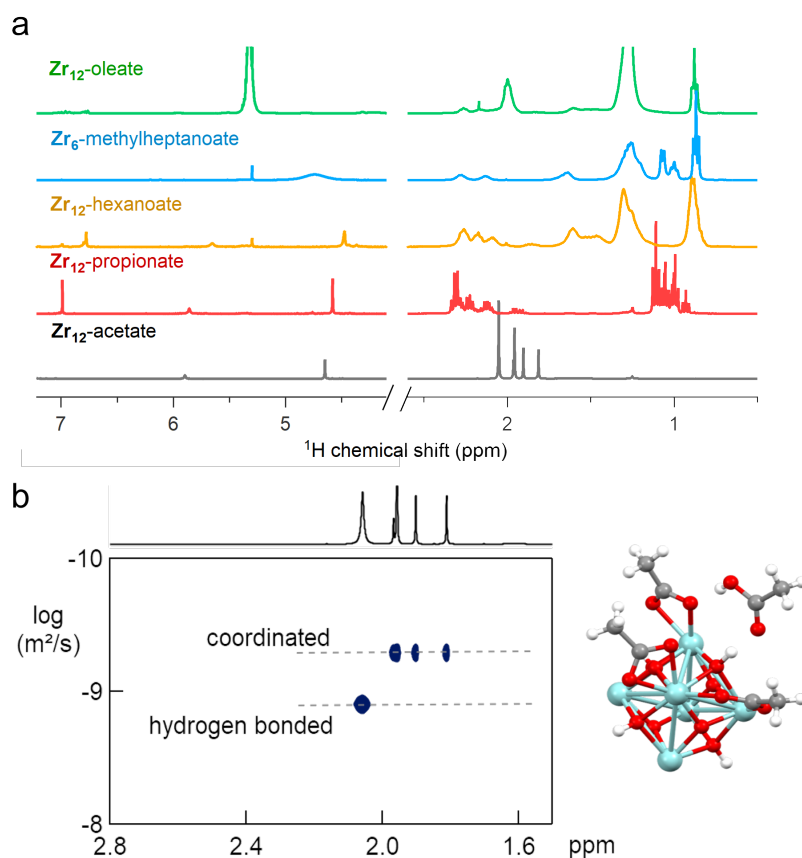

Figure 2.6: (a) NMR spectra in CDCl$_3$ of **Zr$_{12}$**-acetate, -propionate, -hexanoate, -oleate and **Zr$_6$**-methylheptanoate. (b) DOSY of the **Zr$_{12}$**-acetate cluster with one faster diffusing species and a set of three resonances pertaining to a slowly diffusing species corresponding to the cluster.

The signals between 5 and 7 ppm in all clusters spectra are assigned to the exchangeable protons on the cluster core itself since the resonances disappear upon addition of D$_2$O, see Figure A.12. Apart from **Zr$_{12}$**-acetate

and -propionate, all the spectra show significant line broadening, similar to nanoparticle-bound ligands.[31] The longer the ligands, the broader the alpha CH_2 resonance, but the sharper the methyl resonance becomes. Homogeneous line broadening depends on the rotational mobility and it is expected that the methyl group has increased mobility in a longer ligand.[31] The alpha resonance is closest to the surface. Its mobility is not enhanced in a longer ligand and instead, the total rotational mobility of the cluster decreases since it becomes a bigger object. In contrast to nanoparticle-bound ligands, we find little contribution of heterogeneous broadening to the resonances, see Table A.8.

2.2.3   The molecular formula by mass spectrometry

We sought to use electrospray ionization high resolution mass spectrometry (ESI-HR-MS) to obtain the mass of the clusters. Unfortunately, our carboxylate capped clusters show limited solubility in typical ESI-HR-MS solvents such as methanol and acetonitrile. $\mathbf{Zr}_{12}$-acetate clusters dissolve in methanol but no clusters were detected in ESI-HR-MS and NMR analysis provides evidence for cluster degradation in methanol, see Figure A.14-A.15. The limited solubility of $\mathbf{Zr}_{12}$-acetate did not allow for any further HR-MS analysis. On the other end, the $\mathbf{Zr}_{12}$-oleate clusters were too non-polar. The other clusters could be dissolved in tetrahydrofuran (THF) and were analyzed with ESI-HR-MS after adding acetonitrile as co-solvent (full spectra and assignments in Figures A.16-A.23).

The $\mathbf{Zr}_6$ clusters give reasonably clean spectra where the molecular ion can be recognized as $Zr_6O_4(OH)_3(L)_{12}{}^+$ (the cluster minus an OH^- group). The example of $\mathbf{Zr}_6$-methylbutanoate is shown in Figure 2.7. The $\mathbf{Zr}_{12}$ clusters appear less stable and the ion $[Zr_6O_4(OH)_7(L)_9]_2H^+$ was observed in most cases (see Figure 2.7). This ion is the proton adduct of the $\mathbf{Zr}_{12}$ dimer after substituting six carboxylates for six hydroxides. The $\mathbf{Zr}_{12}$ cluster features indeed 6 chelating ligands, which are most labile according to literature.[1] It is thus plausible that such an exchange takes place, further catalyzed by a coordinating solvent like THF. Interestingly, more fragmentation was seen for longer ligands and the monomeric form is even dominant for $\mathbf{Zr}_{12}$-decanoate and $\mathbf{Zr}_{12}$-dodecanoate. Despite the limitations, MS thus confirms the successful formation of oxo cluster with long carboxylate ligands. It is however not the correct technique to distinguish the dimer from the monomer structure.
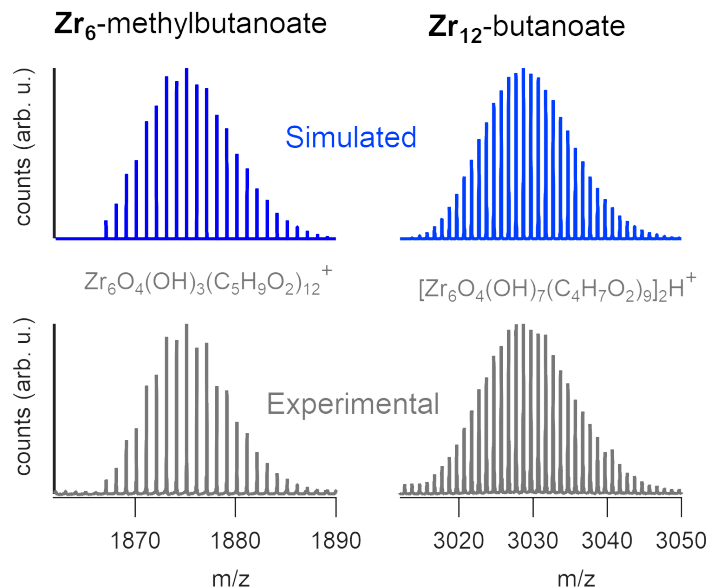
Figure 2.7: ESI-HR-MS analysis of the dimeric **Zr**$_{12}$-butanoate cluster and of the monomeric **Zr**$_6$-methylbutanoate cluster. Both the experimental and simulated spectra are shown.

2.2.4 Ligand exchange reactions

Ligand exchange where all carboxylates are replaced by another type of carboxylate is an interesting way to change the cluster structure and/or functionality. Pucherberger *et al.* previously studied the exchange between methacrylate and propionate/acetate on zirconium oxo clusters by NMR. They inferred that, at room temperature, the monomer and dimer cannot be converted in one another and that the inter-cluster bridging ligands are unavailable for exchange.[1] Here, we re-evaluate the ligand exchange process under more forcing conditions and apply our characterization toolbox to elucidate the cluster structure. Starting from the **Zr**$_{12}$-acetate cluster, we stir it with 1.5 equivalents of new ligand (a carboxylic acid from Figure 2.1) at 70 °C before we evaporate all volatile species. Since acetic acid has a reasonably low boiling point, it is readily removed from the reaction mixture, forcing the ligand exchange to proceed to completion (confirmed by the absence of acetate signals in the ^{13}C NMR, see Figure 2.8 b). The clusters are then purified to remove the excess of high boiling ligand. PDF analysis of the clusters shows that the dimer is obtained for butanoate,

hexanoate, octanoate, decanoate, dodecanoate and oleate, see Figure A.24.
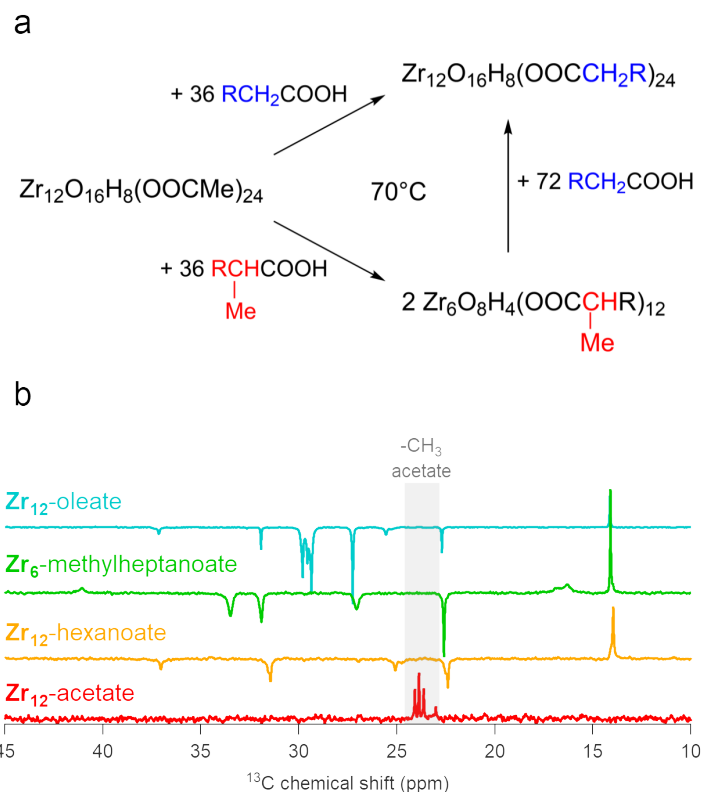
Figure 2.8: Overlay scheme of the exchange reaction (a) of Zr_{12}-acetate cluster with linear or branched carboxylic acids. Alternatively, Zr_6-methylbutanoate can be exchanged to convert monomeric cluster into dimeric clusters. (b) ^{13}C NMR in $CDCl_3$ for the Zr_{12}-hexanoate, -oleate and Zr_6-methylheptanoate synthesised via exchange reaction. Zr_{12}-acetate is added as a reference to prove that the signals of acetate are gone after exchange.

The Zr_6 monomer is retrieved for methylbutanoate or methylheptanoate, showing that the dimer can be broken up under appropriate conditions and with the right structure-directing ligand. Also the IR and NMR spectra look identical to the ones from the clusters that are directly synthesised from zirconium propoxide, see Figure A.25-A.26. We also treated the Zr_6-methylbutanoate cluster twice with 3 equivalents of hexanoic acid. Methylbutanoic acid does not evaporate as easily as acetic acid and a higher

excess of new ligand was needed. The resulting cluster has the typical IR and NMR signatures of a $\mathbf{Zr}_{12}$ cluster, see Figures A.27-A.28. Also the HRMS shows similar results compared to the HRMS of bottom up synthesised $\mathbf{Zr}_{12}$-hexanoate, see Figure A.19 and A.29. The results of the ligand exchanges are summarized in Figure 2.8 a.

2.2.5   Hafnium oxo clusters
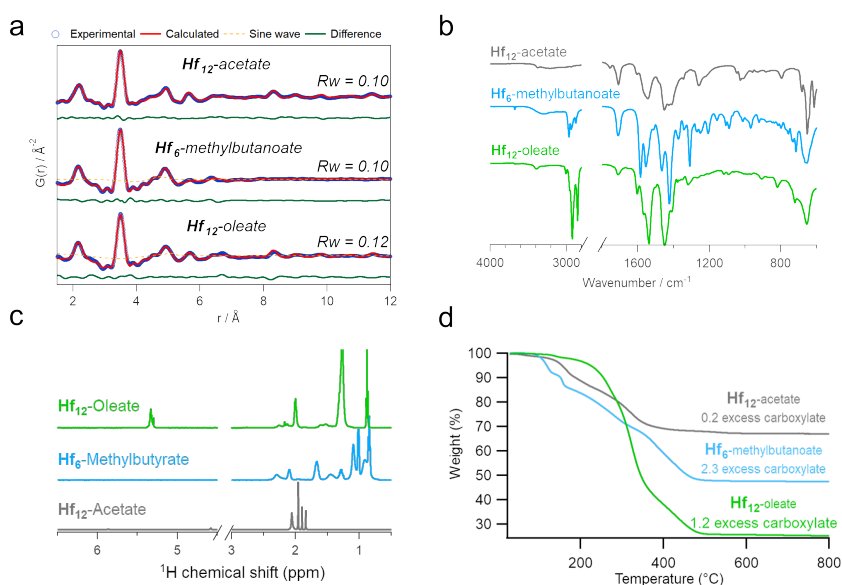
Figure 2.9: (a) PDF fit for $\mathbf{Hf}_{12}$-acetate, $\mathbf{Hf}_6$-methylbutanoate and $\mathbf{Hf}_{12}$-oleate clusters with exponentially dampening sine wave contribution. The refined parameters are indicated in Table A.9. (b) FTIR spectra, (c) ^{1}H NMR spectra in CDCl$_3$ and (d) TGA spectra of the hafnium oxo clusters synthesised via bottom up.

To generalize our methodology to hafnium oxo clusters, we reacted hafnium butoxide with acetic acid, methylbutanoic acid, or oleic acid. After purification, the resulting clusters were characterized by PDF, FTIR, TGA, and NMR. Comparing $\mathbf{Zr}_{12}$-acetate with $\mathbf{Hf}_{12}$-acetate, it is clear from their respective bond distances that they are in fact isostructural. (See Table 2.2) The acquisition and refinement of PDF data are more straightforward for the hafnium oxo clusters since hafnium has a higher scattering cross section, see Figure 2.9 a. All pairs that have at least one hafnium atom

are enhanced in intensity, and all other pairs (e.g. C-C) loose relative intensity. Using a structure model of $\mathbf{Hf}_{12}$-acetate (CCDC-604534),[1] we can readily describe the PDF data of the $\mathbf{Hf}_{12}$-acetate and $\mathbf{Hf}_{12}$-oleate clusters. The goodness of fit is even better than for the respective $\mathbf{Zr}_{12}$ clusters that were refined in an equivalent way, see Figure 2.4. In the absence of a $\mathbf{Hf}_6$ structure model, we constructed a $\mathbf{Hf}_6$ cluster model from the $\mathbf{Hf}_{12}$ structure. This model accurately describes the PDF data, confirming that the $\mathbf{Hf}_6$-methylbutanoate clusters is a monomer. The hafnium oxo clusters thus follow the same structure-directing rules as the zirconium oxo clusters. Also the FTIR spectra (Figure 2.9b) and NMR spectra (Figure 2.9c) show the expected patterns, similar to the case of zirconium. Ligand exchanges can be performed from acetate to oleate or methylbutanoate ligands, forming the expected $\mathbf{Hf}_{12}$ or $\mathbf{Hf}_6$ cluster respectively, based on FTIR and NMR data. Finally, TGA show that there is again free carboxylic acid present on top of the charge balancing ligand shell (Figure 2.9 and Table A.10).

Table 2.2: Bond distances in acetate capped hafnium and zirconium oxo clusters. M=Zr/Hf.[1]

	$\mathbf{Zr}_{12}$-acetate	$\mathbf{Hf}_{12}$-acetate
M-O	2.033-2.396	2.031-2.405
M-M Intra 1	3.448-3.588	3.448-3.588
M-M Intra 2	4.953-4.969	4.953-4.969
M-M Inter 1	5.588-5.684	5.588-5.684
M-M Inter 2	8.270-8.609	8.270-8.609
M-M Inter 3	11.256-11.956	11.256-11.956

2.2.6 Colloidal catalysis

Finally, we take the perspective that these fatty acid capped oxo clusters are the smallest conceivable nanoparticle prototypes.[6,32] While technically not a crystal anymore, such a cluster is the lower limit of scaling down a ligand capped metal oxide nanoparticle. Hence, it has a maximized surface-to-volume ratio. Maximizing surface area is particularly important in heterogeneous catalysis and we thus hypothesized that oxo clusters (diameter = 0.5 nm) would have superior catalytic performance over metal oxide nanoparticles (diameter = 2-10 nm). To test this, we take the previously reported esterification of oleic acid as catalytic model system.[33] We synthesised 5.5 nm tetragonal zirconia nanoparticles, and functionalised their surface with oleate ligands,[34] see Figure 2.10a-b. $\mathbf{Zr}_{12}$-oleate clusters are the atomically precise, smallest conceivable prototypes of such nanoparticles. Given

that both cluster and nanoparticles have the same oleate ligand, the only difference is the inorganic core. In addition, the ligand is identical to the catalytic substrate (oleic acid), thus avoiding competition between ligand and substrate for the surface sites,[33] or the formation of side–products. To compare the efficiency of the two catalysts, we added in both cases 10 mol% Zr to the reaction mixture. We monitored the reactions for the first 5 hours by taking aliquots and quantifying the ester product via NMR, see Figure 2.10c.
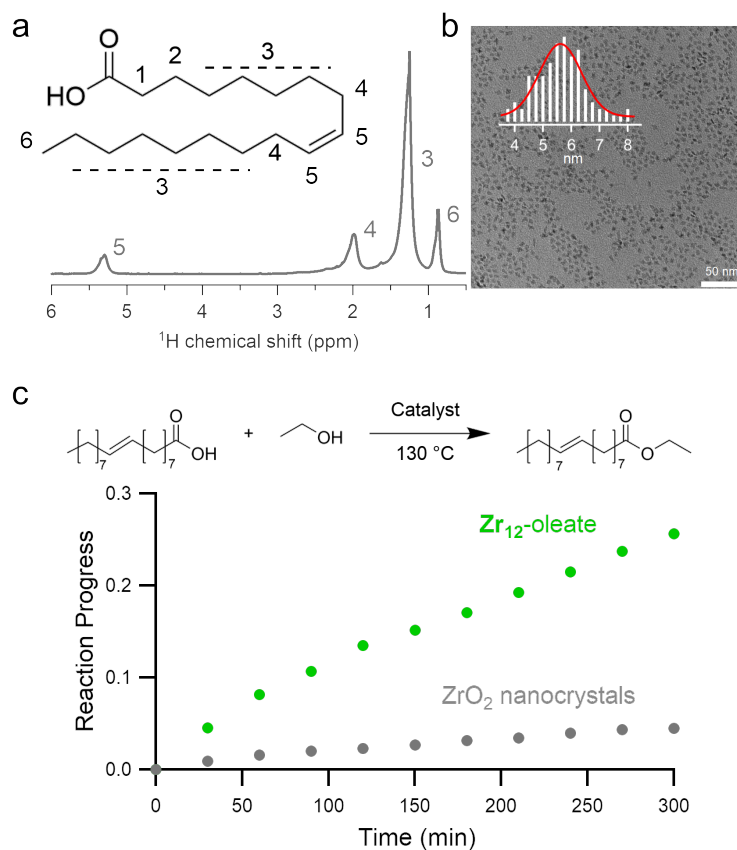
Figure 2.10: (a) ^{1}H NMR of 5.5 nm ZrO_2 nanoparticles in $CDCl_3$ and (b) TEM image of the nanoparticles with their corresponding size distribution. (c) Catalytic esterification of oleic acid with ethanol, catalyzed by either **Zr**$_{12}$-oleate (green) or ZrO_2 nanoparticles (gray). In both cases, 10 mol% Zr, with respect to the carboxylic acid substrate, was added.

The oxo clusters are clearly more catalytically active than the nanoparticles, confirming our hypothesis. An initial rate analysis shows that the rate of the reaction when using $\mathbf{Zr}_{12}$-acetate is 0.3 mM/min while for ZrO_2 nanoparticles it is 0.06 mM/min. The clusters feature thus about a five-fold higher reaction rate, which we relate to a higher surface-to-volume ratio. The cluster has every zirconium atom available at its surface. In contrast, based on the nanoparticle ligand density (5 nm^{-1}), we estimate that 19 % (about one fifth) of the zirconium atoms in the nanoparticles are available for catalysis. The other 81 % is buried under the surface. This estimation agrees well with the five-fold rate enhancement of the clusters. Zirconium and especially hafnium are less abundant elements so ensuring that all metal atoms are available for catalysis and not lost in the bulk is an important step towards a more sustainable catalyst design.[35] These results show that fatty acid capped oxo clusters are an exciting class of materials and they can possess advantages over their larger relatives; oxide nanoparticles. One can thus consider (oxo) clusters for many more catalytic reactions that are currently performed with nanoparticle catalysts. As atomically precise nanoparticle prototypes, the oxo clusters are also better suited for mechanistic studies compared to nanoparticles which feature polydispersity and a more irregular surface structure.[36;37]

2.3   Conclusion

We have synthesised fatty acid capped zirconium and hafnium oxo clusters with a library of linear and branched carboxylic acids. To prove the structure of the oxo clusters, we used X-ray PDF analysis. We showed that the structure models need to include the carboxylate binding groups to obtain excellent refinements. Given the larger scattering power of hafnium, the refinements were even more straightforward for the hafnium oxo clusters. This allowed us to prove the structure of our fatty acid capped oxo clusters, despite the fact that they cannot be crystallized. Because of the lack of crystallization, we developed purification protocols similar to the ones for colloidal nanoparticles, reinforcing the notion that these fatty acid capped oxo clusters are indeed atomically precise nanoparticle prototypes, of the smallest conceivable scale.
We further comprehensively characterized the oxo clusters by FTIR, NMR, TGA and ESI-HR-MS. We find that the cationic cluster cores are charge balanced by chelating and bridging carboxylate ligands and that a small excess of carboxylic acid is hydrogen bonded to the cluster core. Using our characterization tools, we studied carboxylate for carboxylate ligand exchange and found that the $\mathbf{Zr}_6/\mathbf{Hf}_6$ monomer and the $\mathbf{Zr}_{12}/\mathbf{Hf}_{12}$ dimer

structure can be converted into each other, depending on the structure of the final ligand. Finally, we compared the catalytic performance of the clusters with larger oxide nanoparticles. We found that, for the same amount of added zirconium, the oxo clusters show a five time higher esterification rate than oxide nanoparticles, due to their higher surface area. Since oxo clusters represents the limit of downscaling oxide nanoparticles, we thus propose them here as attractive materials, or at least as atomically precise model systems.

2.4   Perspective

Although we have greatly increased the solubility of these systems and therefore their potential applications, many questions remain unanswered. Do these clusters remain stable after catalysis, or does the esterification cause structural changes in the cluster? What types of catalytic reactions can be performed using our atomically precise clusters? Can ligands with other binding groups also bind to the surface of the cluster and does the trend for group 4 metal oxide nanoparticles ligand binding groups (carboxylic acid < phosphinic acid < phosphonic acid)[38;39] apply to clusters? The knowledge gap between the nanoparticle field and the group 4 oxo cluster field is currently very large. The field of nanoparticles has received tremendous interest in the last decades, resulting in numerous mechanistic[8;40] and surface chemistry studies.[41;42] The cluster field, on the other hand, has received little attention since the 1990s which I believe can be mainly ascribed to their limitation in possible ligands and lack of characterization techniques. In order to fully exploit their potential we will need to deepen our understanding of these fascinating materials by addressing the questions raised above.

2.5   Experimental

2.5.1   Synthetic procedures

Chemicals. Zirconium propoxide (70w% in 1-propanol) and hafnium butoxide (99%) are provided by Sigma Aldrich and stored in a Straus flask upon arrival. Acetic acid (>99%) is purchased from Sigma Aldrich and vacuum distilled after which it is stored in a Schlenk flask. Zirconium isopropoxide isopropanol complex (99.9%), Propionic acid (>99.5%), butanoic acid (99%), hexanoic acid (99%), octanoic acid (99%), decanoic acid (>99.5%), dodecanoic acid, oleic acid (90%), methyl-butanoic acid (98%), methyl-heptanoic acid (>98.5%), pivalic acid (99%), and benzyl alcohol

(anhydrous, 99.8%) were bought from Sigma Aldrich and used without any further purificiation. Acetone, dichloromethane (DCM) and diethylether (BHT stabilized) were bought from Biosolve and used without any further purification. Acetonitrile (ACN) HPLC grade was bought from VWR and used without any further purification. All yields reported here are calculated without any co-precipitated molecules unless otherwise specified. Centrifugation was always done at 5000 rcf for 3 minutes, unless otherwise specified. After purification all clusters are stored in a desicator.

Synthesis of Zr_{12}-acetate. A 20 mL vial was equipped with a septum and cycled three times between argon and vacuum. Zirconium propoxide (2.25 mL, 5 mmol, 1 eq.) was added to the vial, together with dry DCM (5.463 mL). Under stirring, distilled acetic acid (2.287 mL, 40 mmol, 8 eq.) was injected, reaching a total reaction volume of 10 mL and thus a zirconium concentration of 0.5 M. After 12 hours at room temperature (19-24 °C), the crystalline powder is isolated by filtration and further washed with 50 mL of a DCM : acetic acid mixture (4 : 1). Finally, the white powder was dried overnight under high vacuum. The powder was stored in a desiccator. The cluster was obtained as a white solid, with a 98% yield, calculated based on the molecular formula: $Zr_{12}O_8(OH)_8(CH_3COO)_{24} \cdot 6\,CH_3COOH \cdot 3.5\,DCM$.

Synthesis of Zr_{12}-propionate. Zirconium propoxide (2.35 mL, 5.22 mmol, 1 eq.) was mixed with propionic acid (3.13 mL, 41.8 mmol, 8 eq.). After overnight reaction the solid was washed with a 1-propanol : propionic acid mixture (ratio 1 : 3.4). After washing, the solid was dried for 8 hours on a Schlenk line. **Zr_{12}-propionate** $(Zr_{12}O_8(OH)_8(CH_3CH_2COO)_{24} \cdot 6\,CH_3CH_2COOH))$ was obtained as a white solid with a yield of 51%, calculated based on the molecular formula.

Synthesis of Zr_{12}-butanoate, hexanoate and octanoate. For butanoate, hexanoate and octanoate capped clusters, zirconium propoxide (2.25 mL, 5 mmol, 1 eq.) was first mixed with DCM, and afterwards 8 equivalents of acid was added. The amount of DCM is adjusted to maintain a Zr concentration of 0.5 M. After stirring for 24 hours at 30 °C the clusters were purified. The butanoate capped cluster was purified by evaporating the solvent using the Schlenk line after which a white waxy solid was obtained. Acetonitrile (15 mL) was added and the clusters were macerated overnight. After centrifugation for 4 minutes at 5000 rcf the supernatant was discarded and the clusters were dried on the Schlenk line for 24 h yielding a white solid. For hexanoate and octanoate clusters the solution was divided over 2 large centrifuge tubes (approximately 5 mL reaction mixture in each) and acetonitrile (10 mL) was added to each centrifuge tube in order to precipitate the clusters. Using centrifugation (5000 rcf, 4 min), the

cluster (viscous oil) was separated from the supernatant and both oils were redissolved in DCM (1 mL). To each tube 6 mL acetonitrile was added to precipitate the cluster. This last step was repeated twice and finally, the clusters were dried overnight under vacuum. **Zr$_{12}$**-hexanoate was obtained as a waxy solid and **Zr$_{12}$**-octanoate was obtained as a viscous liquid. **Zr$_{12}$**-butanoate was obtained with a yield of 49%. Zr$_{12}$-hexanoate was obtained as a waxy solid with a yield of 71%. **Zr$_{12}$**-octanoate was obtained as a viscous oil with a yield of 52%.

Synthesis of Zr$_{12}$-decanoate, dodecanoate and oleate. For decanoic and dodecanoic acid, zirconium propoxide (2.25 mL, 5 mmol, 1 eq.) was mixed with 8 equivalents of acid and diluted with DCM to 0.33 M and 0.25 M respectively in Zr. Decanoic and dodecanoic acids are solids and therefore the concentration had to be lowered in order to dissolve these acids. For oleic acid (which is a liquid), the volume is already 15 mL without DCM. Therefore, no DCM was added and a 40 mL flask was used. After stirring for 24 hours at 30 °C, DCM was evaporated using the Schlenk line for both Zr$_{12}$-decanoate and Zr$_{12}$-dodecanoate, while the oleate sample can be purified as such. The solution for each cluster was divided over 2 centrifuge tubes and ACN (10 mL per tube) was added to precipitate the clusters. Via centrifugation (5000 rcf, 4 min), the cluster precipitate was separated from the supernatant and redissolved in DCM (1 mL). To this 6 mL acetone was added to precipitate the cluster. This last step was repeated twice and finally, the clusters were dried under vacuum. **Zr$_{12}$**-decanoate and **Zr$_{12}$**-dodecanoate were obtained as waxy solids with a yield of 80% and 93% respectively. Finally, **Zr$_{12}$**-oleate was obtained as a viscous oil with a yield of 83%.

Synthesis of Zr$_6$-methylbutanoate and methylheptanoate. Zirconium propoxide (2.25 mL, 5 mmol, 1 eq.) was mixed with 8 equivalents of acid and diluted with DCM to 0.5 M in Zr. After stirring for 48 hours at 30 °C, the solution was dried under vacuum and dissolved again in 1 mL DCM. Afterwards, the solution is divided over 2 centrifuge tubes and acetonitrile (4 mL per tube) was added to precipitate the clusters. Via centrifugation (5000 rcf, 5 min), the cluster precipitate was separated from the supernatant and redissolved in DCM (1 mL each). To both tubes acetonitrile (double the volume) was added to precipitate the cluster. This last step was repeated twice and finally, the clusters were dried overnight under vacuum. **Zr$_6$**-methylbutanoate was obtained as a white solid with a yield of 93%. **Zr$_6$**-methylheptanoate was obtained as a viscous oil with a yield of 55%.

Zr$_{12}$-acetate ligand exchange. The **Zr$_{12}$**-acetate cluster (200 mg, 1.4

mmol acetate, 1 eq.) was weighed into a 20 mL vial. The incoming carboxylic acid (1.5 equivalents) was added together with 1 mL of DCM and stirred for 60 min, after which a clear solution was obtained. Subsequently, the solution was further stirred under vacuum at 70 °C for 1 hour. The sample transforms from a heterogeneous mixture into a viscous liquid. 1 purification step was performed as described above for the respective cluster. Yields: butanoic acid = 82%, methylbutanoic acid = 41%, hexanoic acid = 97.2%, octanoic acid = 95%, and oleic acid = 100%.

Zr_6-methylbutanoate ligand exchange. The **Zr_6**-methylbutanoate cluster (200 mg, 1.27 mmol methylbutanoate, 1 eq.) was weighed into a 20 mL vial. 2 mL DCM together with 3 equivalents of hexanoic acid were added and the solution was stirred for 1 hour at room temperature. Afterwards, the solution is dried under vacuum for 1 hour at 70 °C. One purification cycle was performed by dissolving the sample in 0.5 mL DCM and precipitating it by adding 2 mL ACN. This turbid solution was centrifuged at 5000 rcf for 4 minutes. The whole process was repeated once to ensure full exchange. After the second exchange step the sample was purified twice as described above. **Zr_{12}**-hexanoate was obtained as a viscous liquid with a yield of 56.5%.

2.5.2   Analysis techniques

General instrumentation. Nuclear Magnetic Resonance (NMR) measurements were recorded at 298K on Bruker UltraShield 500 spectrometer operating at a frequency of 500.13 MHz. The IR spectra were recorded on a Perkin Elmer spectrum 2 ATR-FTIR with a diamond crystal.

Mass spectrometry. ESI mass spectra were acquired using a Bruker maXis4G or maXis II high resolution mass spectrometer equipped with an electrospray ionization source. The cluster were dissolved in a mixture of ACN:DCM of which the amount of ACN was maximized while avoiding precipitation of the clusters. The samples were directly introduced into the instrument at a rate of 6 μL/min using a syringe pump. The heated capillary temperature was 200 °C and the capillary voltage was 3.6 kV. The samples were analyzed in positive ion mode. DataAnalysis 4.4 from Bruker was used to process the raw data.

Thermogravimetric analysis. Thermogravimetric analysis were carried out in a temperature range from 30 °C to 800 °C with a heating rate of 5 °C/min. To make sure everything is burned off quantitatively, the sample is kept at 800 °C for 15 minutes. During the measurement the air flow rate is 25 mL/min. and the balance flow is 10 mL/min.

Synchrotron X-ray total scattering experiments. Samples were prepared in 1 mm polyamide kapton tube and were measured either at beamline 11-ID-BM at Advanced Photon Source, Argonne National Laboratory, USA or at beamline P21.1 at DESY in Hamburg, Germany. X-ray total scattering data were collected at room temperature in rapid acquisition mode, using a Perkin Elmer digital X-ray flat panel amorphous silicon detector ($2048 \cdot 2048$ pixels and $200 \cdot 200$ μm pixel size) with a sample-to-detector distance of 180 mm (11-ID-BM) or 380 mm (P21.1). The incident wavelength of the X-rays was $\lambda = 0.2110$ Å (11-ID-BM) or 0.1220 Å (P21.1). Calibration of the experimental setup was performed using a Ni standard.

Analysis of synchrotron X-ray total scattering data. Raw 2D data were corrected for geometrical effects and polarization, then azimuthally integrated to produce 1D scattering intensities versus the magnitude of the momentum transfer Q (where $Q = 4\pi sin\theta/\lambda$ for elastic scattering) using pyFAI and xpdtools.[43;44] The program xPDFsuite with PDFgetX3 was used to perform the background subtraction, further corrections, and normalisation to obtain the reduced total scattering structure function F(Q), and Fourier transformation to obtain the pair distribution function (PDF), G(r).[45;46] For data reduction, the following parameters were used after proper background subtraction: Qmin = 0.8 Å^{-1}, Qmax = 22 Å^{-1}, Rpoly = 0.9 Å. We used the actual chemical composition of each cluster (inorganic core + charge balancing ligands) for data reduction. Modeling and fitting were carried out using Diffpy-CMI.[47] The Debye scattering equation was used to generate the calculated PDF from discrete structure models. The structure models are supplied as xyz files in the supporting information. The refinements were carried out by refining the scale factor, isotropic atomic displacement parameters (Uiso), and delta2 (coefficient for $1/r^2$ contribution to the peak sharpening). The exponentially dampening sine-wave contribution was calculated according to the following equation.

$$y = A\, e^{-\left(\frac{r-r_0}{2\sigma_{eff}}\right)^2} sin\left(2\pi(\frac{r}{\lambda} - \phi)\right)$$

A - Amplitude of oscillation, r - the distance in PDF, λ - wavelength, ϕ - phase shift, σ - effective dampening with $\sigma_{\text{eff}} = \sigma$ / a for r < r$_0$ and $\sigma_{\text{eff}} = \sigma \times a$ for r > r$_0$, a is the asymmetry parameter. r$_0$ is not a physical parameter in real space and is used to describe different dampening behavior.[17]

2.6   Contributions

PDF data processing and fitting was done by Rohan Pokratath. TGA measurements were performed by Eline Goossens. Catalytic experiments were done by Jiskon Pulparayil Mathew. HRMS measurements were performed by Dr. Michael Pfeffer.

References

[1] Puchberger, M.; Kogler, F. R.; Jupa, M.; Gross, S.; Fric, H.; Kickelbick, G.; Schubert, U. Can the Clusters $Zr_6O_4(OH)_4(OOCR)_{12}$ and $[Zr_6O_4(OH)_4(OOCR)_{12}]_2$ Be Converted into Each Other? *Eur. J. Inorg. Chem.* **2006**, *2006*, 3283–3293.

[2] Shen, Y.; Gee, M. Y.; Greytak, A. B. Purification technologies for colloidal nanocrystals. *Chemical Communications* **2017**, *53*, 827–841.

[3] Billinge, S. J. L. The rise of the X-ray atomic pair distribution function method: a series of fortunate events. *Philosophical Transactions of the Royal Society A: Mathematical, Physical and Engineering Sciences* **2019**, *377*, 20180413.

[4] Billinge, S. J. L.; Levin, I. The Problem with Determining Atomic Structure at the Nanoscale. *Science* **2007**, *316*, 561–565.

[5] Christiansen, T. L.; Cooper, S. R.; Jensen, K. M. v. There's no place like real-space: elucidating size-dependent atomic structure of nanomaterials using pair distribution function analysis. *Nanoscale Advances* **2020**, *2*, 2234–2254.

[6] Van den Eynden, D.; Pokratath, R.; De Roo, J. Nonaqueous Chemistry of Group 4 Oxo Clusters and Colloidal Metal Oxide Nanocrystals. *Chem Rev* **2022**, *122*, 10538–10572.

[7] Yang, X.; Masadeh, A. S.; McBride, J. R.; Bozin, E. S.; Rosenthal, S. J.; Billinge, S. J. L. Confirmation of disordered structure of ultrasmall CdSe nanoparticles from X-ray atomic pair distribution function analysis. *Physical Chemistry Chemical Physics* **2013**, *15*, 8480–8486.

[8] Pokratath, R.; Van den Eynden, D.; Rudd Cooper, S.; Katja Mathiesen, J.; Waser, V.; Devereux, M.; J. L. Billinge, S.; Meuwly, M.; Jensen, K.; De Roo, J. Mechanistic insight into the precursor chemistry of ZrO_2 and HfO_2 nanocrystals; towards size-tunable syntheses. *JACS Au* **2022**, *2*, 827–838.

[9] Banerjee, S.; Liu, C.-H.; Jensen, K. M. O.; Juhas, P.; Lee, J. D.; Tofanelli, M.; Ackerson, C. J.; Murray, C. B.; Billinge, S. J. L. Cluster-mining: an approach for determining core structures of metallic nanoparticles from atomic pair distribution function data. *Acta Crystallographica Section A* **2020**, *76*, 24–31.

[10] Cooper, S. R.; Candler, R. O.; Cosby, A. G.; Johnson, D. W.; Jensen, K. M. O.; Hutchison, J. E. Evolution of Atomic-Level Structure in Sub-10 Nanometer Iron Oxide Nanocrystals: Influence on Cation Occupancy and Growth Rates. *ACS Nano* **2020**, *14*, 5480–5490.

[11] Pradhan, S. K.; Mao, Y.; Wong, S. S.; Chupas, P.; Petkov, V. Atomic-Scale Structure of Nanosized Titania and Titanate: Particles, Wires, and Tubes. *Chemistry of Materials* **2007**, *19*, 6180–6186.

[12] Ichikawa, R. U.; Roca, A. G.; Lopez-Ortega, A.; Estrader, M.; Peral, I.; Turrillas, X.; Nogués, J. Combining X-Ray Whole Powder Pattern Modeling, Rietveld and Pair Distribution Function Analyses as a Novel Bulk Approach to Study Interfaces in Heteronanostructures: Oxidation Front in FeO/Fe_3O_4 Core/Shell Nanoparticles as a Case Study. *Small* **2018**, *14*, 1800804.

[13] Jensen, K. M. v.; Juhas, P.; Tofanelli, M. A.; Heinecke, C. L.; Vaughan, G.; Ackerson, C. J.; Billinge, S. J. L. Polymorphism in magic-sized $Au_{144}(SR)_{60}$ clusters. *Nature Communications* **2016**, *7*, 11859.

[14] Beecher, A. N.; Yang, X.; Palmer, J. H.; LaGrassa, A. L.; Juhas, P.; Billinge, S. J. L.; Owen, J. S. Atomic Structures and Gram Scale Synthesis of Three Tetrahedral Quantum Dots. *J. Am. Chem. Soc.* **2014**, *136*, 10645–10653.

[15] Anker, A. S.; Christiansen, T. L.; Weber, M.; Schmiele, M.; Brok, E.; Kjear, E. T. S.; Juhas, P.; Thomas, R.; Mehring, M.; Jensen, K. M. O. Structural Changes during the Growth of Atomically Precise Metal Oxido Nanoclusters from Combined Pair Distribution Function and Small-Angle X-ray Scattering Analysis. *Angewandte Chemie International Edition* **2021**, *60*, 20407–20416.

[16] Williamson, C. B.; Nevers, D. R.; Nelson, A.; Hadar, I.; Banin, U.; Hanrath, T.; Robinson, R. D. Chemically reversible isomerization of inorganic clusters. *Science* **2019**, *363*, 731–735.

[17] Zobel, M.; Neder, R. B.; Kimber, S. A. J. Universal solvent restructuring induced by colloidal nanoparticles. *Science* **2015**, *347*, 292–294.

[18] Chen, Z.; Chen, Z.; Farha, O. K.; Chapman, K. W. Mechanistic Insights into Nanoparticle Formation from Bimetallic Metal-Organic Frameworks. *Journal of the American Chemical Society* **2021**, *143*, 8976–8980.

[19] Hennig, C.; Weiss, S.; Kraus, W.; Kretzschmar, J.; Scheinost, A. C. Solution Species and Crystal Structure of Zr(IV) Acetate. *Inorganic Chemistry* **2017**, *56*, 2473–2480.

[20] Kogler, F. R.; Jupa, M.; Puchberger, M.; Schubert, U. Control of the Ratio of Functional and Non-Functional Ligands in Clusters of the Type $Zr_6O_4(OH)_4(carboxylate)_{12}$ for their Use as Building Blocks for Inorganic-Organic Hybrid Polymers. *J. Mater. Chem.* **2004**, *14*, 3133–3138.

[21] Kickelbick, G.; Schubert, U. Oxozirconium Methacrylate Clusters: $Zr_6(OH)_4O_4(OMc)_{12}$ and $Zr_4O_2(OMc)_{12}$ (OMc = Methacrylate). *Ber. Dtsch. Chem. Ges.* **1997**, *130*, 473–478.

[22] Trimmel, G.; Gross, S.; Kickelbick, G.; Schubert, U. Swelling Behavior and Thermal Stability of Poly(methylmethacrylate) Crosslinked by the Oxozirconium Cluster $Zr_4O_2(methacrylate)_{12}$. *Appl. Organomet. Chem.* **2001**, *15*, 401–406.

[23] Kickelbick, G.; Schubert, U. Hydroxy Carboxylate Substituted Oxozirconium Clusters. *J. Chem. Soc., Dalton Trans.* **1999**, *8*, 1301–1306.

[24] Nateghi, B.; Boldog, I.; Domasevitch, K. V.; Janiak, C. More Versatility than thought: Large Zr_{26} Oxocarboxylate Cluster by Corner-Sharing of Standard Octahedral Subunits. *CrystEngComm.* **2018**, *20*, 5132–5136.

[25] Boyle, T. J.; Ottley, L. A. M.; Rodriguez, M. A. Structurally characterized carboxylic acid modified zirconium alkoxides for the production of zirconium oxide thin films. *Polyhedron* **2005**, *24*, 1727–1738.

[26] Qian, X.; Li, J.; Peng, X. a Liquid-Phase Infrared Strategy for Quantification of Surface Alkanoate Ligands on Colloidal Nanocrystals. *Chemistry of Materials* **2022**, *34*, 7006–7014.

[27] Piszczek, P.; Radtke, A.; Grodzicki, A.; Wojtczak, A.; Chojnacki, J. The New Type of $[Zr_6(\mu_3-O)_4(\mu_3-OH)_4]$ Cluster Core: Crystal Structure and Spectral Characterization of $[Zr_6O_4(OH)_4(OOCR)_{12}]$ (R=But, $C(CH_3)_2Et$). *Polyhedron* **2007**, *26*, 679–685.

[28] Zhang, J.; Zhang, H.; Cao, W.; Pang, Z.; Li, J.; Shu, Y.; Zhu, C.; Kong, X.; Wang, L.; Peng, X. Identification of Facet-Dependent Coordination Structures of Carboxylate Ligands on CdSe Nanocrystals. *Journal of the American Chemical Society* **2019**, *141*, 15675–15683.

[29] Deacon, G. B.; Phillips, R. J. Relationships between the carbon-oxygen stretching frequencies of carboxylato complexes and the type of carboxylate coordination. *Coordination Chemistry Reviews* **1980**, *33*, 227–250.

[30] Fritzinger, B.; Capek, R. K.; Lambert, K.; Martins, J. C.; Hens, Z. Utilizing Self-Exchange To Address the Binding of Carboxylic Acid Ligands to CdSe Quantum Dots. *Journal of the American Chemical Society* **2010**, *132*, 10195–10201.

[31] De Roo, J.; Yazdani, N.; Drijvers, E.; Lauria, A.; Maes, J.; Owen, J. S.; Van Driessche, I.; Niederberger, M.; Wood, V.; Martins, J. C.; et al., Probing Solvent-Ligand Interactions in Colloidal Nanocrystals by the NMR Line Broadening. *Chem. Mater.* **2018**, *30*, 5485–5492.

[32] Schubert, U. Clusters with a Zr_6O_8 core. *Coordination Chemistry Reviews* **2022**, *469*, 214686.

[33] De Roo, J.; Van Driessche, I.; Martins, J. C.; Hens, Z. Colloidal metal oxide nanocrystal catalysis by sustained chemically driven ligand displacement. *Nat. Mater.* **2016**, *15*, 517–521.

[34] Garnweitner, G.; Goldenberg, L. M.; Sakhno, O. V.; Antonietti, M.; Niederberger, M.; Stumpe, J. Large-scale synthesis of organophilic zirconia nanoparticles and their application in organic-inorganic nanocomposites for efficient volume holography. *Small* **2007**, *3*, 1626–1632.

[35] Suess, H. E.; Urey, H. C. Abundances of the Elements. *Reviews of Modern Physics* **1956**, *28*, 53–74.

[36] Hens, Z.; De Roo, J. Atomically Precise Nanocrystals. *J. Am. Chem. Soc.* **2020**, *142*, 15627–15637.

[37] Drijvers, E.; De Roo, J.; Martins, J. C.; Infante, I.; Hens, Z. Ligand Displacement Exposes Binding Site Heterogeneity on CdSe Nanocrystal Surfaces. *Chem. Mater.* **2018**, *30*, 1178–1186.

[38] Deblock, L.; Goossens, E.; Pokratath, R.; De Buysser, K.; De Roo, J. Mapping out the Aqueous Surface Chemistry of Metal Oxide Nanocrystals: Carboxylate, Phosphonate, and Catecholate Ligands. *JACS Au* **2022**, *2*, 711–722.

[39] Dhaene, E.; Pokratath, R.; Aalling-Frederiksen, O.; Jensen, K. M. Ã.; Smet, P. F.; De Buysser, K.; De Roo, J. Monoalkyl Phosphinic Acids as Ligands in Nanocrystal Synthesis. *ACS Nano* **2022**, *16*, 7361–7372.

[40] LaMer, V. K.; Dinegar, R. H. Theory, Production and Mechanism of Formation of Monodispersed Hydrosols. *Journal of the American Chemical Society* **1950**, *72*, 4847–4854.

[41] Yang, Y.; Qin, H.; Jiang, M.; Lin, L.; Fu, T.; Dai, X.; Zhang, Z.; Niu, Y.; Cao, H.; Jin, Y.; Zhao, F.; Peng, X. Entropic Ligands for Nanocrystals: From Unexpected Solution Properties to Outstanding Processability. *Nano Letters* **2016**, *16*, 2133–2138.

[42] Boles, M. A.; Ling, D.; Hyeon, T.; Talapin, D. V. The surface science of nanocrystals. *Nature Materials* **2016**, *15*, 141–153.

[43] Ashiotis, G.; Deschildre, A.; Nawaz, Z.; Wright, J. P.; Karkoulis, D.; Picca, F. E.; Kieffer, J. The fast azimuthal integration Python library:pyFAI. *Journal of Applied Crystallography* **2015**, *48*, 510–519.

[44] Wright CJ, Z. X. Computer-assisted area detector masking. *Journal of Synchrotron Radiation* **2017**, *24(Pt 2)*, 506–508.

[45] Juhas, P.; Davis, T.; Farrow, C. L.; Billinge, S. J. L. PDFgetX3: a rapid and highly automatable program for processing powder diffraction data into total scattering pair distribution functions. *Journal of Applied Crystallography* **2013**, *46*, 560–566.

[46] Yang, X.; Juhas, P.; Farrow, C. L.; Billinge, S. J. xPDFsuite: an end-to-end software solution for high throughput pair distribution function transformation, visualization and analysis. *arXiv preprint arXiv:1402.3163* **2014**.

[47] Juhas, P.; Farrow, C. L.; Yang, X.; Knox, K. R.; Billinge, S. J. L. Complex modeling: a strategy and software program for combining multiple information sources to solve ill posed structure and nanostructure inverse problems. *Acta Crystallographica* **2015**, *A71*, 562–568.

3

Formation mechanism of Zirconium and Hafnium oxo clusters

An experiment is a question which science poses to nature, and a measurement is the recording of nature's answer.
– Max Planck

3.1 Introduction

Several methods are available to synthesise oxo clusters. In aqueous media of low pH, the tetrameric cluster $[Zr_4(OH)_8(OH_2)_{16}]^{8+}$ is present. Upon addition of acetic acid and adjustment of the pH to 1.5, the $\mathbf{Zr_6}$-acetate cluster (with each ligand in bridging mode) was crystallized.[1] The $\mathbf{Zr_{12}}$-acetate cluster was obtained by solvothermal treatment (110 °C) of zirconyl chloride ($ZrOCl_2$) with acetic acid in dimethylformamide (DMF).[2] While it is possible to synthesise MOFs from pre-synthesised oxo clusters,[2–5] the clusters are most often formed *in situ* from $ZrOCl_2$ or $ZrCl_4$.[6] *In situ* Pair Distribution Function (PDF) analysis showed that the $\mathbf{Zr_6}$ clusters are already present in a mixture of $ZrCl_4$, DMF and aqueous HCl, before the addition of difunctional carboxylates.[7] Similar results have been found for

hafnium oxo clusters in MOF reaction mixtures.[8] A slower and more controlled synthesis of oxo clusters involves the reaction of metal alkoxides with carboxylic acid, similar to the synthetic methods developed in chapter 2.[9] A variety of conditions have been reported.[10] While most reactions are performed at room temperature, elevated temperatures appear to be required for rapid cluster formation with sterically hindered carboxylate ligands such as pivalic and benzoic acid.[11;12] The formation mechanism of these octahedron shaped clusters remains unclear. Starting from the usual zirconium propoxide, the unbalanced reaction is written as:

$$6\,\mathrm{Zr(OPr)_4} \,+\, \text{excess}\,\mathrm{RCOOH} \longrightarrow \mathrm{Zr_6O_4(OH)_4(OOCR)_{12}} \,+\, \mathrm{RCOOPr}$$

$$(3.1)$$
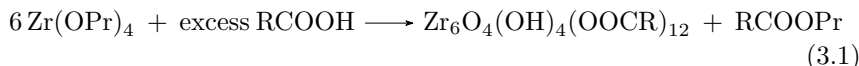
If only a few (i.e. 1 or 2) equivalents of acids are added, ligand exchange takes place.[10;13] The first equivalent of carboxylate exchanges exothermically with one alkoxide.[13]

$$\mathrm{Zr(OPr)_4} \,+\, \mathrm{RCOOH} \xrightarrow{\Delta H < 0} \mathrm{Zr(OPr)_3(OOCR)} \,+\, \mathrm{PrOH} \qquad (3.2)$$
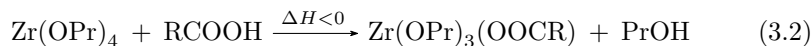
A second equivalent of carboxylic acid also reacts, although there is some evidence that only 80 % of the second equivalent coordinates. If more than two acid equivalents are added, ester is formed.[13] Even alcoholic solutions of $\mathrm{Zr(OPr)_3(OOCR)}$ or $\mathrm{Zr(OPr)_2(OOCR)_2}$ are not stable over extended periods of time and form ester.[13;14] A variety of complexes/clusters (**Zr$_2$**-**Zr$_5$**) have been isolated from various zirconium alkoxides and one equivalent of various carboxylic acids, some of which are displayed in Figure 3.1.[15] Initially, it was hypothesized that free acid and alcohol form ester and water.[13;16] Later, it was found that Zr catalyzes the esterification reaction.[14] A clear solvent dependence on the esterification kinetics was observed with the esterification rate decreasing in the series:

$$\text{dichloromethane} > \text{benzene} \gg \text{tetrahydrofuran}$$

Water formed in the esterification process is hypothesized to cause hydrolysis and condensation of the zirconium complex.

$$\mathrm{Zr(OPr)_2(OOCR)_2} \,+\, 2\,\mathrm{H_2O} \longrightarrow \mathrm{Zr(OH)_2(OOCR)_2} \,+\, 2\,\mathrm{PrOH}$$
$$6\,\mathrm{Zr(OH)_2(OOCR)_2} \longrightarrow \mathrm{Zr_6O_4(OH)_4(OOCR)_{12}} \,+\, 4\,\mathrm{H_2O}$$

$$(3.3)$$
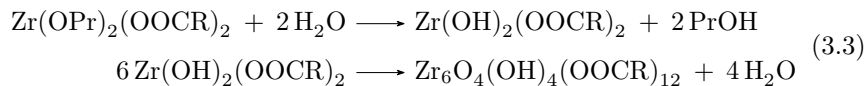
Evidence for a **Zr$_3$** cluster intermediate has been provided by Extended X-ray Absorption Fine Structure (EXAFS),[14] although no precise structure has been provided. Therefore, the leading theory for cluster formation involves ligand exchange, catalyzed esterification, hydrolysis and condensation

through a **Zr**$_3$ intermediate, *en route* towards the **Zr**$_6$ product. However, detailed pathways and quantitative data on the kinetics is lacking. Previous studies have been hampered by the insolubility of the final cluster in solution, precluding, for example, EXAFS studies of the formation kinetics of the final cluster.

a

b

Zr$_2$(μ_2-O^{t}Bu)$_2$(O^{t}Bu)$_4$(^{t}BuCH$_2$COO)$_2$

Zr$_3$(μ_3-O)(μ_2-O^{i}Pr)$_2$(O^{i}Pr)$_3$(CH$_3$COO)$_5$

c

d

Zr$_4$(μ_2-O^{i}Pr)$_4$(O^{i}Pr)$_8$(^{i}PrCOO)$_4$

Zr$_5$(μ_3-O)$_3$(μ_2-O^{t}Bu)$_2$(O^{t}Bu)$_6$(^{t}BuCOO)$_6$
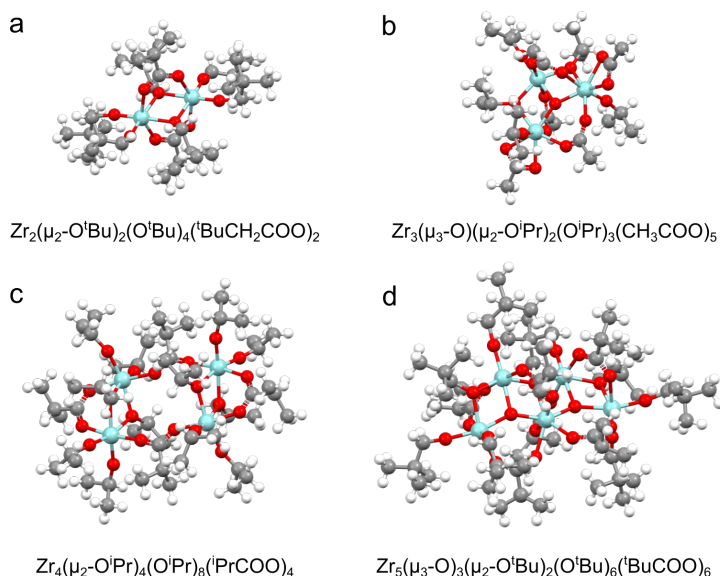
Figure 3.1: Isolated structures by Boyle *et al.* by reacting zirconium (depicted in blue) alkoxide with different equivalents of carboxylic acids with different sterical implications.[15] For every Zr nuclearity in between Zr(OPr)$_4$ and **Zr**$_6$ (i.e. 2-5) one or multiple structures were isolated.

Here, we set out to fully elucidate the reaction mechanism of zirconium (and hafnium) oxo cluster formation. We attempted to identify the mixed alkoxide/carboxylate metal species as well as the reaction intermediates. This was achieved via NMR, FTIR and *in situ* EXAFS. The reaction kinetics were studied by adjusting parameters such as concentration, temperature, equivalents and sterical hindrance to gain more control over the synthesis. We found that the synthesis proceeds equally well in ethylacetate, compared to DCM, making this synthesis more sustainable for the future. Understanding the formation mechanism will aid the development of novel doped clusters. For example, cerium and thorium form isostructural Ce$_6$[17;18] and Th$_6$[19] clusters to Zr$_6$ and Hf$_6$. Knowledge of the reaction kinetics and formation mechanism may be used to rationalise the formation of novel mixed Zr-Hf-Ce-Th clusters.

3.1.1 Model cluster formation reaction

The prototypical reaction, which was optimized in chapter 2, i.e. the reaction between $Zr(OPr)_4$ with 8 equivalents of acid was used as model system. For tracking the ester formation using NMR ,the faster reaction between $Zr(OPr)_4$ and 8 equivalents of acetic acid was preferred. (*vide infra*) Several *in situ* EXAFS experiments were conducted using a synchrotron radiation source. However, here the consideration had to be made that the clusters with short ligands precipitate from the reaction mixture and will therefore not be measured or alternatively clog the flow setup. Thus, for the *in situ* experiments the reaction between $Zr(OPr)_4$ and 8 equivalents of butanoic acid was studied since these clusters stay in solution for the whole duration of the synthesis.

On both of these model synthesis, the reaction conditions were altered and either cluster or side product formation were tracked over time. Obvious conditions such as temperature and concentration of both reagents were tested. Additionally, the influence of sterical hindrance on both the metal alkoxide and the carboxylic acid was studied, i.e. linear molecules versus branched molecules. Finally, also the zirconium alkoxide was exchanged for a hafnium alkoxide.

3.2 Results & discussion

3.2.1 From dimer to trimer

The precursor, $Zr(OPr)_4$ (70 w%) in propanol has a molar ratio of $Zr(OPr)_4$: PrOH of 1 : 2.33. The complex dimerizes and coordinates one equivalent of propanol per zirconium, similar to the crystalline compound $Zr(OiPr)_4$. $iPrOH$.[20;21] (See Figure 3.2) We confirmed the structure of the precursor dissolved in DCM at the relevant concentration for cluster synthesis before injection of the carboxylic acid (0.65 mol/L) by EXAFS, the chemical structure is displayed in Figure 3.2. In the EXAFS analysis, the asymmetric first-shell coordination of Zr is described by including three different two-body ($\gamma^{(2)}$) Zr-O scattering terms, together with a Zr-Zr contribution, which derives from the dimer formation in solution. Indeed, as presented in Table 3.1, the Zr-Zr degeneration is 1, corroborating the dimeric nature of the compound, while the degeneracy of each Zr-O scattering term is 2, which indicates a total coordination number (CN) around zirconium of 6. The retrieved interatomic distances are in good agreement with previous studies of zirconium alkoxides, measured at high concentrations (> 1 mol/kg).[14;21]

R = -CH$_2$CH$_2$CH$_3$
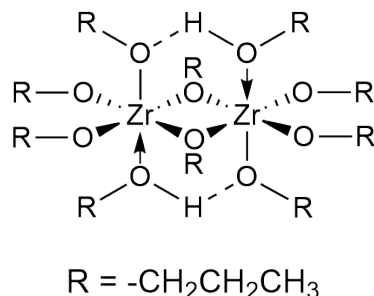
Figure 3.2: Dimeric structure of Zr(OPr)$_4$ where 2 HOPr molecules form H-bridges which increases the coordination number to 6.

Table 3.1: EXAFS results on 0.65 M Zr(OPr)$_4$ in dichloromethane. Four two-body ($\gamma^{(2)}$) terms are used to describe the overall EXAFS signal. Bond lengths, Debye-Waller (DW) factors, and degeneracy values are reported. Values in brackets indicate the error on the last significant figure.

Signal	Bond length / Å	DW factor (σ^2) / Å^2	Degeneracy
$\gamma^{(2)}$(Zr-O1)	1.965(5)	0.003(1)	2.0(2)
$\gamma^{(2)}$(Zr-O2)	2.165(5)	0.016(2)	2.0(3)
$\gamma^{(2)}$(Zr-O3)	2.225(6)	0.008(2)	2.0(2)
$\gamma^{(2)}$(Zr-Zr)	3.51(9)	0.015(5)	1.0(1)

To synthesise oxo clusters, 8 equivalents of carboxylic acid is added to the dissolved precursor. We first monitor the coordination environment at lower acid equivalents added. In the ^{1}H NMR spectrum, a broad resonance at 3.6 ppm increases in intensity upon gradual addition of acetic acid (Figure 3.3a). It is assigned to propanol, but the resonance lacks fine structure, indicating exchange between free and coordinated propanol. Multiple broad resonances between 3.6 and 4.2 ppm are assigned to propoxide, in multiple coordination environments. Given also that free acetic acid is detected in FTIR only after the third equivalent (Figure 3.3b), we conclude that the first two equivalents of acid nearly fully exchange for propoxide. It appears to be nearly full exchange since a very small signal for RCOOH can be observed for the spectrum with 1 and 2 equivalents of acetic acid. The third equivalent does not exchange quantitatively and we also observe the first ester resonance; a triplet at 4 ppm. In FTIR the ester cannot be observed due to it's low concentration and high volatility. The region for acetic acid also shows multiple environments for bound acetate for 1-2 equivalents

added. For 3 equivalents, only one resonance is observed, probably due to exchange between free acetic acid and bound acetate.
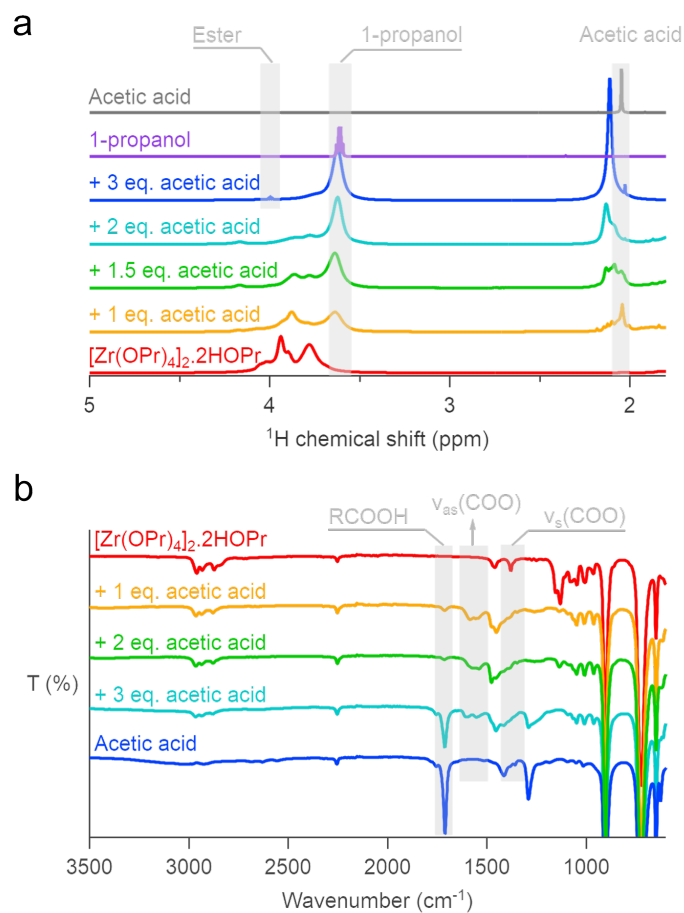
Figure 3.3: The interaction between $Zr(OPr)_4$ and acetic acid. (a) ^1H NMR spectra in $CDCl_3$ of the titration of $Zr(OPr)_4$ with several equivalents of acetic acid in $CDCl_3$ measured at room temperature, $[Zr] = 0.09$ M. (b) Attenuated total reflection (ATR) FTIR spectra of the same titration as in panel a.

$Zr(OPr)_4$ with one or two equivalents of butanoic acid was also analyzed using EXAFS using a flow setup, see Figure A.32. After the addition of 1 equivalent of acid and an equilibration time of 60 minutes, the first-shell coordination of Zr can be fitted with a total $\gamma^{(2)}$(Zr-O) degeneracy

of 8.0(6) and a Zr-Zr contribution with degeneracy equal to 1.3(6) (see Table 3.2). Despite the large error on the second shell contribution due to the low signal/noise ratio of the experimental data, we can assume that, after adding one equivalent, the dimer persists in solution with an altered first-coordination shell, likely due to the ligand exchange. The addition of two equivalents of acid, instead, brings significant structural modifications. (Figure 3.4b) Indeed, according to the EXAFS analysis (Table 3.2), the Zr-O average distance is notably higher and the Zr-Zr path degeneracy increases to $\sim$2, suggesting the formation of a **Zr$_3$** trimer, even before any ester is formed.

Table 3.2: EXAFS results on Zr(OPr)$_4$ with one and two equivalents of butanoic acid. Bond lengths, Debye-Waller (DB) factors, and degeneracy values are reported. Values in brackets indicate the error on the last significant figure.

Signal	Bond length	DW factor	Degeneracy
1 equivalent			
$\gamma^{(2)}$Zr-O1	1.974(6)	0.012(2)	4.0(3)
$\gamma^{(2)}$Zr-O2	2.224(5)	0.006(2)	4.0(3)
$\gamma^{(2)}$Zr-Zr	3.48(6)	0.010(5)	1.3(6)
2 equivalents			
$\gamma^{(2)}$Zr-O1	2.08(1)	0.024(3)	4.0(4)
$\gamma^{(2)}$Zr-O2	2.223(6)	0.004(1)	4.0(3)
$\gamma^{(2)}$Zr-Zr	3.43(3)	0.011(4)	2.2(6)

Comparing with literature, these results are remarkable. Peter *et al.* studied the modification of zirconium alkoxides by acetic acid (1-3 equivalents) through EXAFS, and found that the coordination number remained six and the dimer stayed intact.[22] Peter *et al.* performed their measurements at 0.03 mol/kg in the parent alcohol, which is more than ten-fold more dilute than our measurements. This points to a highly concentration dependent speciation. Our results do agree with the study of Kickelbick *et al.*, where the same trimer and the same Zr-Zr interatomic distance of $\sim$3.4Å was determined.[14] Kickelbick *et al.* performed their measurements *in situ* during a cluster synthesis, and assigned the trimer as an intermediate. Here we find that the trimer is formed before any ester formation and rather than an intermediate, it is the actual precursor for the reaction.
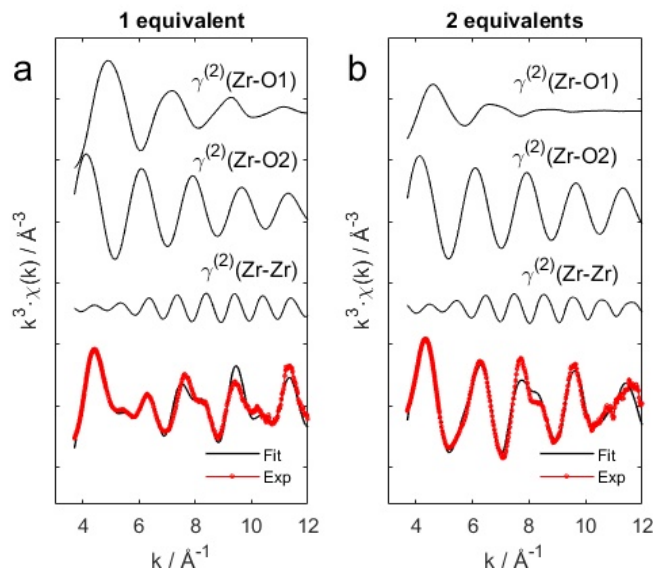
Figure 3.4: EXAFS fit of 0.5 M Zr(OPr)$_4$ reacted with 1 (a) and 2 (b) equivalents of butanoic acid. Considerable structural changes are observed between both samples compared to the Zr(OPr)$_4$ precursor.

3.2.2   Esterification kinetics

Ester is the byproduct of cluster formation and its concentration can be monitored via solution ^{1}H NMR spectroscopy. This delivers a faster and more convenient method to evaluate the reaction kinetics under various conditions, compared to synchrotron experiments. We probed the kinetics by changing the reaction conditions such as temperature, zirconium concentration, acid concentration, HOPr concentration, temperature, nature of alkoxide, solvent and nature of the carboxylic acid. The results are summarized in Figures 3.5 and 3.6.

Figure 3.5a defines the standard reaction. Zirconium propoxide (0.5 M) and acetic acid (4 M, i.e. 8 equivalents) react in dichloromethane at 15 °C. We first varied the concentration of acetic acid, see Figure 3.5 b. The reaction rate clearly increases with the acid concentration, indicating that the acid is part of the rate equation. For any concentration higher than 1 M (= 2 equivalents), one can distinguish a rapid initial build up of ester to approximately 0.17 M (1/3 of the Zr concentration) within the first minutes of the reaction. We assign this to one equivalent of ester per **Zr$_3$** trimer. This is followed by a secondary, slower ester formation for the remainder of the reaction.
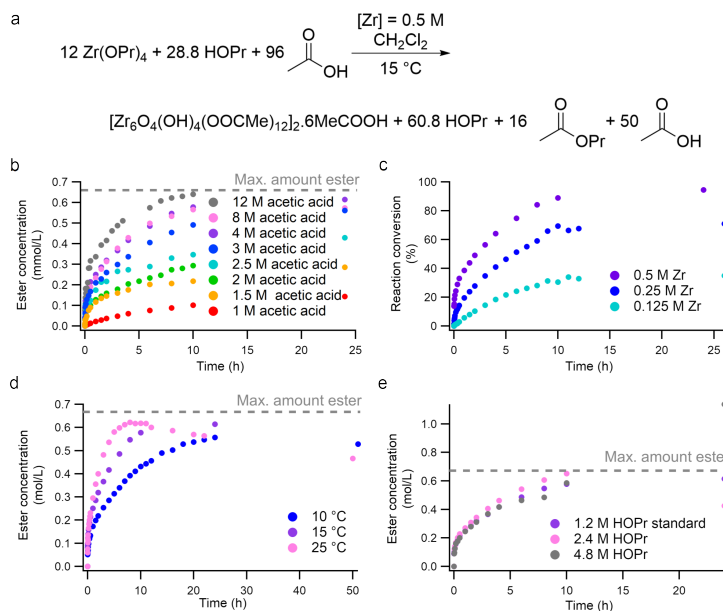
Figure 3.5: (a) Balanced reaction scheme for the standard reaction conditions; 0.5 M Zr(OPr)$_4$, 4 M acetic acid and 1.2 M HOPr at 15 °C. Tracking the ester formation via NMR (in CDCl$_3$) while varying the (b) acid concentration, (c) zirconium concentration (the data is normalised to the maximum amount of cluster), (d) the propanol concentration and (e) the temperature. The maximum amount of ester is indicated by the grey dashed line at 0.66 M.

The maximum concentration of ester reached is 0.66 M. This is a logical consequence of the chemical equation in Figure 3.5a. Based on mass balance, 16 ester molecules provide the necessary bridging O^{2-} and OH$^-$ moieties per **Zr**$_{12}$ cluster. This corresponds to $\frac{16}{12} \times 0.5M = 0.66M$. Given that the ester concentration does not exceed 0.66 M, the ester is purely a byproduct of the cluster formation. Indeed, a control experiment with propanol and acetic acid forms hardly any ester within the time frame of the cluster reaction. (See Figure A.33-A.35) Focusing on the esterification alone (and disregarding cluster assembly), one can write the **Zr**$_6$ cluster formation as

$$Zr_6(OPr)_{12}(OAc)_{12} \; + \; 8\,HOAc \longrightarrow Zr_6(OH)_8(OPr)_4(OAc)_{12} \; + \; 8\,PrOAc$$
$$Zr_6(OH)_8(OPr)_4(OAc)_{12} \longrightarrow Zr_6O_4(OH)_4(OAc)_{12} \; + \; 4\,HOPr$$

$$(3.4)$$
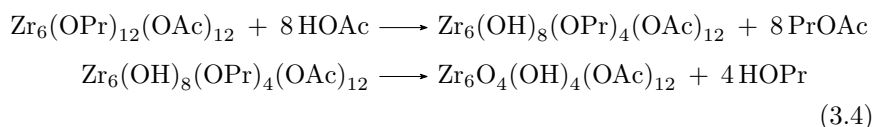
It is clear that not two equivalents of ester are required to form the cluster

but only 1.33 equivalents suffice. ($\frac{8 \ esters}{6 \ Zr} = 1.33$) With an acid concentration < 3 M the ester formation was reduced, indicating that at least 6 equivalents of acid with respect to zirconium is needed to form cluster efficiently.

In Figure 3.5c the zirconium concentration was varied. We plotted the reaction conversion in percent to compare the different reactions. To calculate the reaction conversion, we assumed 1.33 equivalents of ester are formed at full conversion. The reaction rates decrease when the zirconium concentration is decreased. In addition, the lower concentration reactions do not reach full conversion. Only for the standard reaction a quantitative yield is obtained. The reactions where the zirconium concentration is halved and divided by 4 show a conversion of only 74 % and 35 % respectively. This indicates that the reaction mechanism contains concentration dependent equilibria. The temperature variation (Figure 3.5d) shows the expected trend. If the temperature is increased, the reaction reaches completion faster. At room temperature (25 °C), the reaction is completed in less than 10 hours. Curiously, the ester concentration slowly decreases after reaching full yield. The concentration of 1-propanol has little influence on the reaction kinetics and it is thus not part of the rate equation. Why the ester formation for the 4.8 M HOPr sample suddenly spike at 24h is currently unknown.

Finally, both the type of carboxylic acid and metal alkoxides are varied. Figure 3.6a shows that increasing the alkoxide sterical hindrance of the metal precursor from $Zr(OPr)_4$ to $Zr(OBu)_4$ slows down the ester formation. Interestingly, only the second, slower ester formation step is affected, the first 2h the reactions show identical ester formation rates. Since zirconium and hafnium form the same isostructural clusters, $Hf(OBu)_4$ was used to compare with $Zr(OBu)_4$. Interestingly, hafnium shows an intrinsic slower ester formation as compared to zirconium. This might be due to a slightly different M-O bond strength between zirconium and hafnium. When a more sterically imposed alkoxide is used, $Zr(O^iPr)_4$, both the initial ester formation and the secondary ester formation are significantly affected. When the temperature is increased to 40 °C, Figure 3.6b, the ester concentration increases to 0.45 M compared to 0.1 M at 15 °C. Finally, maximizing the sterical hindrance of the alkoxide inhibits the ester formation, as $Zr(O^tBu)_4$ is unreactive at both 15 and 40 °C. (See Figure 3.6b)

Increasing the chain length of the carboxylic acid also slows down the ester formation. Going from acetic acid to hexanoic acid, a chain increase of 4 carbons, the ester formation slows down. The concentration plateau is only reached after approximately 100h ($\sim$ 4 days). Whereas for the acetic acid synthesis the plateau is reached within 26h. Adding steric hindrance by adding a methyl group on the C-alpha of the acid, slows ester formation

down even more, only reaching the plateau after 337h (14 days) for methylheptanoic acid. While the second esterifcation step is greatly affected, the first rapid build up of ester to about 0.17 M is reasonably quick, even for the branched acid.
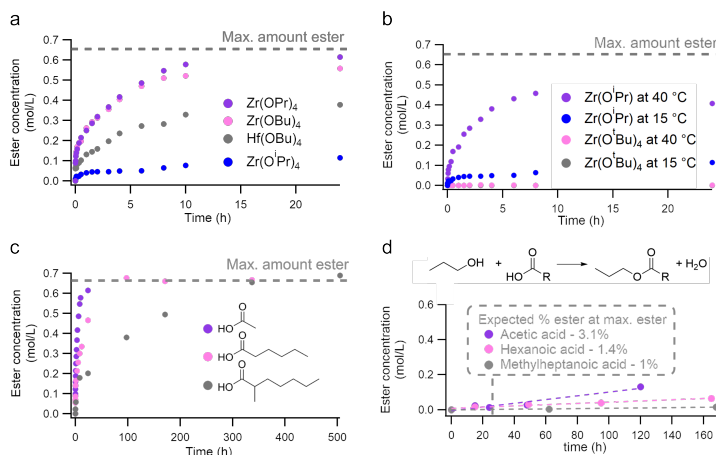
Figure 3.6: Ester formation tracked via NMR in CDCl$_3$, (a) while changing the sterics of the alkoxide at 15 °C, (b) at elevated temperatures for more sterically imposed alkoxides, (c) while changing the sterical hindrance on the carboxylic acid and (d) for the background reaction between free 1-proponol and carboxylic acid. The other parameters are equal to the standard reaction: [M] = 0.5 M, [acid] = 4 M.

In Figure 3.6d, the background ester formation between 1-propanol and acetic, hexanoic and methylheptanoic acid is shown. After 24h, the typical time length of our kinetic studies, reasonably low amounts of ester is formed. These percentages are calculated based on the concentration needed to reach full conversion. This means that even for the highest background ester formation between 1-propanol and acetic acid (~3%), almost 97% of the ester formation is catalyzed by zirconium.

The background ester formation reactions for the kinetic experiments shown in Figure 3.5a-c, can be found in appendix A. (See Figure A.33-A.35) They were all fitted to the following function, $f(x) = a + b * x$, and their fitting parameters are displayed in Table A.11-A.14. All reactions, except one, display a background ester formation of $< 4\%$ again showing that zirconium is responsible for the biggest fraction of the ester formation. The reaction between 1-propanol and 12 M acetic displays the highest amount of background ester formation at 6.4%.

3.2.3   From trimer to cluster
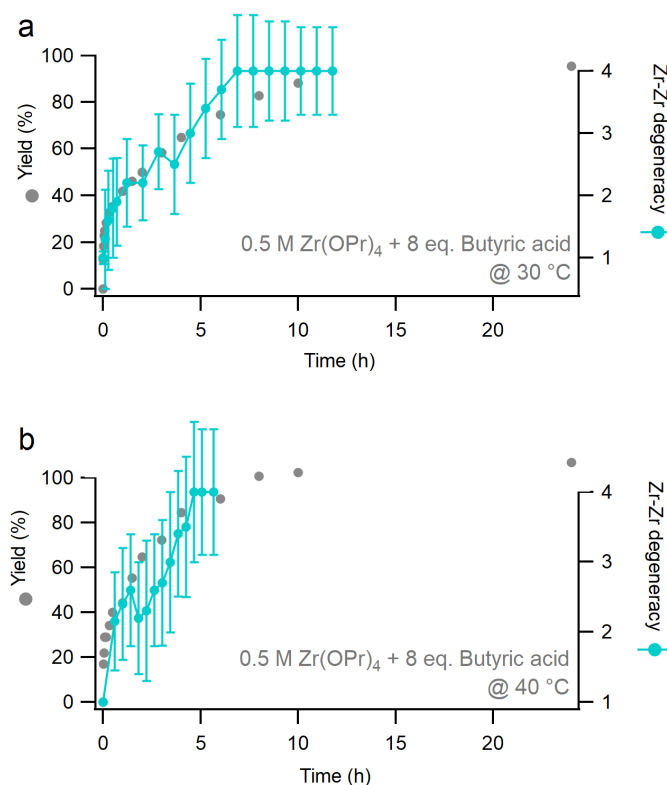
Figure 3.7: Overlay of the ester formation (grey) versus the Zr-Zr degeneracy with associated error bars (teal) for the cluster formation between $Zr(OPr)_4$ and butanoic acid at (a) 30 °C and at (b) 40 °C.

The *in situ* EXAFS experiments have shown us that the dimer converts into a trimeric Zr species even before any ester is formed. Combining this information, with the initial fast ester formation corresponding to 1 oxygen bridge per 3 Zr atoms lead us to believe that our actual precursor has an overall chemical composition of $Zr_3O(OR)_x(OOCR)_y$ with the sum of x and y equal to 10 to ensure charge neutrality. Using EXAFS it was possible to track the Zr-Zr degeneracy over time and compare them to the ester formation. Since the Zr-Zr degeneracy in the final cluster is 4, i.e. every Zr has 4 Zr-Zr interactions, it allows us to follow the cluster formation over time. (See Figure 3.7)

While the error on the Zr-Zr degeneracy is high, a clear trend can be appreciated. The Zr-Zr degeneracy displays the same profile as the ester formation. An initial jump to degeneracy 2, which corresponds to a trimer, followed by a steady increase up to 4, corresponding to the final cluster. This data further supports our claims of the proposed dimer to trimer to cluster mechanism. The data for the same reaction at 40 °C show the same trend except that the reaction is faster.

3.2.4 Proposed mechanism

Combining the knowledge obtained throughout this chapter we proposed a reaction mechanism. The proposed reaction mechanism in Figure 3.8 shows the reaction between $Zr_2(OPr)_8 \cdot 2\,HOPr$ and acetic acid, however we believe that the reaction mechanism is the same for other carboxylic acids. Initially, 2 equivalents acetic acid exchange with $Zr_2(OPr)_8 \cdot 2\,HOPr$ releasing propanol. The dimer persist in solution in the first exchange, after the second exchange a trimer is formed even before ester is formed. These reactions are in equilibrium since a small peak for free acetic acid can be seen in the FTIR titration. (See Figure 3.3b) This could explain the strong zirconium dependency we see in Figure 3.5c, by lowering the zirconium concentration less of the $Zr_3(OPr)_6(OOCCH_3)_6$ intermediate will be formed. This in turn results in a lower cluster yield and therefore less ester formation. The formation of this **Zr$_3$** species is followed by a fast initial ester formation which results in a **Zr$_3$** species with 1 Zr-O-Zr bridge.
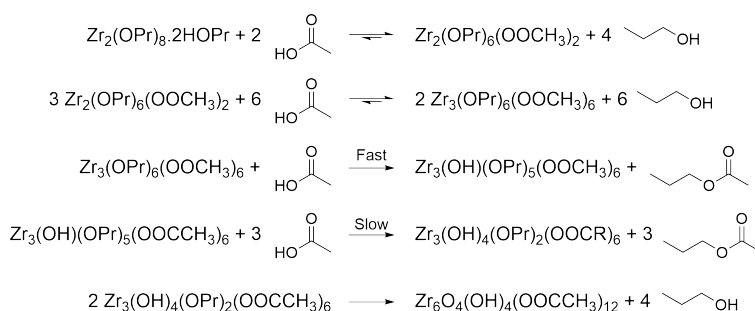
Figure 3.8: Proposed mechanism for the **Zr$_6$** cluster formation. After the initial ligand exchange reactions, the ester formation ensures the formation of Zr-O-Zr bridges to form the final cluster.

Afterwards this species generates ester in a much slower rate. This reaction seems to be heavily depending on the steric hindrance of the carboxylic acid, since the slower ester formation is heavily affected upon increasing the

sterics of the ligand. (See Figure 3.6c) Finally, once enough ester is formed the Zr_3 species can form the final octahedron shaped Zr_6 cluster.

This proposed mechanism is based on our observations while studying this system. We will use COPASI[23] (COmplex PAthway SImulator) in an attempt to fit our data to a mechanism from which quantitative values for reaction rates can be obtained. Additionally, using our *in situ* PDF experiments we will try to obtain realistic structures for the Zr_3 intermediate species both before and after ester formation.

3.2.5   Green cluster synthesis

Dichloromethane is toxic and harmful for the environment.[24;25] Therefore, it would be beneficial if it can be replaced in future synthesis. Ethyl acetate was chosen as the new solvent for the synthesis. First of all, the esterification kinetics should be studied in solution to ensure we have sufficient *in situ* water generation to form the cluster. Figure 3.9a shows that the ester formation follows a nearly identical trend compared to DCM so the amount of ester is sufficient for the cluster to form.
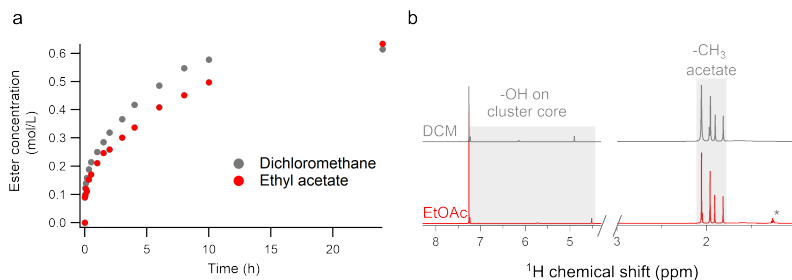
Figure 3.9: (a) The comparison of the esterification process of the standard reaction in DCM and ethyl acetate. (b) The ^{1}H NMR of the purified clusters in CDCl$_3$. The asterisk indicates remaining ethyl acetate in the sample.

In a first attempt we copied the synthesis and purification with DCM completely and replaced the solvent with ethyl acetate. After purification (i.e. filtering and washing with an EtOAc:acetic acid mixture) there was barely any powder left on the filter. After calculating the yield we found that here a yield of merely 14.9% was obtained, in contrast to quantitative yield using DCM. This indicates a higher solubility of the cluster in ethyl acetate, because the ester formation shows that clusters can be formed in quantitative yields. Therefore, we had to improve the purification process in order to

increase the yield. After keeping the reaction mixture at 30 °C for 12 hours, the solvent is evaporated using a Schlenk line. Then the obtained solid is re-suspended in 5 mL of a 1:1 mixture of cold EtOAc (5 °C) and acetic acid and subsequently filtered. The solid is washed once more with 5 mL of the same solution. Finally, the powder is washed with 5 mL of cold EtOAc and dried overnight using the Schlenk line. Using this improved purification method the yield was improved to 97%. It is evident that both reactions yielded the same product in nearly quantitative yield, after comparing the ^{1}H NMR spectra (see Figure 3.9b). This result proves that the cluster synthesis and purification can be carried out in EtOAc, successfully removing all DCM. Some trace ethyl aceate impurities are still present in the ^{1}H NMR (indicated with an asterisk in Figure 3.9b) and could be removed by further drying.

3.3 Conclusion

By studying the interaction between $Zr(OPr)_4$ dimer and acetic acid, using NMR, FTIR and *in situ* EXAFS, we were able to partially elucidate the precursor chemistry. We found that the first 2 equivalents of acetic acid exchange with the $Zr(OPr)_4$ dimer, but this reaction is in equilibrium. With 1 equivalent the dimer seems to persist in solution, whereas with the addition of a second equivalent a **Zr**$_3$ species is formed. NMR has shown us that the ester formation does not start until the third equivalent of acid is added, indicating that the real precursor is most likely a **Zr**$_3$ species without oxygen bridge.

Using ^{1}H NMR we studied the influence of several reaction parameters on the esterification kinetics. We found that lowering the acid concentration or the Zr concentration greatly reduces the amount of ester formed. Changing the temperature shows the expected trend, the higher the temperature the faster the esterification and *vice versa*. The propanol concentration did not seem to have any effect on the esterification kinetics. Increasing the sterics on both the alkoxide or carboxylic acid drastically slows down the ester formation. Increasing the temperature can help to bring these reaction to full yield within a reasonable time frame.

We found that the ester formation and the Zr-Zr degeneracy follow a similar trend, an initial spike followed by a slow and steady increase. This suggested that the ester formation can be used as a measure of the cluster formation. Combining our observations, our current proposed mechanism consists of an initial ligand exchange between $Zr(OPr)_4$ and 2 equivalents of acetic acid, forming a **Zr**$_3$ species. Followed, by a fast ester formation reaction after which the ester formation slows down eventually forming enough

water to form the **Zr**$_6$ cluster. Finally, we found that the reaction happens equally well in EtOAC, excluding the toxic DCM from the synthesis. The elimination of toxic solvents from this synthesis is a major improvement in the sustainability of these materials towards a greener future.

3.4   Perspective

By elucidating the reaction mechanism of group 4 metal oxo clusters we allow for unprecedented control on the reaction conditions. This understanding may allow the synthesis of mixed metal clusters, in a predictable way. As isostructural clusters exist for Zr, Hf, Ce and Th it is possible to envision numerous mixed metal clusters while maintaining the **M**$_6$ octahedron core. Which mixed clusters are energetically favorable remains to be seen. One could use computational calculations to obtain insight into this, otherwise difficult to study, structural information. This precise doping of clusters could be extrapolated to precise doping of nanoparticles, something which the nanoparticle field has been striving towards. Here, the atomically precise clusters can be used as precursors for the nanoparticle synthesis. For iron oxide nanoparticles, it has been shown that their size can be tuned by using different iron oleate clusters as precursors.[26] To the best of my knowledge, only one paper has been published on the use of zirconium clusters as precursors for nanoparticle synthesis.[27] However, the colloidal stability and size of the as synthesised nanoparticles are not discussed, leaving room for improvement.

By understanding that water plays a key role in this mechanism we can start looking for alternative reaction pathways to obtain our clusters. Since Hf(OBu)$_4$ is an expensive precursor (797 CHF for 25 g on Sigma-Aldrich) it would be advantageous to use the cheaper HfCl$_4$ (129 CHF for 50 g on Sigma-Aldrich) as a precursor. Recently, Jerozal *et al.* published a method to synthesise **Hf**$_6$-pivalate clusters in large scale (5.7 g) by adding H$_2$O to a mixture of HfCl$_4$, DMF and pivalic acid.[28] After seeing these results, we immediately wondered if this reaction would also work with other ligands that are not pivalic acid, making the reaction more economically feasible.

3.5 Experimental

3.5.1 Synthetic procedures

Chemicals. Acetic acid (99%) was bought from Sigma Aldrich, dried overnight using $CaSO_4$ and vacuum distilled into a Strauss flask for storage. $Zr(OPr)_4$ (70w% in 1-HOPr) and $Hf(OBu)_4$ (99%) were bought from Sigma Aldrich and stored in a Strauss flask upon arrival. $Zr(OiPr)_4$ (99.9%) and $Zr(OtBu)_4$ (99.999%) were purchased from Sigma Aldrich and stored in a glovebox upon arrival. Butanoic acid (99%), hexanoic acid (99%) and propanol (99.7%) were used as purchased from Sigma Aldrich. Dry DCM was bought from Acros. Ethyl acetate was bought from Biosolve and used without any further purification

Zr_{12}-acetate synthesis. In a typical clusters synthesis, a 20 mL vial was equipped with a septum and cycled three times between argon and vacuum. Zirconium propoxide (2.25 mL, 5 mmol, 1 eq.) was added to the vial, together with dry DCM (5.463 mL). Under stirring, distilled acetic acid (2.287 mL, 40 mmol, 8 eq.) was injected, reaching a total reaction volume of 10 mL and thus a zirconium concentration of 0.5 M. After 12 hours at room temperature (19-24 °C), the crystalline powder is isolated by filtration and further washed with 50 mL of a DCM:acetic acid mixture (4:1). Finally, the white powder is dried overnight under high vacuum. The powder is stored in a desiccator. The cluster was obtained as a white solid, with a 98 % yield (calculated based on the molecular formula: $Zr_{12}O_8(OH)_8(CH_3COO)_{24} \cdot 6\,CH_3COOH \cdot 3.5\,DCM$).[29]
For the synthesis in EtOAc the purification is slightly modified. After synthesis, the solvent is evaporated using a Schlenk line. Then the obtained solid is re-suspended in 5 mL of a 1:1 mixture of cold EtOAc (5 °C) and acetic acid and subsequently filtered. The solid is washed once more with 5 mL of the same solution. Finally, the powder is washed with 5 mL of cold EtOAc and dried overnight using the Schlenk line. The cluster was obtained as a white solid, with a 97 % yield (calculated based on the molecular formula: $Zr_{12}O_8(OH)_8(CH_3COO)_{24} \cdot 6\,CH_3COOH \cdot 3.5\,DCM$).[29]

Ester formation tracking. In order to follow the ester formation over time a metal block was developed which can hold 20 mL vials. An additional plastic cover was used to minimize temperature fluctuations. The metal block (with cover) was put onto a stirring plate inside a refrigerated room (4 °C) and heated to 15 °C. A 20 mL vial with the reagents was added and aliquots were taken during the reaction. For each aliquot, 20 μL was added to 500 μL $CDCl_3$ cooled in brine. Afterwards, the NMR was measured immediately. By measuring the ratio between the -OPr (3.6 ppm) signal

and the ester signal (4 ppm) the concentration of ester could be calculated. All measurements were performed at 15 °C unless specified otherwise.

In these 20 mL vials the reaction mixtures of which the ester formation was studied, were added. The standard reaction, shown above, was modified by changing the amount of carboxylic acid, type of carboxylic acid, the amount of Zr, the amount of propanol, the temperature and the type of metal alkoxide. Upon varying the parameters the total volume of the synthesis was kept constant at 10 mL. So for example, if the equivalents of carboxylic acid is halved this loss of volume is compensated by adding more DCM. For the *in situ* experiments the same ratios were applied however, acetic acid was exchanged for butanoic acid. Also here the total volume was kept at 10 mL.

***In situ* flow setup.** In order to perform the *in situ* experiments at the synchrotron a custom made setup was used. A 25 mL 3-neck flask, fully closed with septa and filled with both the metal precursor and DCM, was attached to a stirring plate and heated to the required temperature (30 or 40 °C) using an oil bath. A Heidolph Hei-flow peristaltic pump equiped wiht a SP-quick head was used to provide the flow within the closes system. Masterflex Viton tubing with an inner diameter of 1.6 mm and Swagelok connectors were used to connect the reaction flask to the sample holder via the perestaltic pump and from the sample holder back to the reaction flask. The flow during the experiment was kept constant at 2.5 mL/min. After the reaction flask was successfully attached and heated the flow was started to ensure a leak free setup. The carboxylic acid was prepared in a separate syringe which was punctured into the reaction flask and attached to a syringe pump. Then the hutch was closed, measurement was started and then the carboxylic acid was added using the syringe pump. Both the sample holder and syringe pump were build by the workshop of the University of Basel.

3.5.2   Analysis techniques

General instrumentation. Nuclear Magnetic Resonance (NMR) measurements were recorded at 298K on Bruker UltraShield 500 spectrometer operating at a frequency of 500.13 MHz. The IR spectra were recorded on a Perkin Elmer spectrum 2 ATR-FTIR with a diamond crystal.

EXAFS data acquisition and processing. The time resolved QEXAFS were measured using at the SuperXAS (X10DA) beamline as the Swiss Light Source, Paul Scherrer Institut in Switzerland. The polychromatic beam of the 2.9 Tesla superbend was collimated by a Si-coated collimating

mirror. The beam was monochromatised by a liquid nitrogen cooled Si(111) channel-cut crystal of the quickXAS monochromator, which oscillated at 1 Hz frequency with an acquisition time of 500 milliseconds per spectrum. Energy calibration was performed using Zr (K edge, Eo = 17 988 eV) foil. A focused beam was used with a spot size of 200 μm (vertical) and 500 μm (horizontal). All spectra were recorded in transmission mode. The resulting raw data were processed, i.e. normalised and averaged, using the ProQEXAFS software.[30] The EXAFS analysis was performed using the GNXAS package based on the multiple scattering theory.[31;32] The samples were flowed through a 1.0 mm Kapton capillary at a rate of 2.5 mL per min. at 30 °C.

3.6   Contributions

EXAFS data acquisition was done at the Paul Sherrer Institute (PSI) in Villigen (CH) by Dietger Van den Eynden, Rohan Pokratath and Dr. Christopher B. Whitehead. EXAFS data processing and fitting was done by Dr. Angelo Mullaliu, a post-doc in the lab of Prof. Dr. Tatjana Parac-Vogt at the University of Leuven (BE). PDF data acquisition was done by Dietger Van den Eynden, Carlotta Seno, Rohan Pokratath and Jibin Muhammed Parammal at the Broohaven National Lab (BNL) in New York (US). PDF data processing and fitting was done by Carlotta Seno. Fitting the kinetic data using COPASI will be done by Jikson Pulparayil Mathew.

References

[1] Hennig, C.; Weiss, S.; Kraus, W.; Kretzschmar, J.; Scheinost, A. C. Solution Species and Crystal Structure of Zr(IV) Acetate. *Inorganic Chemistry* **2017**, *56*, 2473–2480.

[2] Bezrukov, A. A.; Törnroos, K. W.; Le Roux, E.; Dietzel, P. D. C. Incorporation of an Intact Dimeric Zr_{12} Oxo Cluster from a Molecular Precursor in a New Zirconium Metal-Organic Framework. *Chem. Comm.* **2018**, *54*, 2735–2738.

[3] Fidelli, A. M.; Karadeniz, B.; Howarth, A. J.; Huskic, I.; Germann, L. S.; Halasz, I.; Etter, M.; Moon, S.-Y.; Dinnebier, R. E.; Stilinovic, V.; et al., Green and Rapid Mechanosynthesis of High-Porosity NU- and UiO-type Metal-Organic Frameworks. *Chem. Comm.* **2018**, *54*, 6999–7002.

[4] Guillerm, V.; Gross, S.; Serre, C.; Devic, T.; Bauer, M.; Férey, G. A Zirconium Methacrylate Oxocluster as Precursor for the Low-Temperature Synthesis of Porous Zirconium(iv) Dicarboxylates. *Chem. Comm.* **2010**, *46*, 767–769.

[5] Huang, Y.-H.; Lo, W.-S.; Kuo, Y.-W.; Chen, W.-J.; Lin, C.-H.; Shieh, F.-K. Green and Rapid Synthesis of Zirconium Metal-Organic Frameworks via Mechanochemistry: UiO-66 Analog Nanocrystals Obtained in One Hundred Seconds. *Chem. Comm.* **2017**, *53*, 5818–5821.

[6] Cavka, J. H.; Jakobsen, S.; Olsbye, U.; Guillou, N.; Lamberti, C.; Bordiga, S.; Lillerud, K. P. A New Zirconium Inorganic Building Brick Forming Metal Organic Frameworks with Exceptional Stability. *J. Am. Chem. Soc.* **2008**, *130*, 13850–13851.

[7] Xu, H.; Sommer, S.; Broge, N. L. N.; Gao, J.; Iversen, B. B. The Chemistry of Nucleation: In Situ Pair Distribution Function Analysis of Secondary Building Units During UiO-66 MOF Formation. *Chemistry - A European Journal* **2019**, *25*, 2051–2058.

[8] Firth, F. C. N.; Gaultois, M. W.; Wu, Y.; Stratford, J. M.; Keeble, D. S.; Grey, C. P.; Cliffe, M. J. Exploring the Role of Cluster Formation in UiO Family Hf Metal-Organic Frameworks with in Situ X-ray Pair Distribution Function Analysis. *Journal of the American Chemical Society* **2021**, *143*, 19668–19683.

[9] Van den Eynden, D.; Pokratath, R.; Mathew, J. P.; Goossens, E.; De Buysser, K.; De Roo, J. Fatty acid capped, metal oxo clusters as the

smallest conceivable nanocrystal prototypes. *Chemical Science* **2022**, *14*, 573–585.

[10] Van den Eynden, D.; Pokratath, R.; De Roo, J. Nonaqueous Chemistry of Group 4 Oxo Clusters and Colloidal Metal Oxide Nanocrystals. *Chem Rev* **2022**, *122*, 10538–10572.

[11] Kogler, F. R.; Jupa, M.; Puchberger, M.; Schubert, U. Control of the Ratio of Functional and Non-Functional Ligands in Clusters of the Type $Zr_6O_4(OH)_4(carboxylate)_{12}$ for their Use as Building Blocks for Inorganic-Organic Hybrid Polymers. *J. Mater. Chem.* **2004**, *14*, 3133–3138.

[12] Wu, L.; Liu, J.; Vockenhuber, M.; Ekinci, Y.; Castellanos, S. Hybrid EUV Resists with Mixed Organic Shells: A Simple Preparation Method. *Eur. J. Inorg. Chem.* **2019**, *2019*, 4136–4141.

[13] Schubert, U.; Arpac, E.; Glaubitt, W.; Helmerich, A.; Chau, C. Primary Hydrolysis Products of Methacrylate-Modified Titanium and Zirconium Alkoxides. *Chem. Mater.* **1992**, *4*, 291–295.

[14] Kickelbick, G.; Feth, M. P.; Bertagnolli, H.; Puchberger, M.; Holzinger, D.; Gross, S. Formation of Organically Surface-Modified Metal Oxo Clusters from Carboxylic Acids and Metal Alkoxides: a Mechanistic Study. *J. Chem. Soc., Dalton Trans.* **2002**, *20*, 3892–3898.

[15] Boyle, T. J.; Ottley, L. A. M.; Rodriguez, M. A. Structurally characterized carboxylic acid modified zirconium alkoxides for the production of zirconium oxide thin films. *Polyhedron* **2005**, *24*, 1727–1738.

[16] Doeuff, S.; Dromzee, Y.; Taulelle, F.; Sanchez, C. Synthesis and Solid- and Liquid-State Characterization of a Hexameric Cluster of Titanium(IV): $Ti_6(\mu_2-O)_2(\mu_3-O)_2(\mu_2-OC_4H_9)_2(OC_4H_9)_6(OCOCH_3)_8$. *Inorg. Chem.* **1989**, *28*, 4439–4445.

[17] Shirase, S.; Tamaki, S.; Shinohara, K.; Hirosawa, K.; Tsurugi, H.; Satoh, T.; Mashima, K. Cerium(IV) Carboxylate Photocatalyst for Catalytic Radical Formation from Carboxylic Acids: Decarboxylative Oxygenation of Aliphatic Carboxylic Acids and Lactonization of Aromatic Carboxylic Acids. *Journal of the American Chemical Society* **2020**, *142*, 5668–5675.

[18] Dovrat, G.; Pevzner, S.; Maimon, E.; Vainer, R.; Iliashevsky, O.; Ben-Eliyahu, Y.; Moisy, P.; Bettelheim, A.; Zilbermann, I. DOTP versus

DOTA as Ligands for Lanthanide Cations Novel Structurally Characterized CeIV and CeIII Cyclen-Based Complexes and Clusters in Aqueous Solutions. *Chemistry - A European Journal* **2022**, *28*, 202201868.

[19] Niu, Q.; Huang, Q.; Yu, T.-Y.; Liu, J.; Shi, J.-W.; Dong, L.-Z.; Li, S.-L.; Lan, Y.-Q. Achieving High Photo/Thermocatalytic Product Selectivity and Conversion via Thorium Clusters with Switchable Functional Ligands. *Journal of the American Chemical Society* **2022**, *144*, 18586–18594.

[20] Vaartstra, B. A.; Huffman, J. C.; Gradeff, P. S.; Hubert-Pfalzgraf, L. G.; Daran, J. C.; Parraud, S.; Yunlu, K.; Caulton, K. G. Alcohol adducts of alkoxides: intramolecular hydrogen bonding as a general structural feature. *Inorganic Chemistry* **1990**, *29*, 3126–3131.

[21] Peter, D.; Ertel, T. S.; Bertagnolli, H. EXAFS study of zirconium alkoxides as precursor in the sol-gel process: I. Structure investigation of the pure alkoxides. *Journal of Sol-Gel Science and Technology* **1994**, *3*, 91–99.

[22] Peter, D.; Ertel, T. S.; Bertagnolli, H. EXAFS study of zirconium alkoxides as precursors in the sol-gel process: II. The influence of the chemical modification. *Journal of Sol-Gel Science and Technology* **1995**, *5*, 5–14.

[23] Hoops, S.; Sahle, S.; Gauges, R.; Lee, C.; Pahle, J.; Simus, N.; Singhal, M.; Xu, L.; Mendes, P.; Kummer, U. COPASIa COmplex PAthway SImulator. *Bioinformatics* **2006**, *22*, 3067–3074.

[24] Schlosser Paul, M.; Bale Ambuja, S.; Gibbons Catherine, F.; Wilkins, A.; Cooper Glinda, S. Human Health Effects of Dichloromethane: Key Findings and Scientific Issues. *Environmental Health Perspectives* **2015**, *123*, 114–119.

[25] Olaguer, E. P. The distribution of the chlorinated solvents dichloromethane, perchloroethylene, and trichloroethylene in the global atmosphere. *Environmental Science and Pollution Research* **2002**, *9*, 175–182.

[26] Kirkpatrick, K. M.; Zhou, B. H.; Bunting, P. C.; Rinehart, J. D. Size-Tunable Magnetite Nanoparticles from Well-Defined Iron Oleate Precursors. *Chemistry of Materials* **2022**, *34*, 8043–8053.

[27] Sliem, M. A.; Schmidt, D. A.; Bétard, A.; Kalidindi, S. B.; Gross, S.; Havenith, M.; Devi, A.; Fischer, R. A. Surfactant-Induced Nonhydrolytic Synthesis of Phase-Pure ZrO_2 Nanoparticles from Metal-Organic and Oxocluster Precursors. *Chemistry of Materials* **2012**, *24*, 4274–4282.

[28] Jerozal, R. T.; Pitt, T. A.; MacMillan, S. N.; Milner, P. J. High-Concentration Self-Assembly of Zirconium- and Hafnium-Based Metal-Organic Materials. *Journal of the American Chemical Society* **2023**, *145*, 13273–13283.

[29] Puchberger, M.; Kogler, F. R.; Jupa, M.; Gross, S.; Fric, H.; Kickelbick, G.; Schubert, U. Can the Clusters $Zr_6O_4(OH)_4(OOCR)_{12}$ and $[Zr_6O_4(OH)_4(OOCR)_{12}]_2$ Be Converted into Each Other? *Eur. J. Inorg. Chem.* **2006**, *2006*, 3283–3293.

[30] Clark, A. H.; Imbao, J.; Frahm, R.; Nachtegaal, M. ProQEXAFS: a highly optimized parallelized rapid processing software for QEXAFS data. *Journal of Synchrotron Radiation* **2020**, *27*, 551–557.

[31] Filipponi, A.; Di Cicco, A.; Natoli, C. R. X-ray-absorption spectroscopy and n-body distribution functions in condensed matter. I. Theory. *Phys Rev B Condens Matter* **1995**, *52*, 15122–15134.

[32] Filipponi, A.; Di Cicco, A. X-ray-absorption spectroscopy and n-body distribution functions in condensed matter. II. Data analysis and applications. *Phys Rev B Condens Matter* **1995**, *52*, 15135–15149.

4

Radical polymerisation with (meth-)acrylate capped clusters

I am among those who think that science has great beauty.
– Marie Skłodowska-Curie

4.1 Introduction

A recent publication shows that polymerizing oleate-capped, nearly spherical 15 nm iron oxide nanoparticles by heating under high pressure, results in materials with exceptional properties. Hardness values up to 4 GPa and strength values up to 630 MPa were obtained.[1] With our atomically precise Zr_{12}-oleate clusters in hand, we were inspired to attempt polymerising our materials. Previous reports show that it is possible to polymerize clusters with short and rigid ligands, such as methacrylic acid, using radical polymerisation techniques. (*vide supra*) Few publications report the use of clusters with mixed ligand shells.[2;3] We believed that with our recently obtained control over the clusters in both in terms of possible ligands and ligand shell composition, we could create fascinating novel materials. The first part of this chapter deals with the polymerisation of clusters capped

with longer ligands, contrary to existing literature, more specifically $\mathbf{Zr}_{12}$-10-undecanoate, -oleate and -linoleate clusters.

The second part of this chapter, reviews the polymerisation of (meth-)acrylate capped clusters. As stated by the authors, they lacked control over the ligand shell composition,limiting the tunability of their systems.[4] A few years after, they published results where they were able to polymerize clusters with mixed ligand shells. Their clusters were synthesised by mixing $\mathbf{Zr}_4$-methacrylate and $\mathbf{Zr}_4$-pivalate and assumed statistical mixing of the ligands.[3] They found that the T_g decreases with decreasing cross-link density, but they were limited to the use of the short and rigid methacrylic acid alone. Here we set out to create customisable clusters with long flexible (meth-)acrylate ligands that can be used as monomers. By manipulating the monomer/cross-linker, materials with different properties will be obtained. Clusters capped with both 10-undecenoic/oleic/linoleic acid and (meth-)acrylate acid can be synthesised either by bottom up or ligand exchange. However, due to the scalability and the ease of purification of the $\mathbf{Zr}_{12}$-acetate clusters synthesis, the ligand exchange approach was chosen. All ligands used for surface functionalisation are depicted in Figure 4.1.
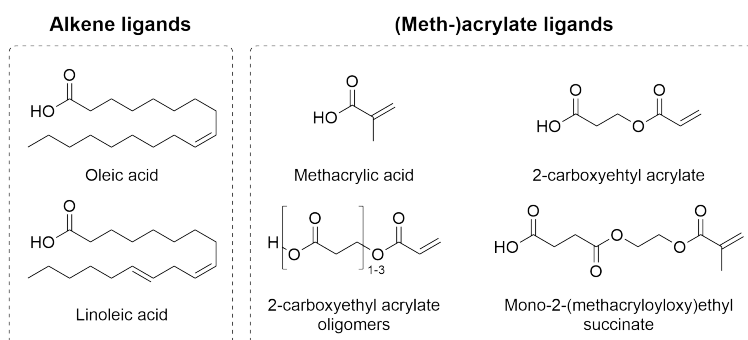
Figure 4.1: Overview of the ligands used in the surface functionalisation of clusters prior to polymerisation. On the left the ligands containing an alkene bond are listed, oleic and linoleic acid. On the right the (meth-)acrylate containing ligands are shown, methacrylic acid, mono-2-(methacryloyloxy)ethyl succinate, 2-carboxyethyl acrylate and oligomers.

Since we now have control over the surface composition, we did not only try to polymerise clusters with a full ligand shell of the previously mentioned ligands, but have also synthesised clusters with a mixed ligand shell. The first consideration is that the second, unreactive ligand should not interfere with the polymerisation process. Therefore, this ligand was chosen

to be shorter or equally long as the reactive ligands. For example, when preparing a mixed cluster with methacrylic acid, propionic acid was used as secondary ligand in order to avoid burying the reactive groups within the ligand shell. For oleic acid, on the other hand, hexanoic acid can be easily used as the secondary ligand. Secondly, it has previously been shown that adding clusters to the equation might affect the polymerisation speed.[3] No clear trend could be observed as to how the amount of clusters affect the polymerisation, but it may be necessary to increase the reaction time.

The two types of clusters mentioned above, alkene or (meth-)acrylate capped, are polymerised using a radical polmyerisation approach. In general, a radical polymerisation consists of a combination of 3 different processes, namely (i) initiation, (ii) propagation and (iii) termination.[5] The initiation can be further divided in 2 steps. First, the homolytic dissociation of the initiator (UV or heat induced) generates radicals. Second, the initiation reaction, where the initiator radical undergoes an addition to the monomers present in the reaction mixture, forming a radical on the monomer. Once this species is present, it can perform the same reaction with multiple monomers, creating a polymer chain, this reaction is called the propagation. Finally, these radicals will terminate each other through a recombination process. Several possible termination reactions can occur. Two propagating polymer chains can find each other and recombine to form a neutral species. Alternatively, they can form two neutral species through a disproportionation process. Finally, the initiator radical can terminate with a propagating polymer chain.

$$\text{Initiator} \xrightarrow{k_d} 2R^\bullet \qquad\qquad \text{Homolytic dissociation}$$

$$R^\bullet + M \xrightarrow{k_i} M_1^\bullet \qquad\qquad \text{Initiation reaction}$$

$$M_n^\bullet + M \xrightarrow{k_p} M_{n+1}^\bullet \qquad\qquad \text{Propagation reaction}$$

$$M_n^\bullet + M_m^\bullet \xrightarrow{k_{tc}} M_{n+m} \qquad\qquad \text{Termination via combination}$$

$$M_n^\bullet + M_m^\bullet \xrightarrow{k_{td}} M_n + M_m \qquad \text{Termination via disproportionation}$$

$$M_n^\bullet + R^\bullet \xrightarrow{k_{prt}} M_nR \qquad\qquad \text{Primary radical termination}$$
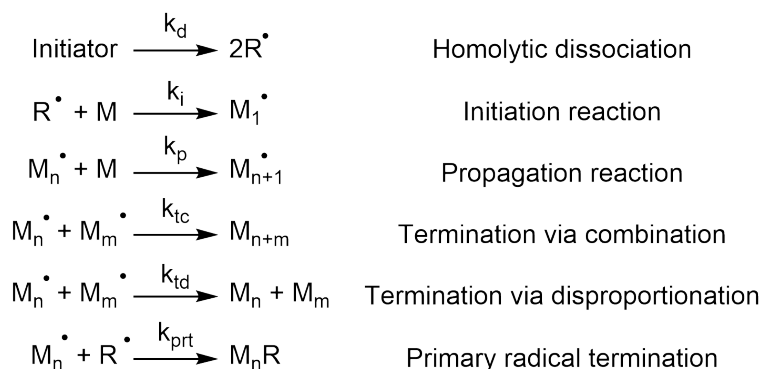
Figure 4.2: Overview of the different steps in a free radical polymerisation. First, the initiation generates radical through homolytic dissociation of the precursor and subsequent addition to a monomer. This species performs the propagation reaction through monomer addition. Finally, the possible termination reactions, which quench the radical polymerisation, are shown.

It is clear that this intricate combination of reactions depends on a variety of factors making it difficult to predict the outcome of a free radical polymerisation. Especially in our case where the amount of clusters, ligands on the surface and type of ligands is varied, further complicating the reaction. The viscosity will also change upon addition of the clusters to the monomer mixture.[6] Since this was an exploration of multiple parameters it was not possible to characterize every sample in depth. We opted to assess the homogeneity and brittleness of the materials, if solid samples were obtained. Additionally, the insoluble fraction and T_g were determined for these samples. The mixed cluster shells were synthesised through a ligand exchange reaction starting from $\mathbf{Zr}_{12}$-acetate. In order to characterize the final surface composition, NMR was used.

4.1.1   Synthesis of alkene capped clusters

Both the $\mathbf{Zr}_{12}$-acetate clusters and the ligand exchange are achieved following a similar procedure to the one in chapter 2. The reaction was scaled up 5 times, yielding 7 grams of clusters in quantitative yields. Again $Zr(OPr)_4$ is reacted with 8 equivalents of acetic acid in DCM. After synthesis, the solution is filtered and the powder is washed with 100 mL of a DCM:acetic acid (4:1) mixture. Finally, the powder is dried on the Schlenk line overnight.

Similarly to the cluster synthesis, the ligand exchange reaction replacing acetate ligands for either oleic or linoleic acid was also scaled up ten-fold. 2 g of $\mathbf{Zr}_{12}$-acetate was weighed into a vial to which 4 mL DCM was added, after 5 minutes of stirring a milky solution was obtained. 1 eq. of the new ligand was added and the solution turns clear after 10 minutes indicating at least partial exchange. After 1 hour of stirring the solution is evaporated at 70 °C using the Schlenk line in order to push the reaction towards completion, via evaporation of acetic acid. This dispersing/evaporation step was repeated once more to ensure full exchange. Finally, the clusters were dried overnight using the Schlenk line.

4.1.2   Synthesis of (meth)-acrylate capped clusters

Since (meth-)acrylate molecules tend to polymerize at elevated temperatures[7] a different exchange reaction had to be developed. Here we chose to reduce the complexity of the system by only adding 1 equivalent of the incoming ligand, avoiding tedious purification, and performing the evaporation step at room temperature, avoiding possible side reactions. By doing so, we open the door for acetic acid to not fully evaporate. This is a compromise we have to make however, since the ligand shell will nevertheless

contain the (meth-)acrylate ligand we believe that some residual acetate ligands should not harm the polymerisation. This results in yields above 100 % since there will always be a slight excess of (meth-)acrylate ligands since not all of the native acetate ligands are replaced. Generally, the exchange reaction from acetate to (meth-)acrylate proceeds via the same method described above. The only difference being 1 eq. of (meth-)acrylate ligands and no heat during the evaporation step.

4.2   Results & discussion

4.2.1   Alkene clusters polymerisation

After obtaining the desired clusters, liquid Zr_{12}-oleate and -linoleate were poured into a Teflon mold and heated to 180 °C in a vacuum oven, similar to the polymerisation of iron oxide nanoparticle (without pressure). After 2, 6 and 24h the consistency of the samples was established, a solid sample indicates successful polymerisation, a liquid sample on the other hand indicates no polymerisation reaction. Unfortunately, both samples did not show any sign of solidifying indicating no or too slow reaction progress. While there was no solidification of the samples, they show discoloration. The samples went from perfectly transparent to slightly yellow for Zr_{12}-oleate and to dark orange for Zr_{12}-linoleate, indicating degradation of the material. (See Figure 4.3)

Figure 4.3: Discoloration of both Zr_{12}-oleate (right) and Zr_{12}-linoleate (left) to light yellow and dark orange respectively after 24h of thermal polymerisation via heating at 180 °C under vacuum.

After this reaction, the liquid was dissolved in $CDCl_3$ and ^{1}H NMR was

measured. (See Figure 4.4) Two observations can be made here, (i) the peaks of the both oleate and linoleate sharper up (i.e. display fine structure) after synthesis and (ii) the CH_3/alkene ratio does not change significantly between the reaction product and the free ligands. This indicates unsuccessful polymerisation, since the double bond clearly did not react and the reaction product dissolved in $CDCl_3$.

Since this attempt was not successful, we decided to add a thermal initiator to the material in order to facilitate the radical polymerisation. Our first choice was azobisisobutyronitrile, or AIBN for short. This initiator has a half life ($t_{1/2}$) of 1h at 85 °C, meaning that in 1h half of the molecules will have decomposed and formed radicals.[8] We performed the reaction at 80 °C overnight, i.e. 16h. The initiator was added to $\mathbf{Zr}_{12}$-oleate and -linoleate in 2, 10 or 20 mol%, based on the amount of double bonds present in the samples. Again no solid samples were obtained after reaction indicating unsuccessful polymerisation. Finally, both the initiator and the ligand shell composition were varied. Also the ligand shell was varied, the amount of oleate/linoleate on the cluster surface ranged from 100 to 50 % (i.e. 12-24 ligands on the cluster surface), the secondary ligand was either methylbutanoate or hexanoate. Dicumyl peroxide ($t_{1/2}$ = 5h at 120 °C)[9] was chosen as a new initiator. These samples were reacted at 110 °C in the vacuum oven overnight. Unfortunately, also here no solid polymer samples were obtained.
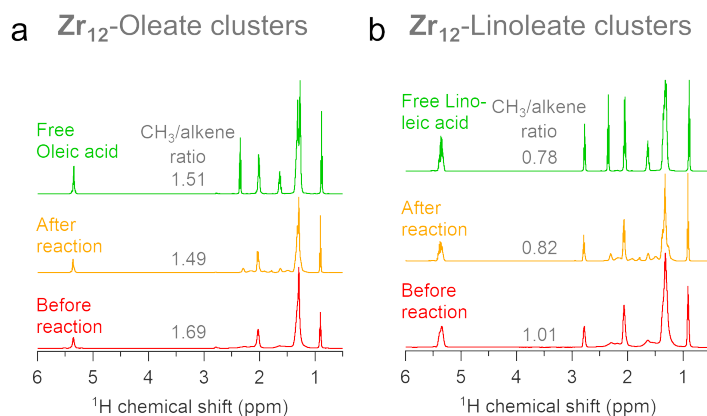
Figure 4.4: (a) Overview figure of the $\mathbf{Zr}_{12}$-oleate before reaction and after heating. (b) Overview figure of the $\mathbf{Zr}_{12}$-linoleate before reaction and after heating. In both reactions the free alekene containing ligand is added on top as a reference. The CH_3/alkene ratio does not change significantly indicating that the double bond did not react. Measured in $CDCl_3$.

Because none of these samples yielded solid polymers, they were not further studied and characterized. From our results it seems that the double bond in oleic acid and linoleic acid is not active enough towards polymerisation as it is shielded from the outside by the tail of the ligand. It appears that if a radical is generated a termination reaction is more plausible than a propagation reaction preventing polymerisation. Indeed, in literature the radical polymerisation of fatty acid derivatives proceeds through an initial chemical transformation which introduces more reactive groups via an esterification reaction.[10;11] Molecules such as 1-tetradecene have been polymerised before however, only at high temperatures and pressure.[12] Therefore, we decided to use 10-undecenoic acid (containing a terminal alkene, see Figure 4.5) as a ligand for the clusters. Using this new ligand, clusters with mixed ligand shells containing 6, 12 or 18 equivalents of 10-undecenoic acid with hexanoic acid as secondary ligand, were synthesised. (see Figure 4.5)
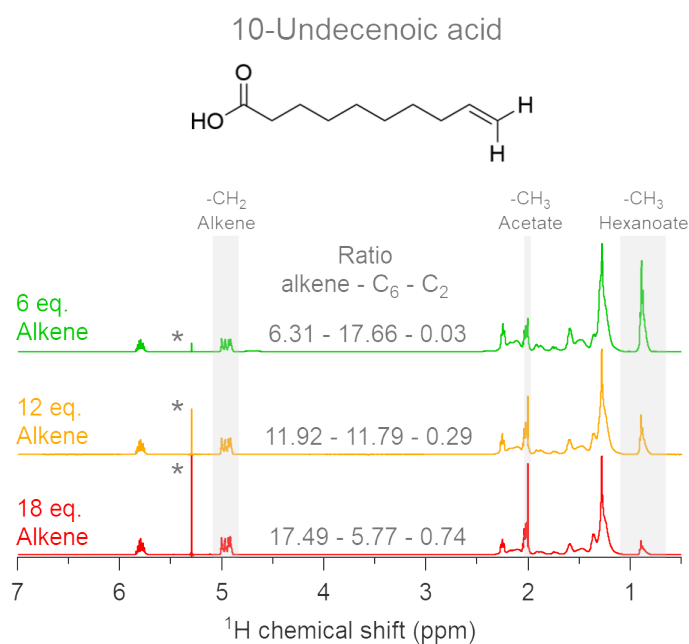
Figure 4.5: Chemical structure of the terminal alkene ligand 10-undecenoic acid. (Top) ^{1}H NMR spectra in CDCl$_3$ of the clusters functionalised with 6, 12 and 18 equivalents 10-undecenoic acid.

After calculating the relative ratios of the ligands it is clear to see that the intended ligand shell composition was achieved with minimal amounts of leftover acetate ligands. The amount of leftover acetate ligands increases

with the increasing amount of 10-undecenoic acid used for functionalisation indicating that the full exchange might be hampered by sterical hindrance. These clusters were then polymerised by adding 1, 5 or 10 w% dicumyl peroxide as initiator and subsequent heating at 110 °C overnight. Solid samples were retrieved after overnight reaction indicating successful polymerisation.

Table 4.1: Insoluble fractions and T_g for the samples with 6, 12 and 18 equivalents of 10-undecenoic acid ligands on the cluster core, via the addition of 1, 5 or 10 w% dicumyl peroxide initiator and subsequent reaction at 110 °C overnight.

	Dicumyl peroxide		
	1 w%	5 w%	10 w%
6 eq.	64.6 %, -2.6 °C	92.6 %, -2.6 °C	91.5 %, -3.2 °C
12 eq.	86.1 %, -3.7 °C	83.8 %, -2.7 °C	93.1 %, -2.8 °C
18 eq.	75.2 %, -3.2 °C	71.7 %, -2.9 °C	95.6 %, -1.6 °C

The insoluble fraction was determined via soaking 50 mg of material in solvent for 2 days. From Table 4.1 we learn that 1 w% initiator is not enough to obtain good insoluble fractions. (i.e. > 90%) It seems that there is sufficient propagation reaction in order to form a network. However, too much monomers remain unreacted allowing them to dissolve upon soaking of the sample in solvent. With 5 w% initiator, only the clusters containing 6 equivalents of 10-undecenoic acid display an insoluble fraction above 90% however, using 10 w% initiator all samples display excellent insoluble fractions.

These results are encouraging since they prove that alkene capped clusters can be polymerised under our current conditions. Switching from a mid-chain alkene to a terminal alkene was the missing key in order to obtain solid polymer networks some of which exhibit excellent insoluble fractions. Now we switch to (meth-)acrylic ligands to decorate the cluster surface, since they are commonly polymerised using free radical polymerisation in industry. These ligands should be more active and clusters containing methacrylic acid have been polymerised before.[3]

$$Zr_{12}O_8(OH)_8(C_6H_{11}O_2)_6(C_{11}H_{20}O_2)_{18}$$

$$Zr_{12}O_8(OH)_8(C_6H_{11}O_2)_{12}(C_{11}H_{20}O_2)_{12}$$

$$Zr_{12}O_8(OH)_8(C_6H_{11}O_2)_{18}(C_{11}H_{20}O_2)_6$$
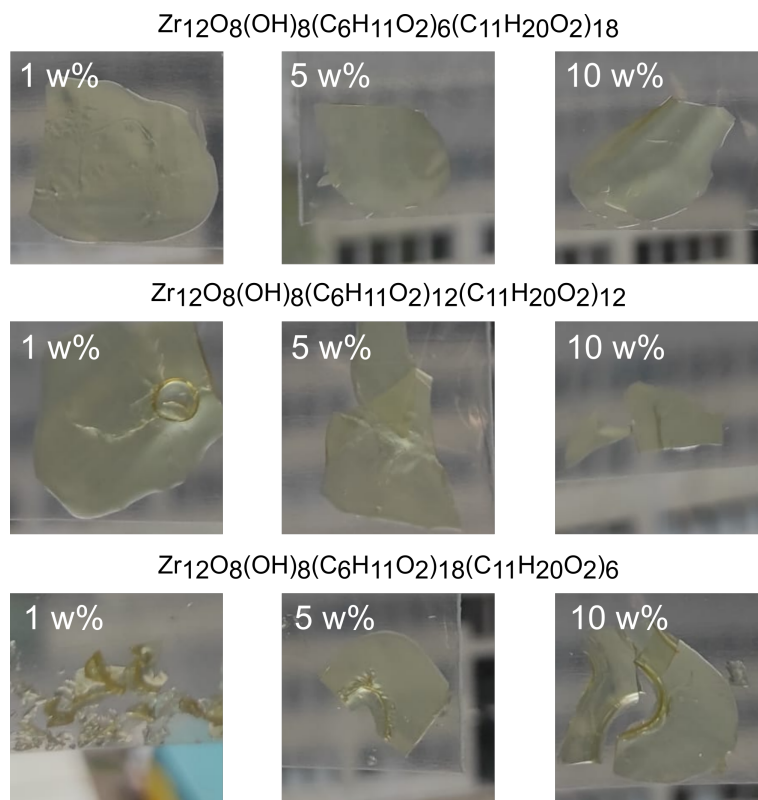
Figure 4.6: Appearance of the polymer samples synthesised from 6, 12 and 18-fold functionalised clusters with 10-undecenoic acid. The materials were reacted with 1, 5 or 10 w% dicumyl peroxide as initiator.

4.2.2 Exploration of acrylate capped clusters

Here we set out to synthesise clusters capped with longer and flexible reactive (meth-)acrylate ligands compared to methacrylic acid. (See Figure 4.1) A mixed ligand shell is created, using hexanoic acid as secondary ligand. As stated above, methacrylic acid capped clusters (even mixed ligands shells) were polymerised before and will therefore not be considered in the remainder of this chapter.[2;3;13]

After the exchange reaction the spectra still contain a signal at 2.1 ppm which originates from acetic acid that is not removed, despite multiple drying steps. This should not come as a surprise, since it was previously shown that at room temperature the clusters do not convert between monomer and dimer because the 4 inter-cluster bridging are not exchanged.[14] The latter

are the most protected i.e. the most difficult to reach and it can easily be imagined that those are the remaining native ligands after exchange. Comparing the ratio between the $-CH$ acrylate ligand signals, the $-CH_3$ acetic acid (2.1 ppm) signal and the $-CH_3$ hexanoic acid (0.89 ppm) signal, one can estimate ligand composition on the cluster core. (See Equations A.12-A.14) Figure 4.7, and the figures for 2-carboxyethyl acrylate (and oligomers) in appendix A (Figures A.36-A.37), show that the value for the remaining acetate is around 4 or lower. This matches approximately with the 4 intercluster bridging acetate ligands that are still present. Despite incomplete ligand exchange, the targeted acrylate/hexanoate ratio was achieved.
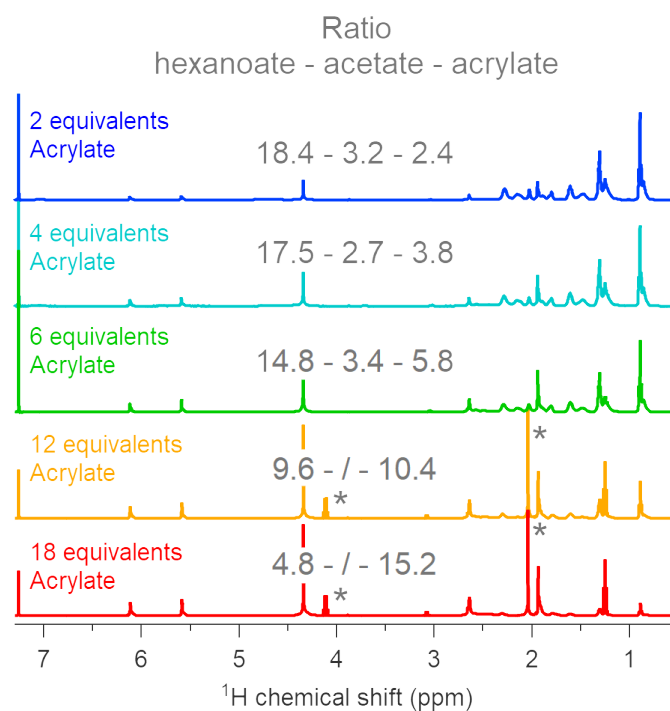
Figure 4.7: ^{1}H NMR spectra of **Zr$_{12}$**-acetate clusters in CDCl$_3$ exchanged with 2, 4, 6, 12 or 18 mono-2-(methacryloyloxy) ethyl succinate and hexanoic acid as secondary ligand. While the exchange is not complete, acetate signal at 2.1 ppm,the overall targeted ratio of acrylate versus hexanoate is obtained. For the samples with 12 and 18 equivalents the amount of acetate could not be determined due to overlap with the solvent peak. For the calculations, the amount of acetate was set to 4. Leftover solvent is indicated with an asterisk.

Since we now have clusters in hand with different ligand shell compositions we attempt to polymerize them by adding co-monomers and a thermal initiator. These viscous clusters were mixed with different amounts (25 - 95 mol%) of methyl methacrylate (MMA) as co-monomer and 5 mol% dicumyl peroxide as initiator. From hereon forth the residual acetate ligands are not displayed when chemical formulas of the clusters are shown, for simplicity reasons. The clusters are depicted with their fully exchanged and ideal ligand shell compositions. We know they are there however, since they reside in the center of the cluster dimer and the reactive ligands are present in the ligand shell, we expect these remaining acetate ligands to have little effect.

4.2.3 High cross-link density & cluster loading

Initially, clusters with 18, 12 and 6 equivalents (out of 24 ligands) of either 2-carboxyethyl acrylate or 2-carboxyethyl acrylate oligomers were polymerised. These viscous clusters were mixed with 25, 50 or 75 mol% methylmethacrylate as co-monomer. Finally, 5 mol% dicumyl peroxide initiator was dissolved in this monomer mixture. After homogenizing, the reaction mixture was poured onto a Teflon sheet and reacted overnight in a vacuum oven at 110 °C after which solid samples were obtained. Unfortunately, most samples rendered only brittle and non-homogeneous samples. (See Figures 4.8 and A.38-A.42)

$$Zr_{12}O_8(OH)_8(C_6H_{11}O_2)_6(C_3H_3O_2(C_3H_4O_2)_n)_{18}$$
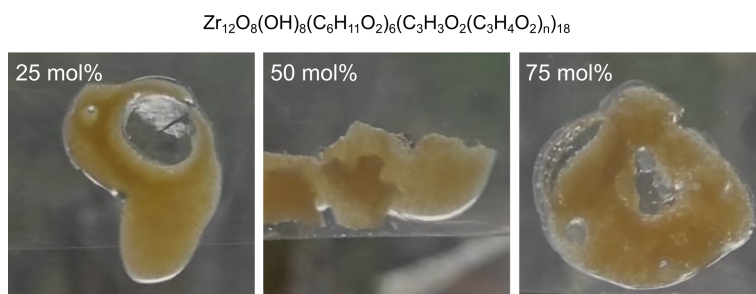
Figure 4.8: Overview of the different polymer samples after the reaction of $Zr_{12}O_8(OH)_8(C_6H_{11}O_2)_6(C_3H_3O_2(C_3H_4O_2)_n)_{18}$ with 25, 50 and 75 mol% methylmethacrylate (from left to right) using 5 mol% dicumylperoxide as initiator. After reacting them in a vacuum oven at 110 °C for 12h, it is clear that the polymers do not form homogeneous samples.

Nearly all samples gave good to excellent insoluble fraction of 90 % or more. Indicating that the polymerisation was successful. In the case of an unsuccessful polymerisation the unreacted monomer would dissolve while

the sample is submerged in solvent and the insoluble fraction would be lower. (*vide supra*) While the differences are small, an increasing trend in insoluble fraction with increasing cross-linking density can be appreciated. Interestingly, the T_g does not show significant differences when any of the parameters are changed. Samples with different amount of clusters, ligand type or the amount of ligands on the core all display a T_g between -4.6 °C and -1.2 °C. (See Table 4.2 & 4.3) One possible explanation for the heterogeneous appearance combined with the excellent insoluble fractions could be that the appearance does not originate from agglomerated monomers. But rather from numerous small solvent bubbles that were trapped during synthesis, unable to escape the matrix due to the high viscosity. Leaving the reaction mixture under vacuum overnight prior to increasing the temperature might circumvent this issue.

Table 4.2: Overview of T_g in °C (first) and insoluble fractions in % (second) for polymers synthesised with different amounts of clusters capped with 2-carboxyethyl acrylate oligomers and cross-link densities.

2-carboxyethyl acrylate oligomers	6 equivalents	12 equivalents	18 equivalents
25 mol% MMA	-3.2 °C, 96.8 %	-1.2 °C, 92.8 %	-2.3 °C, 99.8 %
50 mol% MMA	-3.1 °C, 95.8 %	-2.8 °C, 97.8 %	-3.2 °C, 99.9 %
75 mol% MMA	-4.1 °C, 96.8 %	-3.6 °C, 97.4 %	-2.6 °C, 99.5 %

Table 4.3: Overview of T_g in °C (first) and insoluble fractions in % (second) for polymers synthesised with different amounts of clusters capped with 2-carboxyethyl acrylate and cross-link densities.

2-carboxyethyl acrylate	6 equivalents	12 equivalents	18 equivalents
25 mol% MMA	-3.1 °C, 88.3 %	-4.3 °C, 96.4 %	-4.6 °C, 95.7 %
50 mol% MMA	-3.4 °C, 88.6 %	-3.6 °C, 93.5 %	-4.1 °C, 98.6 %
75 mol% MMA	-3.5 °C, 87.6 %	-3.1 °C, 95.3 %	-4.2 °C, 99.1 %

4.2.4   Reduced cross-link density & cluster loading

In an attempt to reduce the brittleness of the material we decided to lower the cross-link density by reducing the amount of functional ligands on the cluster core equal or below 6. 6-fold cross-linkers are, to the best of my

knowledge, rare while synthesising polymer networks. Commonly found cross-linking agents display a functionality of 2 or 3.[15;16] Cross-linking agent with very high functionalities can be found for the synthesis of so-called "star polymers", a type of polymer where linear polymeric arms originate from a central point referred to as the core.[17] An example is Boltorn H30™, a 32-fold cross-linker used for the synthesis of hyperbranched polymers.[18] For our purpose however, the synthesis of a polymer network, we decided that it would be beneficial if the functionality of the cluster was limited to 6 (or lower) and the mol% of cluster in the reaction mixture was kept below or equal to 20. Additionally, mono-2-(acryloyloxy)ethyl succinate was used as a new ligand. (See Figure 4.1) The temperature was also raised from 110 °C to 130 °C to ensure full conversion of the initiator. No significant difference could be observed between 2-carboxyethyl ligands and the oligomers (*vide supra*), which is why only 2-carboxyethyl oligomer ligands were tested with reduced cluster loading and cross-link density.

$$Zr_{12}O_8(OH)_8(C_6H_{11}O_2)_{20}(C_{10}H_{13}O_6)_4$$

$$Zr_{12}O_8(OH)_8(C_6H_{11}O_2)_{18}(C_{10}H_{13}O_6)_6$$
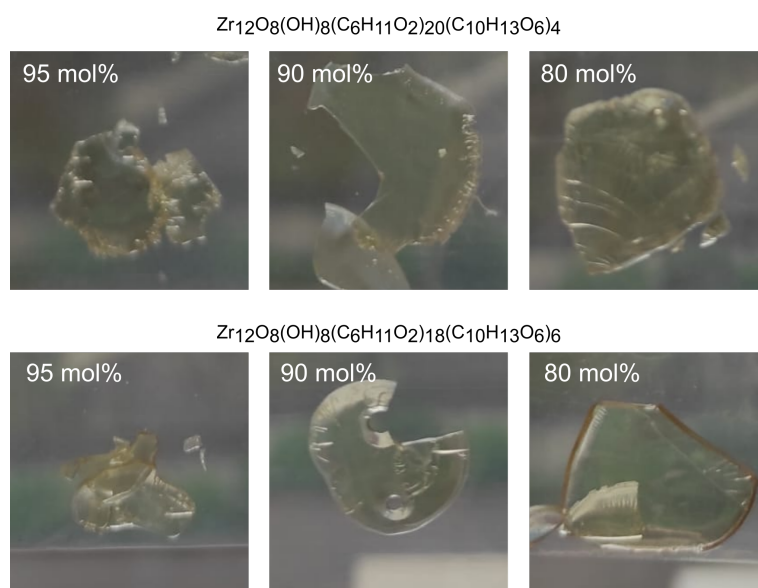
Figure 4.9: Overview of the different polymeric samples after the reaction of $Zr_{12}O_8(OH)_8(C_6H_{11}O_2)_{24-n}(C_{10}H_{13}O_6)_n$ with n = 4 or 6 together with 95, 90 and 80 mol% methylmethacrylate (from left to right) using 5 mol% dicumylperoxide as initiator reacted for 12h in a vacuum oven at 130 °C.

While the samples visually improved i.e. they look homogeneous and transparent, they are still very brittle and their surfaces look strained. The samples synthesised with mono-2-(acryloyloxy)ethyl succinate display the most

promising visual characteristics. The samples look perfectly homogeneous and less brittle compared to previous samples. (See Figure 4.9) Despite the sample looking visually pleasing their insoluble fractions are abominable. Only few samples within this series display an insoluble fraction above 80 % which is insufficient. Here, a clearer trend can be observed among the samples, the higher the amount of cross-linkeable ligands on the cluster surface the higher the insoluble fraction. This implies that high cross-link densities are necessary in order to obtain fully cross-linked materials. Alternatively, it is possible that high cluster loading is necessary when reducing the cross-linker functionality in order to obtain polymer networks. The T_g on the other hand, again does not show significant differences among all samples. All values range from -3.7 to -0.7 °C, similar to previous results.

Table 4.4: Overview of T_g in °C (top) and insoluble fractions in % (bottom) for polymers synthesised with different amounts of clusters capped with 2-carboxyethyl acrylate oligmers and cross-link densities.

2-carboxyethyl acrylate oligmers	2 eq.	3 eq.	4 eq.	6 eq.
80 mol% MMA	-0.7 °C	-0.8 °C	-1.5 °C	-2.7 °C
	42.8 %	49.0 %	62.6 %	72.8 %
90 mol% MMA	-1.7 °C	-1.4 °C	-1.3 °C	-2.2 °C
	33.3 %	51.9 %	59.2 %	88.3 %
95 mol% MMA	-1.5 °C	-1.2 °C	-2.0 °C	-1.8 °C
	34.9 %	53.1 %	72.0 %	84.2 %

Table 4.5: Overview of T_g in °C (top) and insoluble fractions in % (bottom) for polymers synthesised with different amounts of clusters capped with mono-2-(acryloyloxy) ethyl succinate and cross-link densities.

mono-2-(acryloyloxy) ethyl succinate	2 eq.	3 eq.	4 eq.	6 eq.
80 mol% MMA	-2.8 °C	-3.7 °C	-3.0 °C	-3.3 °C
	47.8 %	43.5 %	60.9 %	86.9 %
90 mol% MMA	-3.5 °C	-3.0 °C	-1.9 °C	-2.5 °C
	45.1 %	45.7 %	61.7 %	87.6 %
95 mol% MMA	-3.6 °C	-3.3 °C	-2.8 °C	-1.9 °C
	44.9 %	46.2 %	66.2 %	86.4 %

Plasticizers are commonly added to polymer resins in order to reduce the brittleness of the material.[19] Therefore, we decided to add dioctyl terephtalate (10 mol%) to the reaction mixture before polymerisation. Unfortunately, there seemed to have been a mismatch between our monomer mixture and the plasticizer since the material was heterogeneous after reaction. In contrast to last time now white precipitate is clearly visible in the sample indicating agglomeration of our clusters due to a mixing issue between the reagents.
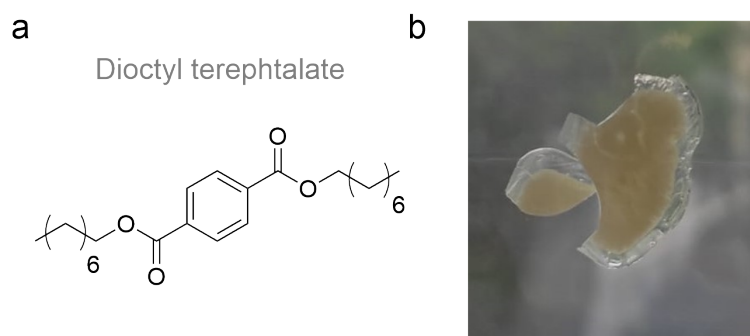
Figure 4.10: (a) Chemical structure of dioctyl terephtalate, a common plasticizer in polymer science. (b) Sample after the reaction of $Zr_{12}O_8(OH)_8(C_6H_{10}O_2)_{21}(C_{10}H_{13}O_6)_3$ with 80 mol% methylmethacrylate, 10 mol% plasticizer and 5 mol% dicumyl peroxide overnight at 110 °C. White precipitation is clearly visible in the sample indicating a chemical mismatch between the reagents.

4.3   Conclusion

Polymerisation of oleate- and linoleate- capped clusters was not successful under the given conditions. None of the chosen approaches, without initiator, adding AIBN, addition of dicumyl peroxide or varying the ligand shell, resulted in solid samples. This suggests that the double bonds are not active enough for radical polymerisation or that the termination rate is too high and propagation does not occur. It is possible that low molecular weight polymers have been formed. However, this was not further investigated as our aim was to synthesise materials with excellent mechanical properties. DOSY or DLS measurements could provide some insight into whether low molecular weight polymers are formed. When a ligand with a terminal alkene group, such as 10-undecenoic acid, is used, solid samples

are obtained. A relatively high amount of intiator (10 w% dicumyl peroxide) is needed to obtain consistently good insoluble fractions. Below this amount, it seems sample dependant if good insoluble fractions are obtained. However, this result is encouraging as it shows that alkene-capped clusters can be successfully polymerised under moderate conditions.

We have shown here that it is possible to polymerise clusters with longer and flexible ligands compared to the rigid methacrylate capped clusters found in literature.[4] We found that the cross-linking agents (i.e. clusters) need a functionality of at least 6, preferably higher, in order to obtain materials with high insoluble fraction which is indicative for a polymer network. Alternatively, it is also possible that the samples containing low functional clusters (< 6) displayed a low insoluble fraction because of the lower cluster loading. The true origin of this incomplete polymerisation should be investigated in more detail. Curiously, despite the very big variation in sample composition (cluster loading, cluster functionality and ligand shell) the T_g does not vary much. The brittleness could be a material property or could originate from the thinness of the samples, this can be checked by synthesising, e.g. 3D rod-shaped materials.

As the samples with mono-2-(acryloyloxy)ethyl succinate ligands show the most promising features, materials with 12- and 18-fold functionalised clusters should be synthesised. One could even try clusters functionalised only with flexible acrylate ligands similar to $\mathbf{Zr}_6$-Methacrylate clusters.[4] Finally, although the T_g does not vary much, it is likely that the mechanical properties of these materials are highly dependent on the functionality of the cross-linker. When studying the mechanical properties of these materials it is beneficial to add the clusters in equal mass% rather than equal mol%.

4.4   Perspective

Despite our issues, I believe it is possible to polymerise $\mathbf{Zr}_{12}$-oleate and -linoleate clusters. One could increase the pressure during the polymerisation. Polyethylene, for example, is also polymerised from ethylene at elevated temperature and very high pressure.[20] Reducing the amount of reactive ligands on the cluster surface might also improve the materials, as this reduces the chance of 2 ligands on the same cluster reacting with each other. An interesting alternative could be the triazolinedione (TAD) chemistry. These molecules perform fast Alder-ene reactions with isolated alkenes and Diels-Alder reactions with conjugated alkenes which can be used to form polymer networks.[21;22]

When polymerising (meth-)acrylate capped clusters it appears that an it-

erative process can be used to find the ideal combination of cluster surface, polymer resin, platicizer and initiator. Mixing the clusters with commercially available resins (e.g. Mercox resin™) might speed up this process. Once could also try to change the co-monomer from MMA to butyl (meth-)acrylate or change the initiator to benzoyl peroxide (BPO). As the available characterization techniques for clusters are relatively limited this optimization process is tedious, for example, it not possible to study the stability of different clusters in polymer resin using dynamic light scattering (DLS). This lengthens the whole process as it becomes more trial and error. Nevertheless, the idea of a liquid tunable inorganic monomer is tempting. The mechanical properties should be studied as it has been shown before that varying cross-link has a large effect on mechanical properties.[23;24] This method implies that additional functionalities can be easily implemented in a polymer network without changing the T_g, while still maintaining a customisable system. Once this process is optimized for heat induced radical polymerisation, his knowledge could be extended to UV-initiated polymerisations. This would enable 3D-printing applications since most resin based printers make use of UV-induced reactions. This technique is very powerful as it gives the user complete control on the size and shape of the printed material and possibly the mechanical properties by adding clusters.

As a second option, one could think of corrosion casting. Corrosion casting is the process where polymer resin is injected into the veins of an animal. After curing of the resin, the soft tissue is corroded away, leaving only the cast which can then be studied.[25;26] However, this corrosion step typically induces data loss in the very fine structures of the cast.[27] In recent research we showed that by adding 5-10 nm HfO_2 nanoparticles to the resin we could bypass the corrosion step by visualising the cast *in situ* using X-ray computed tomography (CT).[28] This allowed us to study very fine veins, arteries and capillaries which was not possible before. While this was a great result, nanoparticles typically suffer from time-consuming and expensive synthesis, limited scaleability and the possibility of leaching out of the resin. Additionally, a small but visible fraction of nanoparticles agglomerated, something which has to be avoided at all costs when higher resolutions are envisioned. This is where **Hf$_{12}$**-acrylate clusters could offer a solution. They actively address all limitations of nanoparticles. Their easy, fast, cheap and scaleable synthesis allowing for the production of large quantities in a single synthesis. By adding reactive groups and tuning of the surface chemistry, they are incorporated into the polymer network and maximize the chemical match between cluster and monomers, reducing the leaching and/or agglomeration to a minimum.

4.5 Experimental

4.5.1 Synthetic procedures

Chemicals. Zirconium propoxide (70w% in 1-propanol) is provided by Sigma Aldrich and stored in a Straus flask upon arrival. Acetic acid (>99%) is purchased from Sigma Aldrich and vacuum distilled after which it is stored in a Schlenk flask. AIBN (98%) is purchased from Sigma Aldrich and recrystallized from hot methanol. Methanol (>99.9%), dicumyl peroxide (98%), propionic acid (>99.5%), hexanoic acid (99%), oleic acid (90%), linoleic acid (>95%), methacrylic acid (99%), methylmethacrylate (99%), dioctyltereph-talate (>96%), 2-carboxyethyl acrylate, 2-carboxyethyl acrylate oligomers and mono-2-(acryloyloxy)ethyl succinate are purchased from Sigma Aldrich and used without further purification. For the acrylates no purity was listed. Ethyl acetate and dichloromethane (DCM) were bought from Biosolve and used without any further purification.

Synthesis of Zr_{12}-acetate. A 100 mL flask was equipped with a septum and cycled three times between argon and vacuum. Zirconium propoxide (11.25 mL, 25 mmol, 1 eq.) was added to the 100 mL flask, together with dry DCM (27.315 mL). Under stirring, distilled acetic acid (11.44 mL, 200 mmol, 8 eq.) was injected, reaching a total reaction volume of 50 mL and thus a zirconium concentration of 0.5 M. After 12 hours at 30 °C, the crystalline powder is isolated by filtration and further washed with 100 mL of a DCM : acetic acid mixture (4 : 1). Finally, the white powder was dried overnight under high vacuum. The powder was stored in a desiccator. The cluster was obtained as a white solid, with a 98% yield, calculated based on the molecular formula: $Zr_{12}O_8(OH)_8(CH_3COO)_{24} \cdot 6\,CH_3COOH \cdot 3.5\,DCM$.

Cluster functionalisation with 10-undecenoic, oleic and linoleic acid. The Zr_{12}-acetate cluster (2 g, 14 mmol acetate, 24 eq. acetate) was weighed into a 40 mL vial. The mixture of new ligands depends on the targeted ligand shell composition, here the example is given for 2 functional groups per cluster core however, these ratios can be easily changed to obtain 3, 4, 6, 12 or 18 functional groups. 2 equivalents (1.17 mmol) of 10-undecenoic (216 mg), oleic (369 µL) or linoleic acid (365 µL) combined with 22 equivalents of hexanoic acid (12.83 mmol, 1.6 mL) were added together with 4 mL of DCM. Afterwards, the solution is stirred for 60 min, after which a clear solution was obtained. Subsequently, the solution was dried under vacuum at 70 °C for 1 hour. The sample transforms from a solid cluster into a viscous liquid. Again, 4 mL of DCM was added with a subsequent stirring step of 1h. Finally, the sample is dried overnight at the Schlenk line.

Cluster functionalisation with acrylates. The Zr_{12}-acetate cluster (2 g, 14 mmol acetate, 24 eq. acetate) was weighed into a 40 mL vial. The mixture of new ligands depends on the targeted ligand shell composition, here the example is given 2 functional groups per cluster core however these ratios can be easily changed to obtain 3, 4, 6, 12 or 18 functional groups. 2 equivalents (1.17 mmol) of 2-carboxyethyl acrylate (139 μL), 2-carboxyethyl acrylate oligomers (172 μL) or mono-2-(methacryloyl) ethyl succinate (226 μL) combined with 22 equivalents of hexanoic acid (12.83 mmol, 1.6 μL) were added together with 4 mL of ethyl acetate. Afterwards, the solution is stirred for 60 min, after which a clear solution was obtained. Subsequently, the solution was dried under vacuum at room temperature for 1 hour. The sample transforms from a heterogeneous mixture into a viscous liquid. Again, 4 mL of ethyl acetate was added with a subsequent stirring step of 1h. Finally, the sample is dried overnight at the Schlenk line.

Recrystallization AIBN. 4.1 g of AIBN (25 mmol) was weighed into a 50 mL Erlenmeyer, 30 mL methanol was added and the solution was heated to 45 °C. After everything dissolved the heating plate was turned off but the Erlenmeyer was left on the heating plate to ensure a slow cooling of the sample. While cooling down needle shaped crystals will start to form which can be filtered of after 30 minutes. After filtration the solid was collected, dried for 3 more hours on the Schlenk line and subsequently stored in the freezer.

Radical polymerisation of clusters. In order to polymerize the surface functionalised clusters they are weighed into a 20 mL vial to which the required amount of co-monomer is added. (0-95 mol% based on the mmol alkene/acrylate) To this monomer mixture the required amount of initiator (2.5-10 mol% based on the mmol alkene/acrylate) is added. This mixture is homogenized using the vortex stirrer until all initiator is dissolved. Finally, this mixture is poured onto a Teflon sheet and reacted overnight in a vacuum oven, at 110 °C (Dicumyl peroxide) or 80 °C (AIBN) respectively.

4.5.2 Analysis techniques

General instrumentation. Nuclear Magnetic Resonance (NMR) measurements were recorded at 298K on Bruker UltraShield 500 spectrometer operating at a frequency of 500.13 MHz.

Determination of the insoluble fraction. For this 50 mg of the polymer sample was weighed and encapsulated in a self-made envelope from filter paper. The sample code is written on the envelope with pencil and the samples are submerged in DCM for 2 days. Afterwards, the envelopes are

dried for an additional 2 days at the Schlenk line. Finally, the samples are weighed again and the insoluble fraction is determined according to Equation 4.1 where m_{begin} is the mass before submerging the sample and m_{end} is the mass after drying.

$$Insoluble\,fraction = \frac{m_{end}}{m_{begin}}.100 \tag{4.1}$$

Differential scanning calorimetry. Differential scanning calorimetry was measured using 10 mg of polymer for each measurement on a DSC 214 Polyma (Netzsch GmbH, Austria) under a nitrogen atmosphere from -50 °C to 180 °C with a cooling rate of 40 $K * min^{-1}$ and a heating rate of 10 $K * min^{-1}$. The first heating run is performed to remove the thermal history of the polymer, DSC curves shown correspond to the second heating curve. The data was analysed using the Netzsch Proteus thermal analysis software.

4.6   Contributions

DSC measurements were performed with the help of John Coats, PhD student in the group of Prof. Dr. Cornelia Palivan at the University of Basel.

References

[1] Dreyer, A.; Feld, A.; Kornowski, A.; Yilmaz, E. D.; Noei, H.; Meyer, A.; Krekeler, T.; Jiao, C.; Stierle, A.; Abetz, V.; Weller, H.; Schneider, G. A. Organically linked iron oxide nanoparticle supercrystals with exceptional isotropic mechanical properties. *Nature Materials* **2016**, *15*, 522–528.

[2] Schubert, U.; Gao, Y.; Kogler, F. R. Tuning the properties of nanostructured inorganic-organic hybrid polymers obtained from metal oxide clusters as building blocks. *Progress in Solid State Chemistry* **2007**, *35*, 161–170.

[3] Kreutzer, J.; Qin, X.-H.; Gorsche, C.; Peterlik, H.; Liska, R.; Schubert, U. Variation of the Crosslinking Density in Cluster-Reinforced Polymers. *Mater. Today Commun.* **2015**, *5*, 10 – 17.

[4] Schubert, U. Organically Modified Transition Metal Alkoxides: Chemical Problems and Structural Issues on the Way to Mater. Syntheses. *Acc. Chem. Res.* **2007**, *40*, 730–737.

[5] Odian, G. In *Radical Chain Polymerization*; John Wiley & Sons Inc., 2004; pp 198–349.

[6] Brooks, B. W.; Melville, H. W. Viscosity effects in the free-radical polymerization of methyl methacrylate. *Proceedings of the Royal Society of London. A. Mathematical and Physical Sciences* **1977**, *357*, 183–192.

[7] Flory, P. J. The Mechanism of Vinyl Polymerizations1. *Journal of the American Chemical Society* **1937**, *59*, 241–253.

[8] Su, W.-F. In *Radical Chain Polymerization*; Su, W.-F., Ed.; Springer Berlin Heidelberg: Berlin, Heidelberg, 2013; pp 137–183.

[9] Spetz, A.; Svanström, M.; Ramnäs, O. Determination of Dicumyl Peroxide in Workplace Air. *The Annals of Occupational Hygiene* **2002**, *46*, 637–641.

[10] Yuan, L.; Wang, Z.; Trenor, N. M.; Tang, C. Robust Amidation Transformation of Plant Oils into Fatty Derivatives for Sustainable Monomers and Polymers. *Macromolecules* **2015**, *48*, 1320–1328.

[11] Tarnavchyk, I.; Popadyuk, A.; Popadyuk, N.; Voronov, A. Synthesis and Free Radical Copolymerization of a Vinyl Monomer from Soybean Oil. *ACS Sustainable Chemistry & Engineering* **2015**, *3*, 1618–1622.

[12] Mortimer, G. A.; Arnold, L. C. Free-radical polymerization of olefins. *Journal of Polymer Science Part A : General Papers* **1964**, *2*, 4247–4253.

[13] Wang, Q.; Cui, H.; Wang, X.; Hu, Z.; Tao, P.; Li, M.; Wang, J.; Tang, Y.; Xu, H.; He, X. Exceptional Light Sensitivity by Thiol-Ene Click Lithography. *Journal of the American Chemical Society* **2023**, *145*, 3064–3074.

[14] Puchberger, M.; Kogler, F. R.; Jupa, M.; Gross, S.; Fric, H.; Kickelbick, G.; Schubert, U. Can the Clusters $Zr_6O_4(OH)_4(OOCR)_{12}$ and $[Zr_6O_4(OH)_4(OOCR)_{12}]_2$ Be Converted into Each Other? *Eur. J. Inorg. Chem.* **2006**, *2006*, 3283–3293.

[15] Elliott, J. E.; Bowman, C. N. Monomer Functionality and Polymer Network Formation. *Macromolecules* **2001**, *34*, 4642–4649.

[16] Baudry, R.; Sherrington, D. C. Facile Synthesis of Branched Poly(vinyl alcohol)s. *Macromolecules* **2006**, *39*, 5230–5237.

[17] Ren, J. M.; McKenzie, T. G.; Fu, Q.; Wong, E. H. H.; Xu, J.; An, Z.; Shanmugam, S.; Davis, T. P.; Boyer, C.; Qiao, G. G. Star Polymers. *Chemical Reviews* **2016**, *116*, 6743–6836.

[18] Zeng, X.; Zhang, Y.; Wu, Z.; Lundberg, P.; Malkoch, M.; Nyström, A. M. Hyperbranched copolymer micelles as delivery vehicles of doxorubicin in breast cancer cells. *Journal of Polymer Science Part A : Polymer Chemistry* **2012**, *50*, 280–288.

[19] Masse, M.; Genay, S.; Feutry, F.; Simon, N.; Barthélémy, C.; Sautou, V.; Décaudin, B.; Odou, P.; for the Armed Study, G. How to solve the problem of co-elution between two compounds in liquid chromatography through the first UV derivative spectrum. A trial on alternative plasticizers to di(2-ethylhexyl) phthalate. *Talanta* **2017**, *162*, 187–192.

[20] Beyer, C.; Oellrich, L. R. *Supercritical Fluids as Solvents and Reaction Media*; Elsevier, 2004; pp 61–84.

[21] Houck, H. A.; De Bruycker, K.; Barner-Kowollik, C.; Winne, J. M.; Du Prez, F. E. Tunable Blocking Agents for Temperature-Controlled Triazolinedione-Based Cross-Linking Reactions. *Macromolecules* **2018**, *51*, 3156–3164.

[22] Türünç, O.; Billiet, S.; De Bruycker, K.; Ouardad, S.; Winne, J.; Du Prez, F. E. From plant oils to plant foils: Straightforward functionalization and crosslinking of natural plant oils with triazolinediones. *European Polymer Journal* **2015**, *65*, 286–297.

[23] Huang, J.; Fu, P.; Li, W.; Xiao, L.; Chen, J.; Nie, X. Influence of crosslinking density on the mechanical and thermal properties of plant oil-based epoxy resin. *RSC Advances* **2022**, *12*, 23048–23056.

[24] Andersons, J.; Cabulis, P.; Kirpluks, M. The Effect of Crosslink Density on the Physical and Mechanical Properties of Bio-Based Polyurethane Foams. *Macromolecular Symposia* **2022**, *404*, 2100329.

[25] Reyes, P.; D'Hooge, D. R.; Cardon, L.; Cornillie, P. From identifying polymeric resins to corrosion casting applications. *Journal of Applied Polymer Science* **2022**, *139*, 52284.

[26] De Spiegelaere, W.; Caboor, L.; Van Impe, M.; Boone, M. N.; De Backer, J.; Segers, P.; Sips, P. Corrosion casting of the cardiovascular structure in adult zebrafish for analysis by scanning electron microscopy and X-ray microtomography. *Anatomia, Histologia, Embryologia* **2020**, *49*, 635–642.

[27] Hossler, F. E.; Douglas, J. E. Vascular Corrosion Casting: Review of Advantages and Limitations in the Application of Some Simple Quantitative Methods. *Microsc Microanal* **2001**, *7*, 253–264.

[28] Goossens, E. et al. From corrosion casting to virtual dissection: contrast-enhanced vascular imaging using hafnium oxide nanocrystals **2023**.

5

Clusters as inorganic monomers for covalent adaptable networks

After a certain high level of skill is achieved, science and art tend to coalesce in aesthetics, plasticity and form. The greatest scientists are artists as well.
– Albert Einstein

5.1   Introduction

We are all aware of the increasing amount of plastic that is accumulating in nature, and with our increasing population, the problem is unlikely to disappear on its own. On the other hand, we can also not imagine a life without plastics. They are used all around us, from the water bottles we use to the cars and airplanes used for transportation. So either we stop using plastics (which, in my opinion, is not very realistic) or we focus our efforts on creating a more circular economy where plastics are recycled rather than left to decompose in nature for decades/centuries.[1] An inventive solution to the latter could be covalent adaptable networks (CANs).[2] These relatively new materials form a bridge between thermoplasts and thermosets. (*vide*

supra) The core idea is that the cross-links of CANs are reversible. They are non-reversible without activation, hence they behave as a thermoset. However, upon activation the cross-links become reversible and they act as thermoplasts.[3] Activation of the reversible cross-links is typically achieved with heat or UV.[4–8] (*vide supra*)

The addition of inorganic particles to polymer resins is typically done to impart novel characteristics to said polymers, e.g. additional mechanical strength.[9] Both titanium and zirconium oxo clusters have been used in recyclable polymers by exploiting the clusters as coordination centers. A **Zr**$_6$-octahedron can be seen as a 12-fold coordination center, a **Ti**$_8$ cluster can be seen as a 16-fold coordination center. They have combined these clusters with a linear polymer, containing multiple carboxylic acid groups. In the case of titanium oxo clusters, the polymer was recycled by the addition of excess free acid, which caused the clusters to become separate entities again. This allowed them to switch between a gel and liquid phase.[10] In the case of the zirconium clusters, the polymers were recycled using a hot plate press.[11] Once the samples were prepared, they were cut into small fragments, placed in a metal mold and pressed in between 2 heated plates that exerted pressure on the sample. However, both of these examples were limited to the short and rigid ligands (pivalic and acetic acid respectively) and did not surface functionalise the clusters after synthesis. In this chapter we will once again exploit our knowledge obtained from the clusters in the previous chapters. Here, the clusters are used as tailor-made inorganic monomers, not for radical polymerisation, but for the synthesis of cluster-reinforced covalent adaptable networks.

5.1.1 Leibler's system

The first vitrimer and inspiration for this chapter was published in 2011 by Ludwig Leibler's group.[12] Inspired by glass, which is solid at room temperature but liquid when heated, they developed a polymer that could be reprocessed at elevated temperatures. By reacting a difuntional epoxide (BADGE) with Pripol 1040 (a mixture of a di- and trifunctional carboxylic acid) a polymer network containing esters and alcohols is formed. (See Figure 5.1) Zn^{2+} is added as catalyst. The transesterification, where an alcohol reacts associatively with an ester, ensured the recyclability of the polymer. At low temperatures, this reaction does not take place and the material behaves as a thermoset. When heated however, this reaction accelerates and the material behaves as a thermoplastic. Legrand *et al.* added epoxy functionalised SiO_2 material to the Leibler system, actively improving the mechanical properties compared to the native material. Transparency of

the materials was lost due to the big size (μm range) of their SiO_2.[13]
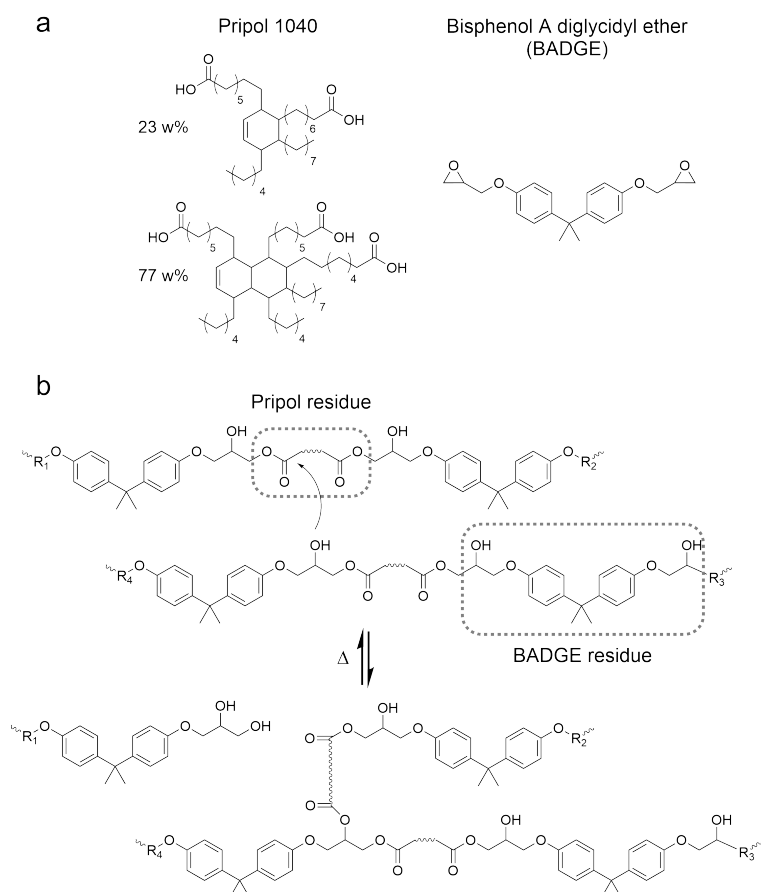
Figure 5.1: (a) The chemicals used in the original Leibler system. A mixture of di- and trifunctional carboxylic acid (Pripol 1040) on the left and a difunctional epoxide Bisphenol A diglycidyl ether (BADGE) on the right. (b) The chemistry of the polymer network, after the carboxylic acid opened the epoxide group an ester and an alcohol functionality are created. This material can be reprocessed because at elevated temperatures a transesterification reaction, catalyzed by Zn^{2+} (not shown), can happen as shown in the figure.

Inspired by this material, we sought to functionalise our clusters with epoxide ligands and create a network similarl to Leibler's system. Unfortunately, neither clusters functionalised with epoxide molecules or straightforward

synthesis of carboxylic acids with epoxide functionalities have been reported in literature. Therefore, we first had to develop a synthesis to obtain our desired tailor-made ligands. We could then use this ligand to functionalise the clusters and polymerize them. Again we took inspiration from the nanoparticle field by using rather long carboxylic acids. Two molecules were chosen for epoxidation. One was a terminal alkene containing molecule (10-undecenoic acid) and the other was the common nanoparticle ligand oleic acid. mCPBA was chosen as epoxidising agent because it reacts at room temperature, minimising side reactions.

5.1.2   Synthesis of polymer networks

5.2   Results & discussion

5.2.1   Synthesis of the epoxide ligands

First of all, the reaction kinetics of the epoxidation in DCM were studied using NMR to track how fast the reaction proceeds. The equivalents of m-CPBA (2.3 equivalents) was based on a publication from 1991.[14] Looking at Figure 5.2 it is evident that the signals corresponding to the double bond, at 5 and 5.8 ppm, gradually decrease as the reaction progresses. This indicates the conversion of the double bond into the epoxide. Additionally, the signal for the carbon adjacent to the double bond disappears. From this it was concluded that the reaction was completed after 8h since there are no more detectable signals for the double bond. To ensure full reaction, this reaction was performed overnight (16h). The purification entails several washing steps with 4.1 m% $NaSO_3$ in H_2O, pure H_2O and brine respectively. Finally, the mixture is applied to a silica plug after which the plug is washed with ethyl acetate to extract our product with a 76% yield. The epoxidation of oleic acid can be synthesised similar to 10-undecenoic acid epoxide in high yields 98.5% and the reaction seems to be complete in a mere 30 minutes. (See Figure A.47)

The purified reaction products were characterized using ^{1}H NMR (See Figure A.48-A.49) and HRMS (See Figures A.50-A.51). In both products there are trace amounts of benzoic acid impurity, which is a side product of the epoxidation. In HRMS the deprotonated carboxylate was found for both products.
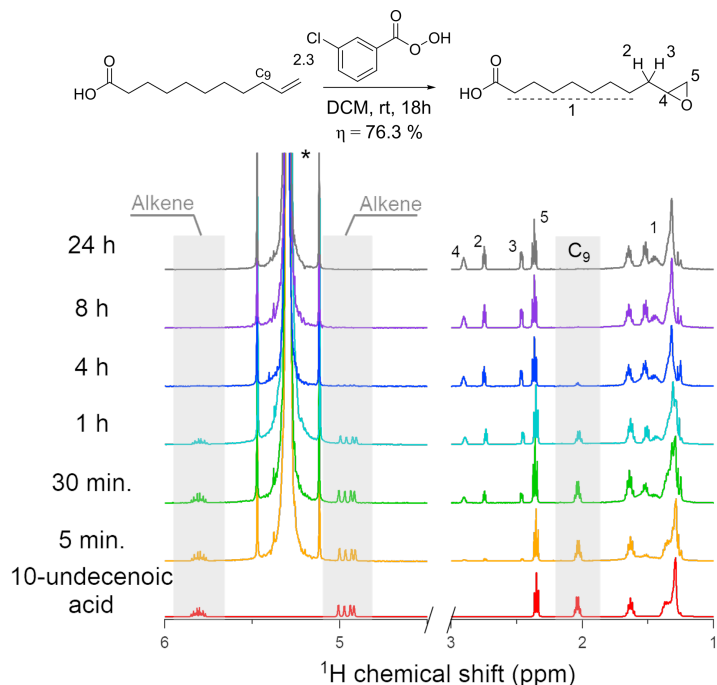
Figure 5.2: ^{1}H NMR in CDCl$_3$ of the epoxidation of 10-undecenoic acid using 2.3 equivalents m-CPBA in DCM. The figure shows the gradual decrease of the signals corresponding to the alkene resonance at 5 and 5.8 ppm together with the decrease of the signal at 2 ppm which corresponds to the carbon adjacent to the double bond. It can be concluded that after 8h the reaction is complete. The solvent (DCM) is indicated with an asterisk.

5.2.2   Cluster functionalisation and polymer synthesis

After synthesis and purification of the epoxide ligand the clusters had to be surface functionalised with the respective epoxide. Initially, clusters with 6, 12 or 18 equivalents of epoxide ligands (both the epoxide of oleic acid as well as the one from 10-undecenoic acid) were targeted with hexanoic acid as secondary ligand. Similar to the (meth-)acrylate functionalisation no heat is used during the ligand exchange to avoid side reactions. Unfortunately, after ligand exchange the ratios were determined using the ^{1}H NMR spectra and it was found that the ratios are not in good agreement with the expected ones. (See Figure A.52-A.53) Nevertheless, they were used as inorganic monomers for the synthesis of CANs, either pure or with 50 mol% BADGE added as co-monomer.

Since BADGE is a solid at room temperature, $(T_m = 40\text{-}44\ °C)$ it is first mixed with the corresponding amount of Pripol 1040 (containing 0, 5 or 10 mol% Zn^{2+}). This mixture is heated using a heating gun in order to, on one side melt BADGE and on the other side reduce the viscosity of Pripol 1040. Once the mixture is homogeneous this yields a transparent solution after vortex stirring. The corresponding amount of cluster, to obtain a 1 to 1 ration epoxide-carboxylic acid, is dissolved in 0.5 mL EtOAc and added drop wise into the BADGE-Pripol 1040 mixture while stirring. Because of the immediate ligand exchange between Pripol 1040 and the cluster the viscosity increases rapidly. Therefore, the mixture is stirred mechanically, using a spatula, to ensure a homogeneous mixture. Finally, the mixture is poured onto a Teflon sheet and cured at 130 °C in a vacuum oven overnight to yield solid transparent samples. Typically, an FTIR spectrum is recorded before and after reaction to make sure that the epoxide signal at ~ 910 cm^{-1} has disappeared, indicating successful polymerisation. (See Figure 5.3)
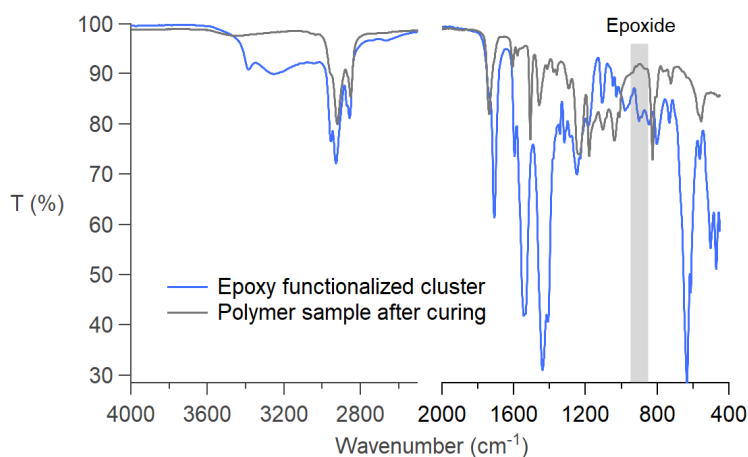
Figure 5.3: FTIR spectra of the cluster before polymerisation (blue) and the polymer sample after curing (grey). The signal around 910 cm^{-1}, indicative for an epoxide group, disappears after curing the sample overnight at 130 °C proving that the polymerisation is successful.

The insoluble fractions, displayed in Table 5.1, are good for nearly all samples synthesised with the epoxide of 10-undecenoic acid, i.e. $> 90\%$. However, for the samples synthesised from the oleic acid epoxide only 1 sample displays a good insoluble fractions. (See Table 5.2) One of the samples even displays an insoluble fraction of nearly 50%, meaning that half of the sample can dissolve again and is not part of the polymer network.

These initial results indicate that the epoxide functionality is shielded by the remaining ligand tail, hampering successful polymerisation.

Table 5.1: The insoluble fraction of covalent adaptable networks synthesised with 6, 12 or 18 equivalents of the epoxide synthesised from 10-undecenoic acid.

Oleic acid epoxide	mol% BADGE	Insoluble fraction (m%)
6 eq. epoxide	0	91.5 %
6 eq. epoxide	50	94 %
12 eq. epoxide	0	95.2 %
12 eq. epoxide	50	96.4 %
18 eq. epoxide	0	93 %
18 eq. epoxide	50	93.5 %

Table 5.2: The insoluble fraction of covalent adaptable networks synthesised with 6, 12 or 18 equivalents of the epoxide synthesised from oleic acid.

Oleic acid epoxide	mol% BADGE	Insoluble fraction (m%)
6 eq. epoxide	0	87 %
6 eq. epoxide	50	83 %
12 eq. epoxide	0	80.7 %
12 eq. epoxide	50	87.3 %
18 eq. epoxide	0	54 %
18 eq. epoxide	50	90.7 %

Because of the divergent ligand ratios and disappointing insoluble fractions we decided to functionalise the cluster surface with only of 2, 4 or 6 equivalents epoxide ligand. Only the epoxide of 10-undecenoic acid was considered from hereon. After exchange we found that the relative ratios between the epoxide and hexanoic acid ligand improved. Here around 4 acetate ligands remain on the cluster and the dimeric structure seemingly persist. (See Figure 5.4)
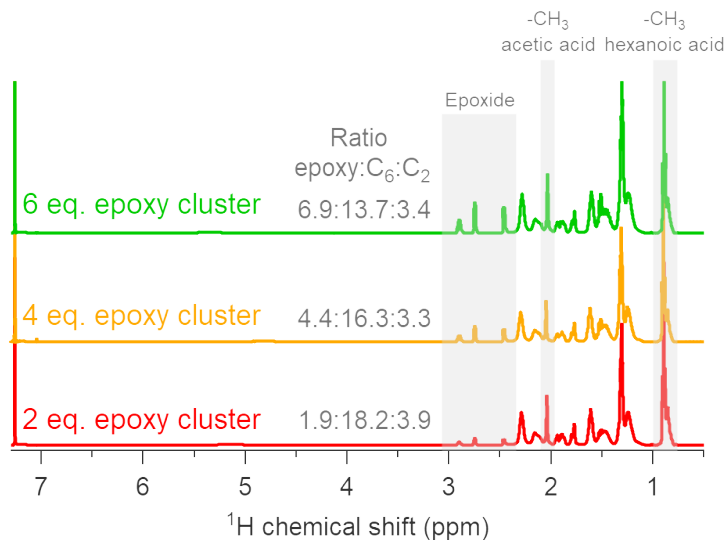
Figure 5.4: ^{1}H NMR in CDCl$_3$ of the clusters functionalised with 6, 4 and 2 equivalents of the synthesised epoxide ligand. Also the ratios between the different ligands are displayed. As it is clear from the signal around 2 ppm some acetate ligands remain on the surface even after exchange.

Now that we have epoxide functionalised clusters they can be used as monomers. Several parameters can be changed in order to synthesise different polymer samples:

- The amount of cross-linkable ligand on the cluster (2, 4 or 6)

- The amount of additional epoxide monomer (BADGE) (0-95 mol%)

- The amount of Zn^{2+} catalyst (0-10 mol%)

This generated numerous distinguishable polymer samples which were synthesised.

5.2.3 Reprocessing the polymers

Once the polymers are synthesised they still contain bubbles originating from trapped solvent in the reaction mixture prior to polymerisation. Since, by definition, these materials should be reshapable they were reprocessed using a hot plate press. This processing step should always be carried out before further characterization as inhomogeneous samples will lead to inconsistent results. In a first attempt the samples were cut up in small fragments added to a metallic mold and pressed for 1h under 1.5 bar pressure.

The samples containing less than 95 mol% BADGE were successfully reprocessed, in contrast to the samples containing 95 mol% which came out of the mold in pieces. After several iterations it was found the all samples can be reprocessed in 30 minutes. Samples containing less than 95 mol% BADGE are reprocessed after 30 minutes at 160 °C using 3 bar pressure. The samples containing 95 mol% BADGE require higher temperatures, they can be reprocessed after 30 minutes at 220 °C using 3 bar pressure. Interestingly, even the samples without additional Zn^{2+} were reprocessable indicating that either the clusters are able to catalyse the transesterification reaction or a different process is responsible for the reversible cross-links.
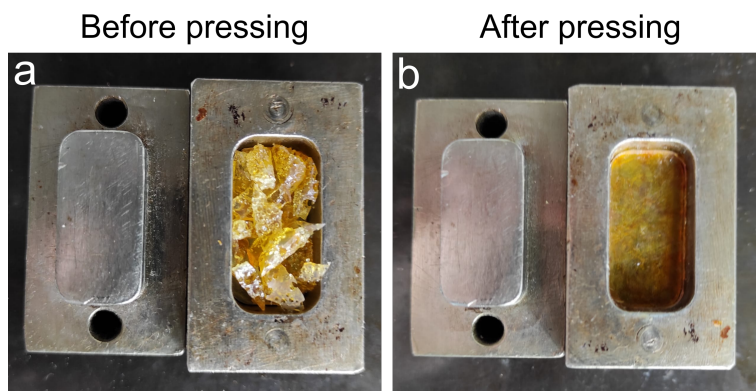
Figure 5.5: Example of reshaping the cluster containing polymers. (a) Cut up sample which still contains bubbles and (b) The same sample after pressing for 30 minutes at 220 °C using 3 bar pressure yielding a homogeneous polymer sample.

5.2.4 Polymer characterization

In order to characterize the obtained materials several techniques were applied. Their insoluble fraction was determined via swelling the samples in DCM and after subsequent drying the weight loss was determined. Differential scanning calorimetry (DSC) was applied to obtain the glass transition temperature, which is defined as the temperature where a hard, glassy polymer switches to a more flexible, soft state. Finally, the thermal degradation was studied using thermogravimetric analysis (TGA).

It was found that nearly all the samples display an insoluble fraction of approximately 10 m%, which is considered a good value for a polymer network. Interestingly, there were no clear trends among the samples, despite showing large variety in composition. It could have been expected that

samples with larger amounts of clusters showed a lower insoluble fraction, as there will be more H-bonded acid and more uncross-linked ligands in the polymers. Since this is not the case one could assume that the clusters are not prone to release their weaker H-bonded acid while submerged in solvent for multiple days.
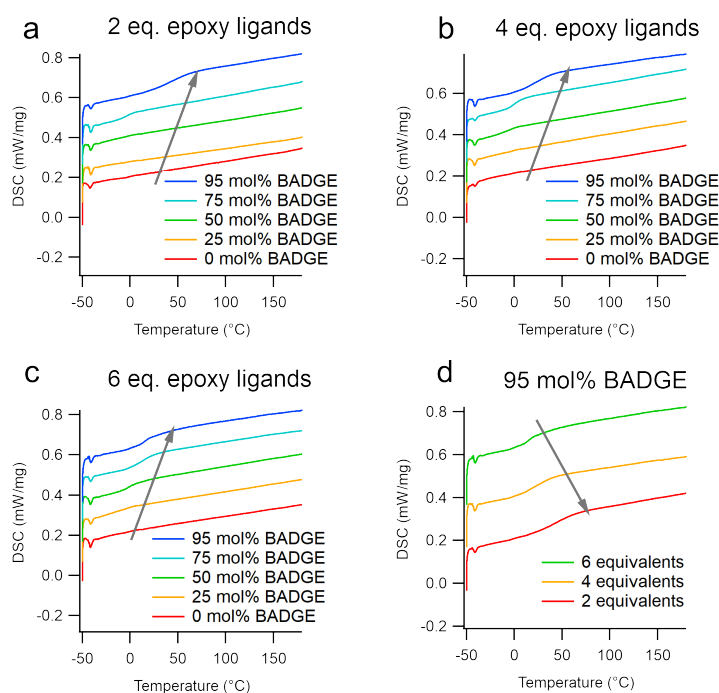
Figure 5.6: Overview of DSC measurements of samples containing 5 mol% Zn with different amounts of epoxide ligands on the cluster surface which are (a) 2 equivalents, (b) 4 equivalents or (c) 6 equivalents. The T_g increase upon decreasing cluster amounts. (d) Comparison of the 95 mol% BADGE containing samples, the T_g increases when the amount of epoxide ligands on the cluster core is reduced.

The glass transition temperature (T_g) was determined using the same temperature range and heating range as in the previous chapter. (-50 - 180 °C, 10 K/min) The samples with high amounts of clusters (0 or 25 mol% BADGE) did not show a clear inflection point in the thermogram, indicating crystallinity of the material. Indeed, they do resemble quite well crystalline MOFs with the only difference being a more flexible linker. The samples with less mol% clusters do show a clear inflection point and the T_g could be

determined accurately. From this we learn that the T_g increases when the amount of BADGE is increased as a co-monomer. (See Figure 5.6)

Finally, the thermal stability was probed with TGA. It appears that the more clusters a sample contains the faster the thermal degradation occurs, i.e. the mass starts decreasing faster. This could be caused by an increased amount of H-bonded ligands because of the higher cluster fraction. Their bond is weaker compared to the chelating or bridging ligands and are thus expected to be burned of first. Alternatively, this initial decrease could be the remaining acetate ligands which were not removed during ligand exchange. Figure 5.7 displays the samples containing clusters functionalised with 2 equivalents of epoxide ligands combined with different amounts of BADGE and 5 mol% Zn, the trend is clearly visible. The red curve (high cluster amount) decreases before the blue curve (low cluster amount). The same trend can be found in all other samples with different compositions. (See Figure A.62-A.69) Another observation, one that confirms the different amount of clusters inside the material, is the different heights of the plateau from 600-800 °C. The higher the cluster amount in the sample, the higher the amount of remaining ZrO_2 will be after the measurement. In our case, it is evident that the plateau is lower for low cluster containing samples (blue) compared to high cluster containing samples (red), confirming that these samples indeed contain different amounts of clusters. (See Figure 5.7)
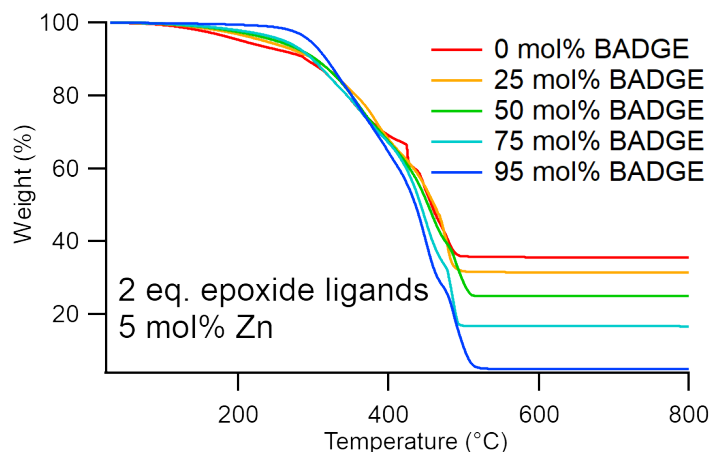
Figure 5.7: Overview of TGA measurements of polymers synthesised from clusters functionalised with 2 equivalents epoxide ligands combined with different amounts of BADGE, containing 5 mol% Zn as catalyst. The trend, more clusters equals faster thermal degradation, is clearly visible.

5.2.5 Relaxation times and activation energies

In order to know the amount of shear strain which can be applied to the sample, without leaving the linear viscoelastic region, is determined via an amplitude sweep. (See Figure A.70) Here, a sample is subjected to an increasing strain while the frequency is constant. For the brittle materials (mol% BADGE < 95) only a small amount of shear strain could be applied. According to the amplitude sweep the linear viscoelastic region ends at 0.15 %. For the more flexible materials (mol% BADGE = 95) a slightly higher shear strain of 0.25 % could be applied. By applying these shear strains to the sample and following the relaxation modulus over time, relaxation times (τ) can be obtained. The relaxation time, of a single measurement, is found when the relaxation modulus is at 37 % of it's initial value. (See Equation 5.4-5.5) Then these measurements are repeated at different temperatures. The natural logarithms of these relaxation times are plotted as a function of the inverse of the temperature (Arrhenius plot) and the activation energy of the exchange reaction can be extracted since the slope of the curve is equal to E_a/R. (See Equation 5.6-5.9)
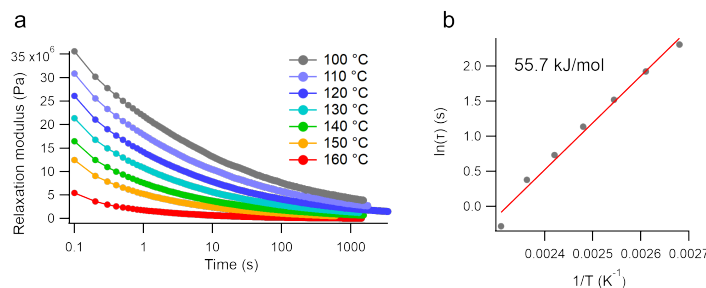
Figure 5.8: The stress relaxation measurement of **Zr**$_{12}$ cluster surface functionalised with 2 equivalents of 10-undecenoic epoxide polymerised with 1 equivalent of Pripol 1040. The samples are able to relax stress within a matter of seconds. E_a was detmined to be 55.7 kJ/mol.

From the decreasing trend in the relaxation modulus, it is clear from graph 5.8 above that the sample can efficiently relax the stress applied to the sample. However, this graph can also provide insights into the relaxation mechanism. The relaxation modulus (y-axis) at time zero increases upon decreasing temperature. This indicates that the mechanism by which the sample relaxes stress is dissociative in nature.[15] Because, the higher the temperature the more the exchange reaction will be towards the dissociated state, lowering the amount of cross-links and thus weakening the sample.

Surprisingly, this is not what Leibler and co-workers observed for their trans-esterification vitrimer.[12] They observed an associative exchange mechanism. One hypothesis which can explain this observation is that the material does not at all display a transesterification reaction, but relaxes via a ligand exchange. Indeed, the ligand exchange onto the cluster has been proven to proceed through a dissociative mechanism.[11] The remaining stress relaxation measurements can be found in appendix A, Figures A.71-A.97.

More interestingly, if the amount of clusters is reduced to 5 mol% the relaxation mechanism seems to shift. Instead of a decreasing exponential looking curve, the curve shows an initial small decrease similar to the decreasing exponential after which the curve seems to take a sigmoidal shape. This sigmoidal shape shares a strong resemblance with the stress relaxation experiments performed by Leibler *et al.* indicating that at least partially the transesterification is happening. This reaction is slow compared to the relaxation times observed before indicating that the presence of the clusters inhibits the transesterification reaction. Also the activation energies seem to shift towards higher values compared to the samples containing more clusters. (See Figure 5.9)
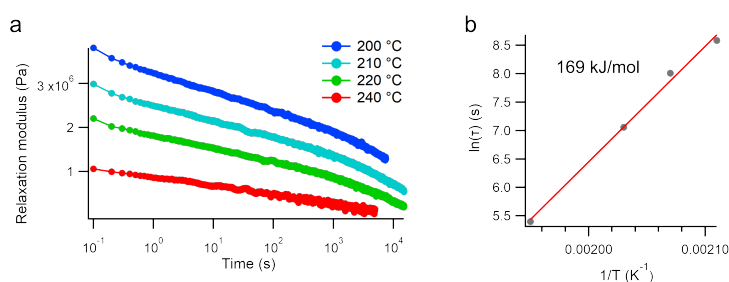
Figure 5.9: The stress relaxation measurement of **Zr**$_{12}$ cluster surface functionalised with 5 mol% 2 equivalents of 10-undecenoic epoxide mixed with 95 mol% BADGE polymerised with 1 equivalent of Pripol 1040. The samples are able to relax stress within a matter of seconds. E_a was determined to be 168 kJ/mol.

A possible pathway how the system can relax stress is shown in Figure 5.10. Starting from a cluster capped with a bridging ligand (initial state), which can dissociate to adopt a monodentate binding mode. This is expected to be a slow step since it reduces the coordination number of 1 Zr atom from 8 to 7 which is less favourable. The vacant site can subsequently be coordinated by a new, free carboxylic acid (in blue). After proton transfer, the native ligand can then leave the cluster. Finally, the new ligand will switch from

its monodentate binding mode to a bidentate mode, arriving back at the initial position with an exchanged ligand.
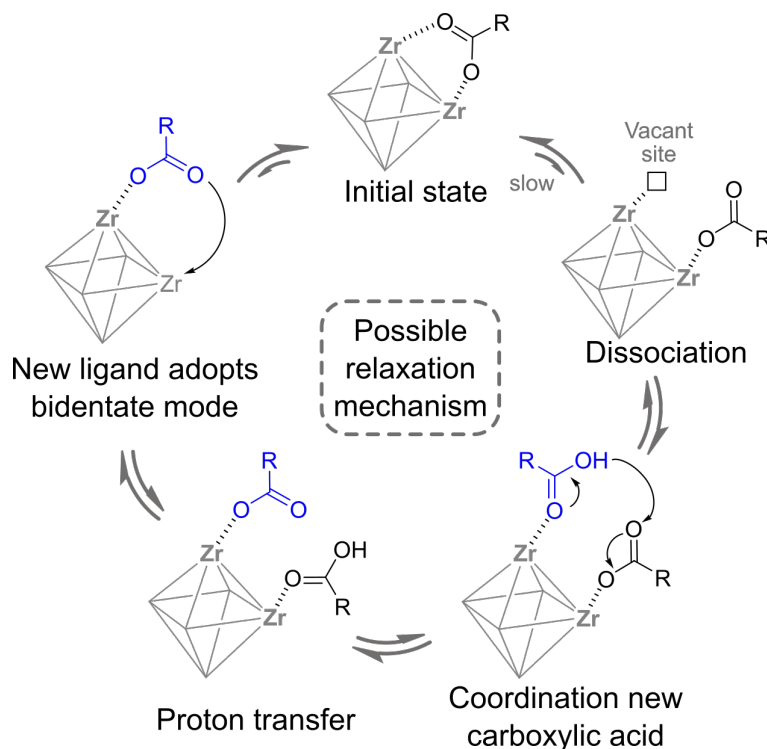
Figure 5.10: Possible relaxation mechanism where a novel ligand exchanges for the native ligand. Via this method the material is able to rearrange its internal structure in order to relax stress applied to the system.

5.2.6   Comparing polymer samples

Because of the large variety of parameters that can be tuned, we compared the polymer samples among each other. The samples were compared on mass% rather than mol% because the relative ratios are quite different. For example, a sample containing 50 mol% of 2 equivalents epoxide capped clusters results in 22 m% clusters, whereas the same sample with 6 equivalents epoxide capped clusters results in only 13.2 m% cluster. Therefore, we decided it was fairer to compare the clusters based on mass% cluster present in the polymer matrix. The most fascinating samples were the ones where no additional Zn^{2+} catalyst was added since they were initially not

expected to relax stress, because they lack the catalyst. The comparison of these samples is shown in Figure 5.11.
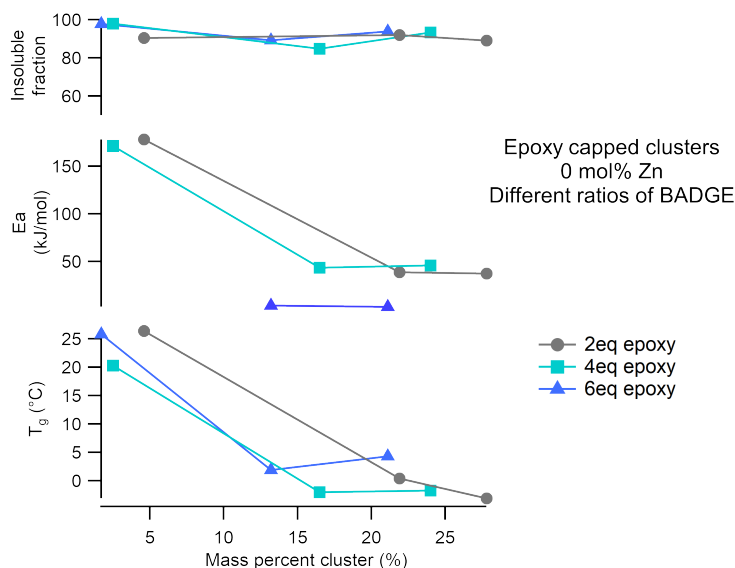
Figure 5.11: Overview of the properties of the polymer samples prepared with 0 mol% Zn using clusters with different amounts of epoxide ligands and different amounts of BADGE. On top the insoluble fractions are displayed. The middle panel showcases the activation energies obtained from the rheological experiments. Finally, at the bottom the T_g is displayed.

The insoluble fraction is around 90% for all samples. Samples with low cluster loading display a slightly higher insoluble fraction ($> 95\%$). Comparing the activation energies, obtained from the stress relaxation measurements, a similar trend for both the samples with 2 and 4 equivalents epoxide ligands was observed. When BADGE was added in 0 or 50 mol% the activation energy seems to hoover around 50 kJ/mol, with a small dip going from 0 to 50 mol% BADGE. When 95 mol% BADGE is added the activation energy increases drastically indicating that the relaxation process changes. The sample with 6 equivalents and 95 mol% BADGE did not result in reliable rheology data and need to be remeasured. Finally, the T_g shows a decreasing trend when increasing the amount of clusters in the samples. With a big difference between the 95 and 50 mol% BADGE and a very small difference going from 50 to 0 mol% BADGE. Note that these conclusions are based on a single measurement and in order to obtain more reliable results these

measurements should be repeated. This will allow for an error estimation on these values. When comparing the samples with 5 and 10 mol% Zn^{2+} the data is even less trustworthy. (see Figure A.98-A.99) The insoluble fractions are, with a few exceptions, very comparable to the samples with 0 mol% Zn^{2+} which means 90 % or higher. Also the T_g shows a similar, generally decreasing trend upon increasing the cluster fraction. The activation energy however, shows a lot of scatter on the data and is therefore difficult to interpret. Especially here more samples have to be measured to calculate the error on these measurements before drawing firm conclusions.

5.2.7 Polymerisation without surface functionalisation

Based on our previous results it looks like the effort of surface functionalising the clusters with a custom made ligand that is capable of reversible chemistry were futile as the relaxation seems to be based on ligand redistribution. So the question arose: "Can we synthesise cluster containing polymers without surface funtionalisation, similar to the few publications discussed before?" The short answer is yes, by simply mixing the clusters ($\mathbf{Zr}_{12}$-acetate, -hexanoate, -oleate, -linoleate and $\mathbf{Zr}_6$-methylheptanoate) with Pripol 1040 solid samples were obtained. The more complex answer is closer to yes, but. After preparing the reaction mixture and curing it in the oven, the samples needed 4 full days before a solid sample was obtained. This indicates that the non-functionalised clusters are rather poor cross-linkers. Additionally, the insoluble fractions were determined and were found to be only 85 m% or lower. (see Table 5.3)

Table 5.3: Insoluble fractions of polymers synthesised via the direct reaction between several clusters and Pripol 1040.

Cluster	Insoluble fraction (m%)
$\mathbf{Zr}_{12}$-acetate	84
$\mathbf{Zr}_{12}$-hexanoate	66
$\mathbf{Zr}_{12}$-oleate	35
$\mathbf{Zr}_{12}$-linoleate	52
$\mathbf{Zr}_6$-methylheptanoate	62

It appears that the bigger the native ligand on the cluster surface the smaller the insoluble fraction of the final polymer, indicating that the sterics of the ligands hamper the polymerisation. Therefore, one can clearly see the merit of surface functionalising the clusters even though it requires the synthesis of a ligand. The polymers cure overnight and give good insoluble fractions.

Because of these unfavorable material properties only polymers without surface functionalisation were not further studied.

5.2.8   Mechanical testing

Since the samples containing 95 mol% BADGE were relatively flexible they could be characterized with dynamic mechanical analysis (DMA). Here a rectangular thin sample is subjected to an oscillating tensional force in a broad temperature range. The storage modulus (E'), i.e. how stiff is a material, is monitored over time. In Figure 5.12 the storage modulus is plotted for three different samples containing either 2, 4 or 6 equivalents of epoxy ligands on the cross-linking agent. Tanδ is defined as the ratio between the loss modulus (E") and the storage modulus (E') and the T_g can be found at the maximum of this curve.
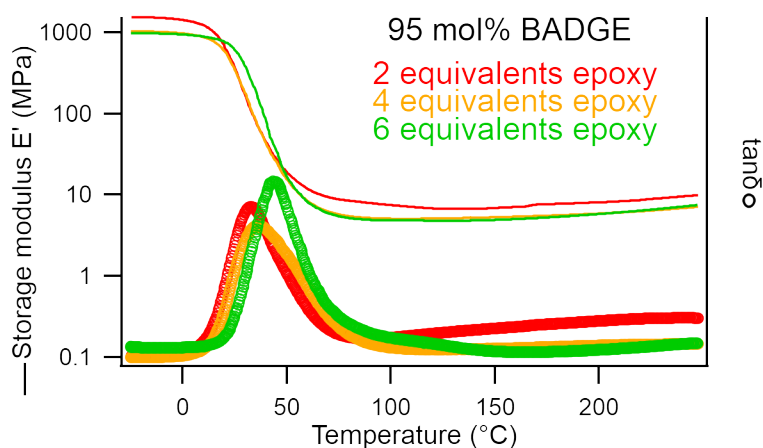
Figure 5.12: Overlay of the DMA measurements for samples synthesised with different amounts of epoxy ligands, 2, 4 and 6 equivalents epoxy per **Zr**$_{12}$ species respectively. The storage modulus (line) is plotted in the left axis while tanδ (circular markers) is plotted on the right axis.

The overview of the DMA results can be found in Table 5.4. At low temperatures (-25 °C) the samples display a storage modulus ∼1-1.5 GPa. The sample which contains 2-fold functionalised clusters displays a slightly higher storage modulus whereas the other 2 seem nearly identical. Upon increasing the temperature, the materials display a mechanical profile similar to previously reported mechanical analysis on dynamic covalent networks.[16] At 25 °C, the storage modulus increases upon increasing cluster functionality,

indicating that the material is stronger when more functional ligands are present on the cross-linking agent. This shows that the mechanical properties of the materials can be tuned by adjusting our inorganic cross-linking agent. The T_g, found at the maximum of the tanδ curve, shows a similar trend however, the error is rather big. The tanδ curve for the sample with 4 equivalents of epoxide ligands is broadened indicating that 2 individual networks might be present.[17;18] The storage modulus shows a rubbery plateau around 100 °C, with 7.5, 5.1 and 4.85 MPa as values for the storage modulus for 2, 4 and 6 eq. epoxide ligand respectively. This suggests that the material with 2-fold functionalised clusters has a higher cross-link density. The materials maintain their mechanical properties throughout the whole temperature range (i.e. the sample does not break) indicated by the smooth continuous curve until 250 °C.

Table 5.4: Overview of the storage moduli (E') and T_g obtained for CANs with 2, 4 and 6 equivalents of epoxide ligands combined with 95 mol% BADGE and 10 mol% Zn^{2+}.

	Storage modulus E' (-20 °C)	Storage modulus E' (25 °C)	T_g
2 eq.	1505 ± 39	310 ± 158	31 ± 4
4 eq.	1087 ± 221	362 ± 167	36 ± 7
6 eq.	975 ± 67	589 ± 22	43 ± 2

By comparing the values to previously reported values for SiO$_2$ reinforced CANs based on Leibler's system we find that our clusters have a more positive effect on the mechanical properties.[13] Their highest obtained value for E' is 44 MPa which is far below our lowest value of 309 MPa at 25 °C, even within error. The value for the bare materials without any fillers was only 36 MPa so there is a clear improvement in the mechanical properties by adding clusters as inorganic monomers. It should be noted that the authors did not specify the thickness of the samples which influences the values obtained from DMA.

The cross-linking density of a material can be calculated according to Flory's expression.[19;20] (See Equation 5.1) Where ν is the cross-linking density in $\frac{mol}{m^3}$, G' is the shear storage modulus at $T_g + 50$ °C in MPa, R is the universal gas constant and T is the temperature in K. The obtained E' (tensile storage modulus) values from DMA can be converted into the shear storage modulus via Equation 5.2.[21]

$$\nu = \frac{G'}{R * T} \tag{5.1}$$

$$G' = 3 * E \tag{5.2}$$

Surprisingly the cross-link density decreases when the functionality of the cluster increases. At first sight, these results seems contradictory with the expected outcome. However, when looking more closely to the system a possible explanation can be found. Since all of these materials were synthesised by adding 95 mol% BADGE, based on the epoxide functionalities, the clusters with more epoxide functionalities need to be balanced with a bigger amount of BADGE for the same amount of clusters. In turn, more Pripol 1040 needs to be added to have a 1:1 ratio epoxide versus carboxylic acid. This actively decreases the amount of clusters and thus cross-linking agents. This could explain the trend in decreasing cross-link density. (See Table 5.1) A fairer comparison would be to synthesise samples with identical mass% of clusters and characterise them with DMA.

Table 5.5: Overview of the cross-link densities calculation according to Equation 5.1. Also the mass percent cluster in the samples is displayed.

	Cross-link density $(\frac{mol}{m^3})$	m% cluster
2 equivalents epoxy	2811.4	4.6 %
4 equivalents epoxy	1753.7	2.6 %
6 equivalents epoxy	1602.8	1.7 %

5.3   Conclusion

Despite our efforts to synthesise covalent adaptable networks with an associative exchange mechanism based on transesterification, we synthesised dissociative CANs. We found that, when the amount of cluster stays below a certain threshold (< 95 mol%) the relaxation mechanism seems to be purely dissociative. This indicates that the transesterification process,

that we tried to introduce using the custom-made ligands, does not occur. Samples without Zn^{2+} catalyst also relax stress, indicating that the transesterification is not the reversible cros-link. An alternative relaxation mechanism could proceed through a dissociative ligand exchange. Despite this unexpected result, the silver lining is that all the samples are able to relax stress, some of them even within a matter of seconds. When the mol% cluster is 5% the regime changes. We observe a fast and relatively small dissociative relaxation, after which the relaxation process resembles the originally reported transesterification. This suggests that the transesterification is not fully inhibited, but the material will rather relax via ligand exchange since this process has a lower activation energy. However, the transesterification is considerably slower compared to the reference samples without clusters, these samples relax within $\sim$ 20 minutes at 190 °C with an activation energy of $\sim$ 80 kJ/mol.[12] This could be due to the lower flexibility of the material, which prevents the Zn^{2+} catalyst from diffusing through the sample, inhibiting efficient transesterification.

Additionally, we have shown that it is possible to use atomically precise metal oxo clusters as tunable monomers for polymer synthesis. From this data, it appears that the T_g can be tuned from -5 to 40 °C by changing the fraction of clusters inside the polymer network. The thermal degradation also changes upon changing the cluster loading. However, this change might occur due to a change in H-bonded acetate ligands being present in the sample. High insoluble fractions combined with the disappearing epoxide signal in FTIR indicate that the polymerisation was successful. However, the lack of consistent results indicates that the samples are not fully homogeneous. Further research should be conducted to add error bars and homogenise the as-synthesised polymer networks. Using the synthesised epoxy ligand shows a clear advantage in the curing speed of the material. When these custom-made ligands are not present on the cluster core, the curing process takes eight times as long, making this a less viable route. Using functionalised clusters also greatly improves the insoluble fraction, suggestion that the polymerisation happens more efficiently.

Finally, using DMA it has been shown that adding clusters to the polymer network, improves the mechanical properties of the material. Furthermore, the mechanical properties can be tuned by changing the cross-link density i.e. amount of epoxy ligands on the cluster core. The higher the amount of epoxy ligands on the cluster the better the mechanical properties at 25 °C. This shows that the clusters can be successfully applied as inorganic monomers that allow tuning of the material properties such as T_g and mechanical strength.

Given the inconsistency in the rheology data and the errors on the DMA

measurements, efforts should be directed towards improving the samples and synthesising a reference sample without clusters. The most likely explanation for these fluctuating results is the heterogeneous distribution of clusters within the polymer network. As the clusters appear to cause relaxation, the properties of the materials (e.g. stress relaxation) will be severely affected if they are not uniformly distributed throughout the material. Finally, it should be confirmed that the cluster structure is maintained within the polymer matrix, for example by PDF measurements.

5.4 Perspective

The approach presented here is a novel alternative for the addition of atomically precise inorganic objects to a polymer network. Rather than mechanical mixing and hoping for good miscibility, here the surface chemistry can even be tuned in order to match the resin as closely as possible. This will enable adding increased amounts of inorganic material inside the material, while minimising the risk of agglomeration simultaneously. Extending this method to other chemistries will lead to novel materials with fascinating properties. I think, for example, about the phtalate monoester covalent adaptable networks which do not require an external catalyst.[22] The clusters could be functionalised with trimellitic anhydride as a ligand and subsequent polymerisation via the reaction with a difunctional alcohol.

The purpose of the clusters shown in this chapter, were merely added to enhance the mechanical properties of the polymer samples. However, this method can be applied to other inorganic materials with fascinating properties such as, (thermo-)luminescence, magnetism or mechanoluminescence. This will produce high-end polymeric materials suitable for several applications, with the added benefit that these materials are recyclable, allowing for the recovery of the inorganic materials. As they often consist of precious metal atoms, it will become increasingly more important to recover them after use. This approach will hopefully redirect the nanocomposite field towards a more circular economy.

5.5 Experimental

5.5.1 Synthetic procedures

Chemicals. Acetic acid (99%) was bought from Sigma Aldrich, dried overnight using $CaSO_4$ and vacuum distilled into a Strauss flask for storage. $Zr(OPr)_4$ (70 w% in 1-HOPr) was purchased from Sigma Aldrich and stored in a Strauss flask upon arrival. 10-undecenoic acid (98%), hexanoic acid (99%), BADGE (100%) and mCPBA (<77%) were purchased from Sigma Aldrich and used without further purification. Pripol 1040 was kindly provided by Crodax. Dichloromethane (DCM) and ethyl acetate were bought from Biosolve and used without any further purification

Epoxidation of 10-undecenoic and oleic acid. 2.515 g 10-undecenoic acid (13 mmol, 1 eq.) or 4.1 mL oleic acid (13 mmol, 1 eq.) is added to 500 mL round bottom flask. 250 mL DCM is added together with a stirring bar. 6.575 g m-CPBA (30 mmol, 2.3 eq.) is weighed separately and added slowly to the stirring acid/DCM mixture. After 16 hours of stirring at room temperature the solution is poured into a 1 L separation funnel to which 250 mL of a 4.1 m% $NaSO_3$ in H_2O is added. The organic fraction is washed twice more using the separation funnel, once with 250 mL of pure H_2O and once with 250 mL brine. Finally, a silica plug is prepared by mixing silica powder with DCM and adding it in a 75 mL por. 4 glass filter on top a small layer of sand. Then, with a pasteur pipette the washed reaction mixture is applied onto the silica plug. The plug is washed twice with 50 mL DCM after which the plug was allowed to fully dry out. Finally, the product is extracted by washing the plug 4 times with 50 mL ethyl acetate. During the extraction step the plug is stirred with a spatula in order to maximize the extraction. 10-undecenoic acid epoxide was obtained in a 76.3% yield and oleic acid epoxide was obtained in a 98.5% yield. Both products contain traces amount of benzoic acid which is a side product of the reaction.

Zr_{12}-acetate synthesis. In a typical clusters synthesis, a 20 mL vial was equipped with a septum and cycled three times between argon and vacuum. Zirconium propoxide (2.25 mL, 5 mmol, 1 eq.) was added to the vial, together with dry DCM (5.463 mL). Under stirring, distilled acetic acid (2.287 mL, 40 mmol, 8 eq.) was injected, reaching a total reaction volume of 10 mL and thus a zirconium concentration of 0.5 M. After 12 hours at room temperature (19-24 °C), the crystalline powder is isolated by filtration and further washed with 50 mL of a DCM:acetic acid mixture (4:1). Finally, the white powder is dried overnight under high vacuum. The powder is stored in a desiccator. The cluster was obtained as a white solid, with a 98 % yield (calculated based on the molecular formula:

$Zr_{12}O_8(OH)_8(CH_3COO)_{24} \cdot 6\,CH_3COOH \cdot 3.5\,DCM$.[23]

Surface functionalisation of clusters with 10-undecenoic epoxide.
Zr$_{12}$-acetate (2g, 14 mmol acetate, 1 eq.) is weighed into a 20 mL vial
together with a stirring bar and 2 mL ethyl acetate. In a separate vial
234.3 mg (1.17 mmol, 0.083 eq.), 468.6 (2.34 mmol, 0.167 eq.) or 702.9 mg
(3.51 mmol, 0.25 eq.) of 10-undecenoic acid epoxide is weighed together
with 1.6 mL (12.83 mmol, 0.917 eq.), 1.46 mL (11.67 mmol, 0.83 eq.) or
1.31 mL (10.5 mmol, 0.75 eq.) hexanoic acid respectively. These amounts
will render clusters which are 2, 4 or 6-fold functionalised with an epoxide
group. This ligand mixture is dissolved in 4 mL ethyl acetate and added
to the milky **Zr**$_{12}$-acetate solution in ethyl acetate. After 2h of stirring the
solution becomes transparent after which the solvent, together with acetic
acid is evaporated using the Schlenk line. This dispersing/evaporation step
is repeated once after which clusters functionalised with the desired amount
of epoxides are obtained.

Preparation of Zn^{2+} containing Pripol 1040. Depending on the tar-
geted mol% Zn^{2+} either 152.3 mg (0.83 mmol, 5 mol%) or 304.6 mg (1.67
mmol, 10 mol%) of $Zn(acetate)_2$ is weighed into a 40 mL vial. 5 g of Pripol
1040 (16.6 mmol acid) is added together with a stirring bar. Next, the vial
is connected to the Schlenk line in order to pull vacuum. The vial is heated
from 110-180 °C with 10 minutes increment and maintaining the mixture
for 30 minutes at every temperature. The mixture will bubble heavily at
the start from the acetic acid which is evaporating. Once the vial is at 180
°C and the bubbling has stopped the Zn^{2+} containing Pripol 1040 is ready.

synthesising polymer networks. In order to synthesise polymer net-
works using the epoxide capped clusters 500 mg is weighed into a 20 mL
vial and 0.5 mL ethyl acetate is added. In another 40 mL vial Pripol 1040
and BADGE are weighed in order to have a 1:1 mmol ratio between epoxide
groups and carboxylic acid. This vial is heated with a heat gun in order to
melt the BADGE, using a vortex stirrer this mixture is homogenized. This
process is repeated until a clear homogeneous liquid is obtained. Using a
Pasteur pipette the mixture containing the cluster is added dropwise to the
Pripol 1040/BADGE mixture while stirring using the vortex mixer. Finally,
this mixture is poured into a Teflon mold which is placed overnight into the
vacuum oven at 130 °C.

5.5.2 Analysis techniques

General instrumentation. Nuclear Magnetic Resonance (NMR) mea-
surements were recorded at 298K on Bruker UltraShield 500 spectrometer

operating at a frequency of 500.13 MHz. The IR spectra were recorded on a Perkin Elmer spectrum 2 ATR-FTIR with a diamond crystal.

Mass spectrometry. ESI mass spectra were acquired using a Bruker maXis4G or maXis II high resolution mass spectrometer equipped with an electrospray ionization source. The epoxides were dissolved in MeOH. The samples were directly introduced into the instrument at a rate of 6 μL/min using a syringe pump. The heated capillary temperature was 200 °C and the capillary voltage was 3.6 kV. The samples were analyzed in negative ion mode. DataAnalysis 4.4 from Bruker was used to process the raw data.

Reprocessing the polymer samples. Before characterization the samples have to be reprocessed to remove remaining air bubbles. 400 mg of polymer sample is cut up in small fragments using scissors and added to a metallic mold. Prior to the addition of the polymer the mold was coated with Marbocoat™ and left to dry for 5 minutes. This mold is put in the middle of the bottom plate of a pre-heated Carver 7.5T manual rubberstamp press. The press is closed and 3 bar of pressure is applied to the mold after which the sample is pressed for 30 minutes. Due to the relaxation of the material, the pressure drops. Therefore, after 10 minutes the pressure is increased to 3 bar again. After pressing the mold is removed from the press and left to cool down for 10 minutes. The samples containing less than 95 mol% BADGE were reprocessed at 160 °C, samples containing 95 mol% BADGE were reprocessed at 220 °C.

Determination of the insoluble fraction. For this 50 mg of the polymer sample was weighed and encapsulated in a self-made envelope from filter paper. The sample code is written on the envelope with pencil and the samples are submerged in DCM for 2 days. Afterwards, the envelopes are dried for an additional 2 days at the Schlenk line. Finally, the samples are weighed again and the insoluble fraction is determined according to Equation 4.1 where m_{begin} is the mass before submerging the sample and m_{end} is the mass after drying.

$$Insoluble\,fraction = \frac{m_{end}}{m_{begin}}.100 \tag{5.3}$$

Differential scanning calorimetry. Differential scanning calorimetry was measured using 10 mg of polymer for each measurement on a DSC 214 Polyma (Netzsch GmbH, Austria) under a nitrogen atmosphere from -50 °C to 180 °C with a cooling rate of 40 $K * min^{-1}$ and a heating rate of 10 $K * min^{-1}$. The first heating run is performed to remove the thermal history of the polymer, DSC curves shown correspond to the second heat-

ing curve. The data was analysed using the NETZSCH Proteus thermal analysis software.

Thermogravimetric analysis. Thermogravimetric analysis were carried out in a temperature range from 30 °C to 800 °C with a heating rate of 5 °C/min. To make sure everything is burned off quantitatively, the sample is kept at 800 °C for 15 minutes. During the measurement the air flow rate is 25 mL/min. and the balance flow is 10 mL/min.

Determination of the relaxation time of covalent adaptable networks. As mentioned above, the stress relaxation of materials is often described using the Maxwell model.[24] In this equation τ indicates the relaxation time.

$$G = G_0 * e^{-\frac{t}{\tau}} \tag{5.4}$$

In order to find the relaxation time we know that the time has to be equal to the relaxation time, i.e. $t = \tau$. By substituting t by τ in Equation 5.4 we find:

$$G = G_0 * e^{-1} \tag{5.5}$$

From this we find that when the relaxation time is reached, G is equal to 1/e or 37% of its original value. Therefore, when measuring the relaxation modulus, the relaxation time is defined as the time needed for the relaxation time to drop to 37% of its original value.

Calculating the E_a of covalent adaptable networks. The activation energy of the reversible cross-links can be calculated using the Arhenius equation, where k is the rate constant, A is the pre-exponential factor, E_a is the activation energy, R is the ideal gas constant and T is the absolute temperature in K:

$$k = A * e^{-\frac{E_a}{R*T}} \tag{5.6}$$

Here the assumption is made that the relaxation is inversely proportional to the rate constant. $(\tau = \frac{1}{k})$ This means that shorter relaxation time correspond to higher reaction rates. The latter can be substituted in the Arhenius equation generating:

$$\frac{1}{\tau} = A * e^{-\frac{E_a}{R*T}} \tag{5.7}$$

This equation can be rewritten as:

$$\tau = \frac{1}{A} * e^{\frac{E_a}{R*T}} \tag{5.8}$$

Finally, the natural logarithm is applied to both sides of the equation:

$$\ln \tau = \ln \frac{1}{A} + \frac{E_a}{R * T} \tag{5.9}$$

Hence, by plotting the $\ln \tau$ as a function the 1/T, the slope will be equal to E_a/R. By multiplying the slope with the ideal gas constant, the activation energy in kJ/mol is obtained.

Rheological measurements. Rheological experiments were carried out using an Anton Paar rheometer equiped with CTD 600 heating device. Amplitude sweeps were performed on polymer discs of 8 mm diameter and a thickness of 3 mm. During this experiment the shear strain was increased from 0.01 to 100% using an angular frequency of 10 Hz, at a temperature lower than the stress relaxation experiments. Samples containing 75 mol% cluster or less were measured at 100 °C and the showed linear behaviour up to 0.15% shear strain. For samples containing 95 mol% BADGE the measurement was done at 170 °C and showed linear behaviour up to 0.25%. For the stress relaxation measurements the shear strain, determined above, was applied to the sample (with the same dimensions as for the amplitude sweep) and the relaxation modulus was measured over time, at different temperatures. The samples containing less than 75 mol% BADGE were measured in a temperature range of 160-100 °C. The samples containing 95 mol% on the other hand, were measured in a range of 240-200 °C.

Dynamic Mechanical Analysis. Dynamic Mechanical Analysis was performed under N_2 on a TA instruments DMA Q800 with a heating rate of 3 °C/min. The rectangular samples (∼10x5x0.3 mm) were attached using tensile clamps and a frequency of 1 Hz, amplitude of 15 μm and force of 0.01 N were applied in a temperature range of -25 °C to 250 °C. with a heating rate of 3 °C/min. Reported mechanical data is the average over 3-5 independent experiments, reported error are standard deviations on the average value.

5.6   Contributions

Rheological experiments were conducted in collaboration with Dr. Tapas Debsharma, post-doc in the group of Prof. Dr. Filip Du Prez, at the University of Ghent (BE). Dynamic mechanical analysis (DMA) was performed by Ilaria Onori from the group of Prof. Dr. Christoph Weder at the Adolphe Merkle Institute (AMI), in Fribourg (CH). DSC measurements were performed with the help of John Coats, PhD student in the group of Prof. Dr. Cornelia Palivan at the University of Basel.

References

[1] Chamas, A.; Moon, H.; Zheng, J.; Qiu, Y.; Tabassum, T.; Jang, J. H.; Abu-Omar, M.; Scott, S. L.; Suh, S. Degradation Rates of Plastics in the Environment. *ACS Sustainable Chemistry & Engineering* **2020**, *8*, 3494–3511.

[2] Kloxin, C. J.; Scott, T. F.; Adzima, B. J.; Bowman, C. N. Covalent Adaptable Networks (CANs): A Unique Paradigm in Cross-Linked Polymers. *Macromolecules* **2010**, *43*, 2643–2653.

[3] Guerre, M.; Taplan, C.; Winne, J. M.; Du Prez, F. E. Vitrimers: directing chemical reactivity to control material properties. *Chemical Science* **2020**, *11*, 4855–4870.

[4] Taplan, C.; Guerre, M.; Du Prez, F. E. Covalent Adaptable Networks Using β-Amino Esters as Thermally Reversible Building Blocks. *Journal of the American Chemical Society* **2021**, *143*, 9140–9150.

[5] Denissen, W.; Winne, J. M.; Du Prez, F. E. Vitrimers: permanent organic networks with glass-like fluidity. *Chemical Science* **2016**, *7*, 30–38.

[6] Yu, K.; Taynton, P.; Zhang, W.; Dunn, M. L.; Qi, H. J. Reprocessing and recycling of thermosetting polymers based on bond exchange reactions. *RSC Advances* **2014**, *4*, 10108–10117.

[7] Yang, Y.; Pei, Z.; Zhang, X.; Tao, L.; Wei, Y.; Ji, Y. Carbon nanotube-vitrimer composite for facile and efficient photo-welding of epoxy. *Chemical Science* **2014**, *5*, 3486–3492.

[8] Obadia, M. M.; Mudraboyina, B. P.; Serghei, A.; Montarnal, D.; Drockenmuller, E. Reprocessing and Recycling of Highly Cross-Linked Ion-Conducting Networks through Transalkylation Exchanges of C-N Bonds. *Journal of the American Chemical Society* **2015**, *137*, 6078–6083.

[9] Kreutzer, J.; Puchberger, M.; Artner, C.; Schubert, U. Retention of the Cluster Core Structure during Ligand Exchange Reactions of Carboxylato-Substituted Metal Oxo Clusters. *Eur. J. Inorg. Chem.* **2015**, *2015*, 2145–2151.

[10] Zhang, G.; Chen, Q.; Xie, C.; Wang, Y.; Zhao, C.; Xiao, C.; Wei, Y.; Li, W. Mechanical-robust and recyclable polyimide substrates coordinated with cyclic Ti-oxo cluster for flexible organic solar cells. *npj Flexible Electronics* **2022**, *6*, 37.

[11] Murali, M.; Berne, D.; Joly-Duhamel, C.; Caillol, S.; Leclerc, E.; Manoury, E.; Ladmiral, V.; Poli, R. Coordination Adaptable Networks: Zirconium(IV) Carboxylates. *Chemistry - A European Journal* **2022**, *28*, 202202058.

[12] Montarnal, D.; Capelot, M.; Tournilhac, F.; Leibler, L. Silica-Like Malleable Materials from Permanent Organic Networks. *Science* **2011**, *334*, 965–968.

[13] Legrand, A.; Soulié-Ziakovic, C. Silica-Epoxy Vitrimer Nanocomposites. *Macromolecules* **2016**, *49*, 5893–5902.

[14] Ayer, W. A.; Craw, P. A. Synthesis of (±) arthrographol. *Canadian Journal of Chemistry* **1991**, *69*, 1909–1916.

[15] Jourdain, A.; Asbai, R.; Anaya, O.; Chehimi, M. M.; Drockenmuller, E.; Montarnal, D. Rheological Properties of Covalent Adaptable Networks with 1,2,3-Triazolium Cross-Links: The Missing Link between Vitrimers and Dissociative Networks. *Macromolecules* **2020**, *53*, 1884–1900.

[16] Chen, X.; Li, L.; Torkelson, J. M. Recyclable polymer networks containing hydroxyurethane dynamic cross-links: Tuning morphology, crosslink density, and associated properties with chain extenders. *Polymer* **2019**, *178*, 121604.

[17] Scobbo, J. J. Dynamic mechanical analysis of compatibilized polymer blends. *Polymer Testing* **1991**, *10*, 279–290.

[18] Koleske, J. V. *Paint and coating testing manual : fifteenth edition of the Gardner-Sward handbook*, 15th ed.; ASTM International West Conshohocken, PA: West Conshohocken, PA, 2012.

[19] Hill, L. W. Calculation of crosslink density in short chain networks. *Progress in Organic Coatings* **1997**, *31*, 235–243.

[20] Guggari, S.; Magliozzi, F.; Malburet, S.; Graillot, A.; Destarac, M.; Guerre, M. Vanillin-Based Epoxy Vitrimers: Looking at the Cystamine Hardener from a Different Perspective. *ACS Sustainable Chemistry & Engineering* **2023**, *11*, 6021–6031.

[21] Beer, F.; Johnston, E.; DeWolf, J.; Mazurek, D. *Mechanics of Materials*; McGraw-Hill US Higher Education, 2018.

[22] Delahaye, M.; Winne, J. M.; Du Prez, F. E. Internal Catalysis in Covalent Adaptable Networks Phthalate Monoester Transesterification As a

Versatile Dynamic Cross-Linking Chemistry. *Journal of the American Chemical Society* **2019**, *141*, 15277–15287.

[23] Puchberger, M.; Kogler, F. R.; Jupa, M.; Gross, S.; Fric, H.; Kickelbick, G.; Schubert, U. Can the Clusters $Zr_6O_4(OH)_4(OOCR)_{12}$ and $[Zr_6O_4(OH)_4(OOCR)_{12}]_2$ Be Converted into Each Other? *Eur. J. Inorg. Chem.* **2006**, *2006*, 3283–3293.

[24] Hajikarimi, P.; Moghadas Nejad, F. In *Chapter 3 - Mechanical models of viscoelasticity*; Hajikarimi, P., Moghadas Nejad, F., Eds.; Elsevier, 2021; pp 27–61.

6

Conclusion and future prospects

6.1 Conclusion

Throughout this thesis we have followed the story of the dormant group 4 metal oxo cluster field. In the past, this field mainly relied on single crystal XRD to obtain structural data. This limited the possible synthesis and introduced tedious and long crystallization processes. Our research has circumvented these problems, reviving this field. We first optimized the synthesis, after which the formation mechanism was studied. Using the obtained knowledge throughout these projects, the clusters were developed and used as tunable inorganic monomers in both free radical polymerisations and covalent adaptable networks.

Firstly, the cluster synthesis was standardised as the reaction conditions in literature were quite divergent. We found that when a metal (Zr or Hf) alkoxide is reacted with 8 equivalents acetic acid, the $\mathbf{M}_{12}$-acetate cluster is consistently formed. After optimising this for a short carboxylic acid, we performed the same reaction with longer carboxylic acids, similar to the nanoparticle field. After purification, we elucidated their structure via PDF measurements, thus eliminating the need for crystalline material. Fitting the data proved that clusters are formed regardless of the carboxylic acid
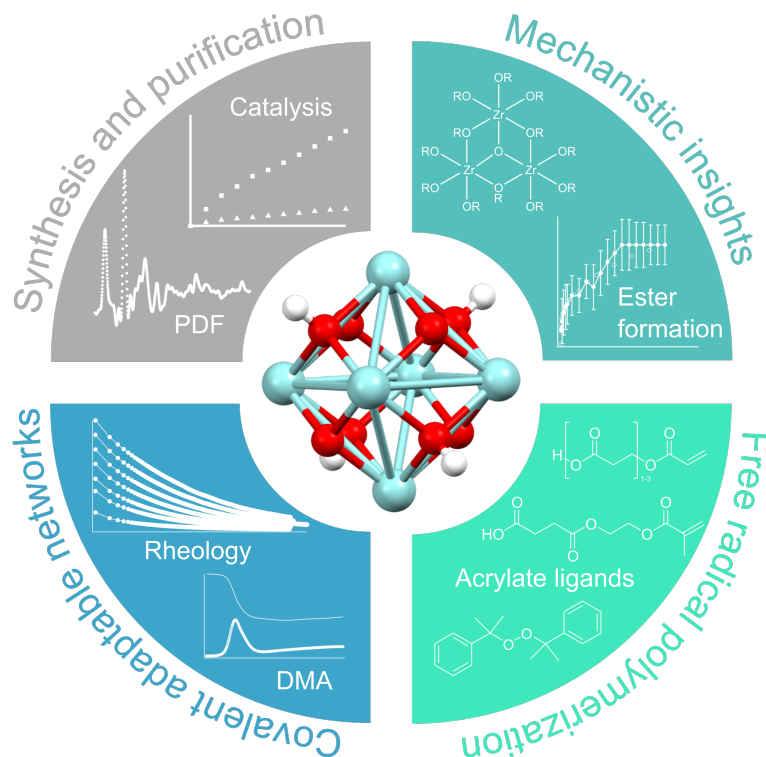
Figure 6.1: Overview figure of the content of this thesis with the **Zr**$_6$ cluster core displayed in the center. Surrounding the cluster, the 4 subjects discussed before are shown.

used during synthesis. The dimerisation of the clusters is controlled only by the sterical hindrance on the α-position of the carboxylic acid, not by it's length. If there is something different from a $-CH_2$ on this position the monomeric M_6 clusters will form, else the dimeric M_{12} clusters are formed. Through ligand exchange under the appropriate conditions (vacuum at 70 °C) it was possible to convert monomers into dimers and *vice versa*. The organic ligand shell was further characterised using NMR, FTIR and TGA. We found that on top of the coordinated ligand shell, which display different binding modes (bridging & chelating), additional H-bonded ligands are present. Applying our toolbox for hafnium clusters we confirmed that the same conclusions are valid. Finally, we tested **Zr**$_{12}$-oleate as catalysts for the esterification reaction between oleic acid and ethanol, since they can be seen as the smallest possible nanoparticle. 5 nm ZrO_2 nanoparticles have been used successfully as esterification catalysts in the past. Interest-

ingly, our clusters showed a 5-fold increase in reaction conversion due to their increased surface to volume ratio, creating a better, cheaper and more sustainable catalyst.

Secondly, the formation mechanism was studied. Using NMR and FTIR we learned that the first 2 equivalents of carboxylic acid exchange with $Zr(OPr)_4$. It appears that this exchange does not go towards completion but is an equilibrium. Only when the third equivalent is added a signal for free acid appears together with an ester signal. *In situ* EXAFS taught us, despite the large error, that the Zr complex after exchange with 1 equivalent of acid is most likely a dimer, while the 2 equivalent sample seems to fit a trimeric structure. By following the ester formation over time by NMR, while varying multiple reaction conditions, we found that the Zr concentration should be high in order to have sufficient ester formation. Increasing the length of the carboxylic acid and/or alkoxide or adding sterical hindrance has a strong negative effect on the ester formation. The Zr-Zr degeneracy, which is 4 in the final cluster, increases simultaneously with the ester formation. Finally, by combining our data a preliminary reaction mechanism was proposed where the initial ligand exchange is followed by a fast ester formation, after which a slow ester formation occurs and finally the $\mathbf{Zr}_6$ cluster is formed.

$\mathbf{Zr}_{12}$-oleate and -linoleate clusters were used unsuccessfully as tunable inorganic monomers for radical polymer synthesis. Under our current conditions, reacting the clusters with AIBN, dicumyl peroxide or without initiator, no polymer networks were formed. It is possible that some low molecular weight polymers were formed but since our objective was to create a polymer network this was not investigated further. Instead, we used 10-undecenoic acid as a ligand, which has a terminal alkene. By reacting these clusters with 10 w% dicumyl peroxide solid polymer networks with excellent insoluble fractions were obtained. This result shows us that the alkene functionalities in oleic and linoleic acid are shielded by the remaining ligand tail, inhibiting successful polymerisation. We then switched from alkene ligands to (meth-)acrylate ligands which are more reactive towards free radical polymerisation. Using our previous knowledge, samples were synthesised with different amounts of reactive ligands on the surface. It was found that samples where the clusters contained 6 reactive ligands or more on the surface resulted in good insoluble fractions, indicative of a polymer network. When fewer reactive ligands were present on the surface, the insoluble fractions were too high. Whether the high insoluble fractions are due to low cluster functionalisation or low cluster loading, is still unclear. Remarkably, the T_g did not change significantly despite the large variation in sample composition, not for the alkene-cluster networks nor the (meth-)acrylate-cluster

networks. For the (meth-)acrylate capped clusters, polymer samples synthesised from mono-2-(acryloyloxy)ethyl succinate containing clusters show the most promising features. However, further research should be done to mechanically characterise these materials.

Finally, the clusters were used as tunable monomers in covalent adaptable networks. The cluster surface was functionalised with different amounts of custom-made epoxy ligands, after which the clusters were reacted into a polymer network. It was found that the T_g ranges from approximately -5 °C to 40 °C and the insoluble fractions were good for almost all samples. The samples were able to relax stress very rapidly, but in a dissociative manner contrary to the intended associative transesterification. We postulate that a ligand exchange on the cluster core is responsible for the fast relaxation of the polymer networks. So far, no clear trend could be observed upon changing the polymer composition by adding co-monomer, different amounts of catalyst or different amount of epoxide ligands. However, DMA measurements showed that the addition of the clusters, even in small amounts, had a positive effect on the mechanical properties. So not only did we switch the reversible chemistry from a transesterification towards a ligand exchange mechanism, but we also improved the mechanical properties of the materials.

6.2   What's next?

I hope that this research invites other people to start studying atomically precise clusters, because they have enormous potential in applications. They can be regarded as very small nanoparticles with the additional advantage that they atomically precise (polydispersity = 0), something the nanoparticle community has been trying to achieve for years. Unfortunately, these materials have received far less attention compared to their bigger counterparts, which resulted in a lack of fundamental knowledge. Our group is currently taking the first steps towards unraveling the inherent differences between clusters and nanoparticles in order to, at least partially, reduce this knowledge gap.

The fact that we have now enabled the cluster field to use whichever carboxylic acid they want, while still forming the same atomically precise cluster, allows for immense tunability of these systems. Their strength truly lies in the fact that people can nearly exchange ligand per ligand on the cluster core, allowing for material synthesis with unprecedented control. As the demands for energy and technology increase, so does the necessity for control on a material science level. This is why we must continue to develop

novel and fascinating materials like our metal oxo clusters. Moreover, these results are likely not limited to group 4 metal oxo clusters.

This thesis displays, to the best of my knowledge, the first example of a tunable inorganic monomer used in covalent adaptable networks. Here, the purpose of the zirconium oxo clusters was to improve the mechanical properties. Which, according to our preliminary data, they seem to have done. One can envision this approach to be applicable for other, more functional nanomaterials (e.g. luminescent or magnetic properties), creating the next generation of high-end polymers. The recyclability of the covalent adaptable networks would ultimately allow for the recovery of the nanomaterials, often consisting of precious metals, from the polymer network. This not only lowers the price of the materials, but also the environmental impact. Especially the latter is something we should all strive for.

This thesis is the result of my passion for science, my enthusiasm and my problem-solving skills. As long as creative minds continue to think outside of the box and think about their research from different perspectives, there is no limit to what fascinating materials can be discovered. As long as people dare to dream, amazing science will result from this. It might, and more likely will, not be easy or straightforward but then again, what is? Coming back to the lecture of Richard Feynman, I'd say there's plenty of room left at the bottom.

A

Supporting Information

A.1 Supporting info of Chapter 1

A.1.1 Nanoparticle mass calculations

Spherical nanoparticles synthesised via both benzylalcohol (BnOH) and tri-octylphosphine oxide (TOPO) synthesis are compared.[1] First, the molar volume (MV) is calculated according to the equation A.1.

$$MV(cm^3/mol) = \frac{M_w\,(g/mol)}{\rho\,(g/cm^3)} \tag{A.1}$$

With M_w as the molecular weight and ρ as the density. (See Table A.1) In order to calculate the volume of 1 nanoparticle (equation A.2), the shape is assumed to be a sphere and the radius is obtained via dividing the diameter (d) by 2.

$$V_{NP} = \frac{4}{3} * \pi * (\frac{d}{2})^3 \tag{A.2}$$

Next, the amount of moles per nanoparticles can be calculated by dividing the volume of 1 nanoparticle by the molar volume. (equation A.3)

$$\frac{mol}{NP} = \frac{V_{NP}}{MV * 10^{21}} \tag{A.3}$$

Finally, the mass of 1 nanoparticle can be calculated by multiplying the moles per nanoparticle with the molecular weight of the respective metal oxide. (Equation A.4)

$$m_{NP} = \frac{mol}{NP} * M_w \tag{A.4}$$

Table A.1: Overview of the material properties for the group 4 metal oxo nanoparticles.

	Molecular weight (g/mol)	Density (g/ml)	Molar volume (cm^3/mol)
TiO$_2$	79.9	4.23	18.9
ZrO$_2$	123.2	5.68	21.7
HfO$_2$	210.5	9.68	21.7

A.2   Supporting info of Chapter 2

A.2.1   Pair Distribution Function analysis

Without carbon atoms   With only first carbon atom   With all carbon atoms
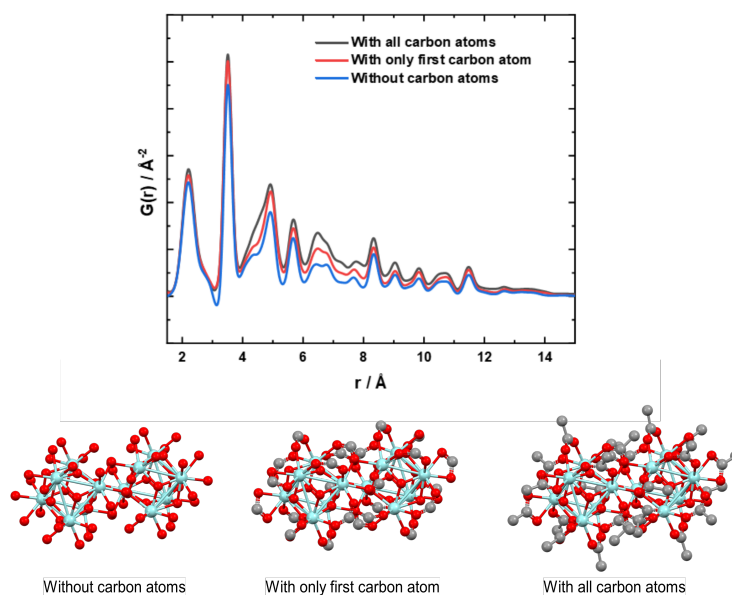
Figure A.1: Theoretically calculated X-ray PDF for the **Zr$_{12}$**-acetate structure, which features bridging and chelating acetate ligands. [2] The hydrogen atoms were not included in any model since hydrogen atoms have an extremely low scattering cross section for X-rays. We used the following atomic displacement parameters (ADP) for the calculation. Zr: 0.007 Å^2, O: 0.02 Å^2, C: 0.02 Å^2. The structures used for calculations are shown.
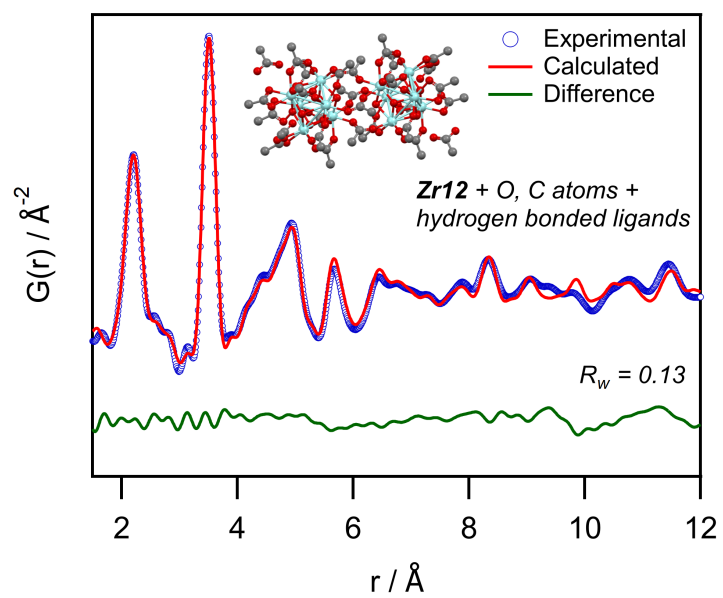
Figure A.2: PDF refinement of the **Zr**$_{12}$-acetate PDF with the **Zr**$_{12}$-acetate cluster model, including the hydrogen bonded ligands. The refined parameters are given in Table A.2.
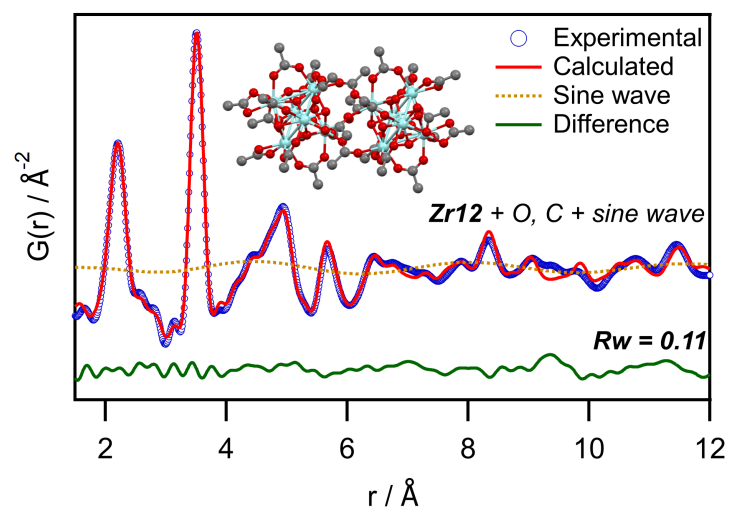
Figure A.3: PDF refinement of the **Zr**$_{12}$-acetate PDF with the **Zr**$_{12}$-acetate cluster model, including an exponentially dampening sine wave contribution. The refined parameters are given in Table A.2.
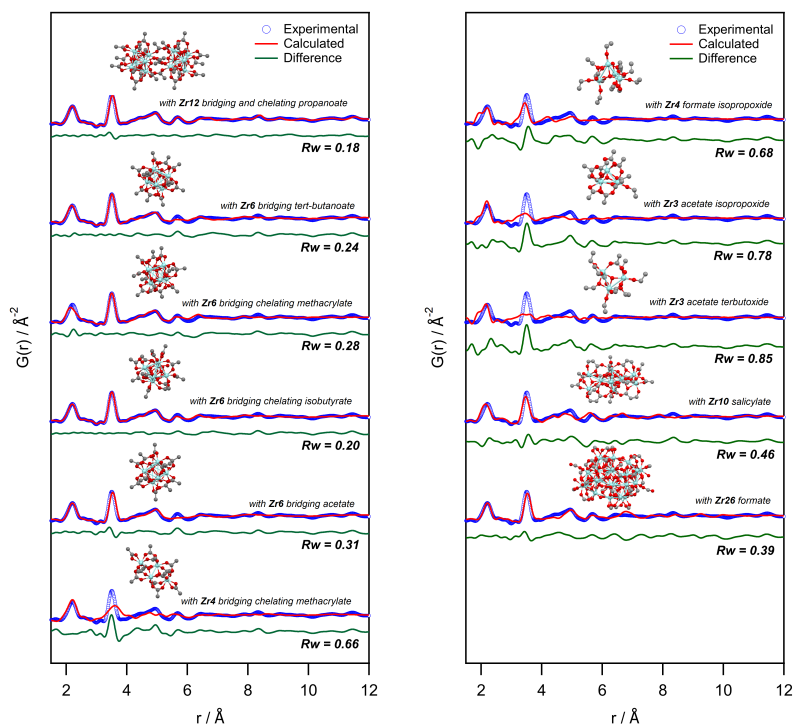
Figure A.4: PDF refinement of the **Zr**$_{12}$-acetate PDF with various cluster structures reported in literature (see main text). For each of the structural models, we removed the excess carbon atoms to arrive at a model with acetate ligands. The refined parameters are given in Table A.3.
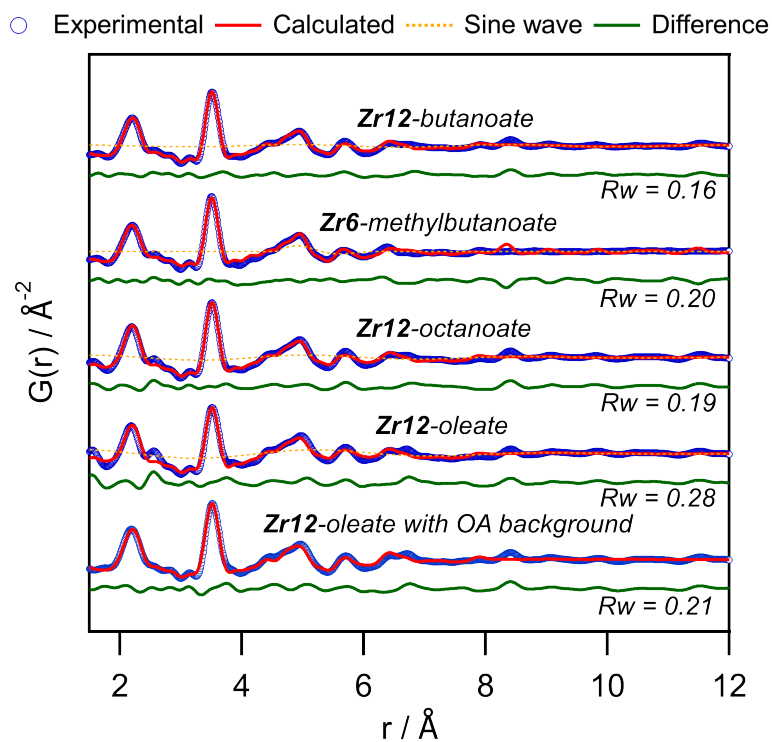
Figure A.5: PDF refinement for Zr_{12}-butanoate (using the Zr_6-acetate structural model), Zr_6-methylbutanoate (using the Zr_{12}-acetate structural model), Zr_{12}-octanoate (using the Zr_6-acetate structural model), and Zr_{12}-oleate (using the Zr_6-acetate structural model). The contribution of the exponentially dampening sine wave is shown (orange dotted lines). The refined parameters are given in Table A.5.
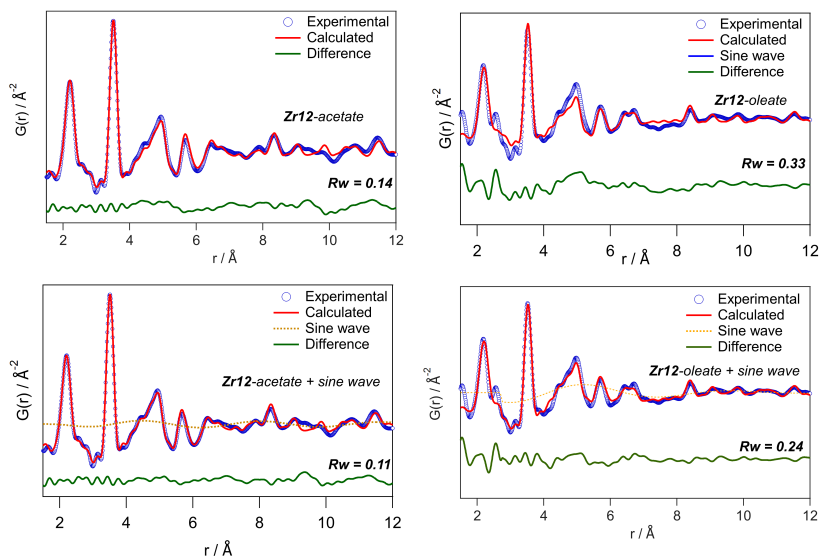
Figure A.6: PDF fit for **Zr$_{12}$**-acetate/oleate cluster with **Zr$_{12}$**-acetate model with/without the exponentially dampening sinusoidal contribution. The refined parameters are given in Table A.6.

Table A.2: Refined parameters after fitting our synthesised **Zr$_{12}$**-acetate cluster with various models, see Figure 2.3, Figure A.2 and A.3. All the models were derived from the crystal structure of **Zr$_{12}$**-acetate,[2] and in all models, the hydrogen atoms were removed. Relative Amplitude = Amplitude / Scale.

Model	Zr$_6$ core	Zr$_{12}$ core	Zr$_{12}$ with all O	Zr$_{12}$ with all O and C	Zr$_{12}$ with H-bonded ligands	Zr$_{12}$ with sine wave
Scale	0.95	0.94	0.66	0.60	0.61	0.60
Uiso Zr (Å^2)	0.004	0.004	0.005	0.004	0.004	0.004
Uiso O (Å^2)	0.005	0.005	0.011	0.011	0.011	0.011
Uiso C (Å^2)				0.013	0.013	0.013
delta2 (Å^2)	2	2	2	2.04	1.96	2.10
Rw	0.48	0.46	0.23	0.14	0.13	0.11
Amplitude (A)						-0.157
Relative Amplitude						0.261
wasyn						1.832
λ						3.616
ϕ						0.474
θ						4.815
wsig						2.701

Table A.3: Refined parameters after fitting our synthesised Zr_{12}-acetate cluster with various models, see Figure A.4. In all models, some carbon atoms were removed in order to form a structure equivalent to an acetate capped cluster and all hydrogen atoms were removed.

Model	Zr4 bridging, chelating methacrylate	Zr$_6$ bridging acetate	Zr$_6$ bridging, chelating isobutanoate	Zr$_6$ bridging, chelating methacrylate	Zr$_6$ bridging butanoate	Zr$_{12}$ bridging, chelating propanoate
Scale	1.01	0.58	0.59	0.55	0.59	0.60
Uiso Zr (Å^2)	0.027	0.004	0.004	0.005	0.005	0.004
Uiso O (Å^2)	-0.014	0.003	0.011	0.029	0.020	0.011
Uiso C (Å^2)	0.022	0.011	0.017	0.035	0.024	0.013
delta2 (Å^2)	-5.88	1.19	1.14	2.85	3.55	2.10
Rw	0.66	0.20	0.31	0.24	0.18	0.11
Amplitude (A)	-0.148	-0.209	-0.220	-0.209	-0.156	-0.157
wasyn	2.04	2.275	0.058	9.917	1.438	1.832
λ	2.949	3.679	3.97	3.541	3.622	3.616
ϕ	1.009	0.432	0.247	0.522	0.462	0.474
θ	4.609	4.406	0.115	2.979	5.181	4.815
wsig	2.413	3.145	0.474	0.904	3.038	2.701
Model	Zr4 formate isopropoxide	Zr3 acetate isopropoxide	Zr3 acetate t-butoxide	Zr10 salicylate	Zr26 formate	....
Scale	0.76	0.85	0.72	0.64	0.50	
Uiso Zr (Å^2)	0.005	0.021	0.036	0.005	0.006	
Uiso O (Å^2)	0.003	-0.013	-0.586	-0.0007	0.009	
Uiso C (Å^2)	0.728	0.183	0.728	0.190	0.052	
delta2 (Å^2)	1.98	1.94	4.08	1.86	4.24	
Rw	0.68	0.78	0.84	0.46	0.39	
Amplitude (A)	-0.198	-0.356	-0.247	-0.369	-0.254	
wasyn	5.021	4.995	0.168	4.716	4.087	
λ	3.908	3.545	3.800	3.647	3.244	
ϕ	0.857	0.578	0.404	0.897	0.475	
θ	3.689	2.487	0.558	3.678	1.478	
wsig	1.985	0.587	2.669	1.119	1.002	

Table A.4: Refined parameters after fitting various zirconium oxo clusters with different ligands, using the Zr_{12}-acetate, Zr_{12}-propionate or the /Zr_6-acetate model. Relative Amplitude = Amplitude / Scale.

	Zr$_{12}$-butanoate	Zr$_6$-methylbutanoate	Zr$_{12}$-octanoate	Zr$_{12}$-oleate	Zr$_{12}$-oleate (background subtracted)
Model	Zr$_{12}$-acetate	Zr$_6$-acetate	Zr$_{12}$-acetate	Zr$_{12}$-propanoate	Zr$_{12}$-propanoate
Scale	0.63	0.56	0.50	0.29	0.64
Uiso Zr (Å^2)	0.004	0.003	0.004	0.005	0.005
Uiso O (Å^2)	0.010	0.011	0.013	0.019	0.017
Uiso C (Å^2)	0.011	0.014	0.010	0.018	0.018
delta2 (Å^2)	2.04	1.54	2.73	3.39	2.87
Rw	0.13	0.13	0.16	0.24	0.15
Amplitude (A)	0.165	0.349	0.331	0.295	
Relative Amplitude	0.262	0.623	0.662	1.01	
wasyn	-0.077	5.163	-4.540	-10.262	
λ	4.290	4.872	3.574	4.532	
ϕ	-1.024	4.677	-4.833	-5.087	
θ	5.191	4.623	2.932	2.767	
wsig	1.173	0.175	-0.332	-0.258	

Table A.5: Refined parameters after fitting various zirconium oxo clusters with different ligands, using the opposite model of Table A.4.

	Zr_{12}-butanoate	Zr_6-methylbutanoate	Zr_{12}-octanoate	Zr_{12}-oleate	Zr_{12}-oleate (background subtracted)
Model	Zr_6-acetate	Zr_{12}-acetate	Zr_6-acetate	Zr_6-acetate	Zr_6-acetate
Scale	0.64	0.53	0.51	0.30	0.66
Uiso Zr (Å^2)	0.004	0.004	0.004	0.004	0.004
Uiso O (Å^2)	0.005	0.023	0.007	0.006	0.004
Uiso C (Å^2)	0.011	0.017	0.010	0.008	0.008
delta2 (Å^2)	2.64	3.37	1.57	1.64	2.13
Rw	0.16	0.20	0.19	0.28	0.21
Amplitude (A)	-0.158	0.662	0.231	0.259	
wasyn	1.027	-5.766	1.174	0.426	
λ	3.553	1.573	3.634	3.996	
ϕ	0.623	-4.112	-0.842	5.066	
θ	6.472	4.602	3.309	3.457	
wsig	3.061	0.091	2.267	-5.372	

Table A.6: Refined parameters after fitting Zr_{12}-oleate cluster with Zr_{12}-propionate model without the exponentially dampening sinusoidal contribution.

	Zr_{12}-oleate
Scale	0.29
Uiso Zr (Å^2)	0.005
Uiso O (Å^2)	0.018
Uiso C (Å^2)	0.016
delta2 (Å^2)	3.32
Rw	0.33

Table A.7: Comparison of the single crystal distance data of different clusters. For methacrylic acid, only the intracluster distances could be compared as this forms a monomer.[2]

Distance	Zr_{12}-acetate (Å)	Zr_{12}-propionate (Å)	Zr_6-methacrylate (Å)
Zr-O	2.03-2.40	2.03-2.41	2.05-2.41
Intra Zr-Zr 1	3.45-3.59	3.47-3.60	3.48-3.55
Intra Zr-Zr 2	4.95-4.97	4.97-5.00	4.96
Inter Zr-Zr 1	5.59-5.68	5.68-5.70	
Inter Zr-Zr 2	8.27-8.61	8.36-8.43	
Inter Zr-Zr 3	11.26-11.96	11.27-12.00	

A.2.2 The organic ligand shell
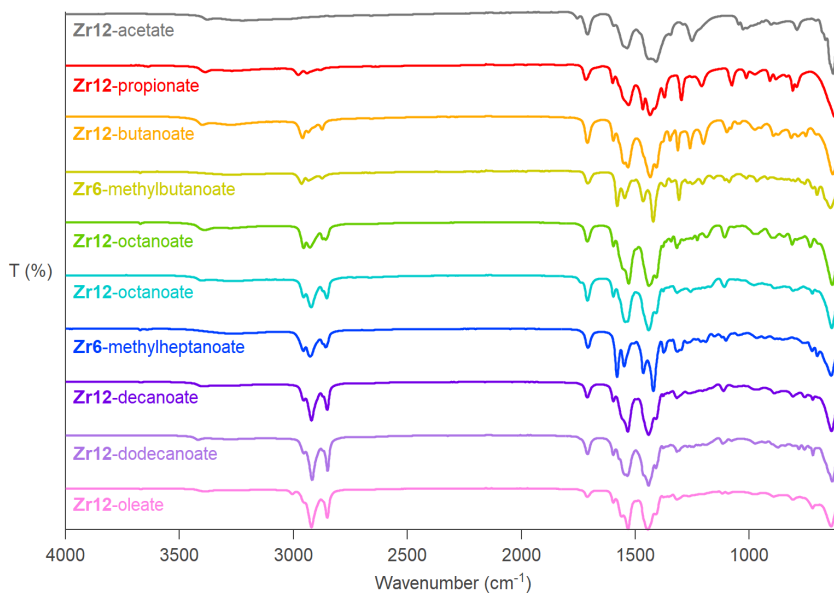
Figure A.7: IR of the all bottom up synthesised clusters.
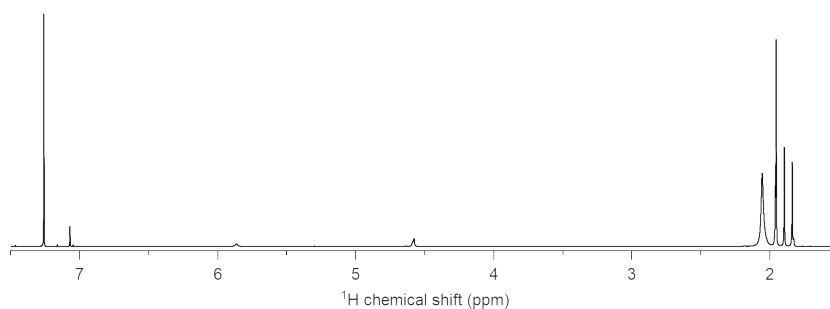
Figure A.8: ^{1}H NMR spectrum in CDCl$_3$ of the **Zr$_{12}$**-acetate cluster. There is no observable signal at 4 ppm indicating that the amount of ester impurity is very low.

In an effort to remove all the hydrogen bonded (protonated) acid from a **Zr$_{12}$**-oleate cluster a non-nucleophilic base (1,8-Diazabicyclo[5.4.0]undec-7-ene or DBU) was added. The base can accept a proton from the hydrogen bonded oleic acid and thus detach it from the cluster. Afterwards, size

exclusion chromatography (SEC) was performed to separate the clusters from the DBU coordinated acid. Only the first fraction of the SEC was obtained as a pure compound (absence of the peak around 1700 cm^{-1}) with a very low yield of 0.8%. From the second fraction onwards, H-bonded acid can be seen in the spectra, see figure A.9).
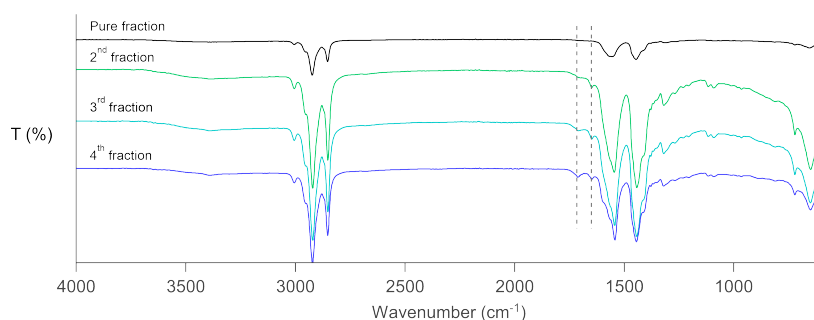
Figure A.9: Fractions collected with size exclusion chromatography

To quantify the amount of hydrogen bonded acid, we measured TGA of our synthesised clusters, see Figure A.10.
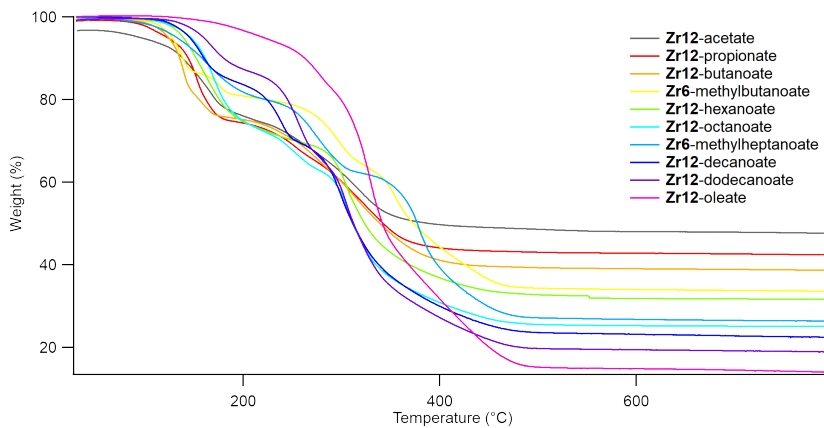
Figure A.10: Thermogravimetric analysis of our bottom up synthesised zirconium oxo clusters.

Assuming a pure cluster, the theoretical mass loss can be calculated from the molecular formula, considering that the end product is zirconia.

$$Zr_6O_8H_4(OOCR)_{12} \longrightarrow 6ZrO_2 + \text{byproducts} \tag{A.5}$$
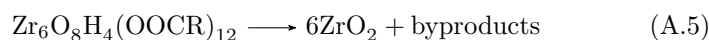
Starting from 100 g of clusters, we can calculate the mass of zirconia at the end:

$$m_{\text{ZrO}_2} = \left(\frac{100}{M_{cluster}}\right) \times 6 \times M_{\text{ZrO}_2} \qquad \text{(A.6)}$$

Where $M_{cluster}$ and M_{ZrO_2} are the molecular weights of the cluster and zirconia, respectively. Note that the calculations are done with the monomeric species and we use the molecular weight of the monomer (which is exactly half of the dimer) for all our calculations. This value is reported in Table 2.1 as the theoretical value. The experimental value is consistently lower than the theoretical one (Table 2.1), indicating an extra organic fraction that is assigned to mostly hydrogen bonded ligands. We quantify its amount by the following procedure. Again assuming that we start from 100 g of clusters, we calculated the molar amount of zirconia in the residual mass (experimental value).

$$n_{\text{ZrO}_2} = \frac{mass}{M_{\text{ZrO}_2}} \qquad \text{(A.7)}$$

From this we can determine the molar amount of monomeric cluster:

$$n_{cluster} = \frac{n_{\text{ZrO}_2}}{6} \qquad \text{(A.8)}$$

We calculate the apparent molecular weight of the cluster by using the molar amount and the starting mass (100 g):

$$M_{apparent} = \frac{100g}{n_{cluster}} \qquad \text{(A.9)}$$

The difference with the theoretical molecular weight is calculated and assigned to the extra organic fraction:

$$\Delta M = M_{apparent} - M_{theoretical} \qquad \text{(A.10)}$$

By dividing ΔM by the molecular weight of the carboxylic acid, we get the number of carboxylic acids that is present per monomer.

$$\frac{\text{extra acid}}{monomer} = \frac{\Delta M}{M_{acid}} \qquad \text{(A.11)}$$

This final value is also reported in Table 2.1.

A.2.3 ^{1}H NMR analysis
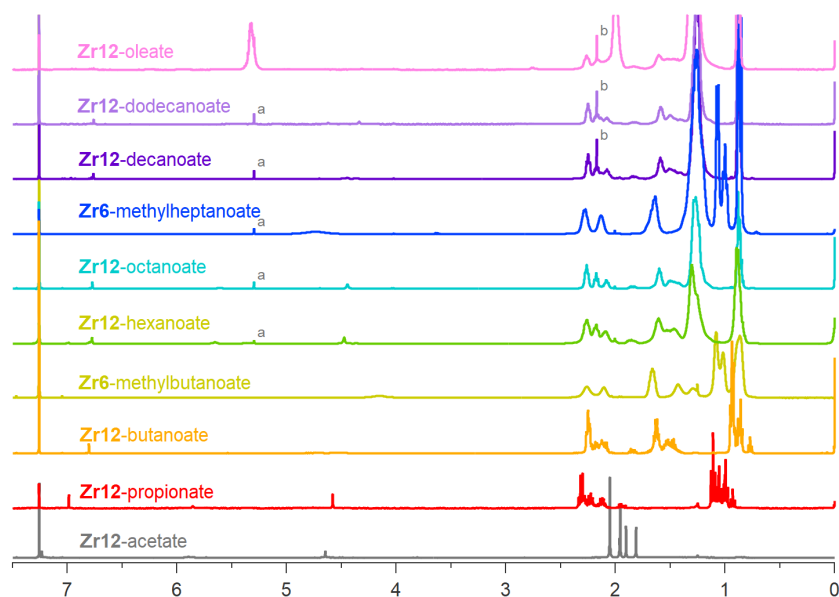
Figure A.11: ^{1}H NMR spectra in CDCl$_3$ of **Zr$_{12}$**-butanoate, octanoate, decanoate, dodecanoate and **Zr$_6$**-methylbutanoate. The peaks indicated with a is remaining DCM, the peaks indicated with b is remaining acetone.
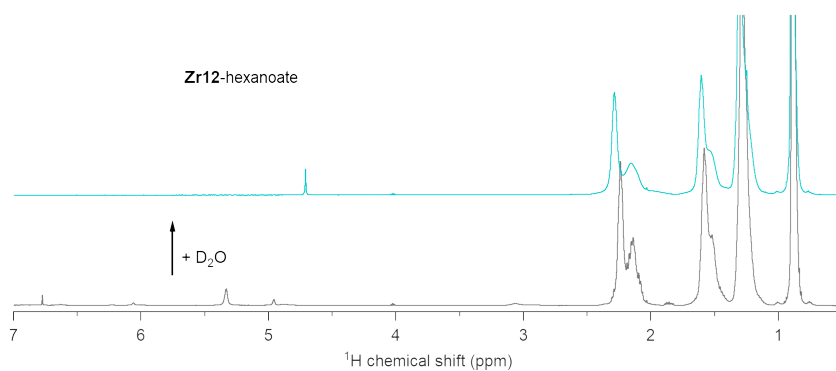
Figure A.12: we added a small amount of D$_2$O (20 μL) to a solution of **Zr$_{12}$**-hexanoate cluster in CDCl$_3$. Upon addition of D$_2$O, the deuterium rapidly exchanges for the protons and all the signals collapse onto a single resonance at 4.77 ppm

Table A.8: Determination of the contribution of homogeneous and heterogeneous broadening for three different resonances in the **Zr**$_{12}$-oleate cluster. We report here the experimental FWHM, the experimentally determined T$_2$ relaxation time constant, the calculated homogeneous line width and finally the homogeneous broadening of the multiplet resonances after simulation of the spectrum with the calculated homogeneous line width. We find that the homogeneous broadening is the main contributor and there is little heterogeneous broadening present.

Resonance	FWHM (Hz)	T$_2$ (ms)	$1/(\pi T_2)$ (Hz)	$\Delta\nu$
αCH$_2$	25.0	30.57	8.92	20
Alkene	11.1	200.0	1.59	9
Methyl	1.53	590.2	0.54	2
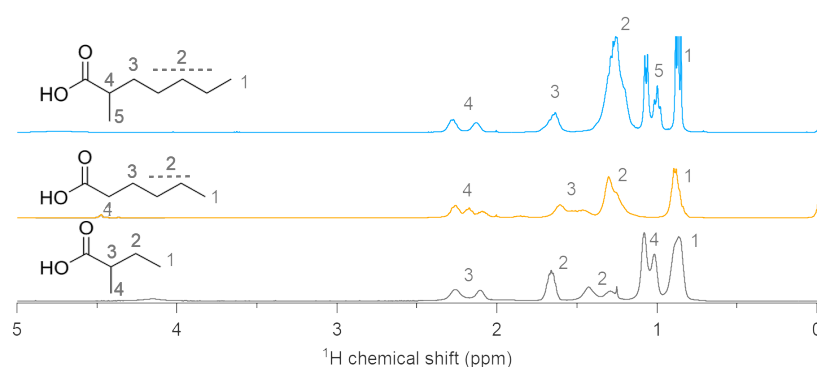
Figure A.13: ^{1}H NMR in CDCl$_3$ of **Zr**$_6$-methylbutanoate, -methylheptanoate and **Zr**$_{12}$-hexanoate with assigned peaks.

A.2.4   HR-MS
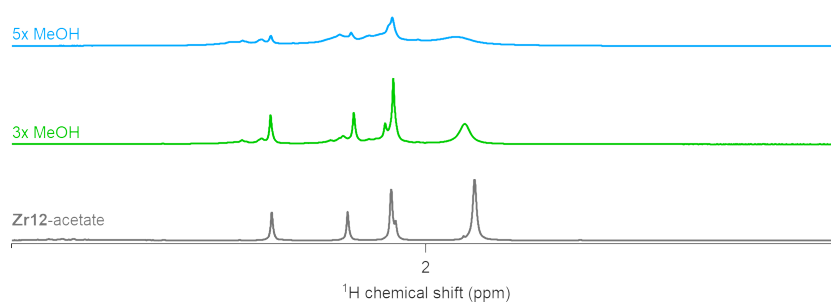
Figure A.14: ^{1}H NMR in CDCl$_3$ of the **Zr**$_{12}$-acetate cluster in CD$_3$OD. All signals disappear after multiple cycles of dissolving/evaporation indicating degradation of the cluster.
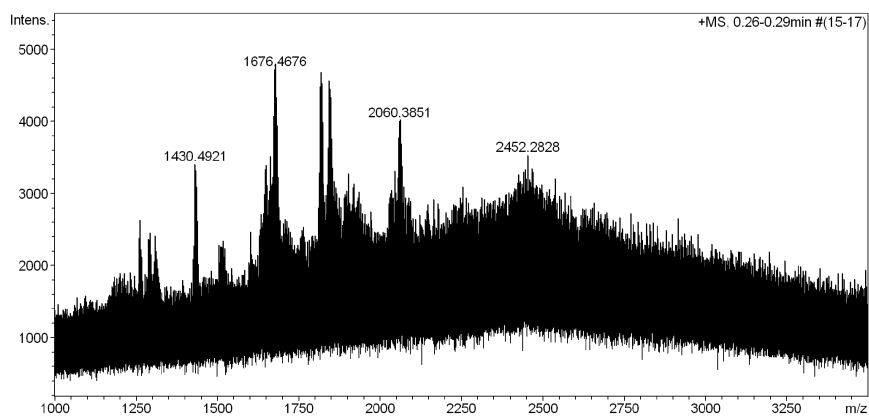
Figure A.15: HRMS of the **Zr**$_{12}$-acetate cluster in MeOH, no signals are close to the target mass (2775.17 g/mol) or could be matched with degradation products.
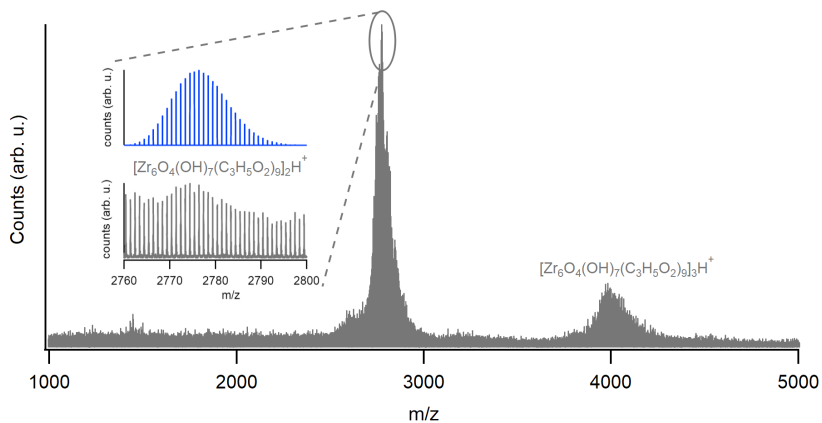
Figure A.16: HRMS of the bottom up synthesised **Zr$_{12}$**-propionate cluster in THF, the grey spectrum (experimental) is compared with the blue spectrum (simulated).
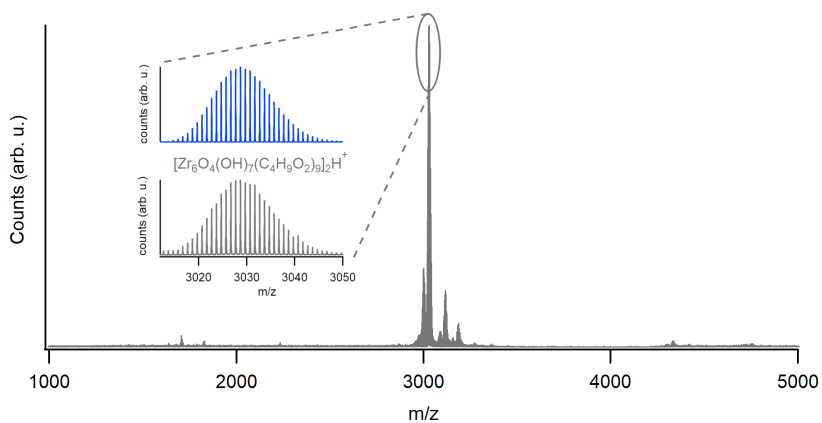
Figure A.17: HRMS of the bottom up synthesised **Zr$_{12}$**-butanoate cluster in THF, the grey spectrum (experimental) is compared with the blue spectrum (simulated).
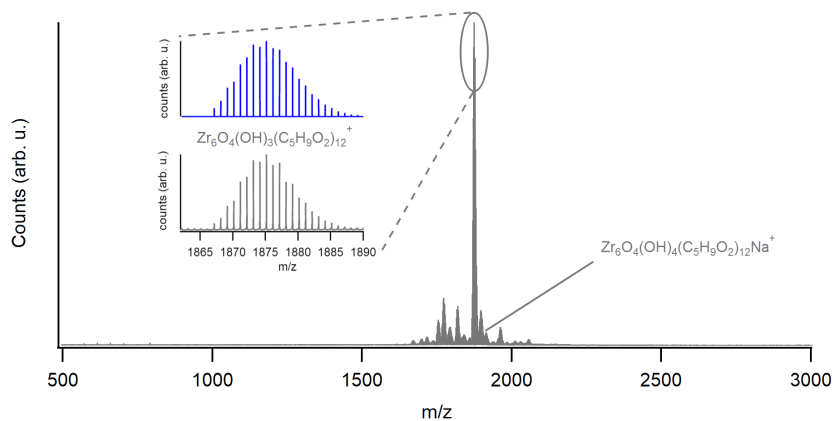
Figure A.18: HRMS of the bottom up synthesised **Zr$_6$**-methylbutanoate cluster in THF, the grey spectrum (experimental) is compared with the blue spectrum (simulated).
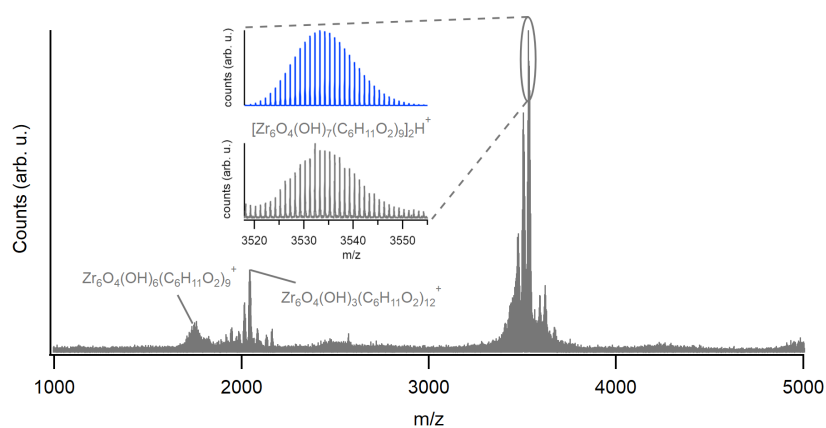
Figure A.19: HRMS of the bottom up synthesised **Zr$_{12}$**-hexanoate cluster in THF, the grey spectrum (experimental) is compared with the blue spectrum (simulated).
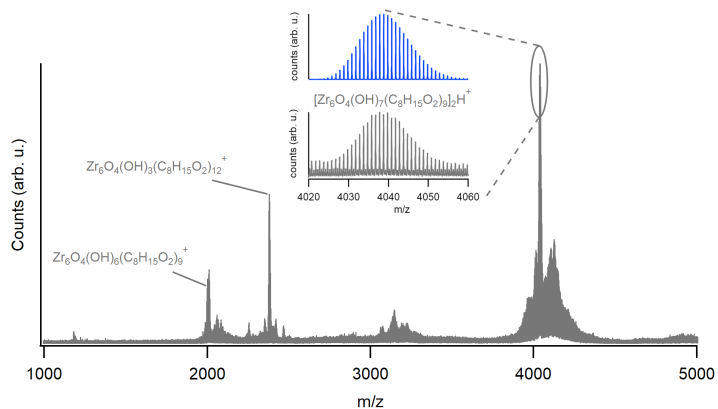
Figure A.20: HRMS of the bottom up synthesised **Zr$_{12}$**-octanoate cluster in THF, the grey spectrum (experimental) is compared with the blue spectrum (simulated).
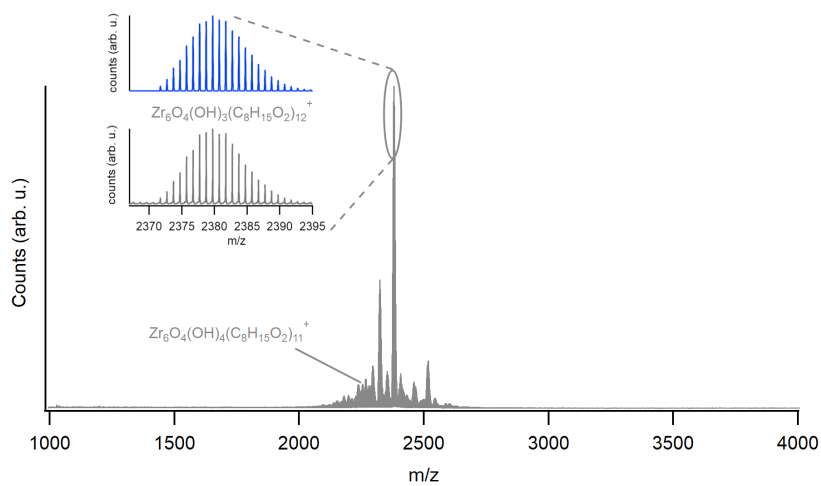
Figure A.21: HRMS of the bottom up synthesised **Zr$_6$**-methylheptanoate cluster in THF, the grey spectrum (experimental) is compared with the blue spectrum (simulated).
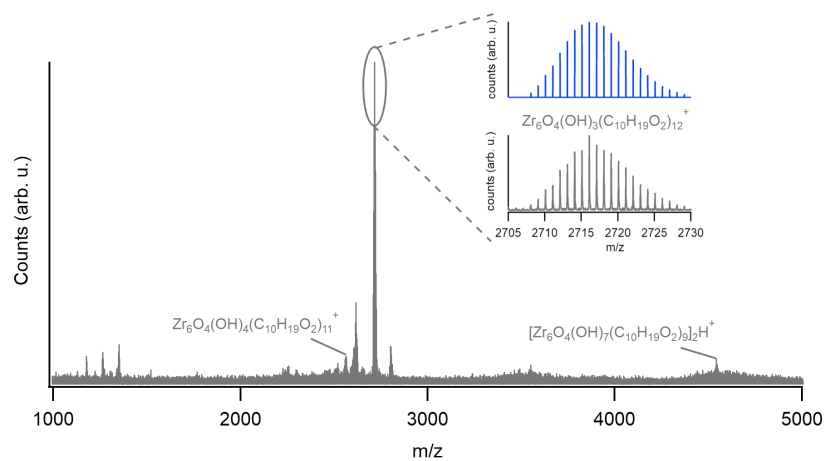
Figure A.22: HRMS of the bottom up synthesised **Zr**$_{12}$-decanoate cluster in THF, the grey spectrum (experimental) is compared with the blue spectrum (simulated).
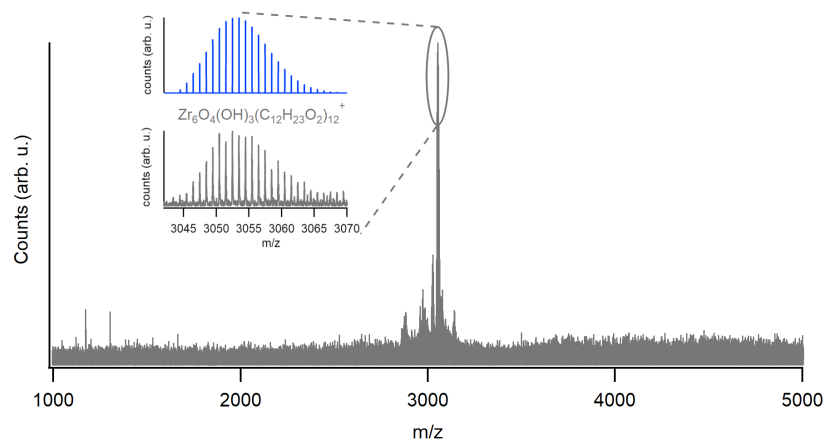
Figure A.23: HRMS of the bottom up synthesised **Zr**$_{12}$-dodecanoate cluster in THF, the grey spectrum (experimental) is compared with the blue spectrum (simulated).

A.2.5 Clusters synthesised by ligand exchange
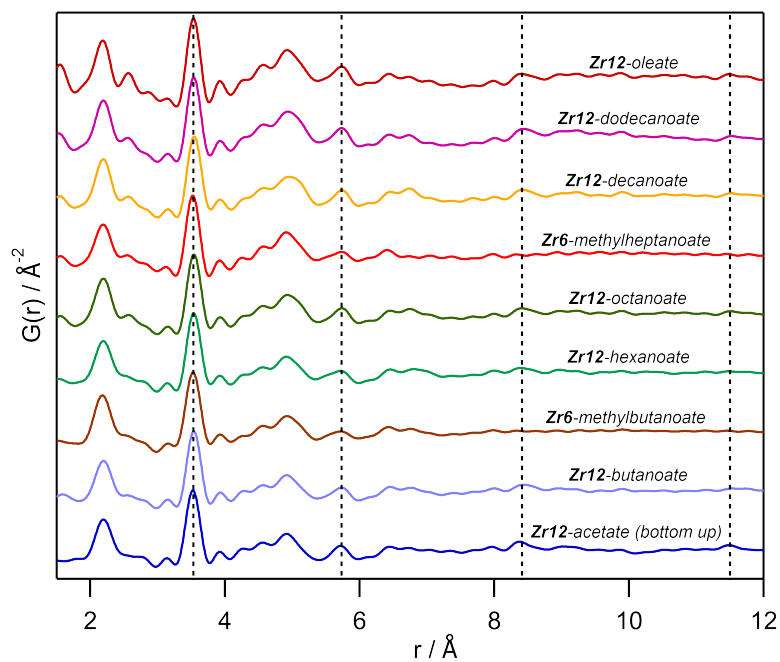
Figure A.24: PDF spectra of the clusters synthesised via the exchange reaction. Note that the acetic acid spectrum is added as a reference spectrum as it is not synthesised via an exchange reaction.
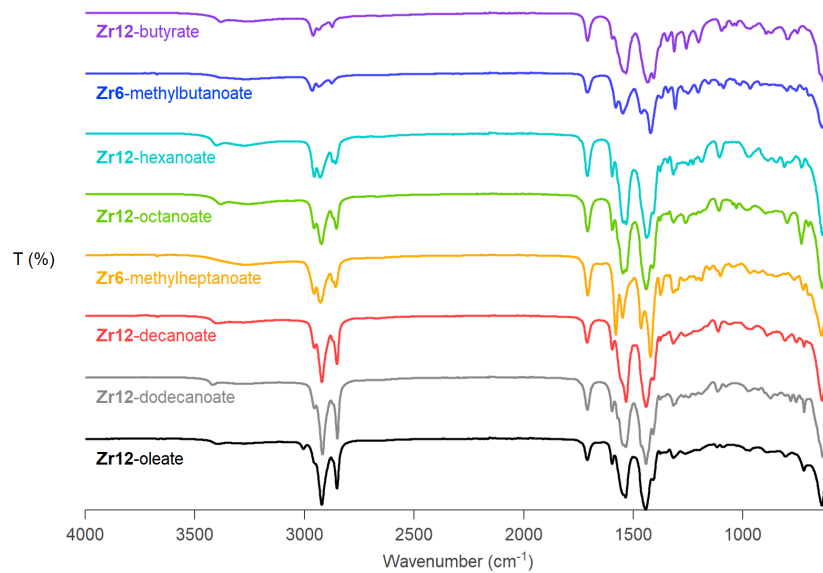
Figure A.25: IR spectra of the clusters synthesised via the exchange reaction.
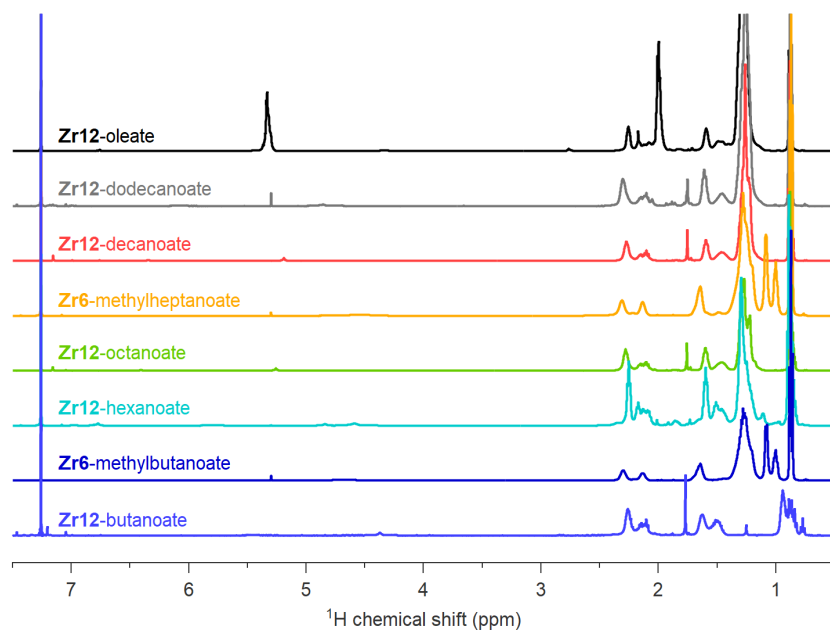
Figure A.26: ^{1}H NMR spectra in CDCl$_3$ of the clusters synthesised via the exchange reaction.
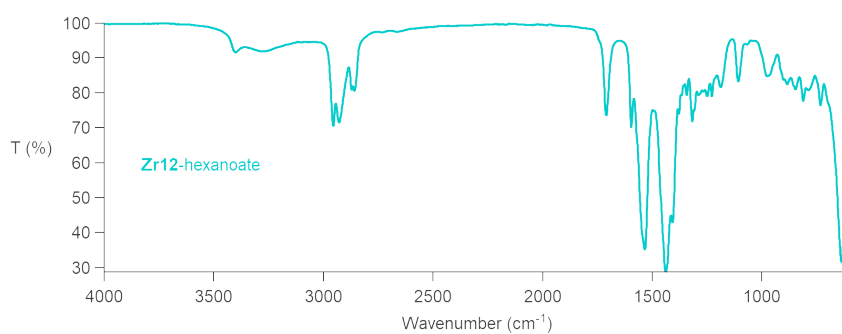
Figure A.27: FTIR spectrum of the cluster obtained via exchanging **Zr$_6$**-methylbutanoate with hexanoic acid.
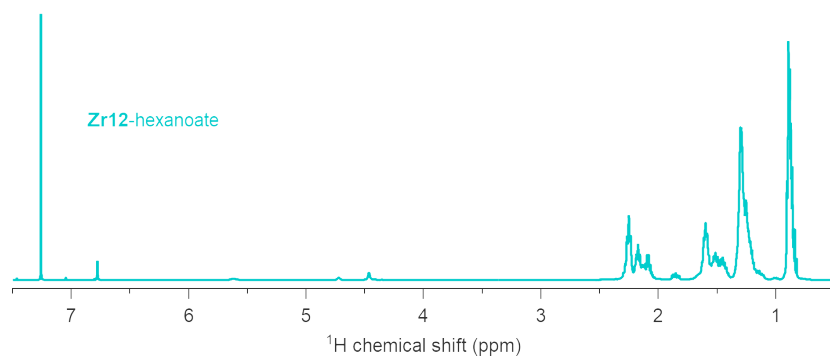
Figure A.28: ^{1}H NMR spectrum in CDCl$_3$ of the cluster obtained via exchanging **Zr**$_6$-methylbutanoate with hexanoic acid.
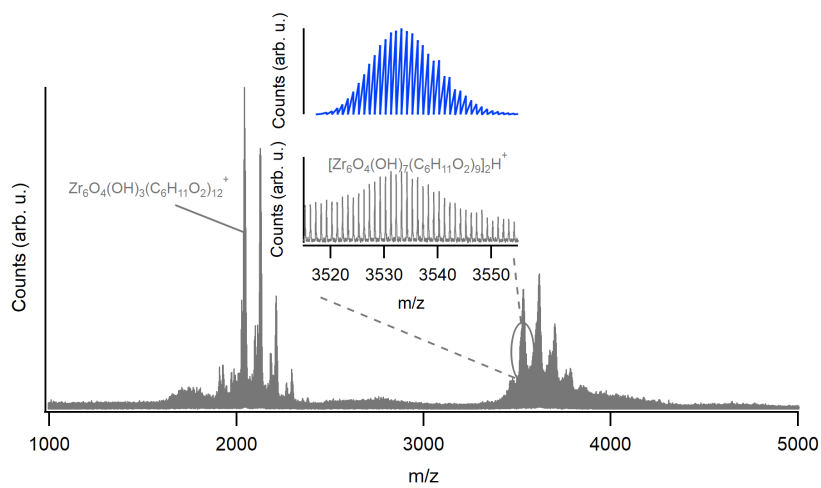
Figure A.29: MS spectrum of the cluster obtained via exchanging **Zr**$_6$-methylbutanoate with hexanoic acid.

A.2.6   Hafnium oxo clusters
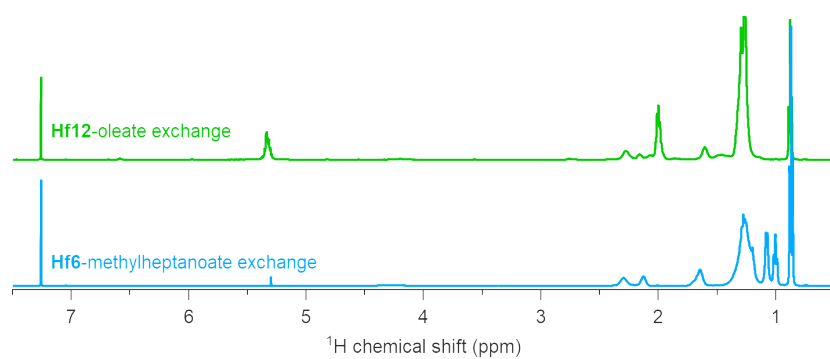
Figure A.30: Overlay of the ^{1}H NMR spectra in CDCl$_3$ for the **Hf**$_6$-methylheptanoate and the **Hf**$_{12}$-oleate obtained via an exchange reaction from **Hf**$_{12}$-acetate.
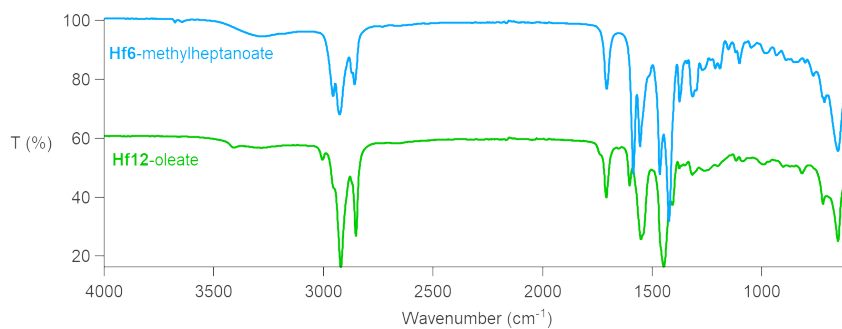
Figure A.31: Overlay IR for the **Hf**$_6$-methylheptanoate and the **Hf**$_{12}$-oleate obtained via an exchange reaction from **Hf**$_{12}$-acetate.

Table A.9: Refined parameters after fitting hafnium cluster with different ligand cappings with **Hf$_{12}$**/**Hf$_6$**-acetate model. **Hf$_6$**-acetate model was created by removing atoms from **Hf$_{12}$**-acetate model.

	Hf$_{12}$-acetate	**Hf$_6$**-methylbutanoate	**Hf$_{12}$**-oleate
Model	**Hf$_{12}$**-acetate	**Hf$_6$**-acetate	**Hf$_{12}$**-acetate
Scale	1.23	1.33	1.24
Uiso Hf (Å^2)	0.005	0.005	0.006
Uiso O (Å^2)	0.016	0.028	0.024
Uiso C (Å^2)	0.015	0.020	0.012
delta2 (Å^2)	3.11	3.44	3.68
Rw	0.10	0.10	0.12
Amplitude (A)		2.314	1.251
wasyn		0.407	-0.145
λ		3.469	3.974
ϕ		0.268	-4.891
θ		4.736	5.120
wsig		0.240	-0.532

Table A.10: TGA data on bottom up synthesised hafnium clusters. The values in the table is the remaining mass of HfO$_2$ in % and are calculated in the same way as shown before for ZrO$_2$ by replacing $M_{cluster}$ and $M_{\mathrm{ZrO_2}}$ with its hafnium counterpart.

Ligand	Theoretical value (%)	Experimental value (%)
Acetic acid	66.1	65.7
Methylbutyric acid	52.3	47.7
Oleic acid	27.6	25.7

A.3   Supporting info of Chapter 3

A.3.1   *In situ* flow setup
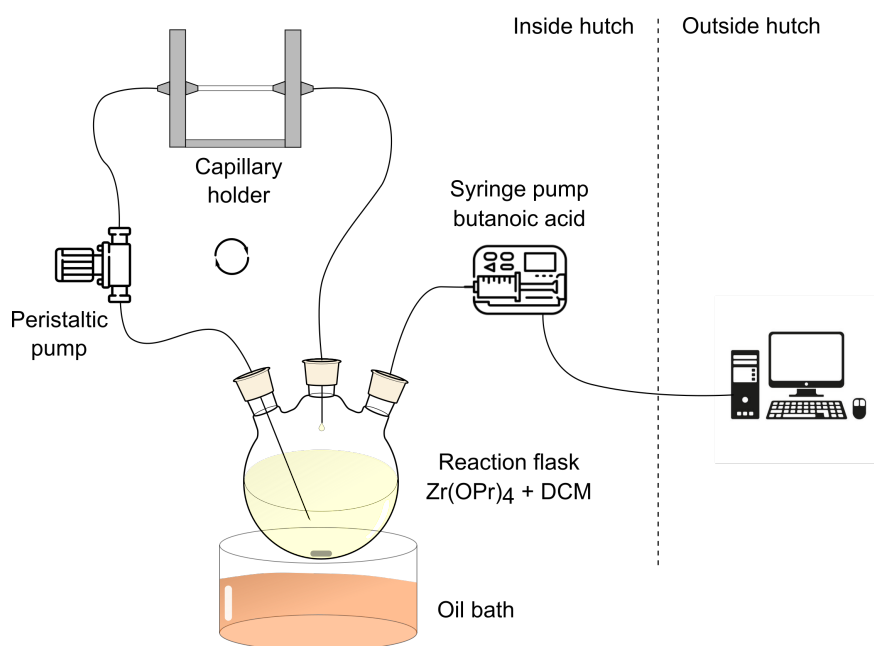
Figure A.32: *In situ* flow setup used for EXAFS synchrotron experiments. First Zr(OPr)$_4$ and DCM are added to an inert 3-neckflask which is stirred and heated to 30 $^\circ$C. This mixture is pumped through the sample holder using a peristaltic pump and cycled back into the flask. After closing the hutch and starting the measurement the carboxylic acid is injected via a remote controlled syringe pump.

A.3.2 Background ester formation
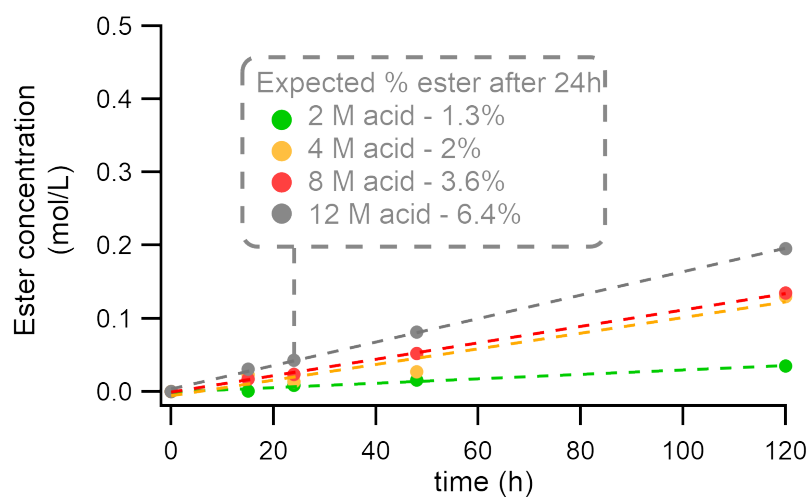
Figure A.33: Background ester formation between 1-propanol and different amounts of acetic acid at 15 °C. The expected amount of ester after 24h, the typical time frame of our kinetic experiments, is displayed. This value is calculated based on the maximum amount of ester formation.

Table A.11: Fitting parameters of the background ester formation between free 1-propanol and different concentrations of acetic acid at 15 °C. Using $f(x) = a + b * x$ as fitting function.

$f(x) = a + b * x$	a	b
2 M	-0.00054647 ± 0.00163	0.00029779 ± 2.75x10^{-5}
4 M	-0.0059273 ± 0.00911	0.0010714 ± 0.000154
8 M	-0.0011637 ± 0.00112	0.001126 ± 1.89x10^{-5}
12 M	0.0034303 ± 0.0017	0.0016053 ± 2.88^{-5}
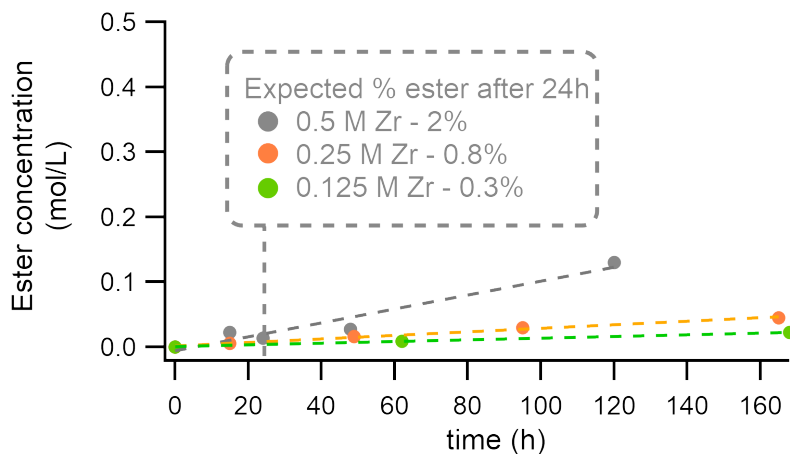
Figure A.34: Background ester formation between acetic acid and different amounts of 1-propanol at 15 °C. The expected amount of ester after 24h, the typical time frame of our kinetic experiments, is displayed. This value is calculated based on the maximum amount of ester formation.

Table A.12: Fitting parameters of the background ester formation between free acetic acid and different concentrations of 1-propanol at 15 °C. Using $f(x) = a + b * x$ as fitting function.

$f(x) = a + b * x$	a	b
0.5 M Zr	-0.0059273 ± 0.00911	0.0010714 ± 0.000154
0.25 M Zr	0.0011991 ± 0.00105	0.00027367 ± 1.19^{-5}
0.125 M Zr	0.0001767 ± 0.000299	0.00013112 ± 2.89^{-6}
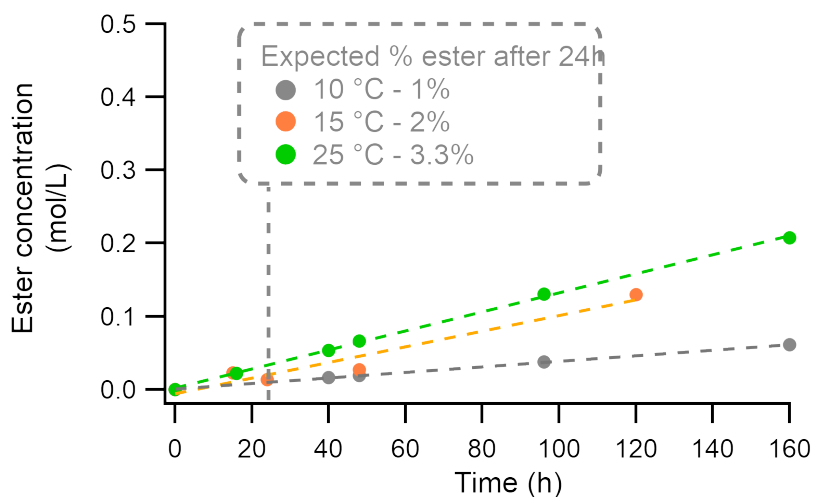
Figure A.35: Background ester formation between acetic acid and of 1-propanol at different temperatures. The expected amount of ester after 24h, the typical time frame of our kinetic experiments, is displayed. This value is calculated based on the maximum amount of ester formation.

Table A.13: Fitting parameters of the background ester formation between acetic acid and 1-propanol at different temperatures. Using $f(x) = a + b*x$ as fitting function.

$f(x) = a + b*x$	a	b
10 °C	-0.0005676 ± 0.000358	0.00037947 ± 4.07^{-6}
15 °C	-0.0059273 ± 0.00911	0.0010714 ± 0.000154
25 °C	0.0016868 ± 0.00159	0.0013036 ± 1.97^{-5}

Table A.14: Fitting parameters of the background ester formation between 1-propanol and different carboxylic acids at 15 °C. Using $f(x) = a + b*x$ as fitting function.

$f(x) = a + b*x$	a	b
Acetic acid	-0.0059273 ± 0.00911	0.0010714 ± 0.000154
Hexanoic acid	-0.0072008 ± 0.00406	0.00035043 ± 4.61^{-5}
Methylheptanoic acid	-0.001417 ± 0.00239	9.418^{-5} ± 2.32^{-5}

A.4 Supporting info of Chapter 4

A.4.1 Calculating ligand shell ratios using ^{1}H NMR

First the spectra are phased, baseline corrected and the peak of CDCl$_3$ is calibrated at 7.26 ppm. Then the integrals of the peaks are calculated for the peaks at 0.89 ppm ($-$CH$_3$ of hexanoate), at 2.05 ppm ($-$CH$_3$ of acetate) and depending on the reactive ligand, at 6.1 ppm ($-$CH of 2-carboxyethyl acrylate and oligomers or mono-2-(methacryloyloxy) ethyl succinate) or at 4.95 ppm (CH$_2$ of 10-undecenoic acid). Since the signal for acetate overlaps with other signals a manual baseline correction has to be done before integrating this peak. Finally, these integrals are normalised via dividing them by the number of protons they integrate for. With the total amount of ligands equal to 24, x the amount of hexanoate ligands, y the amount of reactive ligands and z the amount of acetate ligands we can write the following equation:

$$x + y + z = 24 \tag{A.12}$$

Using the integrals we can additionally calculate the following ratios:

$$\frac{y}{x} \tag{A.13}$$

$$\frac{z}{x} \tag{A.14}$$

By substituting fraction A.13 and A.14 in equation A.12 we can calculate the relative ratios between the different ligands on the cluster core.
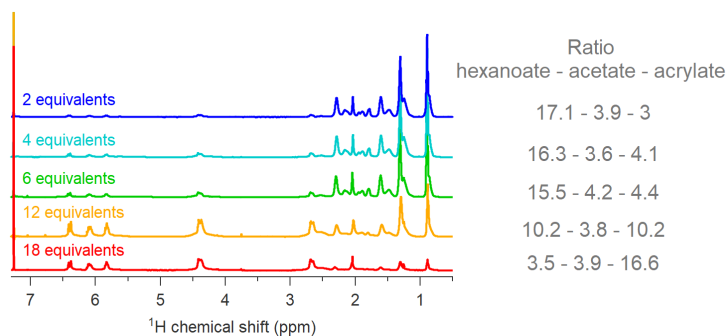
Figure A.36: Overview of **Zr**$_{12}$-acetate clusters exchanged with 2, 4 and 6 2-carboxyethyl acrylate and hexanoic acid as secondary ligand. While the exchange is not complete, acetate signal at 2.1 ppm,the overall targeted ratio of acrylate versus hexanoate is obtained.

Ratio
hexanoate - acetate - acrylate

2 equivalents   18.7 - 3.6 - 1.7
3 equivalents   18 - 3.6 - 2.4
4 equivalents   17 - 4 - 3
6 equivalents   15.4 - / - 4.6
12 equivalents   10.5 - / - 9.5
18 equivalents   5.6 - / - 14.4

^{1}H chemical shift (ppm)
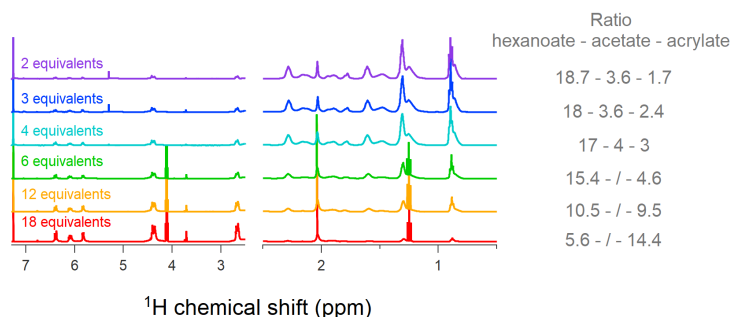
Figure A.37: Overview of **Zr$_{12}$**-acetate clusters exchanged with 2, 4, 6, 12 or 18 2-carboxyethyl acrylate oligomers and hexanoic acid as secondary ligand. While the exchange is not complete, acetate signal at 2.1 ppm, the overall targeted ratio of acrylate versus hexanoate is obtained. For the samples with with 6, 12 and 18 equivalents the amount of acetate could not be determined due to overlap with the solvent peak. For the calculations the amount of acetate was set to 4.

A.4.2   Polymers synthesised from acrylate capped clusters

$Zr_{12}O_8(OH)_8(C_6H_{11}O_2)_{18}(C_6H_7O_4)_6$

25 mol%   50 mol%   75 mol%
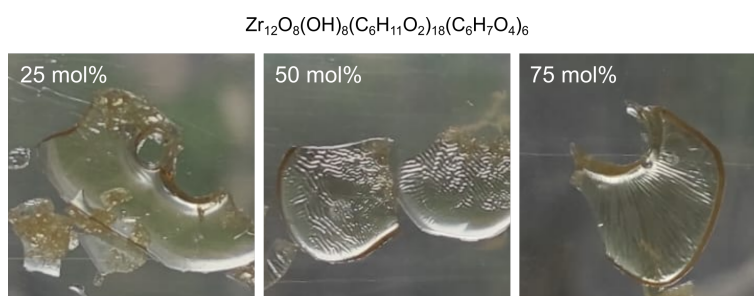
Figure A.38: Overview of **Zr$_{12}$**-clusters capped with a mixed ligand shell of 2-carboxyethyl acrylate and hexanoic acid in a 3 : 1 ratio. polymerised with, from (left to right) 25, 50 and 75 mol% methylmethacrylate using 5 mol% dicumylperoxide as radical initiator.

$Zr_{12}O_8(OH)_8(C_6H_{11}O_2)_{12}(C_6H_7O_4)_{12}$
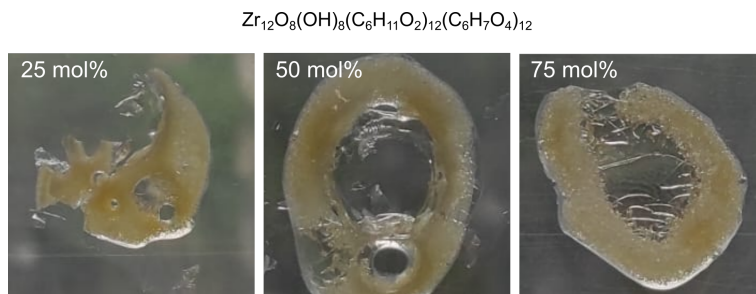
Figure A.39: Overview of **Zr**$_{12}$-clusters capped with a mixed ligand shell of 2-carboxyethyl acrylate and hexanoic acid in a $1:1$ ratio. polymerised with, from (left to right) 25, 50 and 75 mol% methylmethacrylate using 5 mol% dicumylperoxide as radical initiator.

$Zr_{12}O_8(OH)_8(C_6H_{11}O_2)_6(C_6H_7O_4)_{18}$
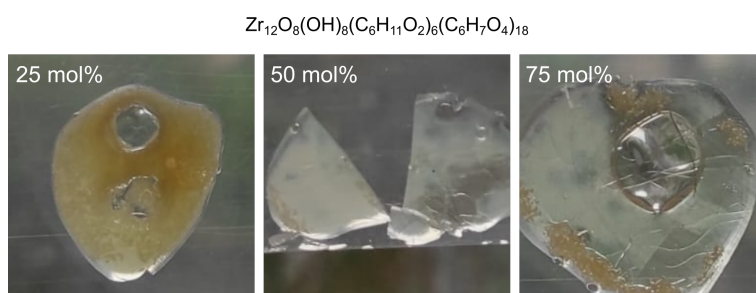
Figure A.40: Overview of **Zr**$_{12}$-clusters capped with a mixed ligand shell of 2-carboxyethyl acrylate and hexanoic acid in a $1:3$ ratio. polymerised with, from (left to right) 25, 50 and 75 mol% methylmethacrylate using 5 mol% dicumylperoxide as radical initiator.
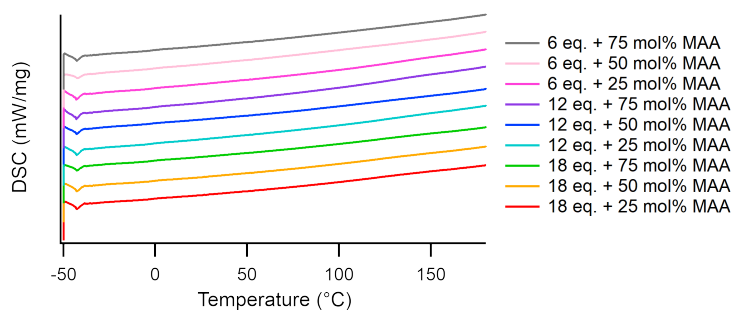
Figure A.41: Overview of DSC measurements for clusters capped with 6, 12 or 18 equivalents 2-carboxyethyl acrylate reacted with 25, 50 or 75 mol% methylmethacrylate.

$Zr_{12}O_8(OH)_8(C_6H_{11}O_2)_{12}(C_3H_3O_2(C_3H_4O_2)_n)_{12}$

$Zr_{12}O_8(OH)_8(C_6H_{11}O_2)_{18}(C_3H_3O_2(C_3H_4O_2)_n)_6$
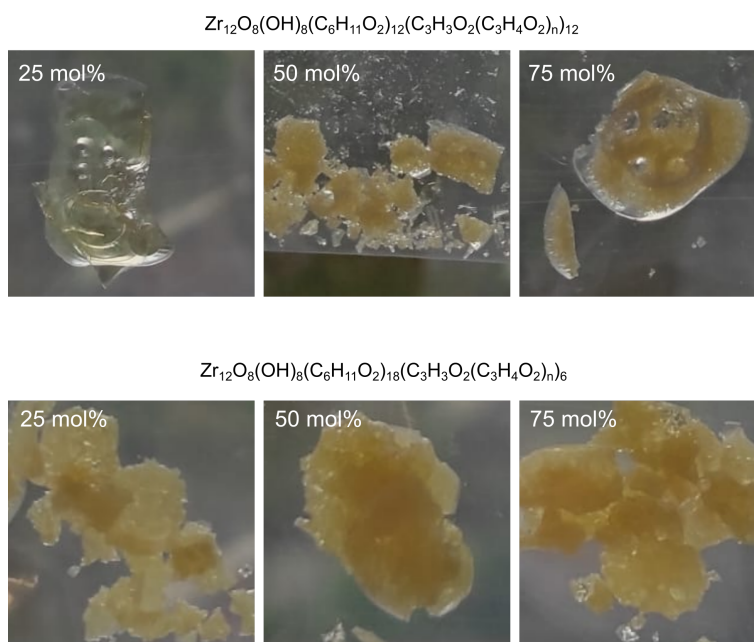
Figure A.42: Overview of **Zr**$_{12}$-clusters capped with a mixed ligand shell of 2-carboxyethyl acrylate oligomers and hexanoic acid in a 1 : 1 ratio (top) and a 1 : 3 ratio. polymerised with, from (left to right) 25, 50 and 75 mol% methylmethacrylate using 5 mol% dicumylperoxide as radical initiator.
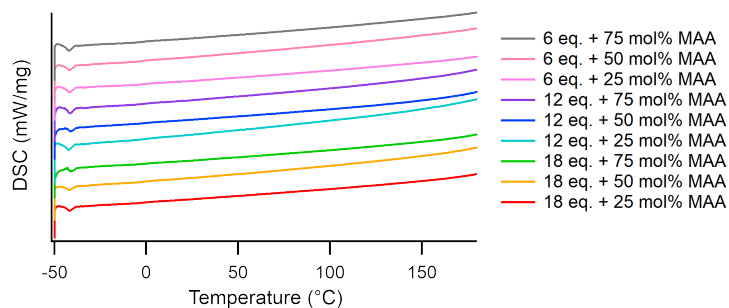
Figure A.43: Overview of DSC measurements for clusters capped with 6, 12 or 18 equivalents 2-carboxyethyl acrylate oligomers reacted with 25, 50 or 75 mol% methylmethacrylate.
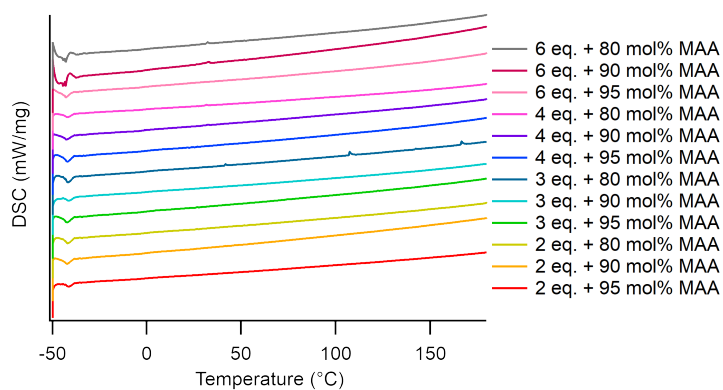
Figure A.44: Overview of DSC measurements for clusters capped with 2, 3, 4 or 6 equivalents 2-carboxyethyl acrylate oligomers reacted with 80, 90 or 95 mol% methylmethacrylate.

$Zr_{12}O_8(OH)_8(C_6H_{11}O_2)_{22}(C_{10}H_{13}O_6)_2$

$Zr_{12}O_8(OH)_8(C_6H_{11}O_2)_{21}(C_{10}H_{13}O_6)_3$
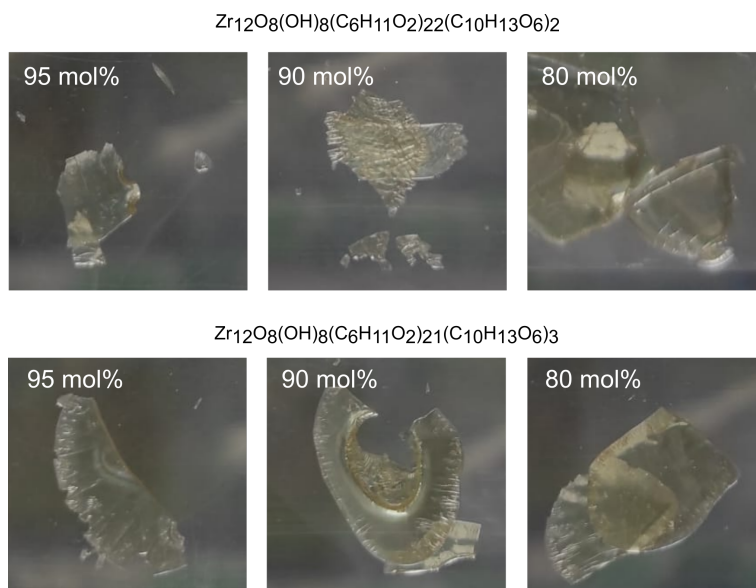
Figure A.45: Overview of **Zr$_{12}$**-clusters capped with a mixed ligand shell of mono-2-(acryloyloxy) ethyl succinate and hexanoic acid in a $1:11$ ratio (top) and a $1:7$ ratio. polymerised with, from (left to right) 95, 90 and 80 mol% methylmethacrylate using 5 mol% dicumylperoxide as radical initiator.
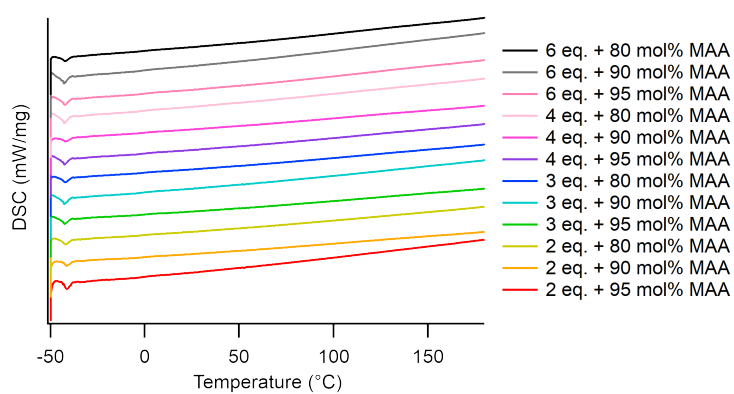
Figure A.46: Overview of DSC measurements for clusters capped with 2, 3, 4 or 6 equivalents mono-2-(acryloyloxy) ethyl succinate oligomers reacted with 80, 90 or 95 mol% methylmethacrylate.

A.5 Supporting info of Chapter 5

A.5.1 Epoxidation of oleic acid
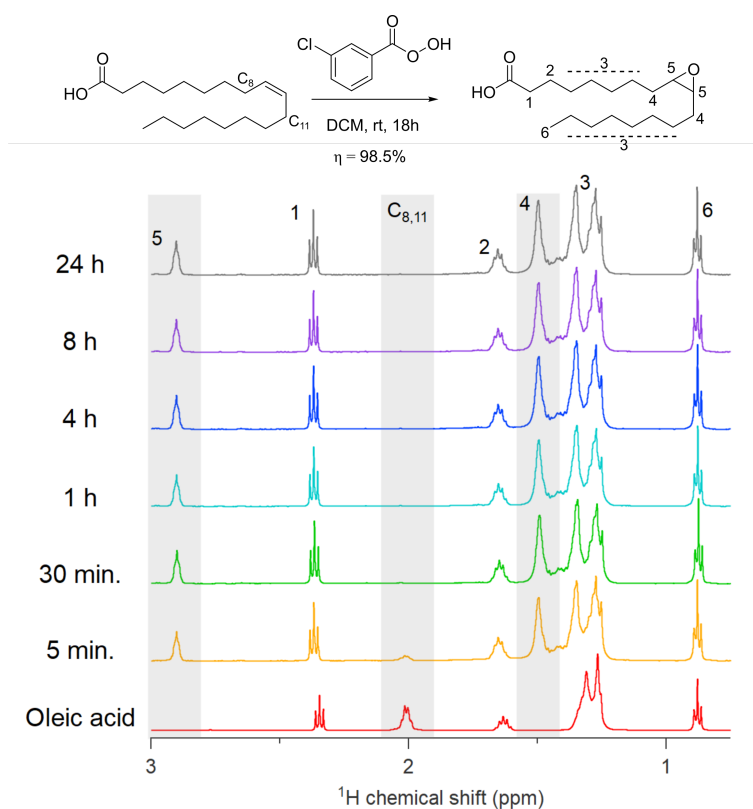
Figure A.47: ^{1}H NMR in CDCl$_3$ of the epoxidation of oleic acid using 2.3 equivalents m-CPBA in DCM. The figure shows the fast decrease of the signals corresponding to the carbons adjacent to the double bond. The double bond signal was impossible to track since it overlapped with the solvent peak. It can be concluded that after 1h the reaction is complete.
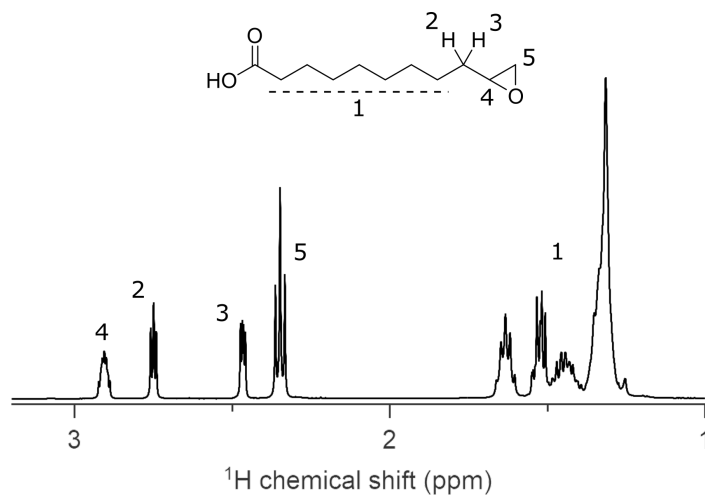
Figure A.48: ^{1}H NMR in CDCl$_3$ of the epoxide ligand from 10-undecenoic acid in CDCl$_3$.
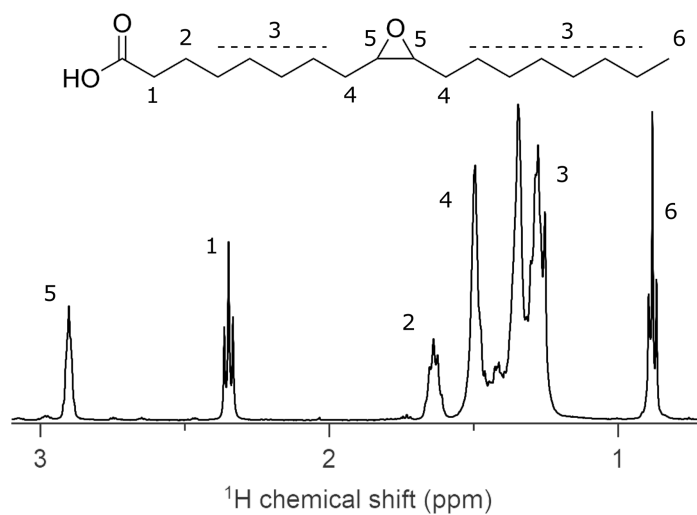
Figure A.49: ^{1}H NMR in CDCl$_3$ of the epoxide ligand from oleic acid in CDCl$_3$.
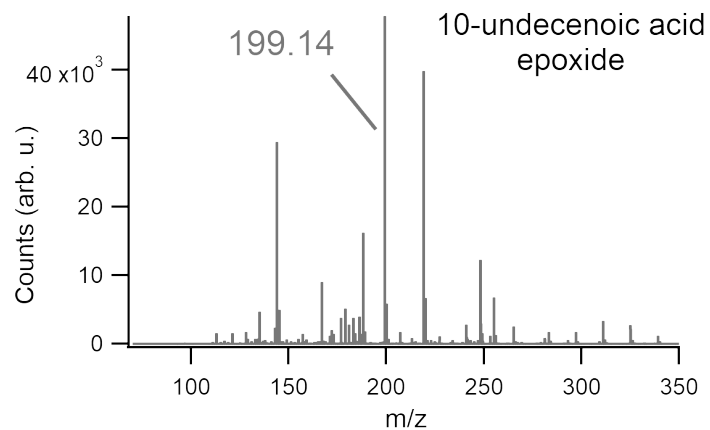
Figure A.50: HRMS of the 10-undecenoic acid epoxide ligand in MeOH. The assigned peak is the mass of the corresponding carboxylate.
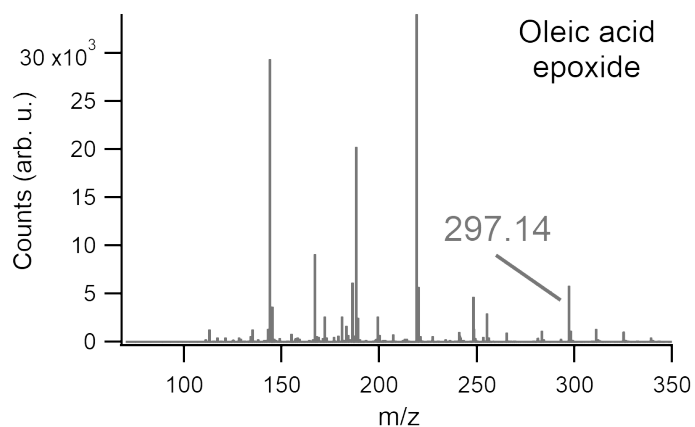
Figure A.51: HRMS of the oleic acid epoxide ligand in MeOH. The assigned peak is the mass of the corresponding carboxylate.

A.5.2   Cluster functionalisation with epoxide
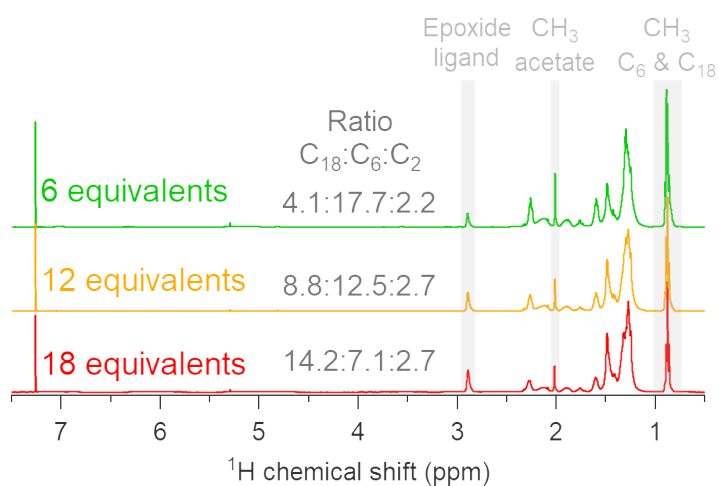
Figure A.52: ^{1}H NMR in CDCl$_3$ of the epoxide ligand, synthesised from oleic acid, capped cluster with either 6, 12 or 18 equivalents.
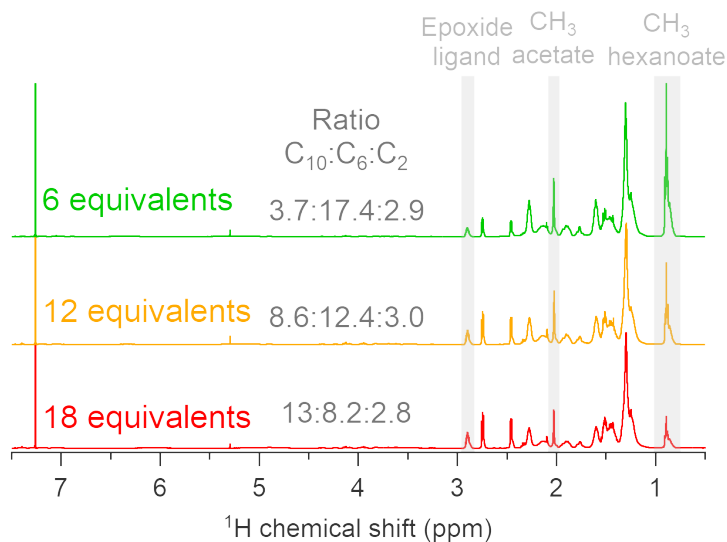
Figure A.53: ^{1}H NMR in CDCl$_3$ of the epoxide ligand, synthesised from 10-undecenoic acid, capped cluster with either 6, 12 or 18 equivalents.

A.5.3   FTIR measurements
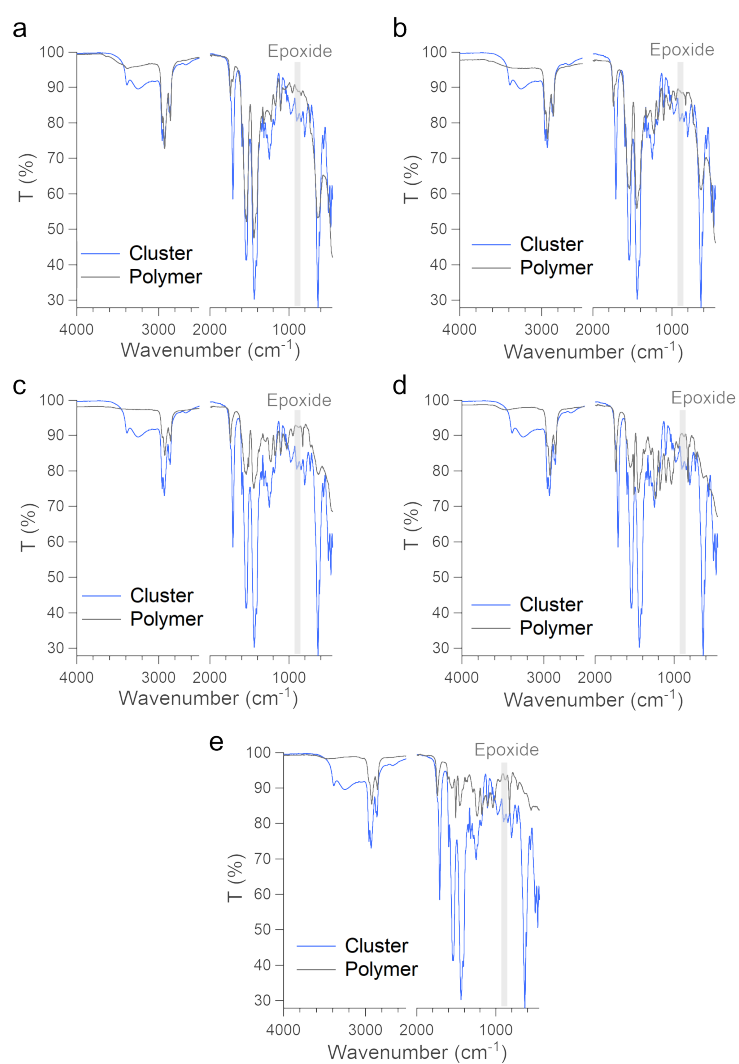
Figure A.54: Overview of FTIR measurements of samples containing 5 mol% Zn and clusters capped with 2 equivalents epoxide ligands on the surface reacted with (a) 0, (b) 25, (c) 50, (d) 75 and (e) 95 mol% BADGE.
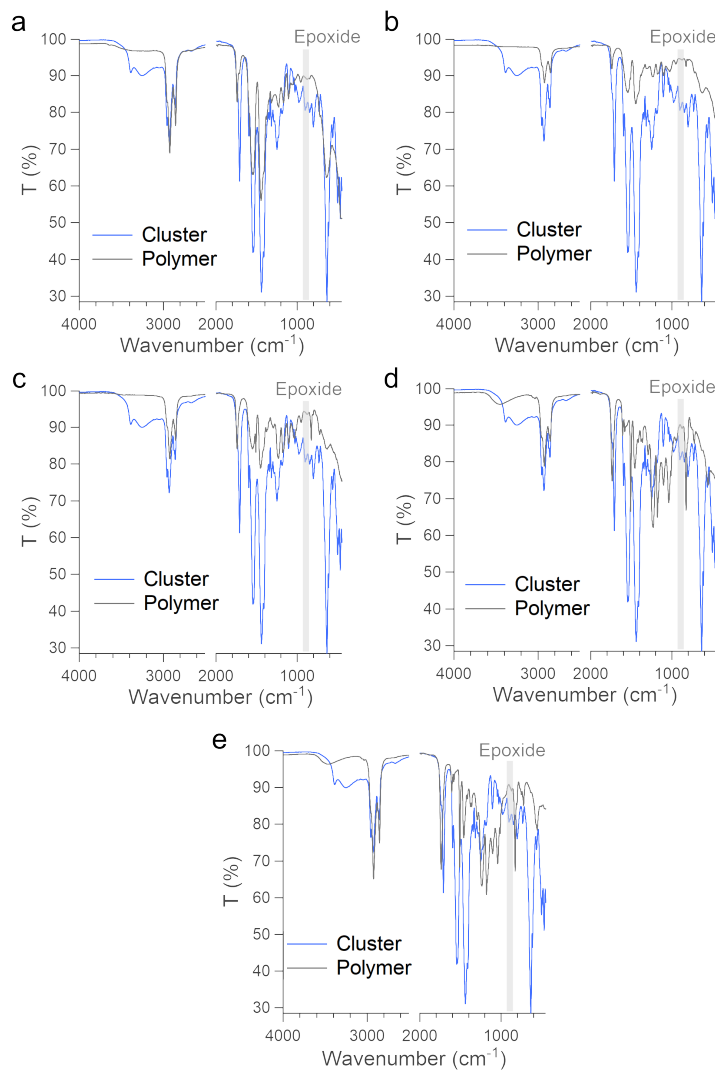
Figure A.55: Overview of FTIR measurements of samples containing 5 mol% Zn and clusters capped with 4 equivalents epoxide ligands on the surface reacted with (a) 0, (b) 25, (c) 50, (d) 75 and (e) 95 mol% BADGE.
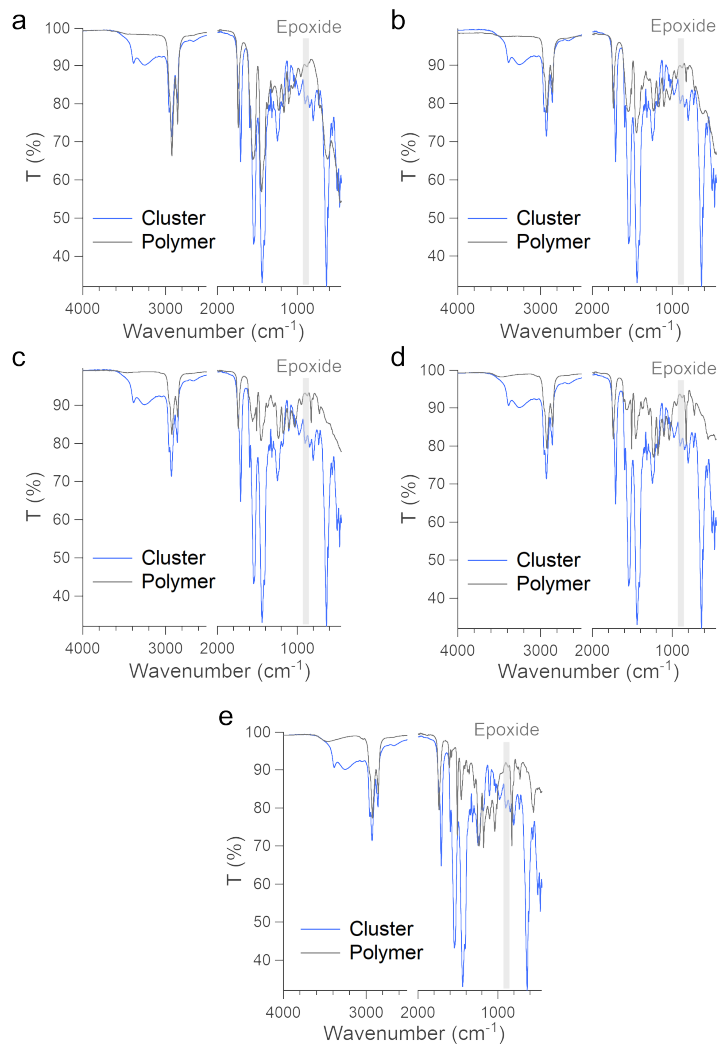
Figure A.56: Overview of FTIR measurements of samples containing 5 mol% Zn and clusters capped with 6 equivalents epoxide ligands on the surface reacted with (a) 0, (b) 25, (c) 50, (d) 75 and (e) 95 mol% BADGE.
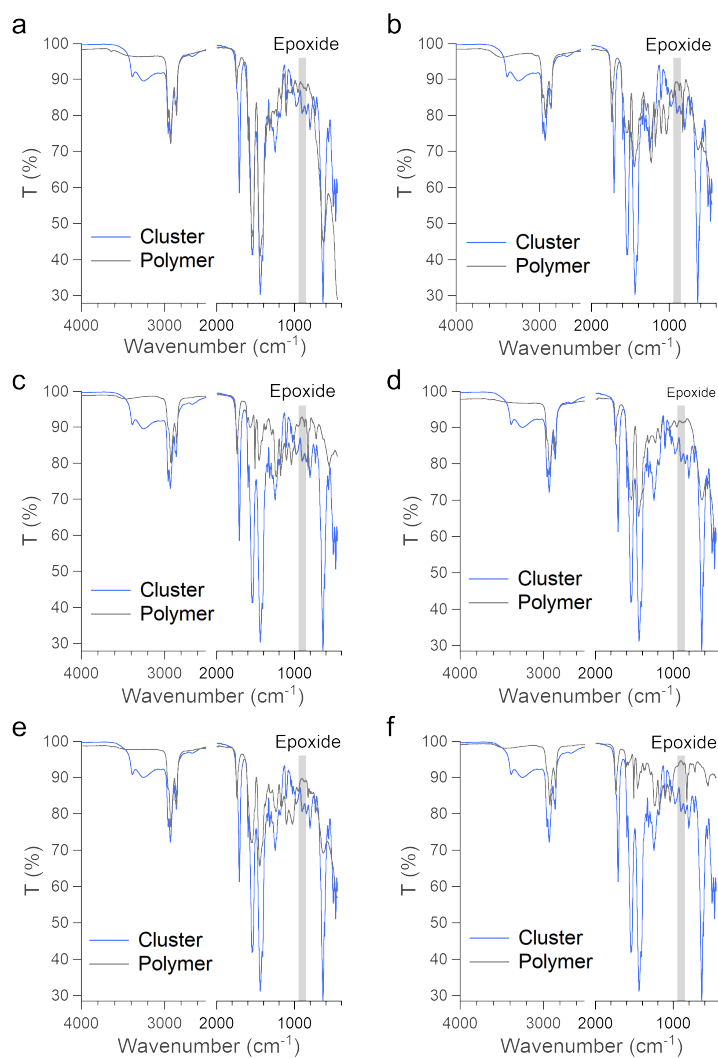
Figure A.57: Overview of FTIR measurements of samples containing 10 mol% Zn and both clusters capped with 2 equivalents epoxide ligands on the surface reacted with (a) 0, (b) 50 and (c) 95 and clusters capped with 4 equivalents epoxide ligands on the surface reacted with (d) 0, (e) 50 and (f) 95 mol% BADGE.
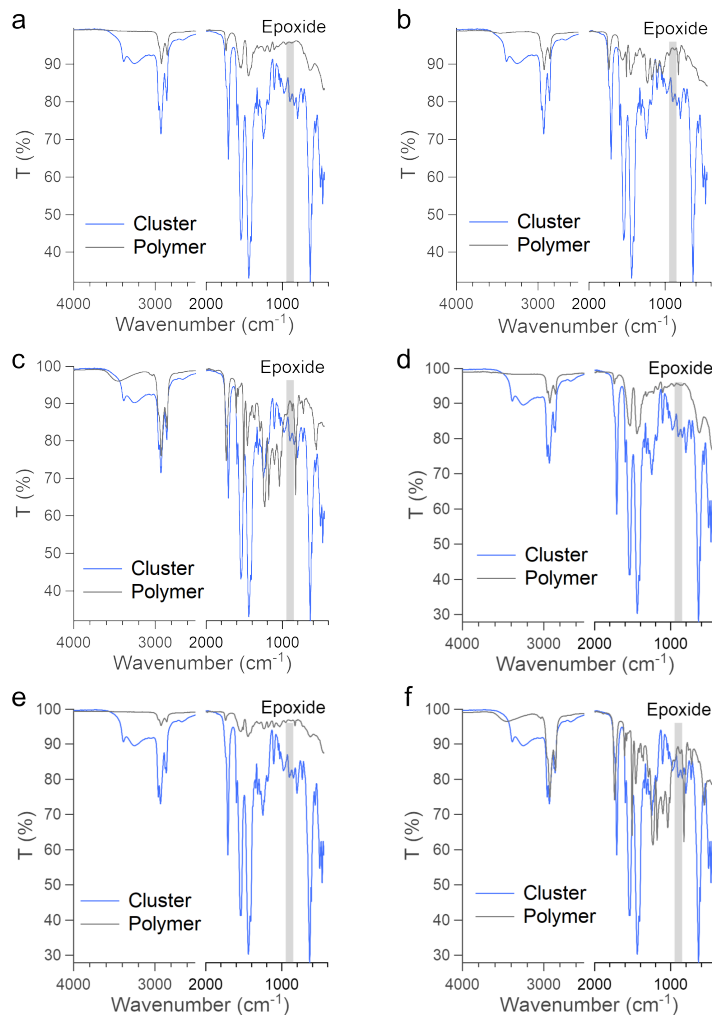
Figure A.58: Overview of FTIR measurements of samples containing 10 mol% Zn and clusters capped with 6 equivalents epoxide ligands on the surface reacted with (a) 0, (b) 50 and (c) 95. Overview of samples containing 0 mol% Zn and clusters capped with 2 equivalents epoxide ligands on the surface reacted with (d) 0, (e) 50 and (f) 95 mol% BADGE.
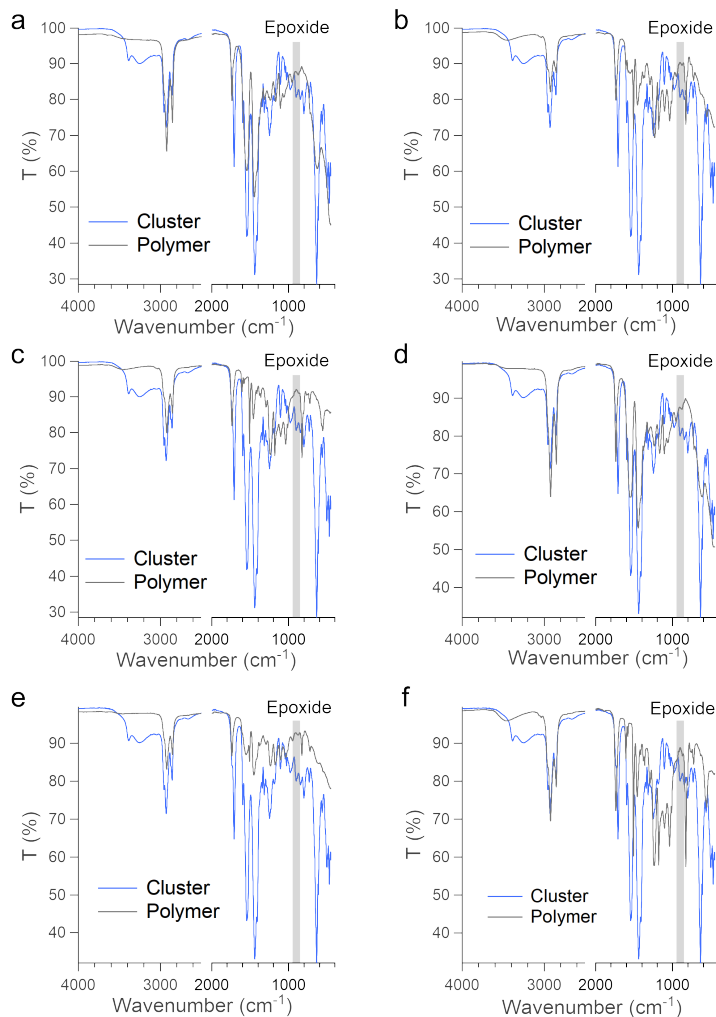
Figure A.59: Overview of FTIR measurements of samples containing 0 mol% Zn and both clusters capped with 4 equivalents epoxide ligands on the surface reacted with (a) 0, (b) 50 and (c) 95 and clusters capped with 6 equivalents epoxide ligands on the surface reacted with (d) 0, (e) 50 and (f) 95 mol% BADGE.

A.5.4 DSC measurements
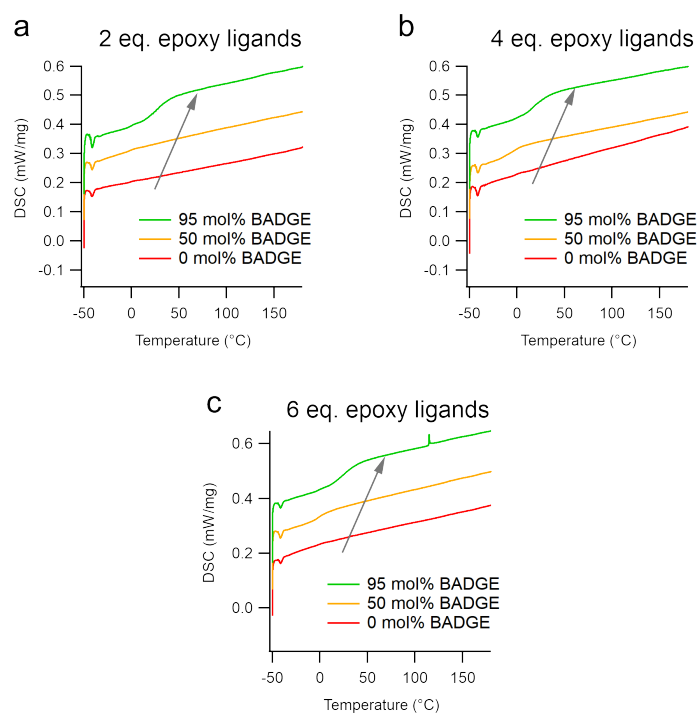
Figure A.60: Overview of DSC measurements of samples containing 0 mol% Zn with different amounts of epoxide ligands on the cluster surface which are 2 equivalents (a), 4 equivalents (b) or 6 equivalents (c).
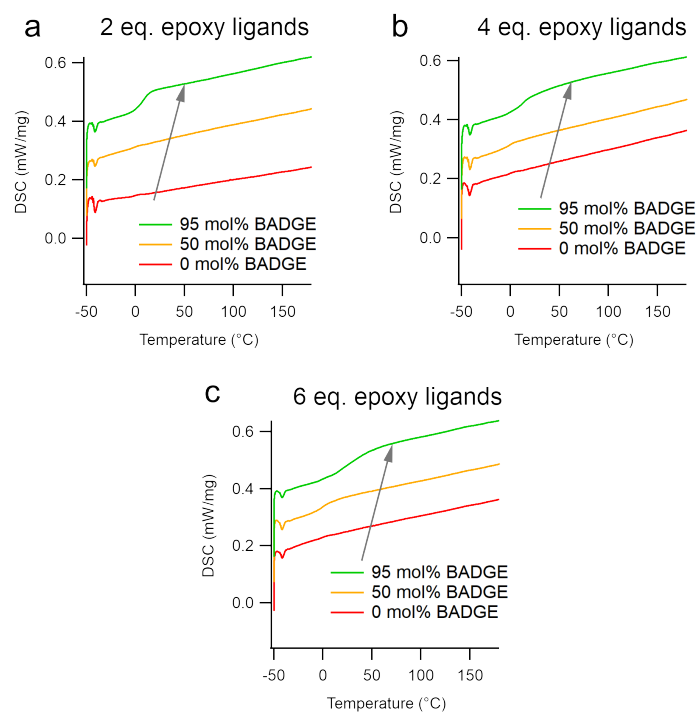
Figure A.61: Overview of DSC measurements of samples containing 10 mol% Zn with different amounts of epoxide ligands on the cluster surface which are 2 equivalents (a), 4 equivalents (b) or 6 equivalents (c).

A.5.5 TGA measurements
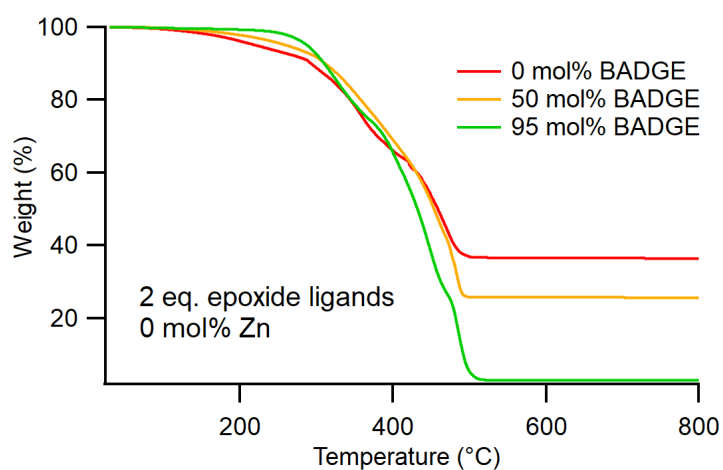
Figure A.62: Overview of TGA measurements of samples containing clusters functionalised with 2 equivalents epoxide and 0 mol% Zn with different amounts of BADGE.
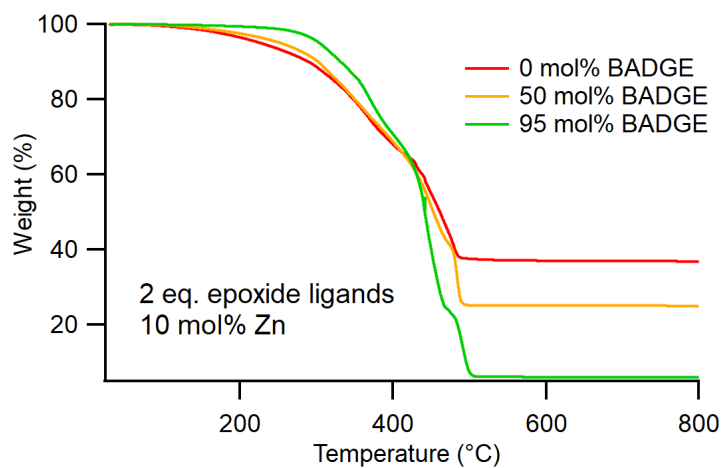
Figure A.63: Overview of TGA measurements of samples containing clusters functionalised with 2 equivalents epoxide and 10 mol% Zn with different amounts of BADGE.
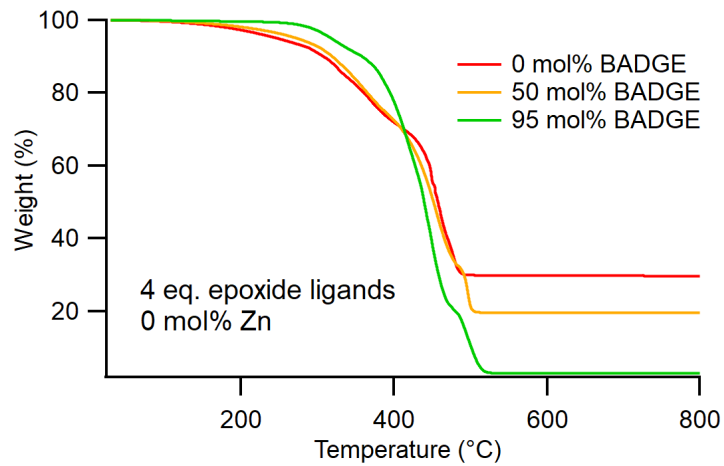
Figure A.64: Overview of TGA measurements of samples containing clusters functionalised with 4 equivalents epoxide and 0 mol% Zn with different amounts of BADGE.
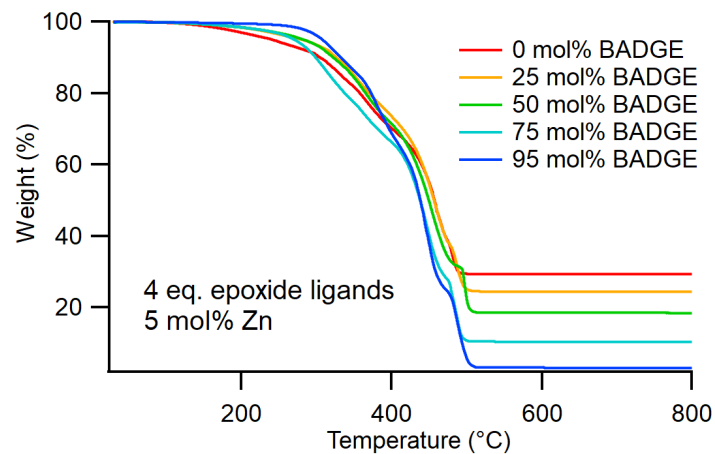
Figure A.65: Overview of TGA measurements of samples containing clusters functionalised with 4 equivalents epoxide and 5 mol% Zn with different amounts of BADGE.
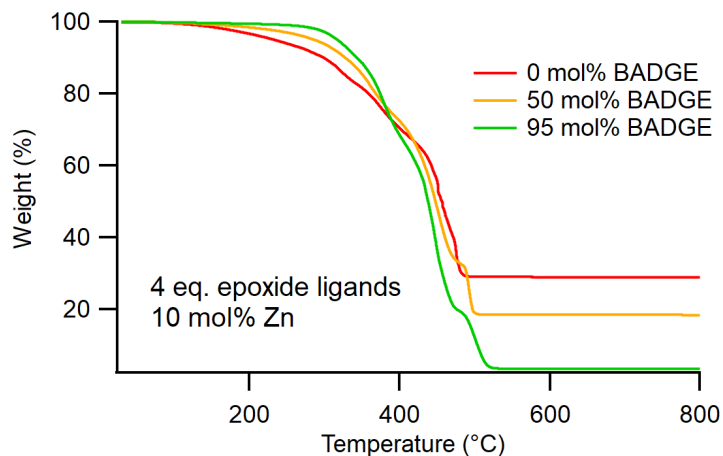
Figure A.66: Overview of TGA measurements of samples containing clusters functionalised with 4 equivalents epoxide and 10 mol% Zn with different amounts of BADGE.
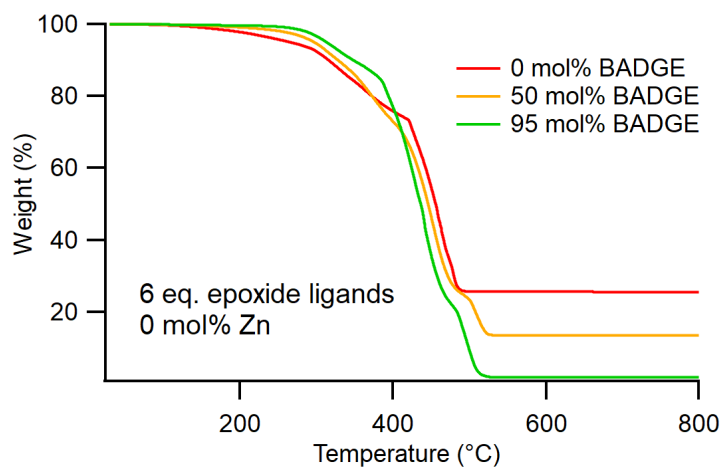
Figure A.67: Overview of TGA measurements of samples containing clusters functionalised with 6 equivalents epoxide and 0 mol% Zn with different amounts of BADGE.
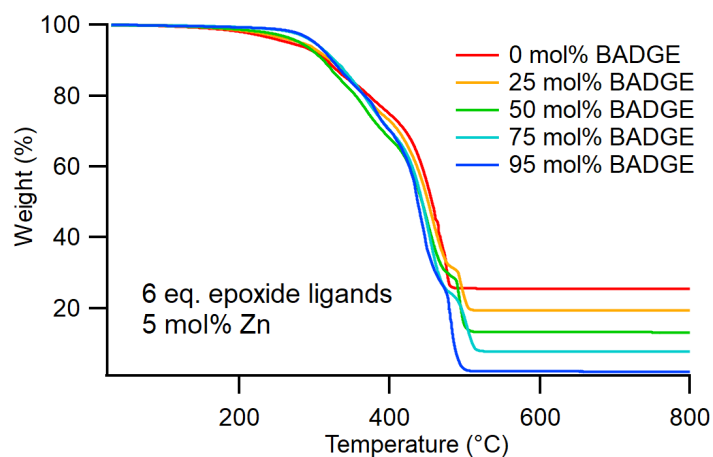
Figure A.68: Overview of TGA measurements of samples containing clusters functionalised with 6 equivalents epoxide and 5 mol% Zn with different amounts of BADGE.
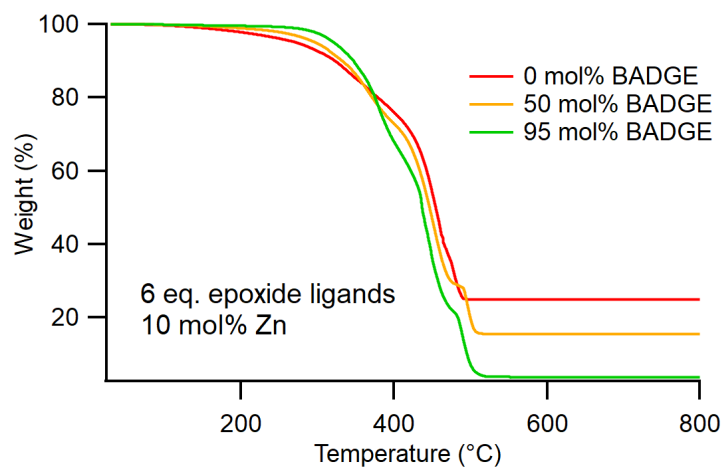
Figure A.69: Overview of TGA measurements of samples containing clusters functionalised with 6 equivalents epoxide and 10 mol% Zn with different amounts of BADGE.

A.5.6   Rheological experiments
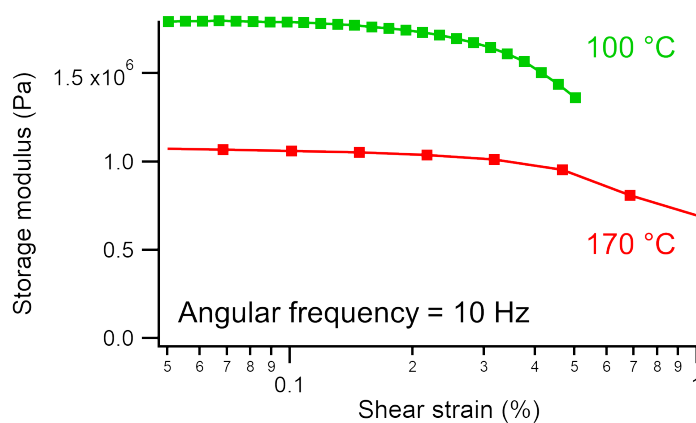
Figure A.70: Amplitude sweep of a polymer sample containing 95 mol% BADGE (red) and a polymer sample containing 50 mol% BADGE (green) with an angular frequency of 10 Hz. The value for the shear strain is obtained by looking to the end of the linear part of the curve.
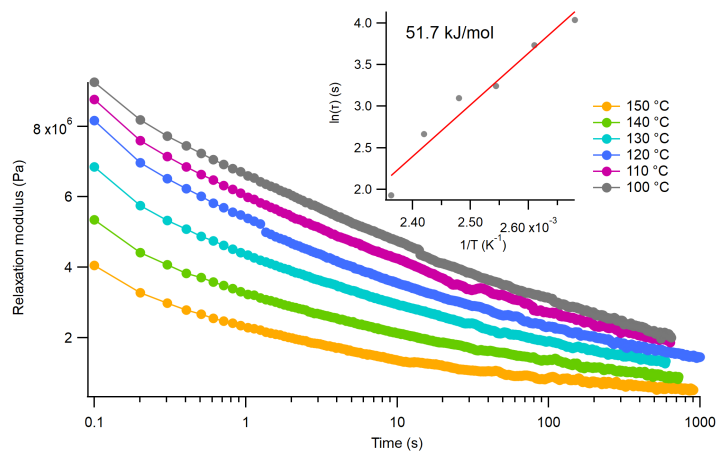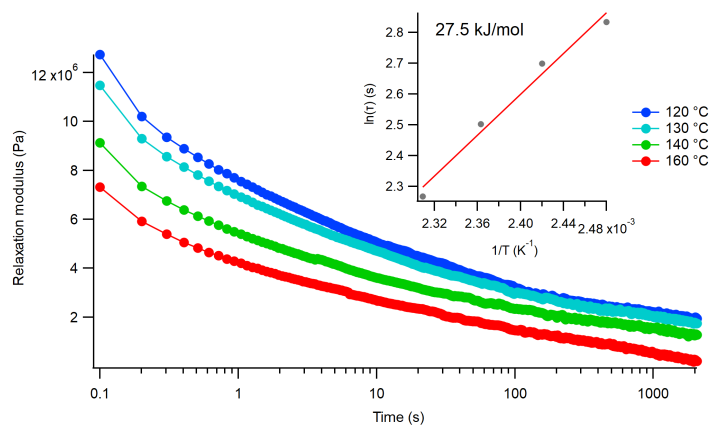

Figure A.71: Stress relaxation measurement of the sample containing 75 mol% clusters with 2 equivalents epoxide, 25 mol% BADGE and 5 mol% Zn.
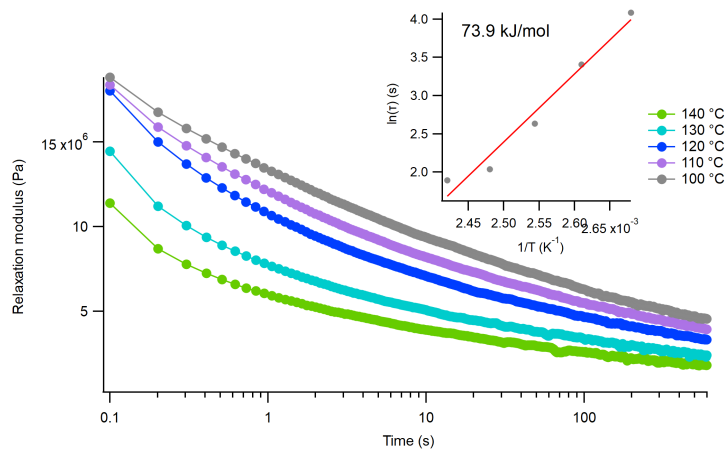
Figure A.72: Stress relaxation measurement of the sample containing 50 mol% clusters with 2 equivalents epoxide, 50 mol% BADGE and 5 mol% Zn.
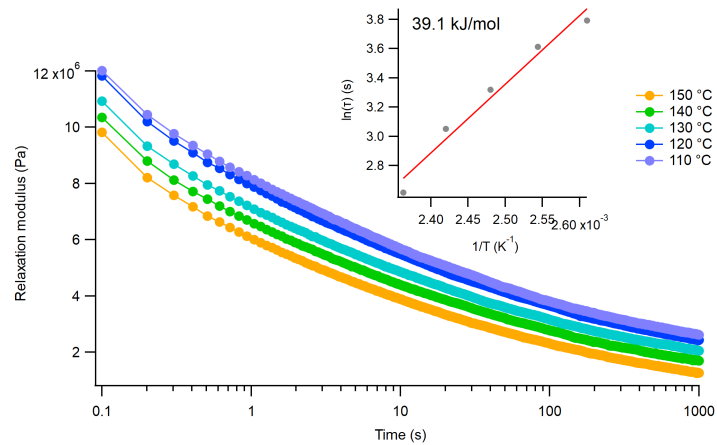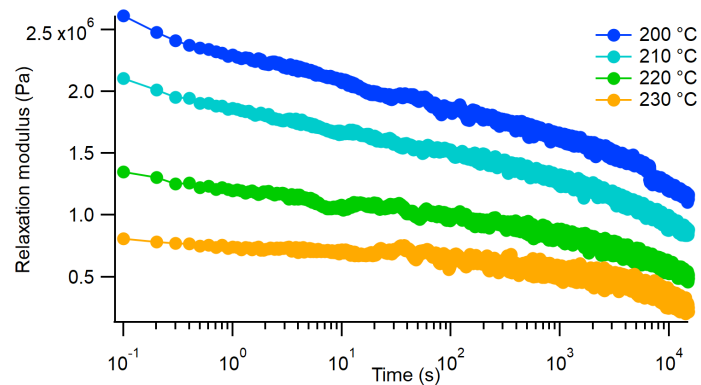

Figure A.73: Stress relaxation measurement of the sample containing 25 mol% clusters with 2 equivalents epoxide, 75 mol% BADGE and 5 mol% Zn.
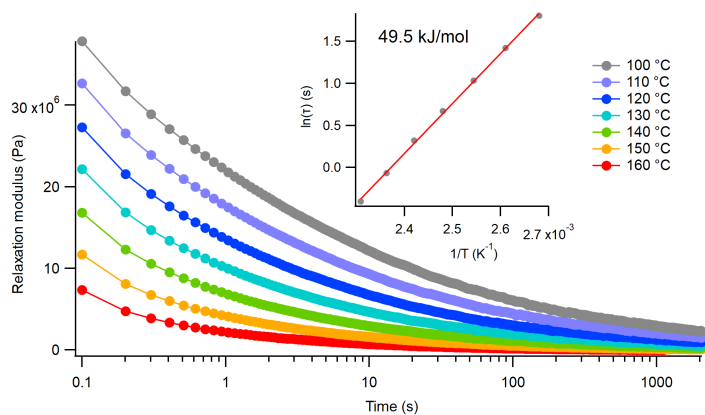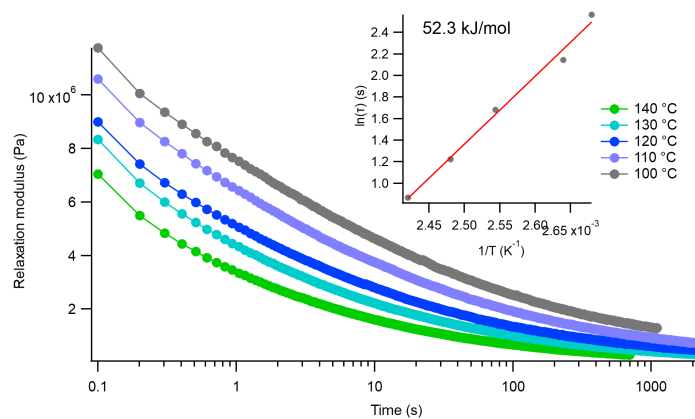
Figure A.74: Stress relaxation measurement of the sample containing 1 equivalent clusters with 4 equivalents epoxide and 5 mol% Zn.
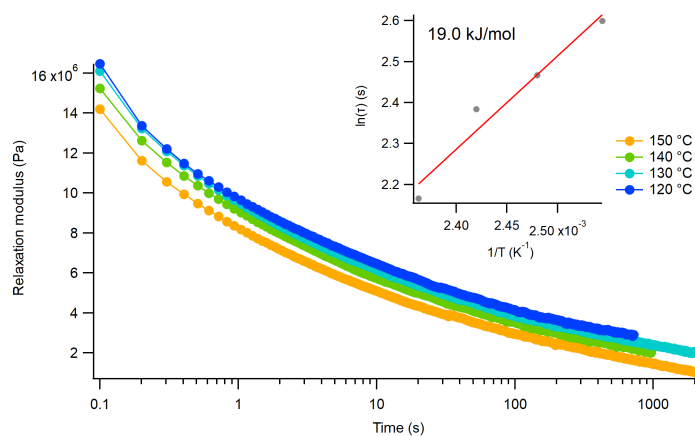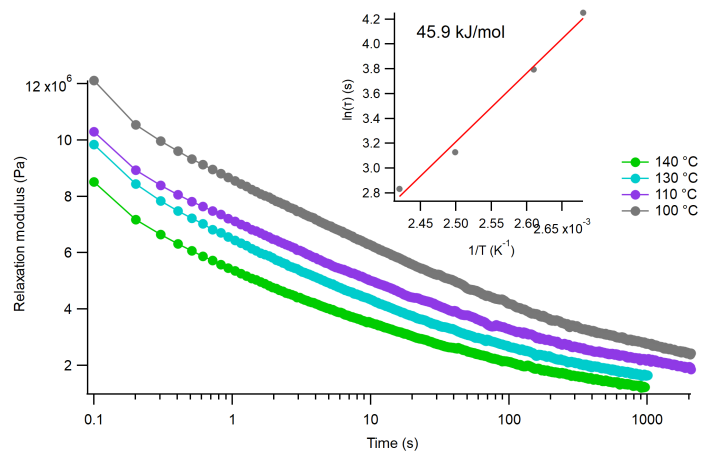

Figure A.75: Stress relaxation measurement of the sample containing 50 mol% clusters with 4 equivalents epoxide, 50 mol% BADGE and 5 mol% Zn.
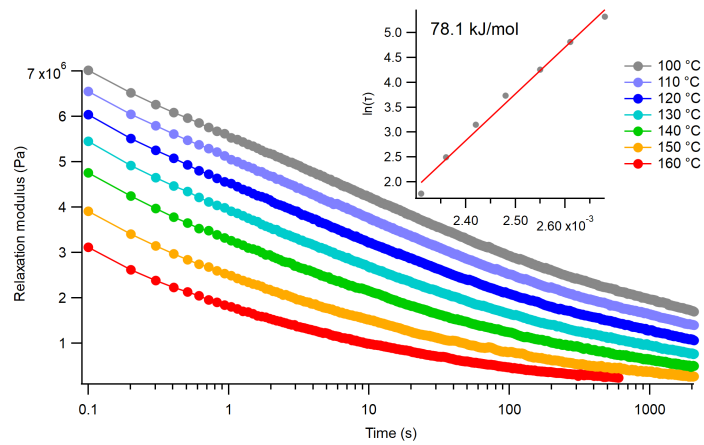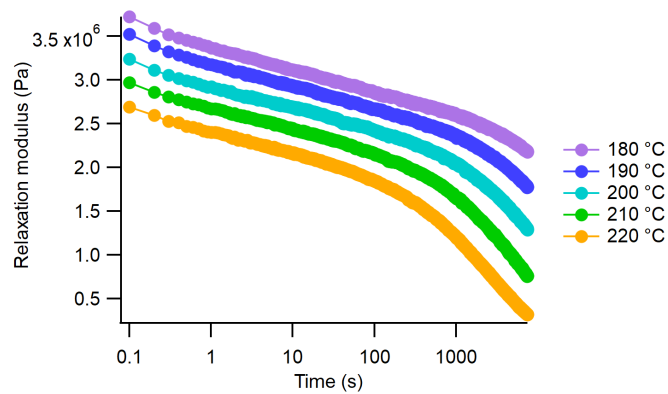
Figure A.76: Stress relaxation measurement of the sample containing 25 mol% clusters with 4 equivalents epoxide, 75 mol% BADGE and 5 mol% Zn.
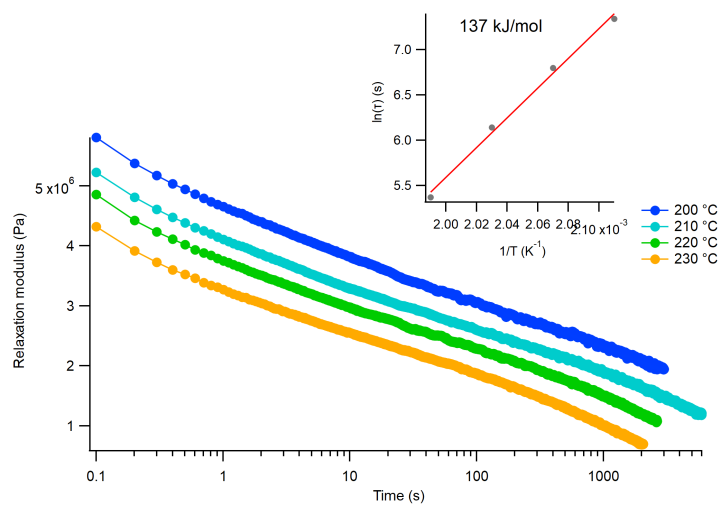
Figure A.77: Stress relaxation measurement of the sample containing 5 mol% clusters with 4 equivalents epoxide, 95 mol% BADGE and 5 mol% Zn.
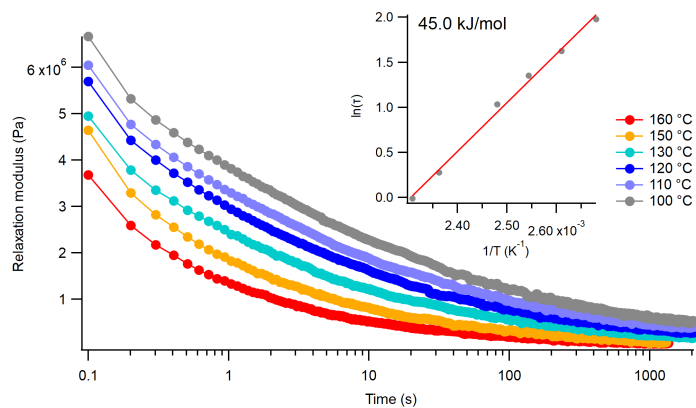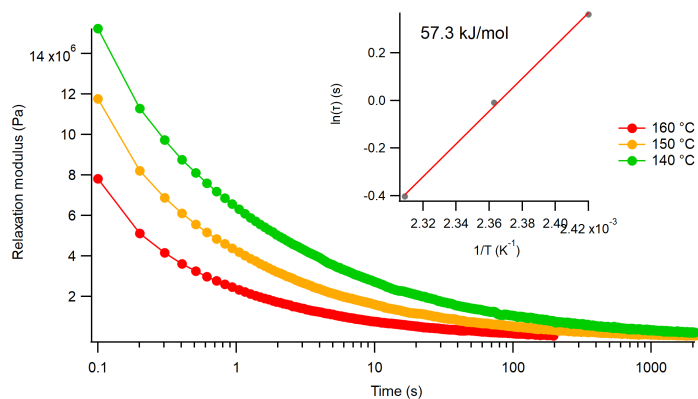
Figure A.78: Stress relaxation measurement of the sample containing 1 equivalent clusters with 6 equivalents epoxide and 5 mol% Zn.
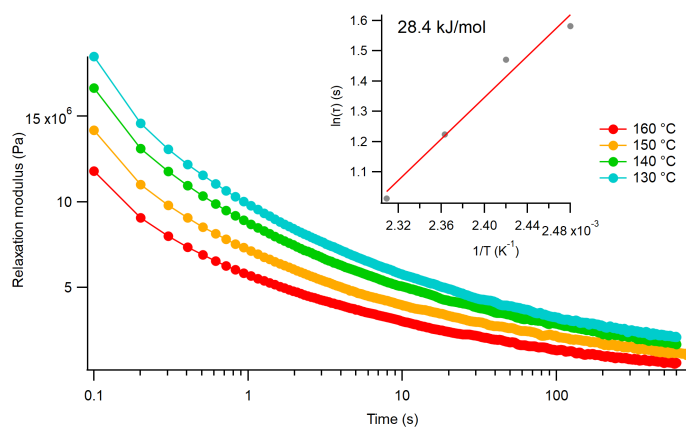
Figure A.79: Stress relaxation measurement of the sample containing 75 mol% clusters with 6 equivalents epoxide, 25 mol% BADGE and 5 mol% Zn.
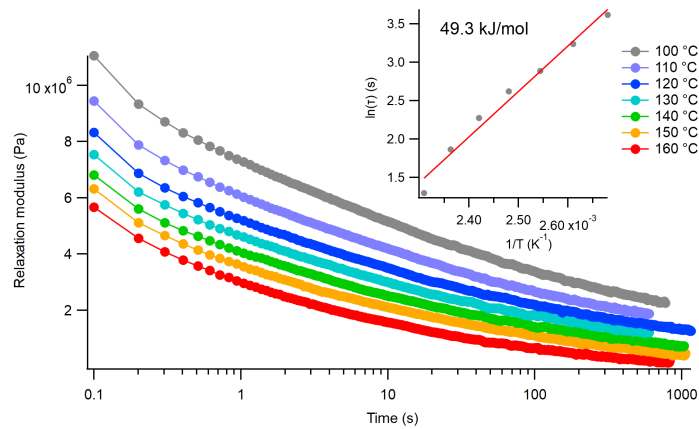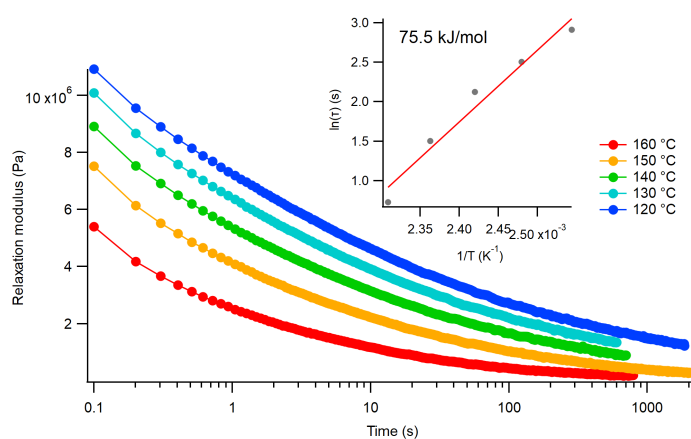
Figure A.80: Stress relaxation measurement of the sample containing 50 mol% clusters with 6 equivalents epoxide, 50 mol% BADGE and 5 mol% Zn.
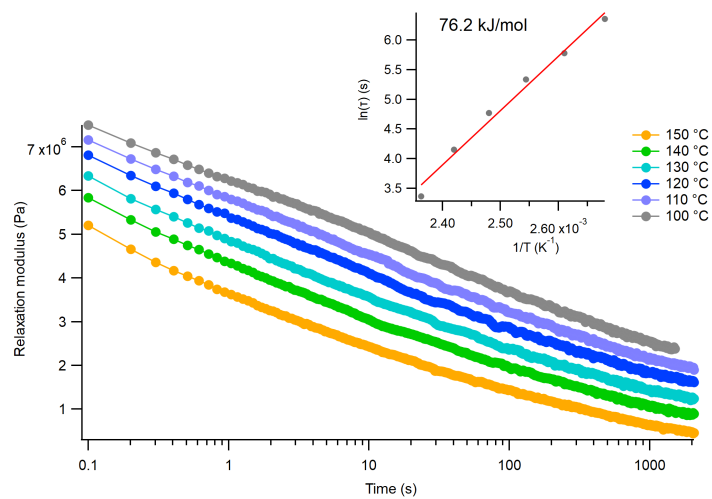
Figure A.81: Stress relaxation measurement of the sample containing 25 mol% clusters with 6 equivalents epoxide, 75 mol% BADGE and 5 mol% Zn.
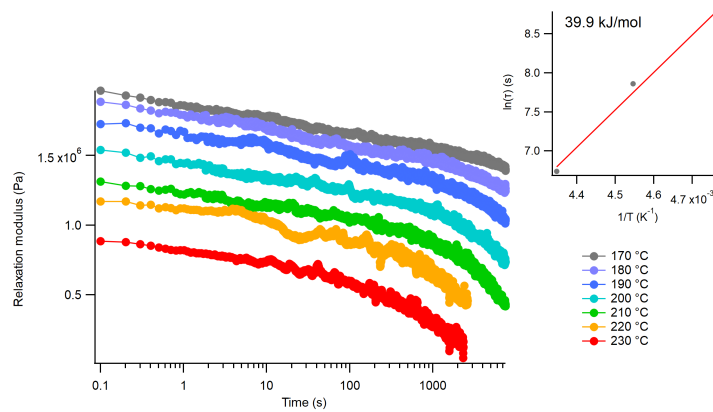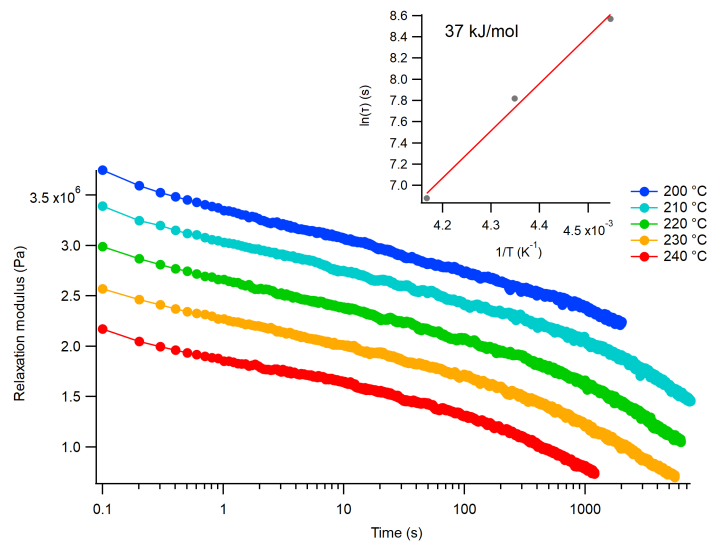
Figure A.82: Stress relaxation measurement of the sample containing 5 mol% clusters with 6 equivalents epoxide, 95 mol% BADGE and 5 mol% Zn.
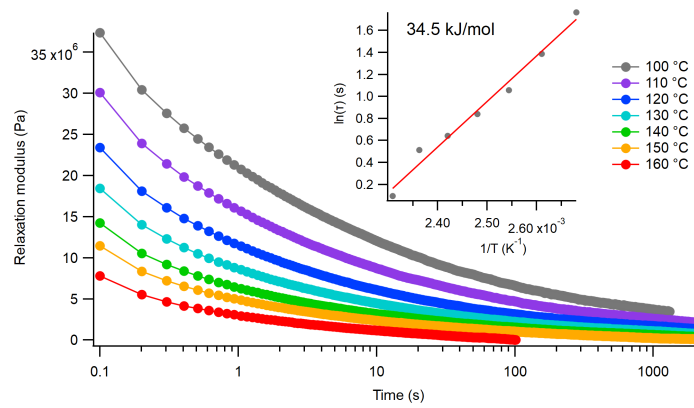
Figure A.83: Stress relaxation measurement of the sample containing 1 equivalent clusters with 2 equivalents epoxide and 0 mol% Zn.

Figure A.84: Stress relaxation measurement of the sample containing 50 mol% clusters with 2 equivalents epoxide, 50 mol% BADGE and 0 mol% Zn.

Figure A.85: Stress relaxation measurement of the sample containing 5 mol% clusters with 2 equivalents epoxide, 95 mol% BADGE and 0 mol% Zn.
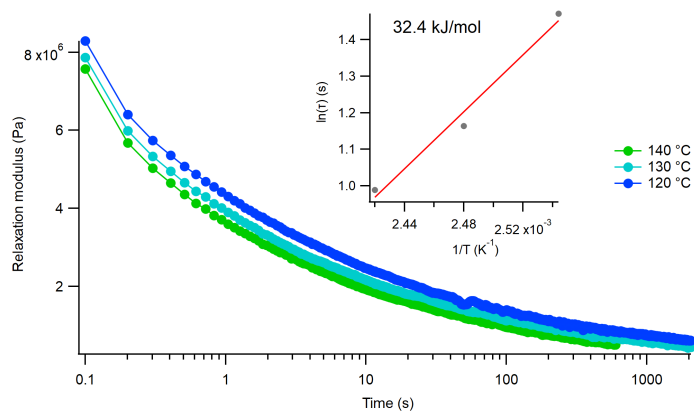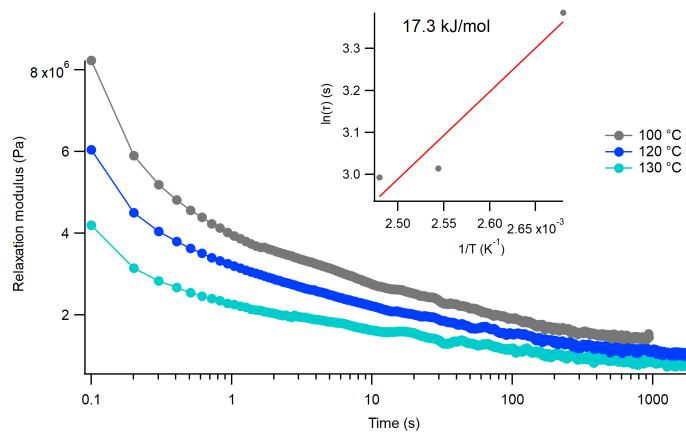

Figure A.86: Stress relaxation measurement of the sample containing 1 equivalent clusters with 4 equivalents epoxide and 0 mol% Zn.

Figure A.87: Stress relaxation measurement of the sample containing 50 mol% clusters with 4 equivalents epoxide, 50 mol% BADGE and 0 mol% Zn.
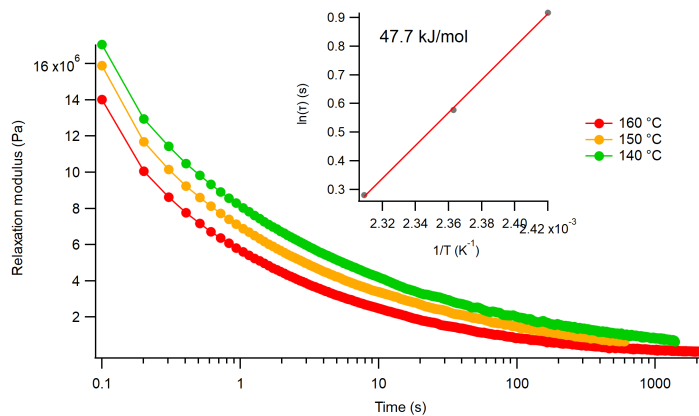

Figure A.88: Stress relaxation measurement of the sample containing 5 mol% clusters with 4 equivalents epoxide, 95 mol% BADGE and 0 mol% Zn.

Figure A.89: Stress relaxation measurement of the sample containing 1 equivalent clusters with 6 equivalents epoxide and 0 mol% Zn.
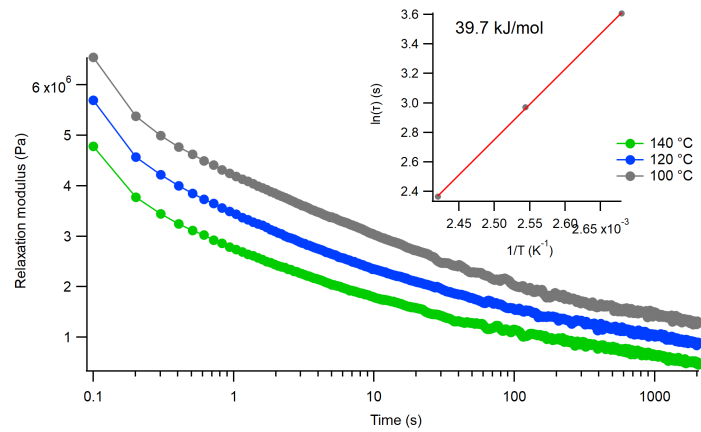

Figure A.90: Stress relaxation measurement of the sample containing 50 mol% clusters with 6 equivalents epoxide, 50 mol% BADGE and 0 mol% Zn.
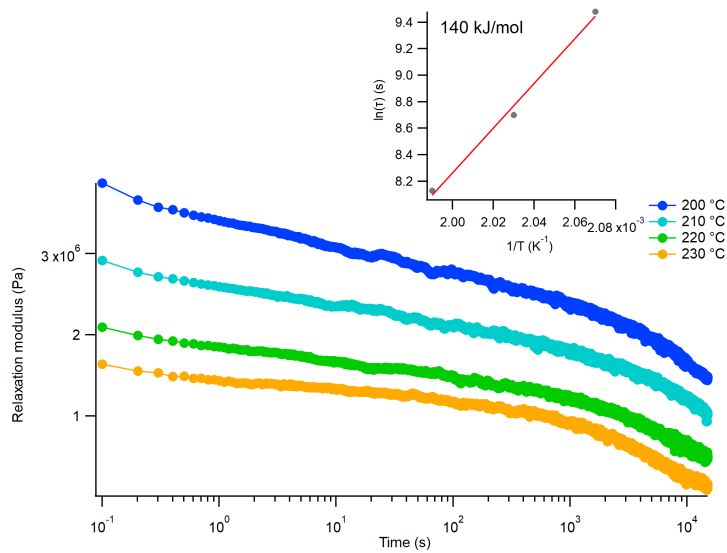
Figure A.91: Stress relaxation measurement of the sample containing 5 mol% clusters with 6 equivalents epoxide, 95 mol% BADGE and 0 mol% Zn.

Figure A.92: Stress relaxation measurement of the sample containing 1 equivalent clusters with 2 equivalents epoxide and 10 mol% Zn.
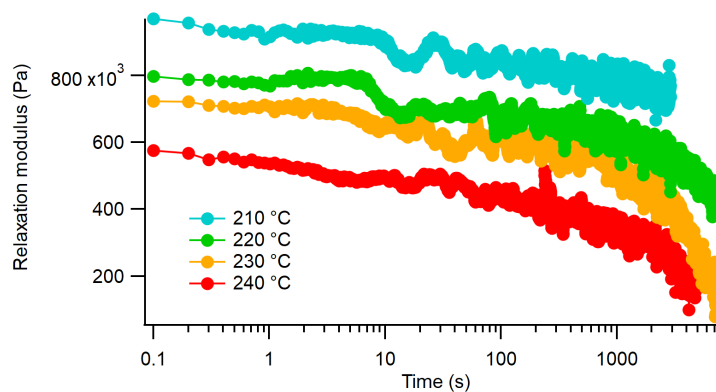
Figure A.93: Stress relaxation measurement of the sample containing 50 mol% clusters with 2 equivalents epoxide, 50 mol% BADGE and 10 mol% Zn.

Figure A.94: Stress relaxation measurement of the sample containing 1 equivalent clusters with 4 equivalents epoxide and 10 mol% Zn.

Figure A.95: Stress relaxation measurement of the sample containing 50 mol% clusters with 4 equivalents epoxide, 50 mol% BADGE and 10 mol% Zn.

Figure A.96: Stress relaxation measurement of the sample containing 5 mol% clusters with 4 equivalents epoxide, 95 mol% BADGE and 10 mol% Zn.

Figure A.97: Stress relaxation measurement of the sample containing 5 mol% clusters with 6 equivalents epoxide, 95 mol% BADGE and 10 mol% Zn.
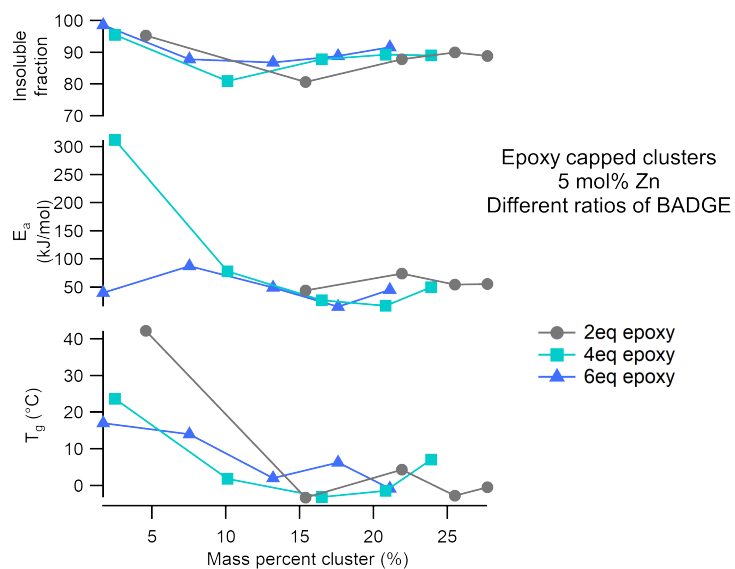

Figure A.98: Overview comparison between (top) insoluble fraction, (middle) activation energy and (bottom) T_g for the polymer samples containing 5 mol% Zn.
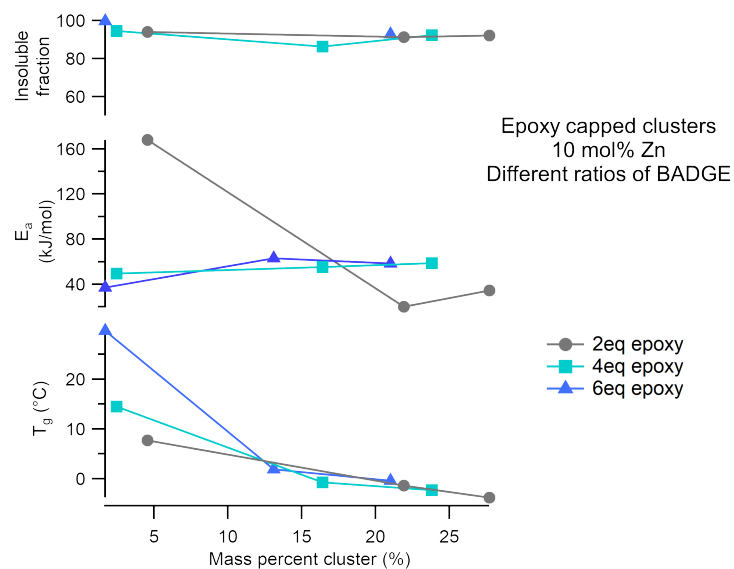
Figure A.99: Overview comparison between (top) insoluble fraction, (middle) activation energy and (bottom) T_g for the polymer samples containing 10 mol% Zn.

References

[1] Van den Eynden, D.; Pokratath, R.; De Roo, J. Nonaqueous Chemistry of Group 4 Oxo Clusters and Colloidal Metal Oxide Nanocrystals. *Chem Rev* **2022**, *122*, 10538–10572.

[2] Puchberger, M.; Kogler, F. R.; Jupa, M.; Gross, S.; Fric, H.; Kickelbick, G.; Schubert, U. Can the Clusters $Zr_6O_4(OH)_4(OOCR)_{12}$ and $[Zr_6O_4(OH)_4(OOCR)_{12}]_2$ Be Converted into Each Other? *Eur. J. Inorg. Chem.* **2006**, *2006*, 3283–3293.

B

Supporting Information

B.1   Publications in peer-reviewed journals

1. Resorcin[4]arene based multidentate phosphate ligands with superior binding affinity for nanocrystal surfaces
   *Nehmat S., **Van den Eynden D.**, Deblock L., Heilmann M., Köster M.J., Parvizian M., Tiefenbacher K., De Roo J.*
   2021, Chemical Communications

2. Ligand conversion in nanocrystal synthesis: the oxidation of alkylamines to fatty acids by nitrate
   *Calcabrini M., **Van den Eynden D.**, Ribot S.S., Pokratath R., Llorca J ., De Roo J ., Ibanez M.*
   2021, JACS Au

3. Mechanistic insights into the precursor chemistry of ZrO_2 and HfO_2 nanocrystals: towards size tuneable synthesis
   *Pokratath R., **Van den Eynden D.**, Cooper S.R., Mathiesen J.K., Waser V., Devereux M., Billinge S.J.L., Meuwly M., Jensen K.M.O., De Roo J.*
   2022, JACS Au

4. The chemistry of Cu_3N and Cu_3PdN nanocrystals
   *Parvizian M., Duran Balsa A., Pokratath R., Kalha C., Lee S., **Van den Eynden D.**, Ibanez M., Regoutz A., De Roo J.*
   2022, Angewandte

5. Nonaqueous chemistry of colloidal group 4 oxo clusters and metal oxide nanocrystals
   ***Van den Eynden D.**, Pokratath R. De Roo J.*
   2022, Chemical reviews

6. Fatty acid capped, metal oxo clusters as the smallest conceivable nanocrystal prototypes
   ***Van den Eynden D.**, Pokratath R., Pulparayil Mathew J., Goossens E., De Buysser K., De Roo J.*
   2022, Chemical science

7. From corrosion casting to virtual dissection: contrast enhanced vascular imaging using hafnium oxide nanocrystals
   *Goossens E., Deblock L., Caboor L., **Van den Eynden D.**, Josipovic I., Reyes Isaacura P., Maksimova E., Van Impe M., Bonnin A., Cornillie P., Boone M., Van Driessche I., De Spiegelaere W., De Roo J ., Sips P., De Buysser K.*
   2023, Submitted

8. Nonaqueous formation mechanism of zirconium and hafnium oxo clusters
Van den Eynden D., Mullaliu A., Seno C., Pulparayil Mathew J., Pokratath R., Whitehead C. B., Clark A. H., Safonova O., Parac-Vogt T. N., De Roo J .
2023, In preparation

9. Lewis acid-base chemistry in the group 4: complexation and disproportionation of metal alkoxy halides
Seno C., Pokratath R., Van den Eynden D., Prescimone A., De Roo J .
2023, In preparation

10. Redefining the gel in nonaqueous sol-gel chemistry: mechanistic insight in the crystallization of metal alkoxides
Goossens E., Aalling-Frederiksen O., Tack P., Van den Eynden D., Jensen K. M. O., De Buysser K., De Roo J .
2023, In preparation

11. Group IV metal oxo-clusters as emerging candidates for catalysis
Pulparayil Mathew J., Seno C., Van den Eynden D., De Roo J .
2023, In preparation

12. Surface chemistry of group IV metal oxo clusters
Parambil A. R. P., Pokratath R., Van den Eynden D., Shahgaldian P., De Roo J .
2023, In preparation

B.2 Oral and poster presentations

1. NanoGe conference – Resorcin[4]arene-based multidentate phosphate ligands with superior binding affinity for nanocrystal surfaces, poster presentation
28.06.2021 – 02.07.2021, online

2. NCCR fellow retreat – Resorcin[4]arene-based multidentate phosphate ligands with superior binding affinity for nanocrystal surfaces, poster presentation
10.05.2021 – 11.05.2021, Grindlewald (CH)

3. PCC research symposium – Resorcin[4]arene-based multidentate phosphate ligands with superior binding affinity for nanocrystal surfaces, invited talk
14.10.2021, University of Basel (CH)

4. International conference on coordination chemistry (ICCC) – Atomically precise group 4 oxo clusters as smallest conceivable nanocrystals, poster presentation
28.08.2022 – 02.09.2022, Rimini (IT)

5. PCC Christmas symposium – Atomically precise group 4 oxo clusters as smallest conceivable nanocrystals, oral presentation
02.12.2022, University of Basel (CH)

6. Research seminar in the group of Prof. T. Parac–Vogt – Group 4 metal oxo clusters; From synthesis to application, invited talk
05.04.2023, University of Leuven (BE)

7. NCCR fellow retreat – Atomically precise group 4 oxo clusters as smallest conceivable nanocrystals, oral presentation
02.05.2023 – 04.05.2023, Grindlewald (CH)

8. Symposium on Materials Chemistry (Matchem) – Atomically precise group 4 oxo clusters as smallest conceivable nanocrystals, poster presentation
14.06.2023, EMPA Dübendorf (CH)
Poster awarded with poster prize

9. Nanax10 – Atomically precise group 4 oxo clusters as inorganic monomers for covalent adaptable networks, poster presentation
03.07.2023 – 07.07.2023, ISTA Vienna (AT)
Poster awarded with poster prize

B.3   Travel awards

1. Swissuniversities travel award
Travel grant to support the travel between the university of Basel and the university of Ghent in the framework of my joint PhD.

2. Swiss Chemical Society travel award
Travel grant to support the research stay at Instituto Italiona de Technologia in Genova Italy

Dietger Van den Eynden

Highly skilled and motivated chemist
With a curious nature

Contact

dietger.vandeneynden@unibas.ch
+41775024776
+32499604013
Palmenstrasse 26, 4055 Basel (CH)
Houtenkruisstraat 36, 9150 Kruibeke (BE)

Skills

Laboratory Skills

Glovebox	●●●●●
Air-free techniques	●●●●●
Nanocrystal synthesis	●●●●○
Polymer synthesis	●●●●○
Computational methods	●●●○○
Organic synthesis	●●●○○

Software and EDV

MS Office	●●●●●
Igor Pro	●●●●○
Gaussian	●●●●○
Python	●●●○○
CP2K	●●●○○
LaTeX	●●●●○
Quantum Espresso	●●●●○

Graphical software

Inkscape	●●●●○
Blender	●●●○○

Operating systems

Windows	●●●●○
Linux	●●●○○

Languages

Dutch (native)	●●●●●
English	●●●●○
French	●●●○○
German	●●●●○

Personal interests

Personal

3D-modeling, sports (surfing, snow-boarding, basketball), Lego

Academic

Thermoresponsive and mechano-luminescent polymers, nanomaterials

Education

10.2019-present
Universität Basel, CH
University Ghent, BE

Joint PhD in chemistry

Joint PhD under the supervision of Prof. J. De Roo (Basel) and Prof. K. De Buysser (Ghent) titled: 'Group 4 metal oxo clusters; from synthesis to application'

06.12.2022-07.12.2022
HEIA Freiburg, CH

Research visit

Learning the nano-indentation technique to study the properties of inorganic-organic polymer composites under supervision of Prof. Hengsberger

20.06.2022-03.07.2022
IIT Genova, IT

Research stay

Learning molecular dynamics to model ligand shells of group 4 metal oxo clusters under supervision of Prof. L. Manna

11.02.2022
EPFL Lausanne, CH

Research visit

Learning the colloidal atomic layer deposition technique (c-ALD) under supervision of Prof. R. Buonsanti

10.2017-09.2019
University Ghent, BE

Master of science in chemistry

Master thesis titled: 'Exploration of group 4 metal oxide nanocrystals as catalysts in covalent adaptable networks' under supervision of Prof. I. Van Driessche and Prof. F. Du Prez. Final grade: magna cum laude

Work related experience

08.03.23–12.03.23
NSLSII New York, US

Lead investigator synchrotron beamtime
In situ PDF experiment

11.05.22 – 13.05.22
PSI Villigen, CH

Lead investigator synchrotron beamtime
In situ EXAFS experiment

04.22-present
Universität Basel, CH

Organization committee symposium
Organization of a symposium on chemists with an unconventional career path

10.19-10.22
Universität Basel, CH

Safety officer
Responsible for general safety in the lab, good organizational skills, making important decisions in absence of the professor

07.18-08.18
XEIKON Lier, BE

Internship in chemical industry
Optimizing polymer scaffolds to improve printing processes

02.18-06.19
MySherpa, BE

Chemistry and physics tutor
Tutoring students in chemistry and or physics from high school to university level

Publications

Lewis acid-base chemistry in the group 4: Complexation and disproportionation of metal alkoxy halides
Seno C., Pokratath R., **Van den Eynden D.**, Prescimone A., De Roo J.
In preparation

From corrosion casting to virtual dissection: contrast-enhanced vascular imaging using hafnium oxide nanocrystals
Goossens E., Deblock L., Caboor L., **Van den Eynden D.**, Josipovic I., Reyes Isaacura P., Maksimova E., Van Impe M., Bonnin A., Cornillie P., Boone M., Van Driessche I., De Spiegelaere W., De Roo J., Sips P., De Buysser K.
https://chemrxiv.org/engage/chemrxiv/article-details/64066d9dcc600523a3c3c5a3

Fatty acid capped, metal oxo clusters as the smallest conceivable nanocrystal prototypes
Van den Eynden D., Pokratath R., Pulparayil Mathew J., Goossens E., De Buysser K., De Roo J.
2022, Chemical Science

Nonaqueous chemistry of colloidal group 4 oxo clusters and metal oxide nanocrystals
Van den Eynden D., Pokratath R., De Roo J.
2022, Chemical Reviews

The chemistry of Cu_3N and Cu_3PdN nanocrystals
Parvizian M., Duran Balsa A., Pokratath R., Kalha C., Lee S., **Van den Eynden D.**, Ibanez M., Regoutz A., De Roo J.
2022, Angewandte

Mechanistic insights into the precursor chemistry of ZrO_2 and HfO_2 nanocrystals; towards size-tunable synthesis
Pokratath R., **Van den Eynden D.**, Cooper S.R., Mathiesen J.K., Waser V., Devereux M., Billinge S.J.L., Meuwly M., Jensen K.M.O., De Roo J.
2022, JACS Au

Ligand conversion in nanocrystal synthesis: the oxidation of alkylamines to fatty acids by nitrate
Calcabrinin M., **Van den Eynden D.**, Ribot S.S., Pokratath R., Llorca J., De Roo J., Ibanez M.
2021, JACS Au

Resorcin[4]arene-based multidentate phosphate ligands with superior binding affinity for nanocrystal surfaces
Nehmat S., **Van den Eynden D.**, Deblock L., Heilmann M., Köster M.J., Parvizian M., Tiefenbacher K., De Roo J.
2021, Chemical Communications

Conferences and talks

Poster presentation at Nanax10
03.07.2023-07.07.2023, ISTA Vienna (AT)

Poster presentation at Matchem23
14.06.2023, EMPA Dübendorf (CH)

Invited lecture by Prof. T. Parac-Vogt
05.04.2023, KU Leuven (BE)

Invited lecture at PCC Christmas symposium
02.12.2022, University of Basel (CH)

Poster presentation at the International conference on coordination chemistry (ICCC)
28.08.2022-02.09.2022, Rimini (IT)

Invited lecture at PCC research seminar
14.10.2021, University of Basel (CH)

Poster presentation on NanoGe conference
28.06.2021-02.07.2021

Additional academic courses

Advanced python and machine learning (University of Basel, 16.03.23-24.03.23)

Project management for researchers (University of Basel, 20.02.23-24.03.23)

Computational materials physics (University of Ghent, 19.09.22-18.12.22)

Entrepreneurship training: business concepts (University of Basel, 27.02.21-19.05.21)

X-ray crystallography: aspects that a chemist needs (University of Basel, 01.02.21-01.06.21)

Colloidal nanocrystals: from synthesis to application (University of Basel, 01.02.20-01.06.20)

Laboratory skills

Schlenk line techniques
Fully trained at air free techniques to perform nanocrystal/precursor synthesis as well as air free purifications

Nanocrystal synthesis
Fully trained in synthesizing and purification of nanocrystals via solvothermal, autoclave or microwave synthesis

Polymer synthesis
Proficient in synthesizing and characterizing polymer networks via radical or thermal polymerizations

Glove box techniques
Fully trained to operate glove boxes for storage and synthesis of air sensitive chemicals

Computational methods
Able to perform geometry optimizations with Gaussian, QuantumEspresso and CP2K as well as molecular dynamics

Organic synthesis
Basic knowledge of organic synthesis and purification of ligands and functionalization

Characterization techniques
Dynamic light scattering (DLS)
Fourrier Transform Infrared (FTIR)
ThermoGravimetric Analysis (TGA)
Gel Permeation Chromatography (GPC)
Gas Chromatography (GC)
Differential Scanning Calorimetry (DSC)

Ultraviolet-Visible Spectroscopy (UV-VIS)
Transmission Electron Microscopy (TEM)
Nuclear Magnetic Resonance (NMR)
Rheology
Hot plate press
MALDI-TOF

Volunteering experience

19.11.2022 — Demonstration chemistry olympiad
Teaching students who participated in the chemistry Olympiad about quantum dots in an interactive session in order to peak their interest for chemistry

09.2016 – 06.2017 — President student association
End responsible for the general functioning of the student association Chemica at the university of Ghent. Ensuring that everyone within the association is living up to their expectations and all of our events are organized correctly.

09.2015 – 06.2016 & 09.2017 – 06.2018 — Course responsible student association
Responsible for the printing and distribution of syllabi for all students in chemistry, biochemistry and biotechnology at the university of Ghent

09.2001 – 06.2014 — Youth movement - Chiro
Youth movement every Sunday afternoon for 12 years. The final two years I was responsible for guiding kids aged 9-12 and 16-18. Also organizing multiple events and a yearly 10-day camp in summer

Awards

Royal Society of Chemistry poster award Nanax10
Poster title: Clusters as inorganic monomers for covalent adaptable networks

Poster award Matchem23
Poster title: Clusters as smallest conceivable nanocrystal prototypes

Swissuniversities travel award
Travel grant to support the travel in the framework of my joint PhD

Swiss Chemical Society Travel award
Travel grant to support the research stay at Instituto Italiona de Technologia in Genova Italy